INVESTIGATION OF NON-NEWTONIAN FLOW IN ANAEROBIC DIGESTERS

by

Jeremy M. Langner

September 2009

A thesis presented to the Faculty of Graduate Studies,

University of Manitoba in fulfillment of the thesis requirement

for the degree of Master of Science in

MECHANICAL ENGINEERING

Department of Mechanical and Manufacturing Engineering

University of Manitoba

Winnipeg, Manitoba, Canada

Acknowledgements

First and foremost, I would like to thank my wife, Sherisse, and my family, Les, Theresa, and Stacie for their constant support, patience, prayer, and love. It goes without saying that without them, all this would not have been possible. I would also like to express my sincere thanks to David Gaden, for his time, wisdom, laughter, and friendship along the way. Thanks to my friends and lab-mates, Amir Birjandi and Andrea Kraj, for their insight and friendship. Many thanks to my summer assistants, Tyra Wedel, and Graham Leverick, whose hard work, creativity, and willingness to step up to any challenge made the task much lighter. Thank you to the Mechanical Engineering technicians, Bruce Ellis, Paul Krueger, and Kim Majury, and to our machinists Daniel Rossong and Irwin Penner. Thank you to Dean Gurney and Shokri Rashwan at Puratone Corp. for their cooperation with the lagoon sampling project. I would also like to thank the members of examination committee, Dr. David Kuhn, Dr. Nazim Cicek, and Mr. Tom Molinski, for the time taken to review my thesis. Finally, I must express my utmost gratitude to Dr. Eric Bibeau, who has not only been an excellent mentor and advisor, but has opened the door to an exciting career in a field that I am passionate about, renewable energy.

Funding for this research was graciously provided through the NSERC Postgraduate Scholarship, and through the NSERC/Manitoba Hydro Industrial Research Chair in Alternative Energy.

Abstract

This thesis examines how the non-Newtonian characteristics of liquid hog manure affect the flow conditions within a steady-flow anaerobic digester. There are three main parts to this thesis. In the first part of this thesis, the physical properties of liquid hog manure and their variation with temperature and solids concentration are experimentally determined. Naturally-settled manure sampled from an outdoor storage lagoon is studied, and density, viscosity, and particle size distribution are measured. Hog manure with total solids concentrations of less than 3.6% exhibits Newtonian behaviour; manure between 3.6% and 6.5% total solids is pseudoplastic, and fits the power law; manure with more than 6.5% total solids exhibits non-Newtonian and time-dependent characteristics. The second part of this thesis investigates the flow of Newtonian and non-Newtonian fluids—represented by tap water and xanthan gum solution, respectively—within four lab-scale reactor geometries, using residence time distribution (RTD) experiments. The effect of reactor geometry, flow rate, and fluid viscosity are evaluated. In the third part of this thesis, flow conditions within lab-scale and pilot-scale anaerobic digester reactors are simulated using three-dimensional modeling techniques. The RTDs of lab-scale reactors as predicted by the 3D numerical models compare well to the experimental results. The 3D models are also validated using data from particle image velocimetry (PIV) experiments. Finally, the viscous properties of liquid hog manure at 3% and 8% total solids are incorporated into the models, and the results are evaluated.

Table of Contents

CHAPTER 1. INTRODUCTION 20

1.1 The hog industry in Manitoba 22

1.1.1 Manure management practices 22

1.1.2 Environmental issues surrounding livestock waste management 24

1.1.3 Manure treatment through anaerobic digestion 26

1.2 Renewable energy from biomass 28

1.3 Anaerobic digestion 30

1.3.1 Mechanisms involved in anaerobic digestion 31

1.3.2 Products of anaerobic digestion 32

1.3.3 Types of anaerobic digesters 32

1.3.4 Biogas production and CHP systems 35

1.3.5 Anaerobic digestion in cold climates 37

1.3.6 Modeling of anaerobic digesters 37

1.4 Thesis overview 38

1.4.1 Physical properties of liquid hog manure 39

1.4.2 Residence time distribution experiments 39

1.4.3 CFD simulations 40

1.4.4 Contribution to research 40

CHAPTER 2. LITERATURE REVIEW 41

2.1 Introduction 41

2.2 Anaerobic digestion – heat transfer and biogas production 42

2.3 Non-Newtonian flow in anaerobic digesters 45

CHAPTER 3. EXPERIMENTAL DETERMINATION OF THE PHYSICAL PROPERTIES OF HOG MANURE 46

3.1 Introduction 46

3.1.1 Overview of the study 46

3.1.2 Naturally settled hog manure 47

3.1.3 Viscosity models – Newtonian and non-Newtonian fluids 48

3.2 Literature review 50

3.3 Sample collection 55

3.3.1 Design of sample collection system 57

3.3.2 Operation of sample collection system 59

3.4 Experimental methods 61

3.4.1 Sample size and storage 61

3.4.2 Mass fraction of total solids and bulk density 62

3.4.3 Particle size distribution 62

3.4.4 Viscosity 64

3.5 Results and discussion 65

3.5.1 Density 65

3.5.2 Total solids concentration vs. depth 66

3.5.3 Particle size distribution 68

3.5.4 Viscosity 75

3.5.5 Recommendations for modeling 84

3.6 Summary of findings 89

CHAPTER 4. DESIGN OF AN EXPERIMENTAL FLUID COLUMN FACILITY 91

4.1 Introduction 91

4.1.1 Overview 91

4.1.2 Design criteria 96

4.2 Description of experiments 97

4.3 Design of acrylic fluid column 99

4.4 Supply and discharge tanks 102

4.5 Pump and plumbing system 103

4.6 Tracer dye injection and sampling stations 108

4.7 PIV system 110

4.8 Design of support and sliding frames 112

4.9 Summary 117

CHAPTER 5. EXPERIMENTAL STUDY OF RESIDENCE TIME DISTRIBUTION 118

5.1 Introduction 118

5.1.1 Overview of the RTD study 119

5.1.2 Residence time distribution 121

5.2 Literature review 126

5.3 Experimental methods 129

5.3.1 RTD experimental procedure 129

5.3.2 Preparation of xanthan gum solution 131

5.3.3 Fluorescence analysis 131

5.4 Initial calculations 132

5.4.1 Geometry and volume calculations 132

5.4.2 Calculation of HRT 133

5.4.3 Inlet and outlet velocities and Reynolds numbers 134

5.4.4 Standard curves for rhodamine B 136

5.4.5 Viscosity calculations for xanthan gum 137

5.5 Results and discussion 138

5.5.1 Visual observations 138

5.5.2 Fluorescence response data and interpretation 142

5.5.3 Residence time distribution – effect of geometry, flow rate, and fluid viscosity 144

5.5.4 Comparison to one-parameter RTD models 150

5.5.5 Comparison to multiparameter RTD models 152

5.5.6 Dead space 159

5.6 Summary of findings 161

CHAPTER 6. CFD STUDY OF AN ANAEROBIC DIGESTER 164

6.1 Introduction 164

6.1.1 Overview 164

6.1.2 Governing equations 165

6.1.3 Modeling assumptions 166

6.1.4 Modeling viscosity 168

6.1.5 PIV validation 169

6.2 Literature review 170

6.3 Model description 172

6.3.1 Geometry 172

6.3.2 Mesh 173

6.3.3 Solver 176

6.3.4 Fluid properties 177

6.3.5 Boundary conditions 177

6.3.6 Transient RTD Studies 178

6.4 Grid independence tests 179

6.5 Results and discussion 183

6.5.1 Reactor geometry 1, centre inlet 184

6.5.2 Reactor geometry 2, side inlet 189

6.5.3 Reactor geometry 3, concentric baffles 194

6.5.4 Reactor geometry 4, radial baffles 198

6.5.5 Effect of flow rate on RTD 202

6.5.6 Pilot-scale simulations 203

6.5.7 Possible sources of error for CFD simulations 210

6.6 Validation of CFD model using PIV 211

6.6.1 PIV experimental procedure 211

6.6.2 PIV calculations 214

6.6.3 PIV results and comparison to CFD model 215

6.6.4 Possible sources of error for PIV experiments 222

6.7 Comparison of CFD results to RTD experiments 223

6.8 Summary of findings 228

CHAPTER 7. CONCLUSIONS AND RECOMMENDATIONS 231

7.1 Objective 231

7.2 Physical and properties of hog manure 231

7.3 Experimental residence time distribution study 233

7.4 CFD simulation of flow conditions in anaerobic digester reactors 234

7.5 Recommendations 235

CHAPTER 8. BIBLIOGRAPHY 238

8.1 Graphic References 248

APPENDIX A. HOG MANURE VISCOSITY RESULTS: FULL DATA SET 249

APPENDIX B. GAMBIT JOURNAL FILES FOR CFD MESHES 252

APPENDIX C. CFD MODEL PARAMETERS AND MESH CHARACTERISTICS 281

APPENDIX D. FULL RESIDENCE TIME DISTRIBUTION EXPERIMENTAL DATA 316

APPENDIX E. RESIDENCE TIME DISTRIBUTION EXPERIMENTAL PROCEDURE 348

APPENDIX F. MATLAB CODE FOR PIV DATA 349

APPENDIX G. FLUID COLUMN DRAWINGS 356

APPENDIX H. FUTURE EXPANSION OF THE EXPERIMENTAL FLUID COLUMN FACILITY 369

APPENDIX I. ANAEROBIC DIGESTER ECONOMIC ANALYSIS 372

List of figures

Figure 1.1: Typical swine manure management practice 23

Figure 1.2: Microbial process of anaerobic digestion..... 31

Figure 1.3: Installation of complete mix digesters at Glenlea Research Facility 33

(NCLE, 2008) 33

Figure 1.4: Plug flow digester at Haubenschild Dairy Farms in Minnesota (Nelson and Lamb, 2002)..... 34

Figure 1.5: Cook Feeders covered lagoon digester near Teulon, MB (Bioterre, 2009) ... 35

Figure 1.6: Diagram of a farm-based biogas CHP system..... 36

Figure 3.1: The power law model 49

Figure 3.2: Sampling locations for Operation 1 and Operation 2. Drawings not to scale. 56

Figure 3.3: Lagoon sample collection system..... 58

Figure 3.4: Ekman dredge and van Dorn bottle sampler 58

Figure 3.5: Sample carrier plate and messenger release mechanism..... 59

Figure 3.6: Sample collection system setup..... 60

Figure 3.7: Sample collection system disassembled and ready for transport 61

Figure 3.8: Particle size distribution – sieve test apparatus 64

Figure 3.10: Density of hog manure as a function of total solids. 66

Figure 3.11: Total solids concentration vs. depth. a) Operation 1; b) Operation 2 67

Figure 3.12: Microphotograph of liquid hog manure, 400X 69

Figure 3.14: Particle size distribution by mass fraction. a) Operation 1; b) Operation 2 . 72

Figure 3.15: Particle size distribution by particle count. a) Operation 1; b) Operation 2. 73

Figure 3.16: Viscosity results for TS < 3.6% 76

Figure 3.17: Shear stress vs. shear rate for Operation 1, TS = 5.09% 78

Figure 3.18: Shear stress vs. shear rate for Operation 1, TS = 5.51% 78

Figure 3.19: Shear stress vs. shear rate for Operation 1, 9.45% TS 79

Figure 3.20: Shear stress vs. shear rate for Operation 2, 6.49% TS 80

Figure 3.21: Shear stress vs. shear rate for Operation 2, 12.9% TS 80

Figure 3.22: Consistency coefficient K ($Pa \cdot s^n$) vs. total solids. 82

Figure 3.23: Comparison of viscosity data with the literature 83

Figure 3.24: Flow behaviour index n vs. total solids. 84

Figure 3.25: Rosin-Rammler fit for a) Operation 1; b) Operation 2 86

Figure 3.26: Recommended Rosin-Rammler distribution of solid particles 87

Figure 3.27: Experimental power law parameters with generalized viscosity model. a) consistency coefficient K; b) flow behaviour index n 88

Figure 3.28: Apparent viscosity as a function of % TS, generalized model 89

Figure 4.1: Diagram of the fluid column facility (not to scale) 91

Figure 4.2: Fluid column test section Geometry #1 with centre inlet 94

Figure 4.3: Fluid column test section Geometry #2 with side inlet 94

Figure 4.4: Fluid column test section Geometry #3 with concentric baffles 95

Figure 4.5: Fluid column test section Geometry #4 with radial baffles 95

Figure 4.6: Acrylic fluid column 99

Figure 4.7: Acrylic fluid column – left, front, and top views 101

Figure 4.8: Acrylic fluid column – 3D view 102

Figure 4.9: Supply and discharge tanks 103

Figure 4.10: Peristaltic pump 104

Figure 4.11: Masterflex® I/P variable speed pump drive and pump head 105

Figure 4.13: Flow control valves 108

Figure 4.14: Dye injection station and sampling station..... 109

Figure 4.15: PIV laser and camera..... 111

Figure 4.16: Fluid column facility with support and sliding frames..... 112

Figure 4.17: 3D rendering of steel support frame..... 114

Figure 4.18: PIV Camera zones 115

Figure 4.19: Aluminum sliding frame 116

Figure 5.1: Four test geometries. a) G1 centre inlet, b) G2 side inlet, c) G3 concentric baffles, d) G4 radial baffles 120

Figure 5.2: The residence time distribution (RTD) curve (Levenspiel, 1972) 122

Figure 5.3: Ideal reactors 123

Figure 5.4: RTD curves for ideal reactors. a) CSTR, b) plug flow reactor 124

Figure 5.5: System diagram of the fluid column facility, indicating dye injection and sampling stations..... 130

Figure 5.6: Tracer dye flowing through G1 test section, flow rate = 0.05 L/s 139

Figure 5.7: Tracer dye flowing through G4 test section, flow rate = 0.05 L/s 141

Figure 5.8: Fluorescence data for G1 centre inlet; H_2O; 0.05 L/s 142

Figure 5.9: Fluorescence data with extrapolation for G1; H_2O; 0.05 L/s..... 143

Figure 5.10: Normalized RTD curves for G1 centre inlet; H_2O; 0.05 L/s..... 144

Figure 5.11: RTD for all four geometries; H_2O; 0.05 L/s..... 145

Figure 5.12: RTD for all four geometries; H_2O; 0.0125 L/s..... 146

Figure 5.13: RTD for all four geometries; xanthan gum; 0.05 L/s..... 147

Figure 5.14: Tanks-in-series fit for G1 and G3; H_2O, 0.05 L/s 151

Figure 5.15: PFR-CSTR series model 153

Figure 5.16: PFR-CSTR series model fit to G1; H_2O; 0.05 L/s 154

Figure 5.17: Modified tanks-in-series model 156

Figure 5.18: Modified tanks-in-series model for G3; H_2O; 0.05 L/s 157

Figure 5.19: Comparison of experimental data and models, H_2O at 0.05 L/s 158

Figure 5.20: Comparison of experimental data and models, H_2O at 0.0125 L/s 158

Figure 5.21: Comparison of experimental data and models, xanthan gum at 0.05 L/s .. 159

Figure 6.1: Reactor geometries as modeled in GAMBIT® 2.2; a) G1 centre inlet, b) G2 side inlet, c) G3 concentric baffles, d) G4 radial baffles. 173

Figure 6.2: Computational mesh for G1 with centre inlet 174

Figure 6.3: Computational mesh for G2 with side inlet 174

Figure 6.4: Computational mesh for G3 with concentric baffles 175

Figure 6.5: Computational mesh for G4 with radial baffles 175

Figure 6.6: Velocity profiles for G1 centre inlet 180

Figure 6.7: Velocity profiles for G2 side inlet 181

Figure 6.8: Velocity profiles for G3 concentric baffles 182

Figure 6.9: Velocity profiles for G4 radial baffles. 183

Figure 6.10: Velocity magnitude and pathlines for G1 centre inlet. a) water; b) 3% TS manure 185

Figure 6.11: Velocity magnitude and pathlines for G1 centre inlet. a) xanthan gum; b) 8% TS manure 186

Figure 6.12: Apparent viscosity for G1 centre inlet. a) xanthan gum; b) 8% TS manure 187

Figure 6.13: Residence time distributions for G1 centre inlet, CFD results 188

Figure 6.14: Velocity magnitude and pathlines for G2 centre inlet. a) water; b) 3% TS manure 190

Figure 6.15: Velocity magnitude and pathlines for G2 centre inlet. a) xanthan gum; b) 8% TS manure 190

Figure 6.16: Apparent viscosity for G2. a) xanthan gum; b) 8% TS manure 191

Figure 6.17: Residence time distributions for G2 side inlet, CFD results 192

Figure 6.18: Comparison of RTD for simulated manure cases, G1 vs G2 193

Figure 6.19: Velocity magnitude and pathlines for G3 concentric baffles. a) water; b) 3% TS manure 195

Figure 6.20: Velocity magnitude and pathlines for G3 concentric baffles. a) xanthan gum; b) 8% TS manure 196

Figure 6.21: Apparent viscosity for G3. a) xanthan gum; b) 8% TS manure 197

Figure 6.22: Residence time distributions for G3 concentric baffles, CFD results 198

Figure 6.23: Velocity magnitude and pathlines for G4 radial baffles. a) water; b) 3% TS manure 199

Figure 6.24: Velocity magnitude and pathlines for G4 radial baffles. a) xanthan gum; b) 8% TS manure 199

Figure 6.25: Apparent viscosity for G4. a) xanthan gum; b) 8% TS manure 200

Figure 6.26: Residence time distributions for G4 radial baffles, CFD results 201

Figure 6.27: RTD comparison, H_2O; 0.05 and 0.0125 L/s 203

Figure 6.28: Velocity magnitude and pathlines for pilot-scale G1. a) water;
b) 8% TS manure 205
Figure 6.29: Velocity magnitude and pathlines for pilot-scale G4. a) water;
b) 8% TS manure 205
Figure 6.30: Apparent viscosity for pilot-scale reactors with 8% TS manure. a) G1; b) G4
..... 206
Figure 6.31: Residence time distributions for pilot-scale simulations..... 207
Figure 6.32: Comparison of variance for G1 and G4, lab-scale vs. pilot-scale..... 209
Figure 6.33: Comparison of dead space for G1 and G4, lab-scale vs. pilot-scale..... 209
Figure 6.34: Setup for PIV experiment..... 212
Figure 6.35: Template used to accurately position the PIV camera 213
Figure 6.36: Calculating the location of the centre of the template square 215
Figure 6.37: Comparison of PIV and CFD results – G1, velocity magnitude and vectors.
a) CFD; b) PIV..... 217
Figure 6.38: Comparison of PIV and CFD results – G1, U velocity. a) CFD; b) PIV ... 218
Figure 6.39: Comparison of PIV and CFD results – G1, W velocity. a) CFD; b) PIV .. 218
Figure 6.40: Comparison of PIV and CFD results – G2, velocity magnitude and vectors.
a) CFD; b) PIV..... 219
Figure 6.41: Comparison of PIV and CFD results – G2, U velocity. a) CFD; b) PIV ... 220
Figure 6.42: Comparison of PIV and CFD results – G2, W velocity. a) CFD; b) PIV .. 220
Figure 6.43: U velocity profiles for G1. a) x = -0.0368 m; b) x = 0.0368 m..... 221
Figure 6.44: U velocity profiles for G2. a) x = -0.0368 m; b) x = 0.0368 m..... 221
Figure 6.45: CFD results for water at 0.05 L/s (experimental results inset)..... 224

Figure 6.46: CFD results for water at 0.0125 L/s (experimental results inset)..... 225

Figure 6.47: CFD results for xanthan gum at 0.05 L/s (experimental results inset)..... 225

Figure 6.48: Comparison of mean values, θ_m 226

Figure 6.49: Comparison of variances, σ_θ^2 227

Figure 6.50: Comparison of the location of peak values, θ_{peak} 227

Figure H.1: Simulating mechanical mixing in the fluid column 370

Figure H.2: Simulating bubble mixing with a draft tube in the fluid column 371

List of tables

Table 3.1: Location and depth of samples collected from two manure lagoons 56

Table 3.2: Summary of hog manure samples: approximate depth, total solids content, and density 68

Table 3.3: Particle size distribution by mass, Operation 1 (dimensions in mm) 74

Table 3.4. Particle size distribution by mass, Operation #2 (dimensions in mm) 74

Table 3.5: Comparison of current results to the literature – distribution of particles by percent mass 75

Table 3.6: Empirical coefficients relating viscosity to total solids concentration 76

Table 3.7: Power law parameters for high-TS samples 81

Table 3.8: Rosin-Rammler fit for particle size distribution 87

Table 3.9: Empirical constants for the generalized viscosity model 88

Table 4.1: Fluid column plumbing system components 106

Table 4.2: Positions of storage tank valves V1, V2, and V6 107

Table 4.3: Positions of flow control valves V3, V4, and V5 108

Table 5.1: RTD experimental test matrix 121

Table 5.2: Fluid column volume 133

Table 5.3: Actual hydraulic retention times for each geometry 134

Table 5.4: Inlet and outlet mean velocities 134

Table 5.5: Inlet and outlet Reynolds numbers 135

Table 5.6: Fluorescence response for rhodamine B dye in water and xanthan gum 137

Table 5.7: Empirical power law parameters for xanthan gum, 1.0 g/L 138

Table 5.8: Overall RTD parameters for all experimental cases 148

Table 5.9: One-parameter tanks-in-series model 152

Table 5.10: PFR-CSTR series model – parameters and standard error 155

Table 5.11: Modified tanks-in-series model – parameters and standard error 157

Table 5.12: Estimated volume fraction of dead space 161

Table 6.1: Power law parameters for the viscosity of working fluids 169

Table 6.2: Computational mesh statistics 176

Table 6.3: Inlet boundary conditions 177

Table 6.4: Non-uniform time step 178

Table 6.5: Summary of CFD cases 184

Table 6.6: Overall RTD parameters, G1 centre inlet 189

Table 6.7: Summary of parameters, G2 side inlet 192

Table 6.8: Summary of overall parameters, G3 concentric baffles 198

Table 6.9: Summary of overall parameters, G4 radial baffles 202

Table 6.10: Comparison of overall parameters, H_2O; 0.05 and 0.0125 L/s 203

Table 6.11: Summary of overall parameters for pilot-scale simulations 208

Table 6.12: Input parameters for PIV experiment 214

Table 6.12: Comparison of maximum U velocity for selected profiles, PIV vs. CFD 222

Viscosity of manure samples with TS < 3.6% 249

Consistency coefficient K and flow behaviour index n for Operation 1, TS = 5.09% and 5.51% 250

Power law parameters for high-TS samples 251

List of copyrighted materials for which permission was obtained

Figure 1.3: Installation of complete mix digesters at Glenlea Research Facility (NCLE, 2008) 33

Figure 1.4: Plug flow digester at Haubenschild Dairy Farms in Minnesota (Nelson and Lamb, 2002).....34

Figure 1.5: Cook Feeders covered lagoon digester in Teulon, MB (Bioterre, 2009) 35

Chapter 1. Introduction

There is a rapidly increasing demand worldwide for sustainable development. Governments and industries are facing greater social and environmental pressures, creating new opportunities for innovation, especially in areas such as waste management, clean air and water solutions, and renewable energy technologies. Anaerobic digestion technology offers opportunity for significant development in all three of these areas.

Anaerobic digestion is the process by which biomass—such as livestock manure, municipal sewage, and organic landfill waste—is converted to biogas through microbial activity in an oxygen-deficient environment. Biogas is a combustible gas composed mainly of methane and carbon dioxide, and can be used to produce clean, renewable heat and power through a variety of energy conversion technologies. As pressure mounts to decrease reliance on fossil fuels, energy demands must be met through the increased use of alternative technologies. Since biomass waste is abundant and widely available, anaerobic digestion may play an important part in Canadian development of a diverse renewable energy portfolio. However, the harsh winter conditions which are prevalent across most of the country demand specific attention to the challenges of implementing anaerobic digesters in a cold climate.

Anaerobic digestion may also play a key role in addressing the environmental issues associated with certain agricultural sectors—in specific, large-scale livestock production. The global demand for meat is growing at a rapid pace; in Canada, intensive livestock operations have become the dominant mode of meat production. The enormous volumes

of manure generated by Canadian hog producers are largely stored in outdoor storage lagoons, which create environmental problems such as uncontrolled greenhouse gas emissions, nutrient overloading in water systems, potential leaching of pathogens, and odour. Anaerobic digestion is an excellent method of treatment for agricultural manures, and can be used to effectively mitigate these problems.

The field of anaerobic digestion research is continually advancing, as scientists and engineers strive to understand and improve this technology. The use of three-dimensional numerical modeling techniques, such as computational fluid dynamics (CFD), will be integral to the development and success of anaerobic digestion technology in Canada. Through the use of CFD, large sets of design parameters are incorporated into sophisticated numerical models; the predicted outcomes and trends can be used to design efficient and cost-effective anaerobic digesters that will perform even in harsh Canadian winters. The aim of this thesis is to investigate one specific aspect of anaerobic digester modeling; the effect of Newtonian and non-Newtonian viscous behaviour on the performance of an anaerobic digester used to treat liquid hog manure. This objective is pursued in three stages: firstly, the physical properties of liquid hog manure are experimentally determined; secondly, the effects of viscosity on flow in four lab-scale reactors are explored through an experimental residence time distribution study; thirdly, a three-dimensional CFD model is developed to predict the effect of viscosity on the performance of continuous flow anaerobic digesters.

1.1 The hog industry in Manitoba

Over the past three decades, the Canadian hog industry has experienced a heavy shift towards intensive livestock production. Manitoba, the largest pig-producing and pig-exporting province in the country, also has the largest number of pigs per farm of any province. From 2001 to mid-2007, the average size of Manitoban hog farms increased from 1495 to 2695 pigs per farm (CEC, 2007). Recently, economic conditions such as increased grain feed prices and market uncertainty, as well as pieces of legislation such as Manitoba's hog moratorium and Country of Origin Labeling (COOL), have had a negative impact on hog producers. As of January 1, 2009, the total number of hogs on Canadian farms had fallen 10.2% from a year earlier, while in Manitoba, hog inventory had fallen 4.6% during the same period (Statistics Canada, 2009). However, the hog industry still remains a vital part of Manitoba's economy, generating the largest cash income of any single commodity in the province (Statistics Canada, 2006).

Bill 17, which came into effect in Manitoba on October 9, 2008, establishes a permanent ban on the building of new hog facilities or expansion of existing facilities in regions of the province where hog production is most concentrated (MLA, 2008). However, this bill makes exception for hog operations that treat manure using anaerobic digestion.

1.1.1 Manure management practices

In 2006, hog farms in Manitoba produced an estimated 346 000 tonnes of manure on a dry basis (CEC, 2007). Most large hog operations in the province rely on slurry manure systems to carry manure from the barn to outdoor storage facility (see Figure 1.1).

Manure from the animals drops through slatted floors, and is collected under the barn along with wastewater. A large volume of water is then used to flush the manure out to the storage facility, a multi-cell earthen lagoon system. Manure slurry initially enters the primary cell, where a large fraction of solids settle, creating a sludge layer at the bottom of the lagoon. The supernatant is allowed to overflow into secondary cells, where further solids separation takes place. Due to the large volume of wastewater and flush water added to the manure slurry, it enters the lagoons at a low solids concentration; further dilution occurs from the accumulation of precipitation within the lagoons. Earthen manure lagoons are lined with a layer of compacted clay to minimize seepage. A minimum of 0.3 m freeboard is required between the surface of the lagoon and the top of its banks (CEC, 2007). To avoid potential leaching or runoff, provincial legislation requires that manure storage facilities are located a minimum of 100 m from waterways, sinkholes, wells, springs, and site boundaries. Additionally, these facilities must be located 0.6 m above the 100 year floodplain level. The regulations for manure storage in Manitoba are generally more stringent than those found in the United States.

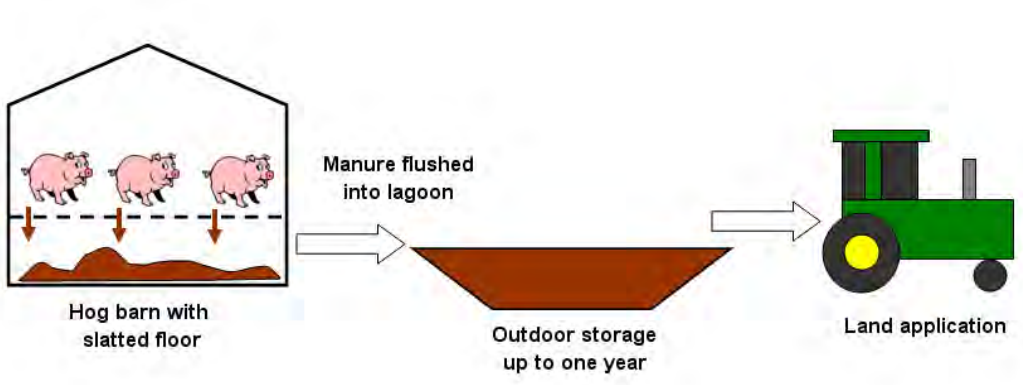

Figure 1.1: Typical swine manure management practice

Annually, the stored manure is agitated, pumped out of the lagoons, and spread onto nearby cropland. Land application most often takes place in the fall, after the crops have been removed from the fields. Pig manure is an excellent source of nutrients for plants; however, it is also very dilute, making transport expensive. In 2006, 73% of hog producers applied manure to their own land (CEC, 2007). Manure is applied to approximately 120 000 ha of land annually, which accounts for only 2.5% of Manitoba's agricultural land base; the majority of this land is located in the south-eastern region of the province. The total value of nitrogen and phosphorus nutrients contained in pig manure is estimated at $30 to $40 million; however, pig farmers that supply manure to crop producers rarely receive compensation.

1.1.2 Environmental issues surrounding livestock waste management

While hog manure may be an excellent source of nutrients, mismanagement of these nutrients can have serious environmental consequences. Hog manure has a relatively low ratio of nitrogen to phosphorus; meaning, manure that is applied to land to meet the nitrogen demand of a certain crop will provide an excess amount of phosphorus. If manure was applied in proportion to the amount of phosphorus required, 500 000 to 700 000 ha of cropland would be required for spreading, compared to the current 120 000 ha (CEC, 2007). Nutrients that are not absorbed by plants may enter water systems, causing serious problems. The main risk for nitrates is leaching to groundwater, whereas phosphorus is more likely to runoff to surface water. Nutrient overloading in lakes and rivers causes eutrophication, altering the overall ecosystem structure and biodiversity of the body of water. Nutrient runoff from intensive agriculture has contributed to the

eutrophication of Lake Winnipeg, the tenth largest freshwater lake in the world, resulting in frequent occurrences of large algal blooms (Cicek et al. 2006).

Another area of growing concern is the risk of water contamination from pathogens and antibiotics found in hog manure. Ninety percent of all food and waterborne illnesses are caused by enteric pathogens such as *E. coli*, *Salmonella*, *Giardia*, and *Cryptosporidium*, which reside in the gut of animals (CEC, 2007). Though these pathogens die slowly in stored manure, the perpetual addition of fresh manure to manure storage lagoons virtually ensures their continued presence; thus, manure that is applied to cropland is very likely to be contaminated with pathogens. While regulations in the United States and Canada require the treatment of municipal sewage waste to kill pathogens, no such regulations apply to animal manure. Recommended best practices for manure management in Manitoba reduce pathogen counts, but do not eliminate their presence.

A third issue of environmental and social concern related to hog manure is that of odour. Anaerobic decomposition of manure in storage lagoons results in the emission of numerous odourous compounds. Strong odours are also released during land application of manure, though direct injection into the soil considerably decreases these odours. Though communities downwind of hog farms may not experience toxic levels of odourous gases, residents may still experience discomfort from the odour, or even indirectly related health problems. Current air quality regulations in Canada focus mainly on industrial pollutants; very little attention is given to odour-related issues. Though separation distances are required in Manitoba between hog operations and populated

areas, these do not take into account factors such as wind direction that affect odour dispersion (CEC, 2007). Some municipalities in the province require straw or synthetic coverings on lagoons to reduce odour emission.

Finally, livestock manure management is a significant contributor to greenhouse gas emissions. In 2006, Canada's agricultural sector produced the equivalent of 69 Mt (megatonnes) of CO_2, an increase of 12 Mt or 21% from 1990 levels (Environment Canada, 2008). 80% of the increase in agricultural emissions is associated with livestock production. Livestock production accounts for 42.2 Mt CO_2, of these emissions, approximately 35% comes from manure management and land application. The decay of manure within outdoor storage lagoons results in uncontrolled releases of methane (CH_4) and carbon dioxide (CO_2) into the atmosphere. Methane has a heat-trapping potential 21 times greater than carbon dioxide (IPCC, 2001). Hamilton et al. (2006) simulated an anaerobic lagoon under typical mid-to-late summer conditions in Oklahoma, and found that the rate of release of CH_4 varied between 200 and 300 kg/ha·da (kilograms per hectare per day), while the rates for CO_2 varied between 380 and 580 kg/ha·da. Based on these rates, a typical three-cell manure storage system, each cell occupying a 60 x 60 m area, would emit between 4.95 and 7.43 tonnes CO_2 equivalent per day in mid-summer.

1.1.3 Manure treatment through anaerobic digestion

Anaerobic digestion is an effective treatment method that can be used to mitigate the current problems associated with hog manure. According to Wilkie (1998), digested effluent shows a 97% reduction in odour from raw manure; in contrast, manure stored for three days was 77% more odourous than raw manure. Anaerobic digestion in the

mesophilic range (35°C to 40°C) can also reduce pathogens by 95% (Lusk, 1998). The issue of nutrients is more complex, however. Anaerobic digestion causes the breakdown of nutrient-rich organic materials, converting organic nitrogen and phosphorus into inorganic forms (CEC, 2007). The inorganic nutrients are released into the liquid effluent, and are absorbed by plants more rapidly and predictably. However, nitrogen, which is converted to ammonia during anaerobic digestion, is more susceptible to volatization, increasing the risk of air pollution. The best way to address this problem is through direct injection of digested manure into the soil. Also, though nutrients are converted to more soluble forms, the ratio of N to P remains the same, so the problem of excess phosphorus still exists even after digestion. Implementing nutrient separation and concentration after digestion is one method of addressing this problem, though this would add to the cost of treatment (MacLeod, 2004).

Perhaps the most obvious benefit of anaerobic digestion is reduction in the emission of greenhouse gases. This benefit is actually two-fold: first, the uncontrolled release of methane gas is prevented; second, biogas can be used to displace fossil fuel for heat and power generation. The biogas may be burned directly in a boiler to provide process or space heat, or it may be used to fuel a reciprocating engine to produce electric power. A third option is combined heat and power (CHP), which produces electricity and recovers the waste heat to satisfy local heating demand. An excellent example is the Highmark Renewables biorefinery near Vegreville, AB, where a biogas-fired CHP system supplies heat and power to an ethanol refinery. Thus, anaerobic digestion is one of many

renewable energy conversion technologies that may contribute to independence from fossil fuels.

1.2 Renewable energy from biomass

Nearly all of the world's industrialized nations rely heavily on fossil fuels such as coal, petroleum, and natural gas to meet their energy and transportation needs. In 2000, fossil fuels supplied 9122 PJ, or 77% of Canada's total energy demand (NRCan, 2006). Fossil fuels are concentrated sources of carbon and hydrocarbons formed by hundreds of millions of years of intense heat and pressure within the earth's crust. They are energy-rich, easy to transport, and have been widely used since the industrial revolution. However, the use of fossil fuels is by far the largest source of anthropogenic greenhouse gas emissions, and thus one of the most significant driving forces behind climate change (IPCC, 2007). Fossil fuels are also a non-renewable resource; reserves that have been produced by nature over millions of years are depleted within a decade or two. Since 1984, global oil production has exceeded discoveries (Hughes, 2006). Studies published between 2004 and 2006 predict that world oil production will peak sometime between 2005 and 2040, with consensus at 2014. The global depletion of fossil fuels is evident in the rising price of petroleum and natural gas, though the economic downturn of late 2008 has temporarily suppressed these prices.

Many European nations have implemented aggressive policies in regards to greenhouse gas emissions and consumption of fossil fuels. Sweden, for example, aims to replace 50% of its energy demand with renewable sources, while eliminating fossil fuels from its transportation sector by 2030 and bringing its net greenhouse gas emissions to zero by

2050 (MoEEC and MoE. 2009). These ambitions policies have facilitated the rapid development of renewable energy technologies in Europe. Biomass energy technologies such as anaerobic digestion have been the focus of much development due to their reliability; whereas wind and solar energy are intermittent sources that rely on fluctuating weather conditions, energy from biomass can be produced to meet demand.

North America, on the other hand, has lagged behind Western Europe in the development of renewable technologies. However, resource-rich nations like Canada and the United States are geographically ideal for the development of renewables due to the vastness of their natural resources. Canada currently produces 1.45×10^8 tonnes of residual biomass per year in such forms as agricultural crop residues, livestock manure and bedding, municipal sewage waste, wood waste and forestry residues, and industrial organic waste (Levin et al. 2007). This amount of biomass translates to approximately 2.28×10^9 GJ of energy, or approximately 22% of Canada's current energy demand. Livestock manure accounts for approximately 1.61×10^7 t (dry basis) or 2.54×10^8 GJ of potential energy. Canada currently exploits only 6% of its biomass resources for energy production (NRCan, 2007).

Biomass energy has several advantages. First, using biomass waste as a source of energy reduces waste disposal costs and diverts material from landfills. Biomass waste is a renewable resource that is produced in abundance by industries such as forestry and agriculture. Furthermore, energy from biomass is carbon neutral, since the carbon dioxide released during combustion would normally be released through natural decomposition.

In fact, in circumstances where the biomass decomposes in anaerobic environments, using it for energy actually decreases emissions by producing carbon dioxide instead of methane. Finally, unlike intermittent energy sources such as wind or solar, biomass is a reliable energy source that can produce heat or power on demand. However, most biomass resources—agricultural crop residue or livestock manure, for example—are distributed across large regions, in contrast to fossil fuels, which are found in concentrated deposits. As well, biomass resources have relatively low energy densities in comparison to fossil fuels. For these reasons, large, centralized generating stations dedicated to producing power from biomass often require significant subsidization to be feasible. The economics become more favourable when biomass can be used for distributed energy generation, especially when CHP generation is implemented, and the heat is used locally.

1.3 Anaerobic digestion

Anaerobic digestion is not a new technology, though it has been the subject of renewed interest in recent decades. The first AD plant was built in Bombay, India in 1859; AD was later introduced to England in 1895 to treat sewage and provide fuel for streetlamps (Lusk, 1998). An estimated 6 to 8 million small, low-tech digesters are currently in use around the globe, providing fuel for cooking and lighting. AD technology has been expanding in China and India, while it has become well-established in several European countries. Denmark is a leader in large-scale anaerobic digestion; there are currently 20 large joint biogas plants that process a total of 1.1 million tonnes of animal manure and 400 000 tonnes of industrial waste annually (DEA, 2003). All of these biogas plants were

built with 20% to 40% subsidization. As well, over 60 small, farm-based biogas plants operate in Denmark.

1.3.1 Mechanisms involved in anaerobic digestion

Anaerobic digestion is a microbial process that converts organic material into simpler, inorganic compounds through the action of anaerobic bacteria. A complex consortia of bacteria are involved in this process, including hydrolytic bacteria, acidogens, acetogens, and methanogens. Though a complete mapping of the microbial pathways involved in AD would produce a very complicated diagram, the basic process can be described in a simplified fashion in Figure 1.2.

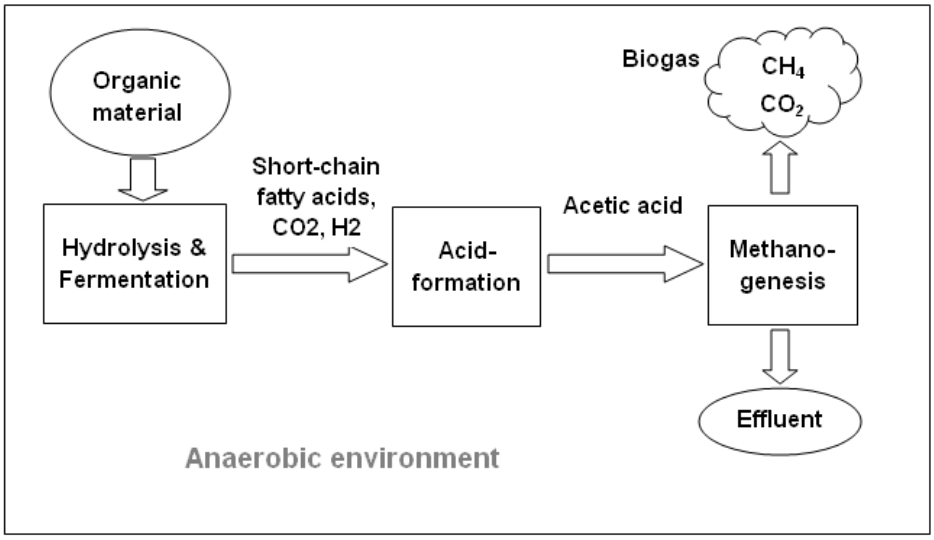

Figure 1.2: Microbial process of anaerobic digestion

The action of the anaerobic bacteria is dependent on several environmental factors, such as temperature, pH, and chemical composition of the liquor. The physical mechanisms that determine the performance of an anaerobic digester are (Fleming, 2002):

- Advection

- Settling of suspended solids
- Mixing
- Bubbling
- Heat loss through boundaries
- Internal heat transfer

The interaction of all of these mechanisms within an anaerobic digester produces a complex system.

1.3.2 Products of anaerobic digestion

The end-products of anaerobic digestion are biogas and digestate, which consists of a liquid fraction and a fibrous solid fraction. The liquid fraction of digestate contains nutrients in soluble form; it is nearly odourless, and may be used as a high-quality fertilizer. The biogas is composed of methane and carbon dioxide, with traces of hydrogen sulfide, ammonia, and water vapour; typically, methane content is approximately 60% by volume, though this varies depending on process parameters. With a methane content of 60%, the lower heating value of biogas is 19.7 MJ/m^3 at 298 K and 101.3 kPa. Traces of hydrogen sulfide in the biogas greatly increase the potential for corrosion issues.

1.3.3 Types of anaerobic digesters

Though numerous reactor designs are used for anaerobic digestion, only three types are common in farm-based AD—complete mix, plug flow, and covered lagoon digesters.

Complete mix digesters typically use cylindrical stainless steel or concrete tanks that are mechanically agitated. Mechanical impellers, bubble mixing, or external recirculation loops may be used to agitate the manure, though the former is most common. Manure is typically limited to less than 10% TS (total solids). Mesophilic or thermophilic temperatures may be used, and retention times of 10 to 20 days are common. Complete mix digesters are the most complex AD systems used in farm applications; capital investments and operation and maintenance costs are typically high. A pilot AD system installed at the University of Manitoba's Glenlea Research facility, shown in Figure 1.3, uses complete mix digester tanks (NCLE, 2008). Complete mix systems are also common in the large biogas plants found in Denmark and other European countries.

Figure 1.3: Installation of complete mix digesters at Glenlea Research Facility (NCLE, 2008)

A common plug flow digester design consists of a long, below-ground, cement channel with a flexible cover that traps the biogas. Variations on this design include horseshoe-shaped channels and above-ground stainless steel tubes. Fresh manure is introduced at

one end of the digester, and digested manure (digestate) is removed at the other end. No forced mixing is used inside the digester; however, plug flow systems typically include a mixing tank, where the manure is pre-mixed, heated, and diluted to the proper concentration (10% to 15% TS). Plug flow digesters are most often operated in the mesophilic regime, with retention times of 20 to 30 days. A plug flow digester is generally less expensive and complex than a complete mix digester with similar capacity. The most successful applications of plug flow digesters in North America have been on dairy farms, such as the Haubenschild Farms project shown in Figure 1.4, near Princeton, Minnesota (Nelson and Lamb, 2002).

Figure 1.4: Plug flow digester at Haubenschild Dairy Farms in Minnesota (Nelson and Lamb, 2002)

Covered anaerobic lagoon digesters are the simplest and least costly farm-based anaerobic digesters, especially if an existing manure storage lagoon is used. A flexible cover floating on top of the lagoon traps the biogas that is produced; often a black cover is used to absorb solar radiation and heat the digester. In cooler climates, heating coils are required to maintain the lagoon at the proper temperature. Covered lagoon digesters are operated in either the mesophilic or psychrophilic (less than 25°C) temperature regimes. These systems are most often implemented at hog operations that use slurry-based flush

systems, due to the low solids content of the manure (normally less than 2%). Year-round operation of covered lagoon digesters becomes uneconomical in colder climates, due to compensation for heat losses in the winter months. The Cook Feeders hog farm near Teulon, MB (see Figure 1.5) uses novel psychrophilic digestion technology developed by Bio-Terre Systems Inc. in a covered lagoon digester (Bio-Terre, 2009).

Figure 1.5: Cook Feeders covered lagoon digester near Teulon, MB (Bioterre, 2009)

1.3.4 Biogas production and CHP systems

The anaerobic digester is central to any biogas energy generation system; an example of such a system is shown in Figure 1.6. The most effective method of harnessing the energy from biogas is combined heat and power (CHP), which burns the biogas to produce electricity, and recovers the waste heat for local use. There are several methods of energy generation available: these include external combustion cycles such as steam Rankine cycles, organic Rankine cycles, or Stirling engines; a Brayton cycle using a gas turbine or microturbine; and internal combustion engines (ICE's). Connecting an ICE to an electric generator is the most common method of biogas energy generation, since it is relatively cheap and easy to maintain. The heat recovered from the ICE can be used for a

number of purposes, such as on-farm process heat or space heating, or in the district heating system of a local community. CHP systems operate at maximum thermal efficiency when the heat load is well-matched to the electric load. Thus, a consistent process heat load is preferred to a seasonally-variable space heating load.

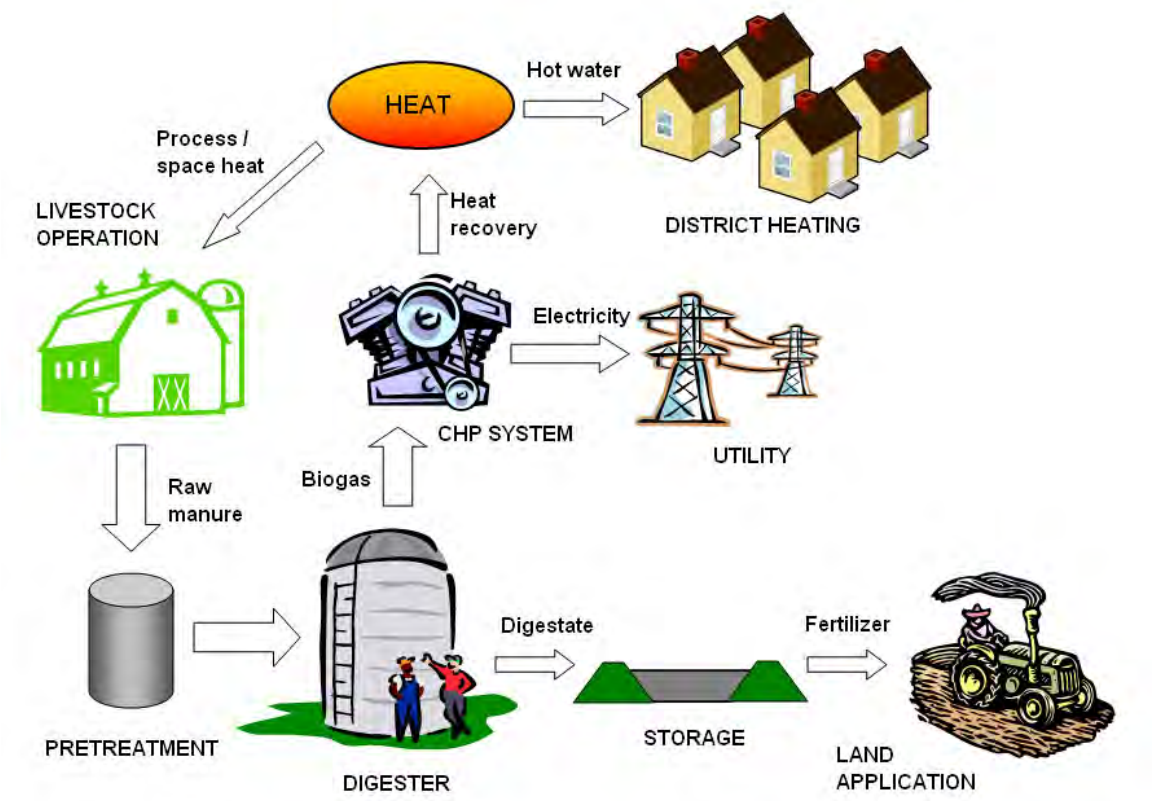

Figure 1.6: Diagram of a farm-based biogas CHP system

Depending on the type of livestock operation and the specific digester requirements, a pretreatment step may be required. Here, manure is either diluted or dewatered to meet the target solids concentration, then mixed and heated to the working temperature of the digester. After digestion, the digested manure is collected in a storage facility until it is applied to cropland. Optional post-digestion steps are solid-liquid separation of the digestate, and precipitation of solubles.

1.3.5 Anaerobic digestion in cold climates

Climate has a major impact on the economic feasibility of anaerobic digestion. Most digesters operate in either the mesophilic (35°C to 40°C) or thermophilic (52°C to 57°C) temperature regimes. In countries with warm climates year round, sustaining these temperatures is not difficult. However, lower ambient temperatures lead to higher heating requirements, so that the net energy output of the digester decreases significantly as the temperature drops. Thus, the harsh Manitoban winter poses a major obstacle for the development of AD technology in the province. Sophisticated modeling techniques such as computational fluid dynamics (CFD) can play a key role in adapting this technology to be effective in cold-climates.

1.3.6 Modeling of anaerobic digesters

As described in Section 1.3.1, there are numerous physical, chemical, and microbial mechanisms involved in anaerobic digestion, and the interaction of these mechanisms creates a complex system. The behaviour of such a system cannot be predicted using simple calculations. Experimental data often provides the best understanding of these systems, yet such experiments are expensive, especially in large scales. Experimental data is typically also limited to overall parameters, since localized instrumentation is difficult to implement. However, numerical experiments can be performed at a fraction of the cost of the physical experiment through the use of sophisticated modeling techniques such as CFD. Using CFD, the complex mechanisms of anaerobic digestion can be modeled, and detailed investigations can be performed on the impact of various

parameters such as weather, geometry, mixing rate, and manure characteristics. Thus, CFD is an indispensable tool for the development of AD technology in cold climates.

1.4 Thesis overview

This thesis examines how the non-Newtonian characteristics of liquid hog manure affect the flow conditions within a steady-flow anaerobic digester. All manure slurries exhibit non-Newtonian viscous behaviour, with the exception of very dilute manure. The non-Newtonian characteristics of manure significantly influence how the manure flows within a digester. Thus, an AD reactor geometry that is designed for a Newtonian fluid (such as water) may perform poorly when a non-Newtonian fluid is introduced. The first part of this thesis experimentally determines the non-Newtonian characteristics of liquid hog manure sampled from an outdoor storage lagoon, and the variation of these characteristics with temperature and solids concentration. The second part of this thesis investigates the flow of Newtonian and non-Newtonian fluids within four lab-scale reactor geometries, using residence time distribution (RTD) experiments. Finally, the properties of liquid hog manure are incorporated into 3D numerical models that recreate the RTD experiments, and the experimental and numerical results are compared. The results produced during these studies are intended for use within a complete CFD anaerobic digester model.

1.4.1 Physical properties of liquid hog manure

The experimental investigation of the physical properties of hog manure is found in Chapter 3. Hog manure sampled from an outdoor storage lagoon at different depths and locations is used in these experiments, and represents a variety of solids concentrations. Density, total solids, particle size distribution, and viscosity are measured as received. Correlations are developed for density, particle size distribution, and viscosity as a function of total solids. A specific problem with digesting hog manure from large operations is the large amount of water added to the manure, and thus, the low solids concentration. Settling is a method of increasing solids concentration before digesting, so settled manure from a lagoon is used instead of freshly scraped manure diluted to target concentrations.

1.4.2 Residence time distribution experiments

Residence time distribution (RTD) is an overall parameter that may be used to assess certain aspects of reactor performance; it can be measured using relatively simple experimental techniques. Chapter 4 describes the design of the experimental fluid column facility that simulates flow conditions in an anaerobic digester. Chapter 5 describes the RTD tests and compares the data obtained for different geometries, flow rates, and fluids. Newtonian and non-Newtonian flows are compared using water and a 1 g/L xanthan gum solution as the working fluids. Four AD reactor geometries are studied; two out of four geometries use baffles to direct flow within the reactor. The study is limited to continuous-flow conditions with no mechanical agitation.

1.4.3 CFD simulations

Chapter 6 explores the use of CFD to simulate the flow conditions in an anaerobic digester. First, the lab-scale experiments described in Chapter 5 are recreated as 3D numerical simulations; the results of these simulations are compared with the experimental data. The properties of liquid hog manure at two solids concentrations—as described in Chapter 3—are then incorporated to simulate manure flowing through a digester. Finally, the models are scaled up to represent 2000 L pilot AD reactors with a retention time of 17 days. The results of these simulations are compared with the lab-scale simulations to determine the effect of size and flow rate on reactor performance.

1.4.4 Contribution to research

The aim of this thesis is to advance knowledge in the field of anaerobic digestion by focusing on the specific problem of non-Newtonian flow within the AD reactor. The physical properties of naturally settled hog manure have not been studied before in the literature; this is a novel contribution to the field of AD research, and to agricultural science in general. RTD is a critical but often neglected aspect in the design of an anaerobic digester; the experimental work described here demonstrates that RTD, which is significantly impacted by non-Newtonian characteristics, must be considered to maximize the effectiveness of AD technology. This thesis also demonstrates the use of CFD techniques to study the impact of process parameters on the overall performance of an AD reactor. This is an important contribution to the development of a fully integrated 3D model of anaerobic digestion.

Chapter 2. Literature review

2.1 Introduction

In recent decades, a significant amount of research has been performed in the field of anaerobic digestion. Anaerobic digestion is a multistage process that involves a complex system of biochemical and microbial pathways. Several researchers have developed integrated mathematical models that link heat transfer mechanisms to the reaction kinetics. Most of these models are zero-dimensional (assuming complete mix) or one-dimensional (assuming plug flow). Much effort has also been directed to the study of digester designs apart from the traditional designs (ie. complete mix, covered lagoon, and plug flow); these include the upflow sludge anaerobic blanket reactor (USABR or USAB), the expanded granular sludge bed reactor (EGSB), the anaerobic sequential batch reactor (ASBR), the anaerobic baffled reactor (ABR), and the periodic anaerobic baffled reactor (PABR).

Typical feed materials for anaerobic digesters—such as animal manure, wastewater, and slurries from food processing plants—often possess unique properties, especially in terms of rheological behaviour. Most of these liquids are non-Newtonian to some degree. Several researchers have studied the non-Newtonian characteristics of these fluids; the most research in this area has been conducted on dairy and beef cattle manure. Also, some studies have been performed that examine the flow characteristics of non-Newtonian fluids in reactor tanks. However, at this point, no studies exist that link non-

Newtonian flow mechanisms to heat transfer and reaction kinetics in a three-dimensional model.

2.2 Anaerobic digestion – heat transfer and biogas production

O'Neil (1985) reviewed the existing literature on anaerobic digestion, with a focus on the flow characteristics of anaerobic digesters. He found that the rheology of biomass slurries changes with the degree of digestion; as the slurries are digested, they become more Newtonian in character. Complex non-Newtonian flow can increase the severity of non-ideal flow conditions. Incomplete mixing in a complete mix digester can lead to short-circuiting; in a plug flow digester, settling of solids at the bottom of the digester leads to non-uniform flow, creating a stagnant zone at the bottom of the digester. O'Neil compared the reaction kinetics of ideal and non-ideal plug flow digesters, and found that an ideal complete mix reactor is superior to an ideal plug flow reactor at conversion fractions under 85%; that is, a complete mix digester will require less time to reach the target percent conversion, unless a very high percent conversion is required. However, in non-ideal flow situations, plug flow digesters will often out-perform complete mix digesters, due to the effect of short-circuiting in the latter. O'Neil concluded that there was a significant lack of knowledge on the rheology of biomass slurries, and the effect of complex rheology on digester flow and performance.

Chen and Shyu (1996) studied the performance of four types of anaerobic reactors with very dilute dairy manure: a complete mix reactor, an upflow anaerobic sludge blanket reactor (UASB), an upflow anaerobic filter reactor (UAF), and a baffled reactor. Several

hydraulic retention times and organic loading rates were tested. The effluent suspended solids and chemical oxygen demand (COD) were tested and compared for all cases studied.

Dugba et al. (1999) simulated two-stage digestion using two anaerobic sequential batch reactors (ASBR). The first ASBR was simulated using thermophilic conditions, while the second was simulated using mesophilic conditions. Zhang et al. (2000) experimentally evaluated two-stage digestion of dairy and swine manure using ASBRs, comparing a thermophilic-mesophilic system to a system with two mesophilic reactors.

Axapoulos et al. (2001) investigated the heat transfer and biogas production of a solar-heated plug flow anaerobic digester in Greece. A mathematical heat transfer and kinetic model was used to predict the thermal behaviour and methane production of the digester; these predictions compared well with the measured experimental data.

Fleming (2002) developed a novel simulation of an anaerobic covered lagoon digester. This model integrated the physical, chemical, and biological mechanisms that are active in a lagoon digester: advection, heat transfer, settling, bubbling, chemical reactions and microbial pathways, and biogas formation. The model was validated using performance data from full-scale covered lagoon digesters in North Carolina.

Zupancic and Ros (2003) compared the heat requirements and biogas production of mesophilic and thermophilic complete mix anaerobic digesters for waste water treatment.

Retention times of 1 to 10 days were studied. Thermophilic digesters exhibited more rapid biogas production than mesophilic digesters, but required approximately twice as much heat. Most of the heat required was used to heat the influent; very little heat was required to make up for heat lost from the digester. Using heat regeneration from the effluent to preheat the influent significantly decreased the heat requirements of the digesters.

Karim et al. (2005) studied the effect of recirculated biogas mixing at various rates on biogas production within a lab-scale digester. They found that rate of mixing had very little effect on the biogas production; however, air leaks in the recirculation system and the small size of the digester may have significantly affected these results.

Gebremedhin et al. (2005) constructed a comprehensive mathematical model from fundamental equations to predict the energy requirements for a plug flow digester. Gebremedhin and Inglis (2007) combined this model with a biogas production model to determine the usable energy produced by a digester. The model was validated using one year of test data from a digester in New York State.

Wen and Chen (2006) studied a system of sequential, complete mix anaerobic digesters in series. The biogas produced from dairy manure was measured; biogas production was found to be highest in the first tank and lower in each subsequent tank. Wen and Chen attempted to create a two-stage digester system, with acidogenesis in the first tank and

methanogenesis in the second tank; however, this attempt failed due to high alkalinity in the influent manure.

Pontes and Pinto (2006) integrated mathematical kinetics and flow models to simulate three types of anaerobic digesters: a batch digester; an upflow anaerobic sludge blanket (USAB) digester; and an expanded granular sludge bed (EGSB) digester.

2.3 Non-Newtonian flow in anaerobic digesters

The chapters to follow investigate the non-Newtonian properties of hog manure, and the characteristics of non-Newtonian flow within simulated anaerobic digester tanks. Chapters 3, 5, and 6 each contain a review of the literature that pertains to that chapter. In Chapter 3, the literature on the rheology and physical properties of livestock manures is reviewed; Chapter 5 contains a literature review of experimental investigations into the residence time distribution of various reactors; and Chapter 6 includes a review of the literature that pertains to the three-dimensional modeling of anaerobic digesters and similar reactors. To avoid duplication, literature pertaining directly to these topics is not discussed here.

Chapter 3. Experimental determination of the physical properties of hog manure

3.1 Introduction

3.1.1 Overview of the study

The objective of this study is to experimentally determine the physical properties of liquid hog manure and develop mathematical models to describe these properties as functions of the total solids content. Specifically, bulk density, particle size distribution, and rheology were investigated. The literature contains several studies on the physical properties of hog manure; however, most studies focus on manure scraped from the barn floor and diluted to target concentrations. In the current study, manure was extracted from various depths and locations within two outdoor storage lagoons; the samples collected varied between 0.67% and 37.1% total solids concentration by mass. Bulk density and particle size distribution were empirically determined at room temperature for all samples. Particle size distribution was determined using both microscopic imaging and sieve tests; particles detected ranged between 1 μm to several mm. The Rosin-Rammler distribution provides a good fit for the distribution of particle diameters. The rheology of the manure was investigated for samples between 0.67% to 13.1% total solids at temperatures of 15°C, 25°C, 40°C, and 60°C and shear rates ranging from 0.0066 s^{-1} to 44 s^{-1}. Surface samples with total solids concentrations under 3.6% exhibit Newtonian behaviour; however, bottom sludge samples with over 6.5% TS show both non-Newtonian and time-dependent characteristics. Two intermediate samples behave as

pseudoplastic fluids, and could be described using the power law. In general, apparent viscosity increases exponentially with total solids concentration, but decreases with temperature according to the Arrhenius equation.

3.1.2 Naturally settled hog manure

The physical properties of manure determined by this study will be used to represent the properties of manure within an anaerobic digester. However, obtaining manure that accurately represents that found within a digester is not straight-forward, for several reasons. First of all, several different manure handling and pre-treatment processes may occur before digestion; these processes vary depending on such factors as the type of digester used. For example, a covered lagoon digester accepts manure with 1% to 2% TS, yet a plug-flow digester performs best with manure between 10% and 15% TS. A complete mix digester will work with low-solids manure, but biogas production is much better in the range of 5% to 10% TS. Manure properties also vary depending on the diet of the animals, and these properties change even during the digestion process. Thus, it is difficult to predict the exact properties of manure that should be used in an anaerobic digester model.

In this study, naturally settled manure was collected from an outdoor storage lagoon, rather than scraped from the barn floor. There are several reasons for choosing this method. First, manure stored in a lagoon most accurately reflects the dominant mode of manure handling for large hog operations, where the manure is mixed with large volumes of water and flushed from the barn. Second, covered lagoon digesters are often used for

hog operations; thus, settling that occurs within a covered lagoon digester would be similar to settling within a conventional storage lagoon. Finally, if a plug flow or complete mix digester were to be installed at a hog barn with a flush manure system, concentrating the solids would give better digester performance, and allow for a smaller digester. The simplest method of solids concentration is through the use of a settling chamber; in this case, the concentrated manure would be similar to naturally settled manure within a conventional storage lagoon.

3.1.3 Viscosity models – Newtonian and non-Newtonian fluids

Viscosity is the material property that determines how a fluid behaves under shearing. Fluids that exhibit a linear relationship between shear rate and shear stress are classified as Newtonian, and can be described by the Newtonian constitutive equation:

$$\tau = -\mu\dot{\gamma} \tag{3.1}$$

where τ is shear stress, μ is the dynamic viscosity of the fluid, and $\dot{\gamma}$ is the rate of shear (*du* / *dy*). Non-Newtonian fluids are any fluids whose response to shearing cannot be described by Equation 3.1. The generalized Newtonian fluid (GNF) model may be used to describe many non-Newtonian fluids (Morrison 2001):

$$\tau = -\eta(\dot{\gamma})\dot{\gamma} \tag{3.2}$$

where $\eta(\dot{\gamma})$ is the apparent viscosity, and is a function of shear rate. The GNF model can describe fluids that do not exhibit a linear proportionality between shear rate and shear stress, such as shear-thinning, shear-thickening, and yield stress fluids. The power law model is one of the most commonly used GNF models, since it adequately describes

many pseudoplastic (shear-thinning) and dilatant (shear-thickening) fluids using only two parameters:

$$\eta(\dot{\gamma}) = K\dot{\gamma}^{n-1} \tag{3.3}$$

Thus, the relationship between τ and $\dot{\gamma}$ is:

$$\tau = -K\dot{\gamma}^{n} \tag{3.4}$$

where *K* is the consistency coefficient and *n* is the flow behaviour index. Using S.I. units, the consistency coefficient *K* has units of Pa·s^n, while flow behaviour index *n* is dimensionless. These parameters can be determined empirically by plotting shear stress vs. shear rate on a logarithmic plot (see Figure 3.1). Note that for Newtonian flow, *n* = 1.

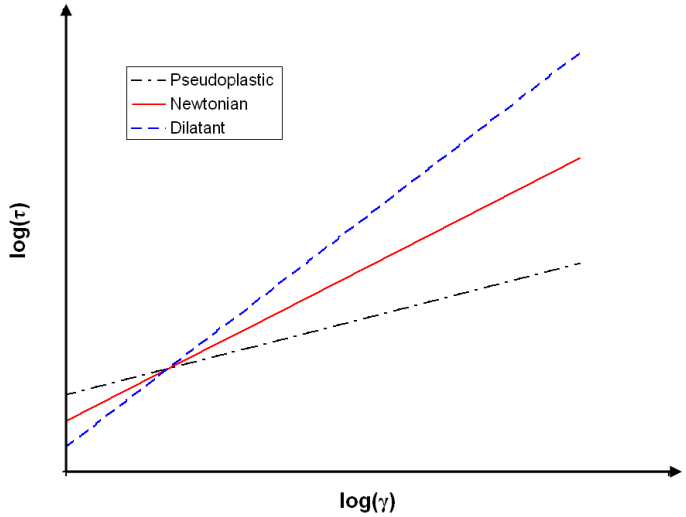

Figure 3.1: The power law model

Two other GNF models are the Carreau-Yasuda model and the Bingham Plastic model. The Carreau-Yasuda model uses five parameters to describe a fluid whose apparent viscosity approaches limits at high and low shear rates. The Bingham Plastic model can be used to describe fluids that exhibit yield stress. Non-Newtonian fluids may also exhibit memory effects, such as thixotropy—decreasing viscosity with time—and rheopexy—

increasing viscosity with time. Viscoelasticity is a memory effect whereby the fluid exhibits a combination of viscous and elastic behaviour. Thixotropic, rheopectic, and viscoelastic fluids cannot be described by the GNF model.

3.2 Literature review

The rheology and physical properties of animal manures has been the topic of several studies in the literature. Most of these studies have been aimed towards the design of pumps and manure spreaders, though some authors have mentioned anaerobic digestion as a motivation for studying manure properties. The most thorough research in this field has been performed on dairy and beef cattle manure (Kumar et al. 1972, Chen 1986, Achkari-Begdouri and Goodrich 1992, El-mashad et al. 2005). While hog manure has also been studied in the literature, the data is much less comprehensive and cohesive with regards to the ranges of temperature and total solids concentration. Also, most of the studies have used manure scraped from a barn floor and diluted to target concentrations; the physical properties of naturally settled hog manure in an outdoor storage lagoon have not previously been described in the literature.

Albert Einstein set the stage for studying the viscosity of suspensions in his doctoral dissertation (Einstein, 1905). Using hydrodynamic theory, Einstein found that the Newtonian viscosity of a dilute suspension of very small solid spheres could be related to the volume fraction occupied by the spheres using the following:

$$\mu^* = \frac{\mu_{susp}}{\mu_l} = 1 + 2.5\phi \tag{3.7}$$

where μ^* is the relative viscosity of the suspension with respect to the liquid phase; μ_{susp} is the viscosity of the suspension; μ_l is the viscosity of the liquid solvent phase; and φ is the volume fraction of solid particles. While most notable for its contribution to the field of molecular theory and the prediction of Avagadro's number, Einstein's thesis also sets a theoretical basis for the study of the viscosity of suspensions.

Kumar et al. (1972) used a custom-designed constant torque viscometer to study the effect of temperature, dilution, and sawdust content on the viscosity of dairy cattle manure. The manure was sampled directly as excreted, from a manure gutter, and from a liquid manure storage tank. They found that below 5.15% TS, Newtonian behaviour was observed, while above 5.15% TS, the flow was non-Newtonian. Fit to the power law, n varied between 0.26 and 0.54 for TS > 5.15%. Particle size distribution was also studied.

Hashimoto and Chen (1976) studied the rheology of fresh and aerated poultry, swine, and dairy cattle slurries. Using the power law, they developed correlations for K and n based on the volume fraction of solids:

$$K = b_1 \phi_L^{\,b_2} \tag{3.8}$$

$$n = b_3 + b_4 \ln \phi_L \tag{3.9}$$

where φ_L is the volume fraction of solids; and b_1, b_2, b_3, and b_4 are empirical constants.

Barker and Driggers (1981) performed viscosity experiments on dilute swine manure for the purpose of designing an alternative flushing system. Under 3% TS, they proposed the following relation for Newtonian viscosity:

$$\mu = 3.084(1.626)^{TS} \tag{3.10}$$

where μ is the Newtonian viscosity, and *TS* is the % concentration of total solids, by mass.

Chen (1986) investigated the rheology of sieved beef cattle manure slurries, scraped from concrete floors. The slurries were diluted to target concentrations between 2.6% and 19.6% TS; temperatures between 14°C and 64°C and shear rates ranging from 0.1 to 200 s^{-1} were used. It was observed that the power law was acceptable for TS < 2.84%; however, slurries with higher solids concentrations were fit to the curve:

$$\tau = \eta_o \dot{\gamma} + K'' \dot{\gamma}^{n''} \tag{3.11}$$

For the 2.84% slurry, fit to the power law model, K was found to decrease with increases in temperature, while n remained relatively constant with temperature at 0.695. For TS > 4.5%, the following correlations were proposed:

$$\eta_o = 5.24 \times 10^{-6} \exp\left(0.0868TS + \frac{18.1}{RT}\right) \tag{3.12}$$

$$K'' = 2.428 \times 10^{-3} \exp\left(0.2499TS + \frac{7.39}{RT}\right) \tag{3.13}$$

$$n'' = 0.307 \quad \sigma = 0.054 \tag{3.14}$$

where *R* is the universal gas constant [8.314 J/kg·K]; *T* is the absolute temperature [K]; and *TS* is the % concentration of total solids, by weight..

Achkari-Begdouri and Goodrich (1992) studied the viscous behaviour of scraped Moroccan dairy cattle manure. Over the total solids and temperature ranges of 2.5% to 12% and 20°C to 60°C respectively, the manure slurries were found to behave as shear-thinning, and could be fit to the power law. Over this range, the data fit the following correlations:

$$K = \left\{ 8.722 \exp\left[\left(\frac{4830}{T} \right) + 0.58319 TS \right] \right\} \times 10^{-10} \tag{3.15}$$

$$n = 0.6894 + 0.0046831(T - 273) - 0.042813 TS \tag{3.16}$$

where T is the absolute temperature [K].

Benali and Kudra (2002) conducted laboratory tests to determine the drying characteristics of raw hog manure. Using a rotational viscometer (unknown shear rate) they determined that the viscosity remained Newtonian and relatively constant between 4.5% and 16% TS.; between 16% and 60% TS., the apparent viscosity increased exponentially according to:

$$\eta = \exp(0.1493 TS) \tag{3.17}$$

where η is the apparent viscosity in mPa·s.

Landry et al. (2004) studied the bulk density, particle size distribution, and flow properties of liquid and semi-solid manure from dairy cattle, sheep, poultry, and swine. For swine manure, total solids concentrations of 10% and higher were investigated. They found that the following correlation described the bulk density of swine manure:

$$\rho = -0.0235 TS^3 + 1.19 TS^2 + 11.2 TS + 1000 \quad [\mathrm{kg/m^2}] \tag{3.18}$$

Using the power law, they fit the data to the following relations:

$$\eta_{app} = 4 \times 10^{-6} TS^{4.6432} \quad \dot{\gamma} = 10 \text{s}^{-1} \tag{3.19}$$

$$K = 0.33TS^2 - 7.87TS + 46.91 \tag{3.20}$$

The flow behaviour index, n decreased with increasing solids content; however, no correlation was stated.

Massé et al. (2004) compared the particle size distribution of raw manure with digested manure in an anaerobic sequential bath reactor (ASBR). They found that anaerobic digestion decreased the TS concentration of the manure. As well, the digested manure contained higher concentrations of smaller particles than raw manure.

El-Mashad et al. (2005) studied the effects of temperature and shear rate on dairy cattle manure. Solids concentrations of 91 g/L and 107 g/L were studied with no dilution. The manure was described as “real plastic”; in other words, pseudoplastic behaviour was observed at low shear rates, but the apparent viscosity approaches a constant value at higher shear rates. The Arrhenius model was applied to describe the effect of temperature.

Keener et al. (2006) performed viscosity tests on dairy cattle and hog manure. For hog manure, solids content ranged from 1.4% to 22.4%. A rotational viscometer was used; however, only two speeds (30 and 60 RPM) were tested. Particle size distribution was tested for dairy cattle manure, but not for hog manure.

3.3 Sample collection

With the cooperation of Puratone Corp. of Niverville, Manitoba, manure was sampled from two large hog operations. Operation #1 was a 3100 sow farrow to nursery farm located near Grunthal, MB. Operation #2 was a 3200 head grower/finisher farm located near Niverville, MB. The lagoon storage capacity for each farm was 4.5 million gallons (20.5×10^6 L) and 3 million gallons (13.6×10^6 L), respectively. Samples were collected in early July and before agitating in mid August.

Manure was extracted from several depths and locations within outdoor storage lagoons; all experiments were performed on the samples at their original solids concentrations. Manure was drawn from the open lagoons in 1.5 to 2.0 L samples using the novel cable-and-pulley sample collection system described below. The collection system was set up diagonally across the lagoons to avoid discharge pipes, wet wells, and other obstacles, as shown in Figure 3.2. Each of the samples was poured into three or four 500 mL containers for storage at approximately 5°C. In total, 16 samples were collected from Operation #1, and 10 samples were collected from Operation #2. All samples were kept separate and stored for 2 to 21 days at 5°C before testing. Table 3.1 gives a summary of the samples collected.

Table 3.1: Location and depth of samples collected from two manure lagoons

Operation	Location	Distance from bank (m)	Depth (m)
1	1	3	0.15
1	1	3	0.30
1	1	3	1.50
1	2	6	0.15
1	2	6	0.25
1	2	6	0.45
1	2	6	0.60
1	3	12	0.15
1	3	12	0.40
1	3	12	0.50
1	3	12	0.75
1	3	12	1.50
1	4	30	0.15
1	4	30	0.60
1	4	30	1.20
1	4	30	1.50
2	1	25	0.15
2	1	25	0.45
2	1	25	0.75
2	1	25	1.20
2	2	15	0.15
2	2	15	0.60
2	2	15	1.50
2	3	5	0.15
2	3	5	0.60
2	3	5	1.80

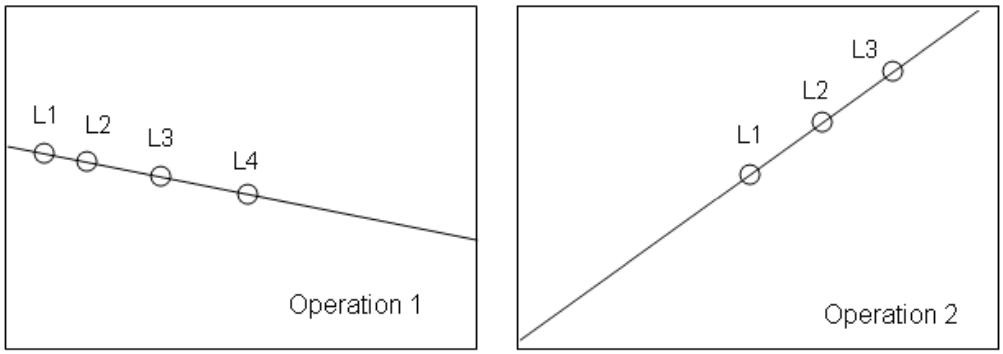

Figure 3.2: Sampling locations for Operation 1 and Operation 2. Drawings not to scale.

3.3.1 Design of sample collection system

Collection of manure samples from various depths and locations within an outdoor storage lagoon requires a novel sample collection system. This system is designed according to the following design criteria:

1. The sample collection system must be easy to transport by small trailer or pick-up truck.
2. The system can be operated by two people.
3. The system can be set-up and taken down in a day.
4. The system can collect samples from the middle of a lagoon that is up to 60 m wide.
5. The system can draw 2 L of manure from the lagoon at a time.
6. The system can be used to draw manure from several locations and depths within a reasonable degree of accuracy and repeatability.
7. The system must be built for less than $1500.

The design that best fits these criteria is a cable-and-pulley system that stretches the length of the lagoon. This system contains the following components (see Figure 3.3):

- Two wood structures (approximately 3 m tall × 3 m long × 1.2 m wide) equipped with pulley systems
- Aircraft cable
- Sampling devices (Ekman dredge and van Dorn bottle sampler, see Figure 3.4)
- Sampler carrier and release mechanism
- Sampler line and spindle

- Signal line and spindle

Figure 3.3: Lagoon sample collection system

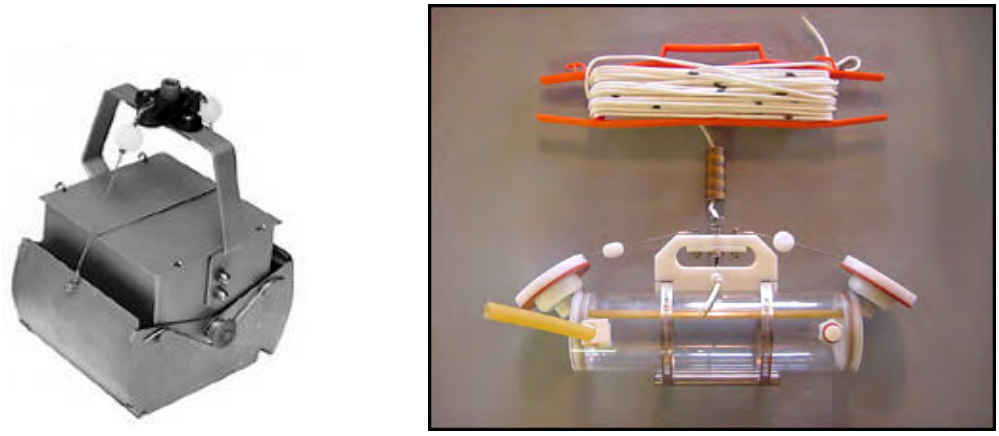

Figure 3.4: Ekman dredge and van Dorn bottle sampler

The sample carrier plate (Figure 3.5) is designed to perform a number of functions. It is connected to both ends of the cable to form a loop; a winch is attached to the plate to tighten the cable. The sampling device is hung below the plate on a hook, with a line

stretching back to the operator on the lagoon bank. A 350 g messenger triggers the sampling device. This messenger is connected to a pin that is held in place at the release mechanism. Pulling on the signal line releases the pin and drops the messenger.

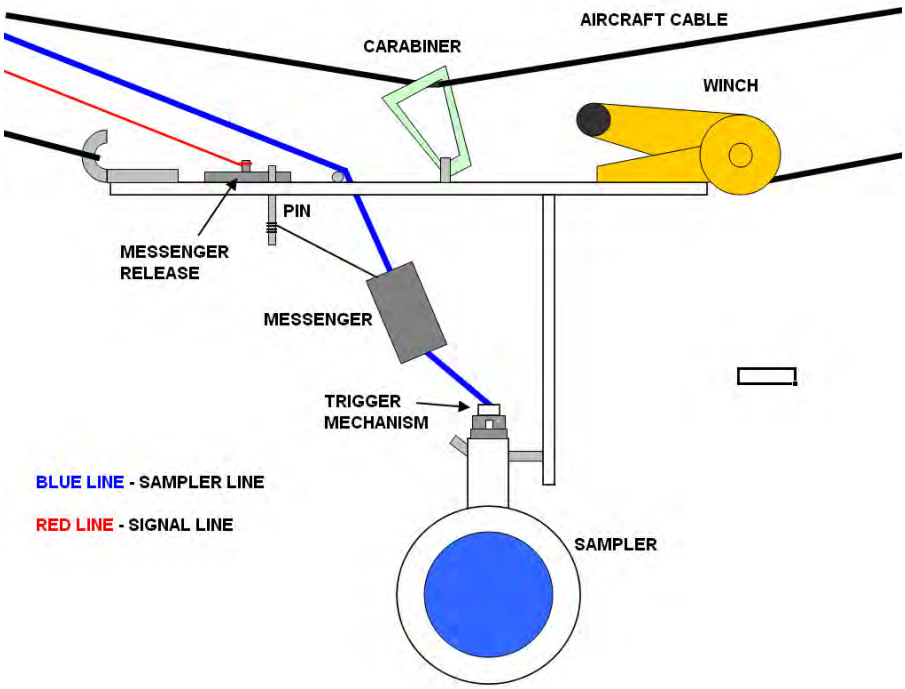

Figure 3.5: Sample carrier plate and messenger release mechanism

3.3.2 Operation of sample collection system

The system is set up at a lagoon as shown in Figure 3.6. The wood structures are placed on opposite banks of the lagoon; stakes are driven into the ground to keep the wheels from moving under the tension of the cables. The steel cable is strung from one structure to the other and winched to the appropriate tension. Care must be taken to keep the cables from dipping into the lagoon.

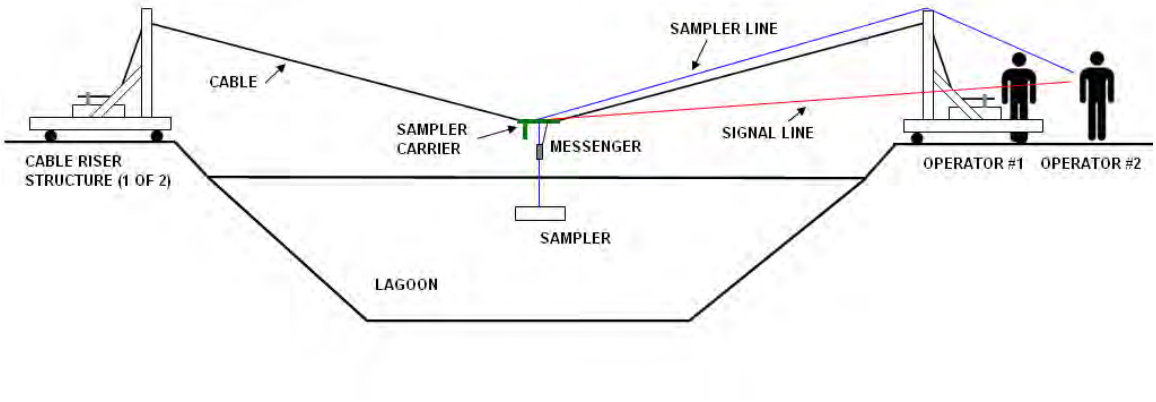

Figure 3.6: Sample collection system setup

Two operators are required to use the sample collection system. Operator #1 draws the sampler and carrier plate out into position over the lagoon using the aircraft cable. While the sampler and carrier plate is being drawn into position, Operator #2 ensures that the sampler line and signal line are fed at an appropriate rate, and do not get tangled. Once the sampler and carrier plate are in the proper location, Operator #2 releases the sampler by first pulling on the sampler line (to bring the sampler off of the hook), then lowering the sampler into the lagoon. Once the desired depth is reached, Operator #2 drops the messenger by tugging on the signal line. The impact of the messenger on the sampler's trigger mechanism closes the sampler, trapping the liquid manure inside. The sampler is then drawn out of the lagoon and emptied into sample containers.

Sample collection is complicated by a few factors. The most significant of these is that the depth of the lagoon is difficult to judge. The distribution of settled solids on the bottom of the lagoon is often non-uniform; in certain locations, the samplers only penetrate about 1 m deep, due to the thickness of sludge. Some solids also float on the

surface of the lagoon; this further complicates the sampling process. Despite these factors, however, the sample collection system worked successfully, and a total of 26 samples were collected.

The sample collection system was designed to be easily assembled and disassembled, as shown in Figure 3.7. The system was transported using an aluminum flat-bed trailer pulled behind an SUV. The total weight of the system was no more than 150 kg.

Figure 3.7: Sample collection system disassembled and ready for transport

3.4 Experimental methods

3.4.1 Sample size and storage

Manure was drawn from open lagoons in 1.5 to 2.0 L samples. In total, 26 samples were collected; 16 from Operation 1, and 10 from Operation 2. Each of these samples were mixed and poured into three or four 500 mL containers for storage. Samples were stored

at 5ºC for 2 to 21 days before testing to avoid decomposition. Other than settling, no significant changes in the samples were observed during storage.

3.4.2 Mass fraction of total solids and bulk density

To determine the total solids content of the manure, 50 mL samples were measured, weighed, and dried overnight at 103°C. The dried samples were weighed again, and the mass fraction of total solids was calculated as:

$$TS = \frac{m_{dry}}{m_{wet}} \times 100 \tag{3.21}$$

where TS is the mass percentage of total solids, m_{dry} is the mass of the dried manure, and m_{wet} is the initial wet mass of the manure (50 mL sample). This test was performed four times for each sample, and the average value was taken. Also, the bulk density of the manure was calculated as:

$$\rho_{manure} = \frac{m_{wet}}{V_{wet}} \tag{3.22}$$

where ρ_{manure} is the bulk density of the manure, and V_{wet} is the volume of the wet manure.

3.4.3 Particle size distribution

Two separate tests were used to determine the size distribution of particles within the manure. The distribution of larger particles was measured using a sieve test, while the distribution of smaller particles was determined by microscopic analysis.

The sieve tests were performed using a series of sieves in a transparent column. The column was set over a vacuum flask, and wet manure was poured through the sieves (see

Figure 3.8). Distilled water was used to rinse the sieves to ensure that smaller particles would pass through to the next sieve. The sieves were placed in the drying oven overnight at 103°C. The dried mass on each sieve was then weighed. The sieves used were US Standard #6 (3.353 mm), #10 (1.829 mm), #18 (1.016 mm), #35 (0.508 mm), #60 (0.229 mm), #100 (0.140 mm), and #270 (0.053 mm).

Small particles (1 to 500 μm) were observed under a microscope. Each sample was diluted using distilled water; samples with less than 6% total solids were diluted 100:1, while samples greater than 6% total solids were diluted 250:1. Five millilitres of diluted manure was dropped into a Petri dish and placed under a microscope. Digital micrographs were taken at 3 magnifications: 20X, 50X, and 400X; several different micrographs were taken for each sample to ensure a good representation. Using a commercial software package, particles were counted and measured according to area, length, and mean diameter. This information was then used to create a particle size distribution graph for each sample.

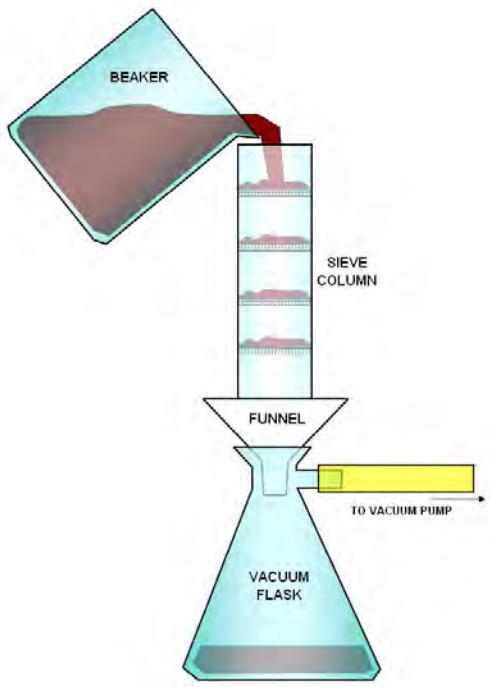

Figure 3.8: Particle size distribution – sieve test apparatus

3.4.4 Viscosity

Viscosity tests were conducted using the Brookfield DV-II+PRO viscometer with an LV spring (see Figure 3.9). 600 mL Griffin beakers were filled with manure samples taken directly from refrigeration. Samples were brought to temperature using a constant temperature bath (25°C, 40°C, and 60°C), then placed in foam wrap insulation. The 15°C samples were taken out of the refrigerator and warmed to 15°C in the ambient air before wrapping with insulation. Low solids content samples (TS < 6%) were tested at nine speeds (40 to 200 RPM), while thicker samples were tested at lower speeds (0.05 to 0.4 RPM for 13.1% TS) to avoid exceeding the torque range of the viscometer. The Brookfield #61 spindle was used for all viscosity tests. Samples with TS < 6% could be tested at all nine speeds consecutively; each speed was held for 30 s, and measurements were recorded every 10 seconds. Samples with higher solids content yielded time-

depended results; thus, each speed was held for up to 45 min. Recordings were taken every 10 s and extrapolated to achieve a steady-state value. These samples were kept in the temperature bath during testing to avoid losing too much heat during the test.

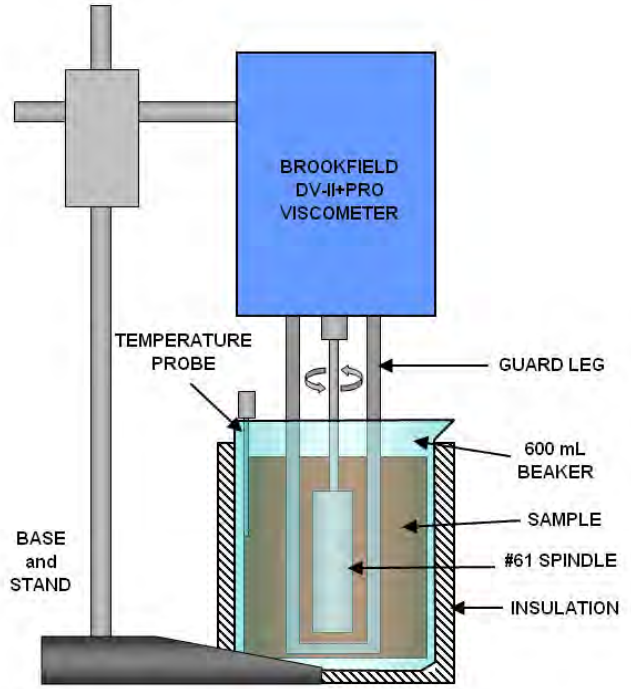

Figure 3.9: Setup diagram for Brookfield viscometer

3.5 Results and discussion

3.5.1 Density

Figure 3.10 shows the measured density of the hog manure samples as a function of total solids concentration at room temperature (25°C). For TS < 17%, the density increases linearly with increasing total solids, according to Equation 3.23.

$$\rho = 3.446\mathrm{TS} + 1001 \tag{3.23}$$

where ρ is the density [kg/m^3], and TS is the percent total solids concentration, by mass. For TS = 0%, the above equation predicts a density of 1001.1 kg/m^3. This agrees with the accepted density of water at 25°C, 997 kg/m^3 (Fox et al., 2004), within a reasonable margin of error. The density increases as total solids increases, in agreement with Landry et al. (2003).

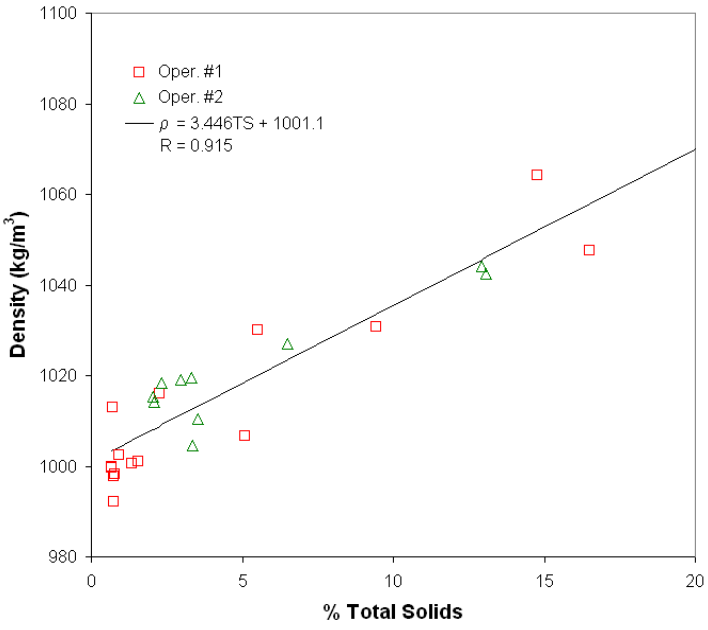

Figure 3.10: Density of hog manure as a function of total solids.

3.5.2 Total solids concentration vs. depth

The total solids concentration measured as a function of depth is shown in Figure 3.11 for both operations. For Operation 1, the solids concentration increases slowly with depth until a certain depth; past this depth, the increase in TS is much greater. This is evidence of stratification within the lagoon. The transition depth varies from location to location, probably influenced by proximity to the inlet, distance from the lagoon bank, and

convection. In general, the transition depth occurs somewhere between 0.45 and 1.5 m. Similarly, the data from Operation 2 shows a similar trend, indicating a transition depth somewhere between 0.75 and 1.2 m. Note that the solids concentration for Operation 1 at shallow depths is much lower than for Operation 2 (less than 1.0% TS compared with 2.0 to 3.5% TS, respectively). Table 3.2 summarizes the data for depth, total solids, and density.

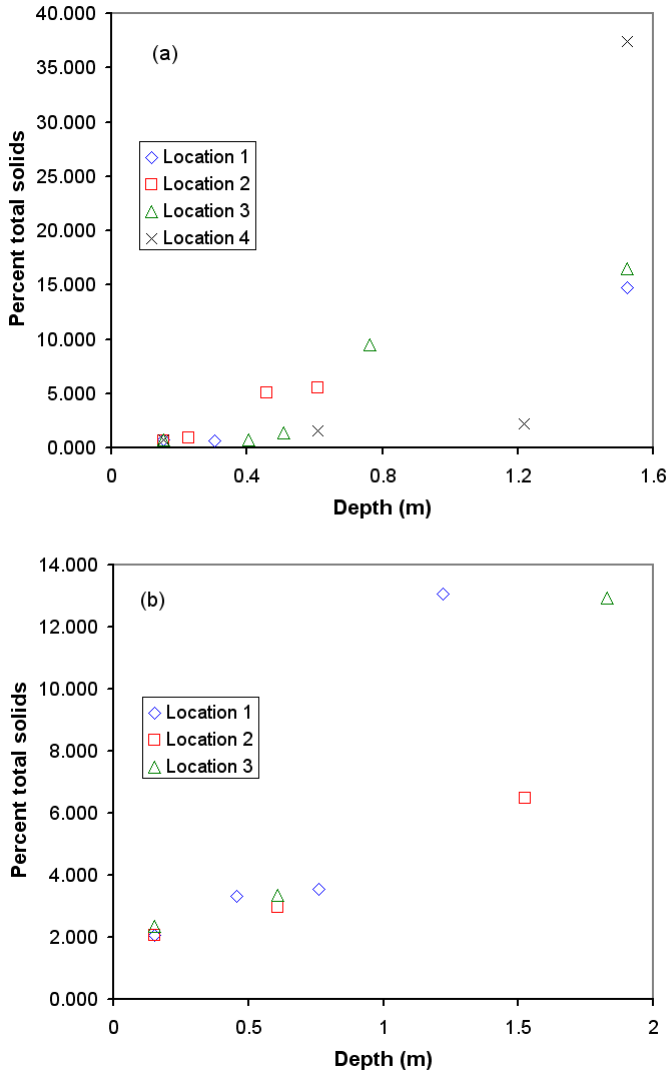

Figure 3.11: Total solids concentration vs. depth. a) Operation 1; b) Operation 2

Table 3.2: Summary of hog manure samples: approximate depth, total solids content, and density

Operation	Depth (m)	% T.S	Density
1	0.15	0.75	992
1	0.15	0.69	1000
1	0.15	0.74	998
1	0.15	0.72	1013
1	0.25	0.90	1002
1	0.30	0.67	1000
1	0.40	0.78	998
1	0.45	5.09	1007
1	0.50	1.36	1001
1	0.60	5.51	1030
1	0.60	1.54	1001
1	0.75	9.45	1031
1	1.20	2.25	1016
1	1.50	14.8	1064
1	1.50	16.5	1048
1	1.50	37.4	1277
2	0.15	2.05	1015
2	0.15	2.07	1014
2	0.15	2.34	1018
2	0.45	3.33	1020
2	0.60	2.97	1019
2	0.60	3.37	1005
2	0.75	3.55	1011
2	1.20	13.1	1043
2	1.50	6.49	1027
2	1.80	12.9	1044

3.5.3 Particle size distribution

A microphotograph of liquid manure is shown in Figure 3.12. The original total solids concentration for this sample is 5.09%. Before analysis, the sample was sieved through a series of sieves of 0.23 mm and greater, then diluted 100:1 with distilled water. The photograph is magnified 400X.

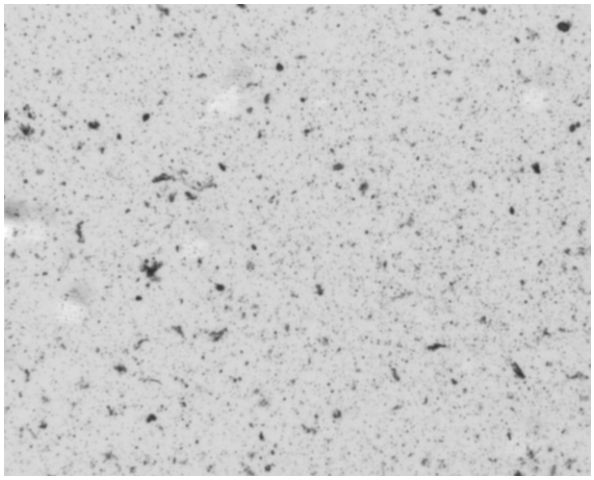

Figure 3.12: Microphotograph of liquid hog manure, 400X

Two distinct parameters are used in the analysis of particle size distributions: the fraction of particles counted with a diameter less than d (N_d), and the mass fraction of particles with a diameter greater than d (Y_d). Each of these parameters reveals different characteristics. N_d is weighted towards the smaller particles and thus reveals more detail in the range where d is very small; conversely, Y_d is weighted towards the large particles, revealing more detail in the range where d is very large. These parameters are defined in Equations 3.24 and 3.25:

$$N_d = \frac{\sum_{di=d\,\min}^{d} n(d_i)}{\sum_{di=d\,\min}^{d\,\max} n(d_i)} \tag{3.24}$$

$$Y_d = \frac{\sum_{di=d\,\min}^{d} m(d_i)}{\sum_{di=d\,\min}^{d\,\max} m(d_i)} \tag{3.25}$$

where $n(d_i)$ is the number of particles with a diameter of d_i; $m(d_i)$ is the mass of particles with a diameter of d_i; d_{min} is the minimum diameter measured (approximately 1 μm); and d_{max} is the maximum diameter measured (on the order of 1000 μm)

It is important to note that two different experimental analyses were used—sieve tests and microscopic analysis—and the data presented below is the product of merging the results of these analyses. Particle mass can not be determined directly from the microscopic images. Thus, it is assumed that the density is uniform over the entire range of particles; particle mass can then be estimated according to particle volume, calculated as the volume of a sphere with a diameter of d_i. Additionally, the particle count can not be determined using the sieve tests; however, this is neglected, since N_d is weighted so heavily towards small particles.

Figure 8 shows how particle size distribution varies with depth within the lagoon. The presence of large particles (d_i > 100 μm) heavily influences the profiles of Y_d for individual samples. In general, only a few of these particles are present in the microscopic images for each sample, yet in the samples collected from the bottom sludge zone of the lagoon, they occupy up to 80% of the mass fraction of solid particles observed (since mass fraction is proportional to d_i^3). As depth and % TS increase, the distribution shifts to the right, indicating the settling of larger particles within the lagoon.

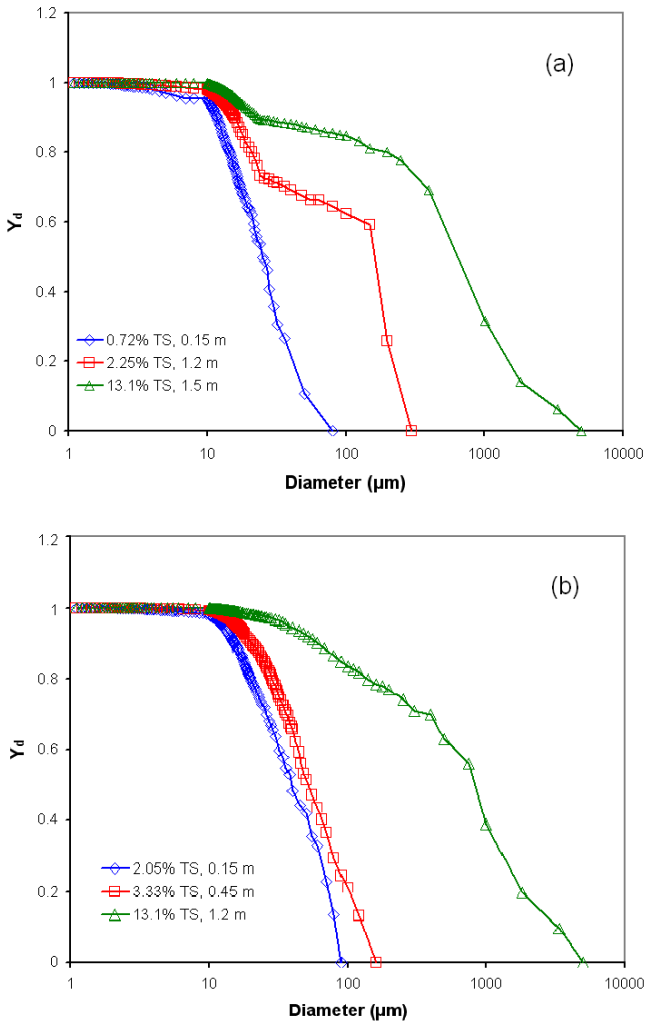

Figure 3.13: Particle size distribution by mass fraction. a) Operation 1, Location 1; b) Operation 2, Location 2

Figure 3.14 summarizes Y_d for all samples. These plots show the average values of d_i that correspond to Y_d = 0.368, 0.5, 0.75, and 0.9. Similarly, Figure 3.15 shows the average values of d_i that correspond to N_d = 0.5, 0.75, 0.9 and 0.95 for all samples. In general, the TS > 5% profiles show higher values than the TS < 5%. Both operations show similar profiles for Y_d; however they produce different results for N_d (see Figure 3.15). Operation #1 (a sow farm) exhibits a much higher profile for TS > 5% than for TS < 5%;

Operation # 2 (a grower/finisher farm) on the other hand, shows nearly identical profiles for high and low solids content samples.

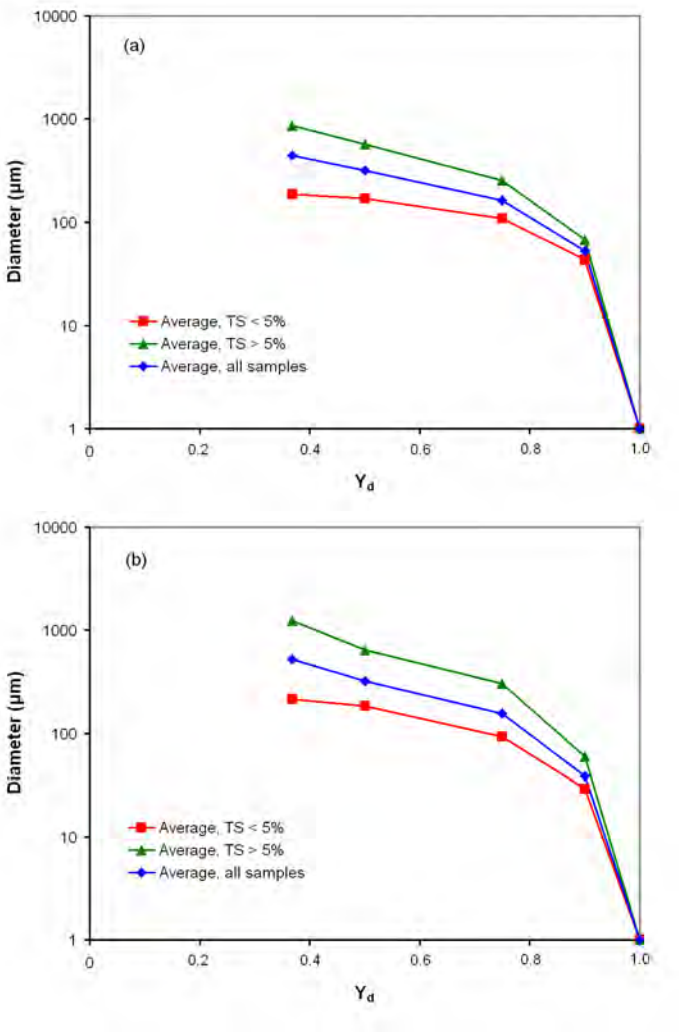

Figure 3.14: Particle size distribution by mass fraction. a) Operation 1; b) Operation 2

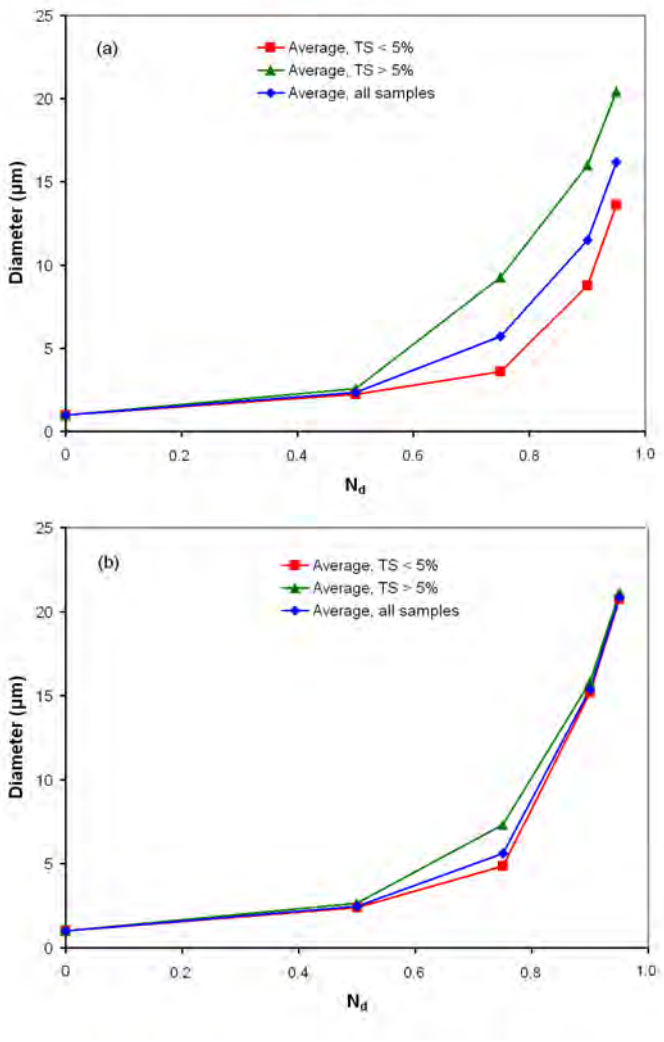

Figure 3.15: Particle size distribution by particle count. a) Operation 1; b) Operation 2

The particle size distributions by mass for Operation 1 and 2 are shown in Tables 3.3 and Table 3.4. These tables represent the average diameter at which Y_d = x, for all samples, samples with high solids content (TS > 5%), and samples with low solids content (TS < 5%). Standard deviations are also shown.

Table 3.3: Particle size distribution by mass, Operation 1 (dimensions in mm)

	All samples		TS < 5%		TS > 5%	
	Avg.	St. dev	Avg.	St. dev	Avg.	St. dev
Yd = 0.368	438.8	477.1	187.0	195.5	858.3	545.6
Yd = 0.50	317.3	321.7	167.6	186.5	566.7	378.6
Yd = 0.75	162.5	163.3	108.0	179.5	253.3	95.04
Yd = 0.90	52.13	54.00	42.80	60.12	67.67	48.95

Table 3.4. Particle size distribution by mass, Operation #2 (dimensions in mm)

	All samples		TS < 5%		TS > 5%	
	Avg.	St. dev	Avg.	St. dev	Avg.	St. dev
Yd = 0.368	519.1	521.2	214.5	195.7	1230	157.2
Yd = 0.50	320.7	284.1	182.5	175.0	643.2	220.3
Yd = 0.75	156.2	150.1	92.75	91.31	304.2	171.6
Yd = 0.90	38.24	20.40	29.20	16.30	59.33	11.02

Table 3.5 compares the results of the current study to those of Masse et al. (2004). The results of the latter study have been converted from units of concentration (g/L) to percentage of the total mass of solids. It is apparent that the results of Masse et al. show much higher percentages of smaller particles than the current study. The current study shows that, for all samples, 99.21% of particles are larger than 10 μm; Masse et al., however, show 48.89% and 20.67% for raw and digested manure. The current study shows that samples over 5% TS contain much higher percentages of larger particles than samples below 5% TS. In general, Operation #1 shows slightly higher fractions of larger particles than Operation #2.

Table 3.5: Comparison of current results to the literature – distribution of particles by percent mass

	> 1000 µm	> 250 µm	> 50 µm	> 10 µm	> 0.45 µm
Masse et al. raw	15.96	22.47	28.48	48.89	81.16
Masse et al. AD	1.21	4.08	6.95	20.67	56.00
All samples	12.05	47.48	72.03	99.21	--
Operation 1, < 5% TS	0.00	40.80	66.92	98.59	--
Operation 2, < 5% TS	0.00	32.19	62.95	99.27	--
Operation 1, > 5% TS	47.49	79.86	89.80	99.83	--
Operation 2, > 5% TS	40.65	74.94	91.60	99.87	--

3.5.4 Viscosity

The viscous characteristics of liquid hog manure vary significantly with total solids content and temperature. Samples with total solids concentrations less than 3.6% exhibit Newtonian behaviour; these samples originate from shallower depths in the lagoon, and thus contain fewer large particles. Samples with TS > 6.5%, generally collected from the bottom sludge of the lagoon (1.2 m or deeper), exhibit non-Newtonian, time-dependent characteristics. Two samples represent a transition zone between the dilute surface samples and the thick sludge samples; these samples contain 5.09% and 5.51% TS, and were collected at approximately 0.45 and 0.6 m from the lagoon surface. These samples are non-Newtonian, but their viscosity is not time dependent. Thus, the power law is a good fit for these samples.

The viscosities of the samples with TS < 3.6% were tested at nine shear rates between 8.8 and 44 s^{-1}. Figure 3.16 displays the viscosity data for the low-solids samples at 15°C, 25°C, 40°C, and 60°C. The data shows a clear upward trend as TS increases. Viscosity also decreases as the temperature is increased from 15°C to 60°C. At any given

temperature, the relationship between solids content and viscosity may be expressed by Equation 3.26.

$$\mu(TS) = \exp(a + bTS) \tag{3.26}$$

where TS is the percent total solids concentration, and a and b are empirical coefficients given in Table 3.7. The full set of viscosity results is found in Appendix A.

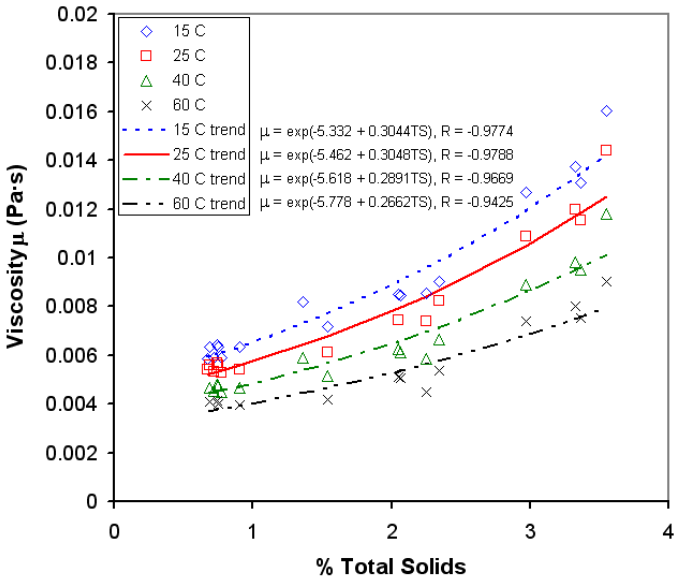

Figure 3.16: Viscosity results for TS < 3.6%

Table 3.6: Empirical coefficients relating viscosity to total solids concentration

Temperature (°C)	a	b	Corr. coeff. R
15	-5.332 ± 0.0348	0.3044 ± 0.0170	0.9774
25	-5.462 ± 0.0368	0.3048 ± 0.0177	0.9788
40	-5.618 ± 0.0429	0.2891 ± 0.0204	0.9669
60	-5.778 ± 0.0649	0.2662 ± 0.0285	0.9425

The temperature dependence of the low-TS samples may be expressed using the Arrhenius relationship. Incorporating this into Equation 3.26, the viscosity may be expressed as a function of both temperature and total solids using Equation 3.27:

$$\mu(T,TS) = \exp(-8.629 + \frac{946.2}{T} + 0.2911TS) \quad (3.27)$$

where T is the temperature in Kelvin. The standard error for this correlation is 7.08×10^{-4}. The form of this equation is similar to the relationship between correlation coefficient, temperature, and total solids given by Achkari-Begdouri and Goodrich (1992).

As mentioned earlier, two samples represent a transition zone between the dilute samples near the surface of the lagoon, and the sludge found at the bottom. These samples, both collected from Operation 1, have solids contents of TS = 5.09% and 5.51%. As shown in Figures 3.17 and 3.18, the shear stress vs. shear rate curves for these samples are well-fitted to the power law. In general, K is greater and n is smaller for the sample with TS = 5.51%, with the exception of 60°C. As expected, K decreases with temperature for both samples. The flow behaviour index n increases marginally as the temperature increases from 15°C to 40°C. At 60°C, n increases substantially for both samples, from 0.530 to 0.912 for TS = 5.09%, and from 0.498 to 0.605 for TS = 5.51%. It is possible that moisture loss at 60°C may play a factor in the viscosity readings.

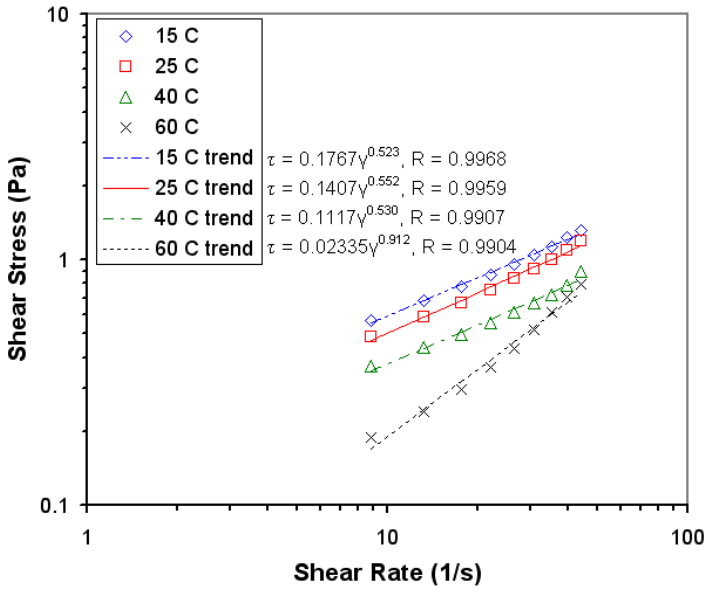

Figure 3.17: Shear stress vs. shear rate for Operation 1, TS = 5.09%

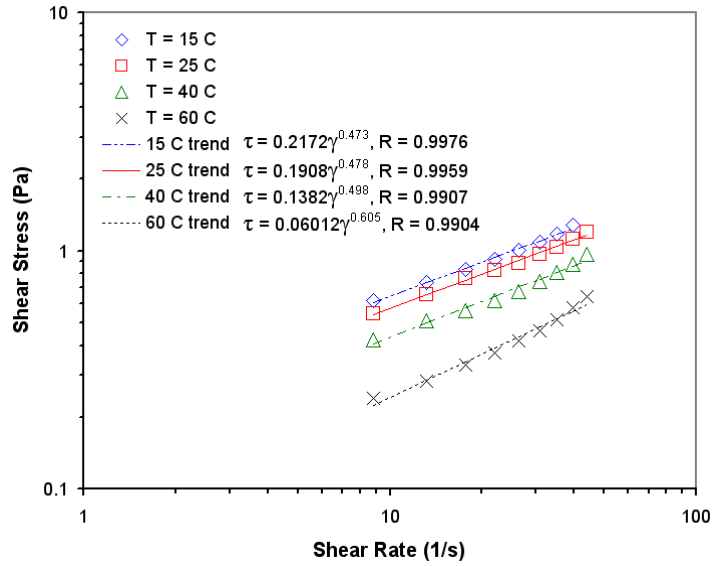

Figure 3.18: Shear stress vs. shear rate for Operation 1, TS = 5.51%

The viscous behaviour of samples collected from the sludge zone is non-Newtonian and time-dependent. Operation 1 (9.45% TS) and Operation 2 (12.9% TS) exhibit decreasing apparent viscosity with time; the viscosity exponentially decays to a steady state value.

However, the apparent viscosity of the 6.49% TS sample from Operation 2 increases with time, exponentially approaching a steady-state value. Less shear rates were tested for these samples, due to the length of time required to collect the time-dependent data. The steady state values are shown in Figures 3.19, 3.20, and 3.21. The power law parameters K and n are shown in Table 3.9; it is apparent that the power law provides a poorer fit for these samples than for the previous samples at 5.09% and 5.51% TS.

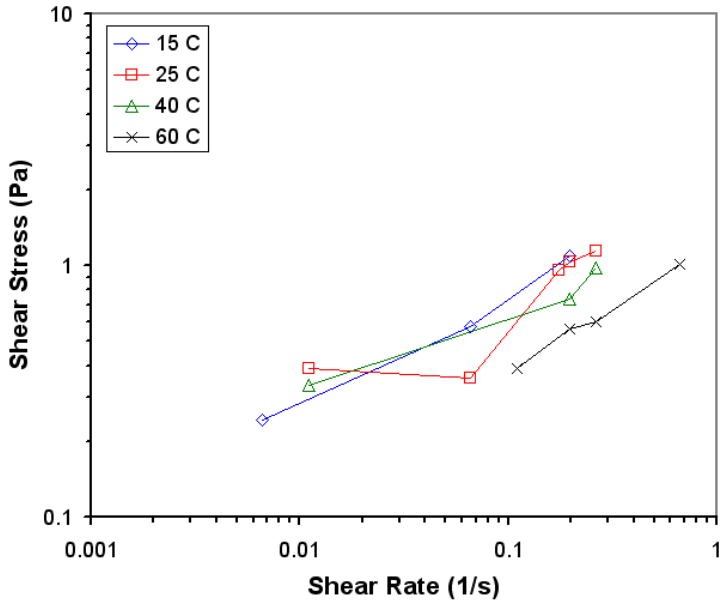

Figure 3.19: Shear stress vs. shear rate for Operation 1, 9.45% TS

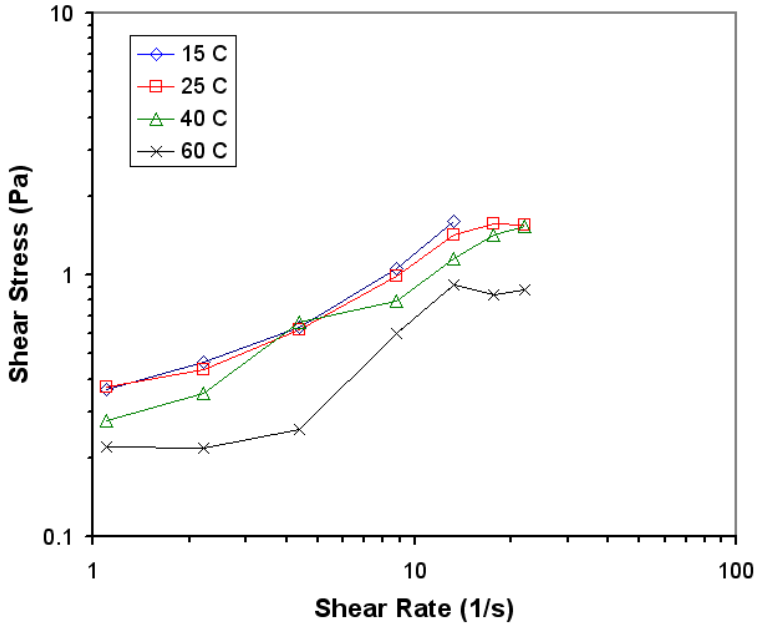

Figure 3.20: Shear stress vs. shear rate for Operation 2, 6.49% TS

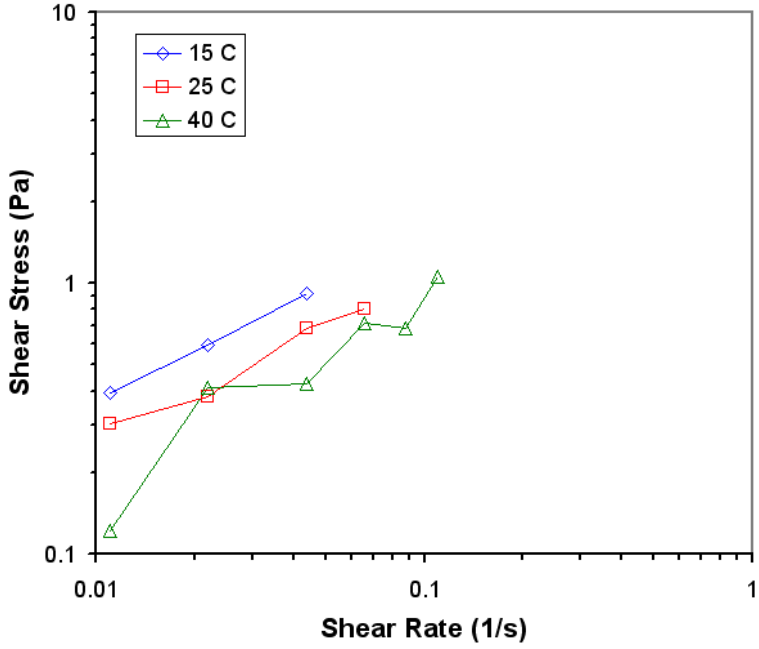

Figure 3.21: Shear stress vs. shear rate for Operation 2, 12.9% TS

Table 3.7: Power law parameters for high-TS samples

Oper.	% T.S.	Temp (°C)	K (Pa·s^n)	n	Corr. Coeff.	Shear rates (s^{-1})			Data pts.
1	9.45	15	2.054	0.4322	0.9926	0.0066	to	0.198	3
1	9.45	40	1.349	0.3112	0.9834	0.011	to	0.264	3
1	9.45	60	1.245	0.5217	0.9962	0.11	to	0.66	4
2	6.49	15	0.3075	0.5894	0.9802	1.1	to	13.2	5
2	6.49	25	0.3139	0.5392	0.9863	1.1	to	22	7
2	6.49	40	0.2478	0.5909	0.9918	1.1	to	22	7
2	6.49	60	0.1622	0.5673	0.9413	1.1	to	22	7
2	12.9	15	6.154	0.6116	0.9998	0.011	to	0.044	3
2	12.9	25	3.900	0.5798	0.9837	0.011	to	0.066	4
2	12.9	40	3.470	0.6080	0.9585	0.011	to	0.11	6

Figure 3.22 plots K against TS for all samples. Examination of Figure 3.22 shows that the consistency coefficient, K, follows a clearly-defined upward trend. There are two distinct regions—K in the low TS region increases more gradually than in the high TS region. The transition happens somewhere between 3.6% and 5.0% TS; however, there are no data points that fall in this transition zone. The 60°C series fits poorly with the rest of the data above 5.0% TS, possibly because of rapid moisture loss at this high temperature. To simplify the analysis and avoid error caused by this possible loss of moisture, the 60°C series is omitted from the calculation of trends.

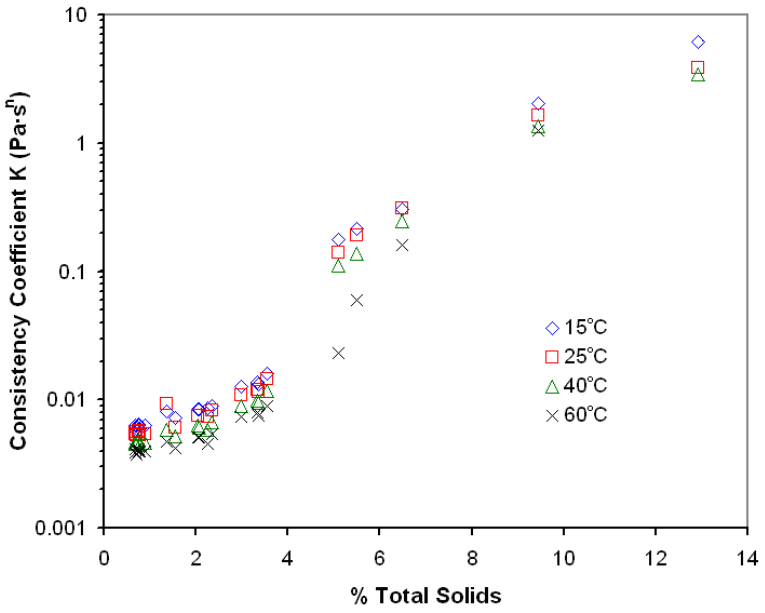

Figure 3.22: Consistency coefficient K (Pa·s^n) vs. total solids.

The trend observed in Figure 3.22 compares well qualitatively with the trends observed by Chen (1986) and Achkari-Begdouri and Goodrich (1992), though these studies were conducted using beef and dairy cattle slurries, respectively. Both studies propose exponential functions to describe K as a function of total solids. These trends also agree qualitatively with the results of Landry et al. (2004); however, Landry et al. studied slurries of higher solids content (10% to 20% TS) and describes the data using a quadratic function. However, none of the above-mentioned studies describe a transition zone between low-solids and high-solids content. Kumar et al. (1972), Barker and Driggers (1980), and Benali and Kudra (2002) describe the slurries as Newtonian at low TS and non-Newtonian at high TS, though the position of this transition is different for each.

Figure 3.23 compares the present viscosity results to data given by Barker and Driggers (1981) and Landry et al. (2004). Results are given the consistency coefficient K, taken at room temperature. The correlation given by Barker and Driggers for TS < 3% matches data from the present study quite well, though a steeper slope is implied. The values for K given by Landry et al. correspond to four samples between 10.7% and 22.8% TS.

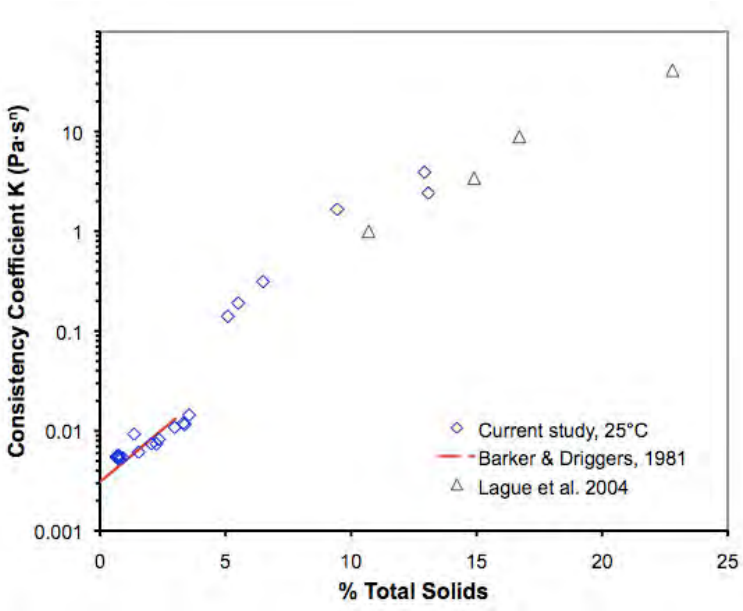

Figure 3.23: Comparison of viscosity data with the literature

The flow behaviour index n shows a large amount of scatter when plotted against TS (see Figure 3.24). Below TS = 3.6%, n is equal to 1.0, since the fluid is Newtonian in this region. However, between TS = 5.0% and TS = 12.9%, n varies between 0.91 and 0.31. The sample at 9.4% TS appears especially out-of-place when compared with the other data points.

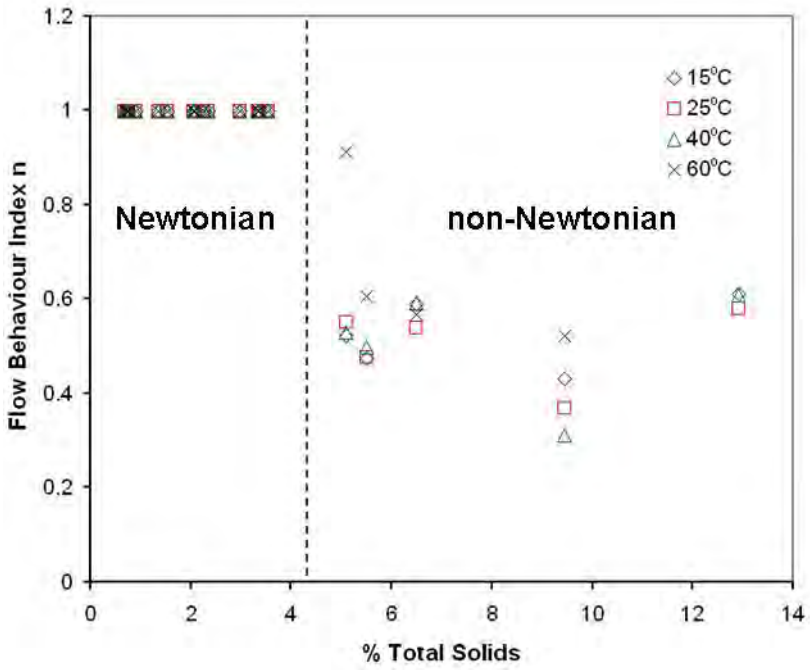

Figure 3.24: Flow behaviour index n vs. total solids.

3.5.5 Recommendations for modeling

The above results show that the physical properties of liquid hog manure are complex, varying with temperature, total solids, and shear rate (in the case of viscosity), as well as the type of hogs and process parameters. However, for this data to be useful from the perspective of research and design of anaerobic digesters, it is necessary to interpret the data in terms of appropriate mathematical models. In this section, recommendations will be given for implementation of these models in a commercial CFD package such as Fluent®, CFX®, and OpenFOAM®.

3.5.5.1 Density

The density of hog manure can be described using Equation 3.23, from 0% to 16.5% TS (repeated below):

$$\rho = 3.446\text{TS} + 1001 \text{ [kg/m}^3\text{]} \tag{3.23}$$

Using this formula, the density only changes about 5% over the given range.

3.5.5.2 Particle size distribution

Though discrete phase models have several limitations, they can be used to trace particle motion within an anaerobic digester model, especially for systems with low total solids. Fluent uses the Rosin-Rammler function (see Equation 3.28) to describe the diameter distribution of a particle injection (Fluent, 2005):

$$Y_d = \exp\left[-\left(\frac{d}{d_m}\right)^n\right] \tag{3.28}$$

where Y_d is the mass fraction of particles with a diameter greater than d; d is the particle diameter; d_m is the mean particle diameter; and n is the spread parameter (not to be confused with the flow behaviour index used for non-Newtonian fluids).

A value for d_m is found by estimating d such that $Y_d = e^{-1} \approx 0.368$. Figure 3.25 shows the Rosin-Rammler distribution fit to the data for both operations. Table 3.10 gives the empirical constants d_m and n used for these curves. Values for a generalized model, determined by taking the average of Operation 1 and Operation 2, are also recommended in Table 3.10. The particle size distribution described by this recommended model is shown in Figure 3.26.

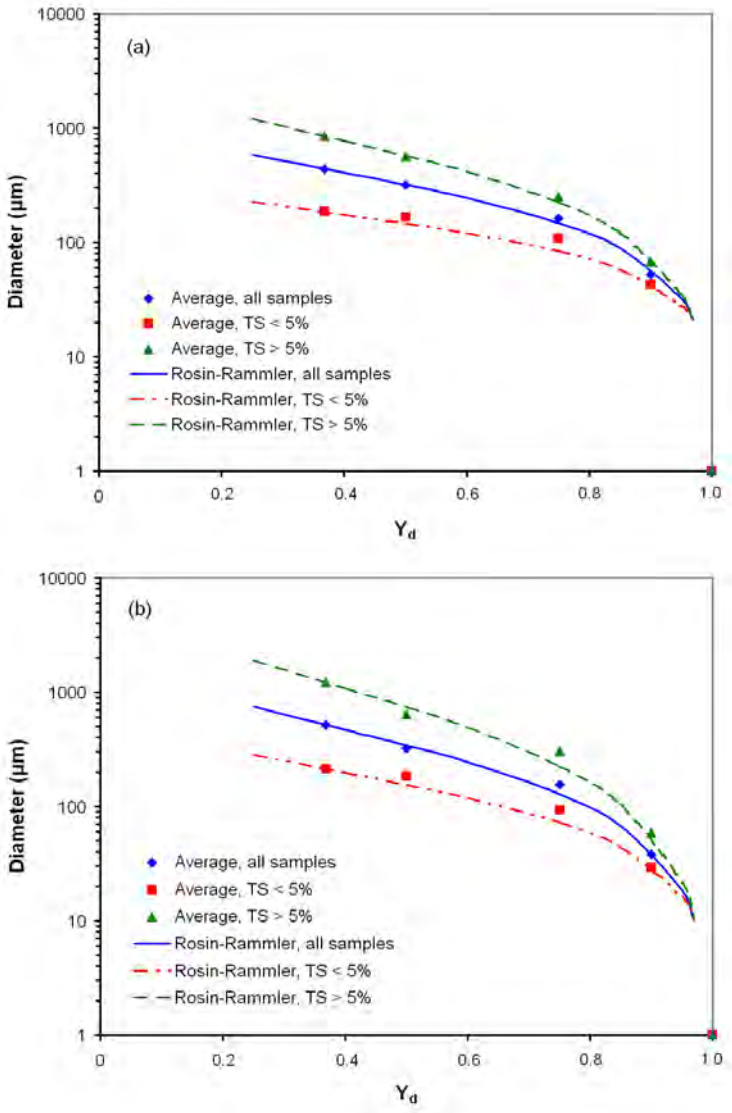

Figure 3.25: Rosin-Rammler fit for a) Operation 1; b) Operation 2

Table 3.8: Rosin-Rammler fit for particle size distribution

	d_m (µm)	n	d_{max} (µm)	d_{min} (µm)
Operation #1 – All	519.1	0.887	1204.2	1.1
Operation #1 – TS < 5%	214.5	1.150	283.3	1.1
Operation #1 – TS > 5%	1230.0	0.733	3353.0	1.1
Operation #2 – All	438.8	1.147	1043.6	1.1
Operation #2 – TS < 5%	187.0	1.570	236.3	1.1
Operation #2 – TS > 5%	858.3	0.930	2389.1	1.1
General – All	479	1.0	1124	1.0
General – TS < 5%	201	1.4	260	1.0
General – TS > 5%	1044	0.8	2871	1.0

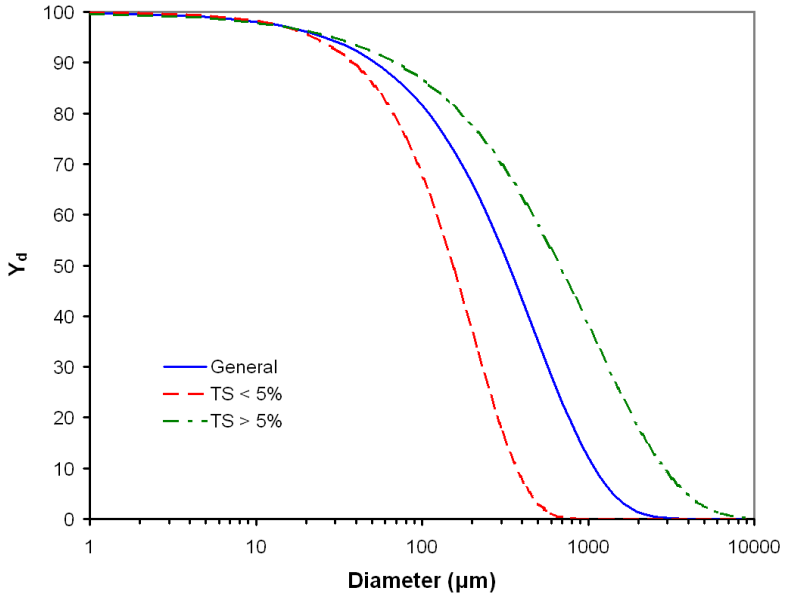

Figure 3.26: Recommended Rosin-Rammler distribution of solid particles

3.5.5.3 Viscosity

As described above, the power law (see Equation 3.3) was used to characterize the apparent viscosity η of hog manure as a function of shear rate. The power law parameters, K and n, can be described as functions of temperature and TS using Equations 3.29 and 3.30:

$$K(T,TS) = \exp(a_1 + \frac{a_2}{T} + a_3 TS) \ [\text{Pa·s}^{n-1}] \tag{3.29}$$

$$n = a_4 \tag{3.30}$$

where T is temperature [K], TS is % total solids, and a_1 through a_4 are empirical coefficients. Separate coefficients are used for the high- and low-TS regions. A transition zone between the low- and high-TS regions was also developed, preserving zero-order continuity; in this transition zone, the coefficients are linear functions of TS. Table 3.11 shows the empirical constants a_1 through a_4 for the general viscosity model. Figure 3.27 superimposes these correlations on the data for K and n, respectively. The apparent viscosity described by this generalized model is shown in Figure 3.28.

Table 3.9: Empirical constants for the generalized viscosity model

	0.7% to 3.6% TS	3.6% to 5.0% TS	5.0% to 12.9% TS
a_1	-8.58	-1.29 × TS + (-3.93)	-10.4
a_2	937	642 × TS + (-1380)	1836
a_3	0.287	0.118 × TS + (-0.137)	0.452
a_4	1.0	-0.3483 × TS + 2.254	0.5123

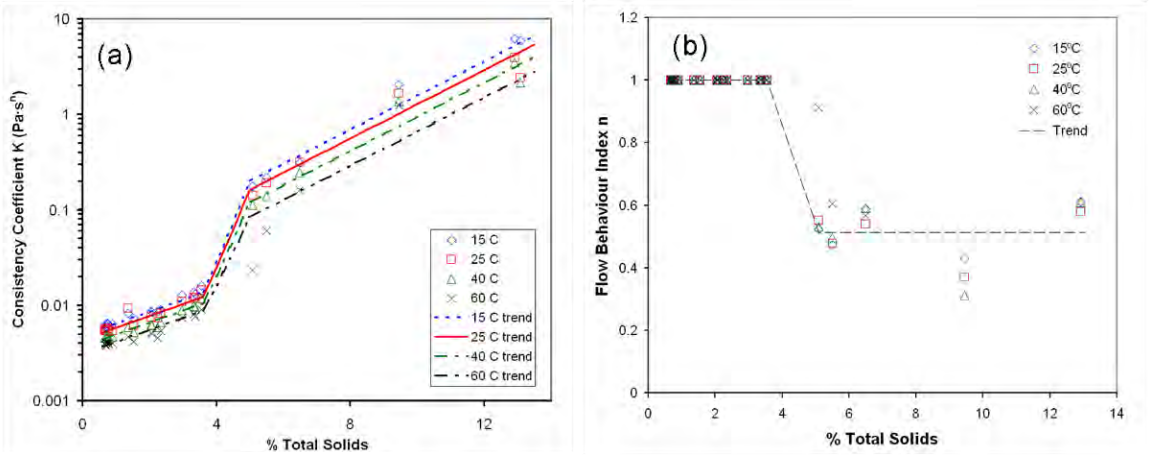

Figure 3.27: Experimental power law parameters with generalized viscosity model. a) consistency coefficient K; b) flow behaviour index n

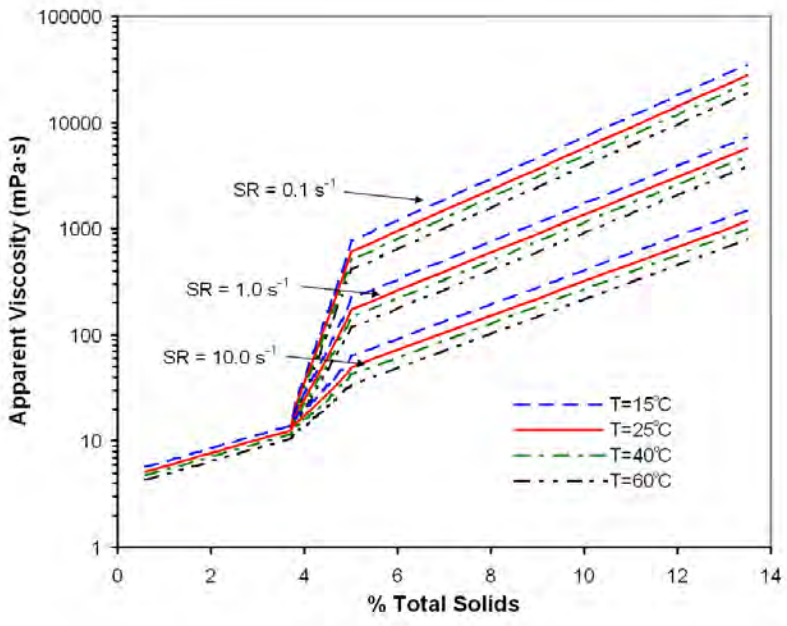

Figure 3.28: Apparent viscosity as a function of % TS, generalized model

3.6 Summary of findings

Hog manure was collected from several depths and locations within two outdoor storage lagoons. The total solids concentration of the samples collected ranged from 0.67% to 3.6% for surface samples, up to 37.1% in the sludge zone at the bottom of the lagoon. It was found that the bulk density increased linearly with total solids content. The particle size distribution was measured on a mass fraction basis and on a particle count basis. Samples collected deeper in the lagoon exhibited higher fractions of large particles than samples collected near the surface, due to the settling of large particles within the lagoon. The maximum particle diameters observed were between 1.0 and 3.4 mm for samples with high solids concentrations (TS > 5%) and approximately 250 μm for samples with

low solids concentrations. The smallest particles observed were about 1 μm in diameter; however, this value is determined by the resolution of the microscopic imaging instruments. The viscosity of liquid hog manure was measured over the range of 0.6% to 12.9% TS and at temperatures of 15°C, 25°C, 40°C and 60°C. The range of shear rates used was 0.0066 to 44 s^{-1}; lower shear rates were used for thicker samples. Newtonian behaviour was observed under 3.6% TS; non-Newtonian, time-dependent characteristics were observed above 6.5% TS; and intermediate samples were pseudoplastic and were fitted to the power law.

Chapter 4. Design of an experimental fluid column facility

4.1 Introduction

4.1.1 Overview

An experimental fluid column facility was designed and built to simulate the flow of Newtonian and non-Newtonian fluid within an anaerobic digester. This fluid column facility was used to investigate the effects of geometry, flow rate, and fluid properties on the velocity fields and residence time distribution (RTD) of a continuous-flow reactor. The results of these studies are also used to validate CFD simulations. This facility, as shown in Figure 4.1, can be separated into the following systems: acrylic fluid column; storage tanks; pump and plumbing system; tracer dye injection and sampling stations; PIV system; and support and sliding frames.

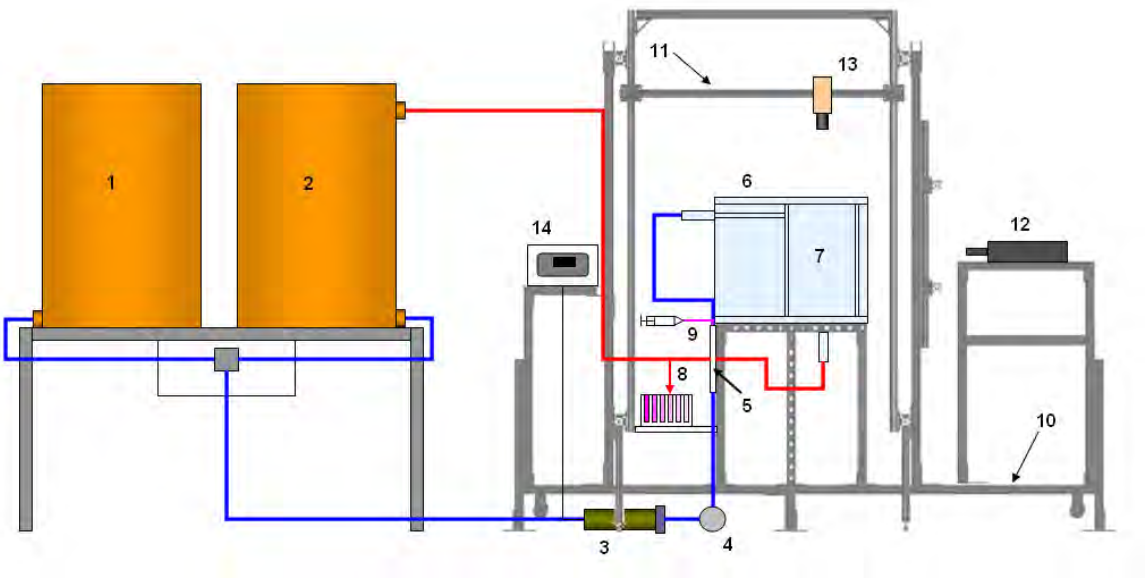

Figure 4.1: Diagram of the fluid column facility (not to scale)

As shown in Figure 4.1, the components of the fluid column facility are:

1. Supply tank
2. Discharge tank
3. Masterflex I/P peristaltic pump
4. Pulse dampener
5. Flow control valves
6. Acrylic fluid column
7. Test section
8. Sampling station
9. Tracer dye injection station
10. Steel support frame
11. Aluminum sliding frame
12. Gemini-PIV dual-head laser
13. Kodak Megaplus digital camera
14. Digital pump controller

The test section of the fluid column is a vertical cylindrical tank operating in continuous flow without mixing. The test section has one inlet and one outlet, whose locations vary according to the desired configuration. The test section is covered, with the fluid filled right to the top cover; there is no free surface when the fluid column is filled. The test section is designed to study four different reactor geometries, two without baffles and two with baffles, as shown in Figures 4.2 through 4.5. These reactor geometries were chosen

to study the effect of geometrical configuration and the placement of baffles on the residence time distribution. The four geometries are described below:

Geometry #1 (G1) – a cylindrical tank with no baffles (Figure 4.2). A horizontal inlet is located at the top of the test section, directed towards the centre of the test section. A vertical outlet is located in the centre of the test section floor.

Geometry #2 (G2) – this geometry is similar to G1, with the inlet directed tangential to the cylindrical wall of the test section (Figure 4.3). G2 is designed to produce a swirling flow in the test section.

Geometry #3 (G3) – a cylindrical tank with two concentric, cylindrical baffles (Figure 4.4). The inlet is in the same location as G2, tangential to the wall of the test section. The two baffles extend the full height of the test section. Each baffle has a circular hole, located such that the flow changes direction (from down to up and vice versa) as it crosses each baffle. The outlet is in the same location as G1 and G2.

Geometry #4 (G4) – this geometry is annular, with eight flat, radial baffles (Figure 4.5). Four baffles extend the full height of the test section; these baffles alternate with four short baffles. Three of the four long baffles have circular holes at the top, while the fourth is solid, and separates the outlet from the inlet. Both outlet and inlet horizontal and are situated at the top of the test section. When looking from the top, fluid flows clockwise around the test section, switching vertical directions as it passes each baffle. This geometry is a much-simplified version of the periodic anaerobic baffled reactor (PABR) design as presented by Skiadas and Lyberatos (1998).

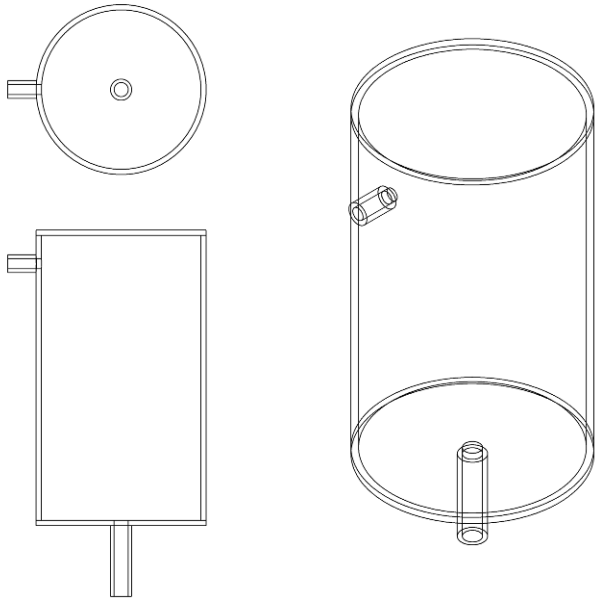

Figure 4.2: Fluid column test section Geometry #1 with centre inlet

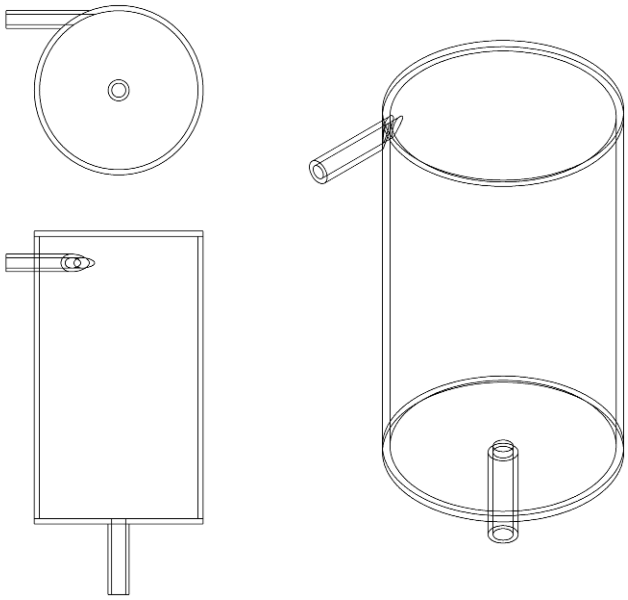

Figure 4.3: Fluid column test section Geometry #2 with side inlet

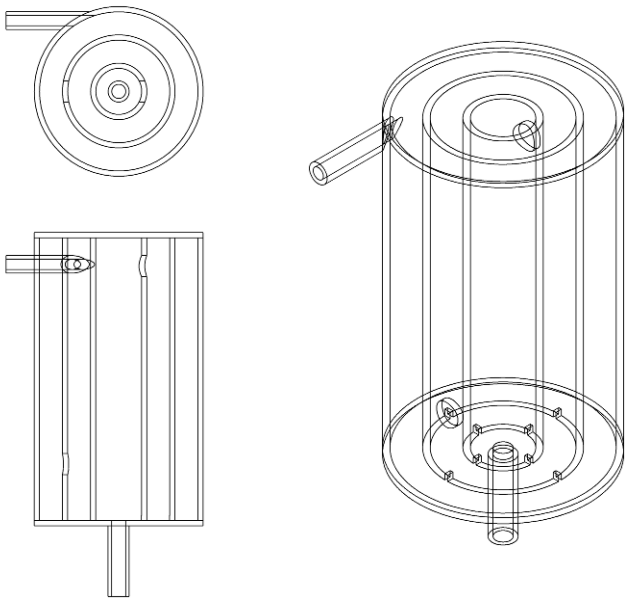

Figure 4.4: Fluid column test section Geometry #3 with concentric baffles

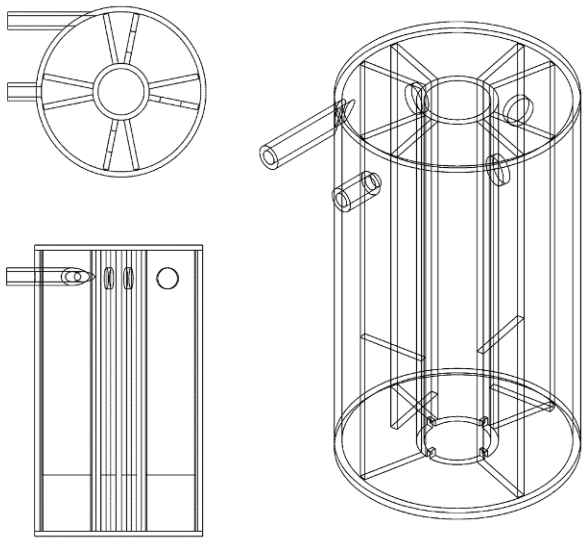

Figure 4.5: Fluid column test section Geometry #4 with radial baffles

4.1.2 Design criteria

As stated above, the aim of the fluid column facility is to study the relationship between reactor geometry, fluid properties, flow conditions, and residence time distribution in an anaerobic digester. The design criteria for the fluid column facility are:

1. The Reynolds number within the test section must be comparable to the Reynolds numbers experienced within a full-scale anaerobic digester.
2. Two experiments must be accommodated: a residence time distribution study; and a PIV study.
3. Accurate control of flow rates is required.
4. The hydraulic retention time of the test section may be varied between approximately 5 and 60 minutes (600 to 3600 s).
5. The working fluid can be interchanged. Water (Newtonian) and a 0.1% xanthan gum solution (non-Newtonian) may be used as the working fluid.
6. The system must have the ability to operate in open-loop and closed-loop modes. The closed-loop mode is required to recycle particles in the PIV study. The open-loop mode is required for the RTD tracer dye study.
7. The capability to select different inlet/outlet configurations is required.
8. The design of the facility must allow for future expansion. Specifically, the effects of mixing using mechanical agitation, jets, or bubble draft tubes may be studied in the future.

The technical criteria for the fluid column facility, which are more specific, are:

1. The fluid column facility can be operated by one person.

2. The test section is transparent, undistorted, and unobstructed to allow visual observation and PIV analysis.
3. Vibrations caused by the pump must be isolated from the laser, camera, and test section.
4. Tracer dye can be inject shortly upstream of the inlet without disrupting the flow.
5. The fluid can be sampled easily shortly downstream of the outlet without disrupting the flow.
6. The test section geometry can be changed without difficulty.
7. The usable volume of the supply and discharge tanks must be at least five times the volume of the test section.
8. The acrylic fluid column, supply tanks, and plumbing system must be watertight.
9. No significant corrosion issues may exist.
10. The system may be easily drained.

4.2 Description of experiments

The fluid column facility is designed to allow two separate sets of experiments: measuring the residence time distribution; and studying the flow field using particle image velocimetry. The RTD is an overall parameter that may be used to understand certain characteristics of the flow within a reactor. PIV is a technique by which the velocity and turbulence fields in a 2D plane are measured. A brief description of both of these techniques is provided below; for a more complete description, see the appropriate sections in Chapter 5.

The RTD of a reactor measures the time it takes for particles of fluid to travel from inlet to outlet. Since each particle of fluid will take a different path as it travels through the reactor, the RTD is not a single value, but rather a distribution. Experimentally, RTD can be determined by injecting a discrete pulse of tracer dye at the inlet of the reactor and measuring the concentration of dye at the outlet at regular intervals of time. This experiment should be performed over the course of several hydraulic retention times. One hydraulic retention time (HRT) is the theoretical time required for all of the fluid in the reactor to be replaced at a specified flow rate. Thus,

$$HRT = \frac{V}{Q} \tag{4.31}$$

where HRT is the hydraulic retention time of the reactor [s], V is the volume of the reactor [m^3], and Q is the volumetric flow rate through the reactor [m^3/s].

Particle image velocimetry uses microscopic, reflective particles to capture the flow characteristics in a 2D plane. The particles are illuminated by a double-pulsed sheet of laser light as they follow the flow through the test section. A high-speed digital camera is used to capture the locations of the particles at each pulse. When the correct density of particles is used, an instantaneous velocity field may be calculated from a pair of images; turbulence data and mean flow velocities may be calculated when an adequate number of images are taken over time.

4.3 Design of acrylic fluid column

The acrylic fluid column, as shown in Figure 4.6, is the central component of the fluid column facility. The fluid column is composed of two sections: the outer tank, and the test section. Within the test section, the flow conditions of an anaerobic digester are simulated. This test section can accommodate a variety of experiments, including tracer dye tests and PIV studies. The geometry of the test section can also be varied, as described in Section 4.1.1. The rectangular outer tank houses the test section, and is filled with water. The main purpose of the outer tank is to minimize the problems that are caused by the refraction of light in the cylindrical test section. This feature is especially important for PIV experiments. The refractive index of acrylic is 1.49, while that of water is 1.333. Housing the test section in the outer tank also allows greater flexibility in the geometry of the test section.

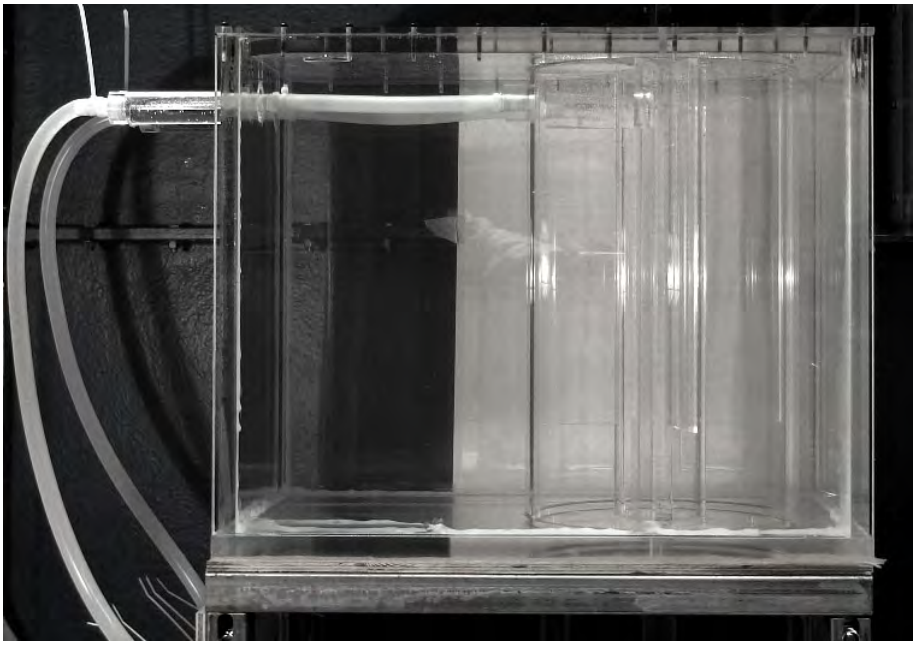

Figure 4.6: Acrylic fluid column

The outer tank is composed of a 25.4 mm (1 in.) thick floor piece, four 19 mm (3/4 in.) thick walls, and a 25.4 mm (1 in.) thick lid. All parts are cell cast acrylic. The walls and floor are bonded together using Weld-On #3, and sealed with silicone sealant. Three inlet/outlet tubes are also attached using Weld-On #16; two 152 mm (6 in.) tubes are attached to the left wall, and one 254 mm (10 in.) tube is attached to the floor. These tubes accommodate HDPE hose-barb fittings with an NPT thread; which in turn connect to flexible tube. The lid is countersunk, and is attached to the tank using machine screws. A 3.2 mm (1/8 in.) rubber O-ring sits in a groove around the perimeter of the lid, and creates a water-tight seal with the tank walls when the machine screws are fully tightened. The lid can be secured or removed in approximately two minutes, for easy access to the tank and test section. A 9.5 mm (3/8 in.) threaded hole drilled through the lid allows access to the test section. This hole is plugged with an acrylic screw when the fluid column is operating. The interior dimensions of the outer tank are: base 628 × 374 mm (24.75 × 14.75 in.); depth 495 mm (19.5 in.). The outer tank holds approximately 116 L, including the test section volume.

The test section is contained within a vertical acrylic cylinder with an outer diameter of 305 mm (12 in.). This acrylic cylinder is interchangeable; depending on the desired geometry, a cylinder with a centre port, side port, or double port may be used. The cylinder extends the full inner height of the acrylic tank. Two circular grooves—one in the floor of the tank, and the other in the lid—keep the cylinder in position. Each groove holds a rubber O-ring that seals the test section from the outer tank. The ports on the cylinder are connected to the inlet/outlet tubes on the left wall using flexible tubing. The

outlet tube in the floor of the tank is concentric with the test section cylinder. Cylindrical or flat baffles may be inserted into the test section to vary the geometry. The two cylindrical baffles have 102 and 203 mm (4 and 8 in.) outer diameters; each baffle contains a 38 mm (1.5 in.) diameter hole. The "flat baffle" assembly consists of a 51 mm (2 in.) diameter central tube, and eight flat baffles extending radially outwards to the test section cylinder wall. Four of these baffles are 394 mm (15.5 in.) long, while the other four extend the full height of the test section. The baffles and cylinders are all constructed from 9.5 mm (3/8 in.) thick acrylic. The working volume of the test section is approximately 32 L when no baffles are in place.

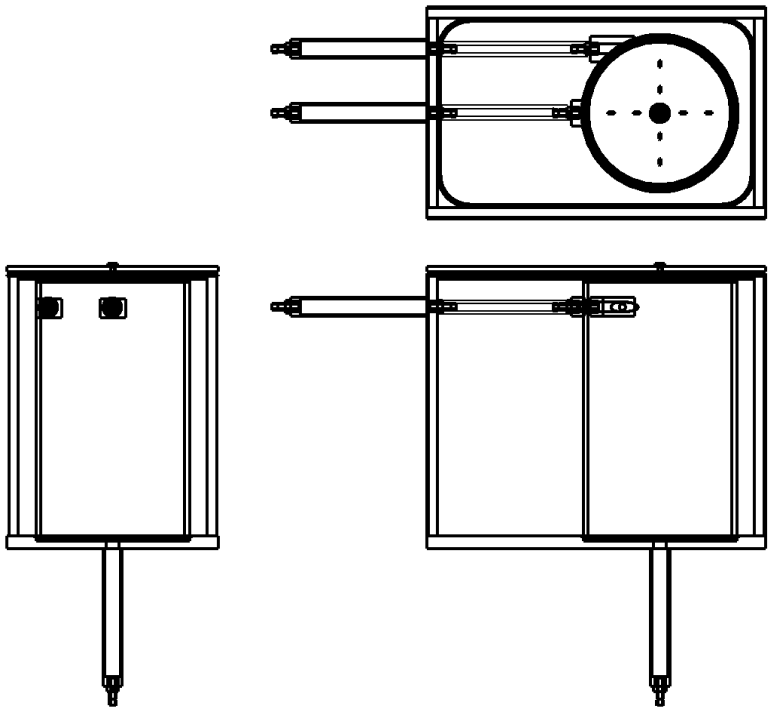

Figure 4.7: Acrylic fluid column – left, front, and top views

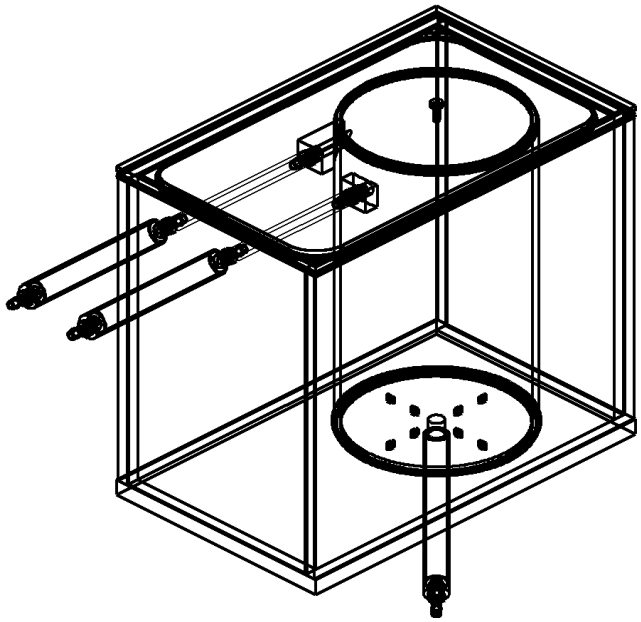

Figure 4.8: Acrylic fluid column – 3D view

4.4 Supply and discharge tanks

The supply and discharge tanks are two large plastic storage tanks elevated approximately 0.81 m (32 in.) off the ground (see Figure 4.9). Both tanks are open at the top to allow filling or mixing. The tanks drain from the bottom. When the system is running in open-loop mode, the working fluid flows from the supply tank through the pump, then through the fluid column, and into the discharge tank. When operating in closed-loop mode, only the discharge tank is used. The water flows from the discharge tank, through the system, and returns to the discharge tank. In general, the RTD studies were run in open-loop mode, so that the tracer dye injected before the fluid column would not be recycled during the experiment. Conversely, the PIV experiments were performed using closed-loop mode, in order to recycle the seeding particles. The capacity of each tank is approximately 180 L. Since the volume of the test section is approximately 32 L,

the fluid column facility can be run continuously for over five hydraulic retention times in open-loop mode. For instance, at a flow rate of 3 L/min, the pump runs for approximately one hour before exhausting the supply tank. In closed-loop mode, the system can be run as long as necessary.

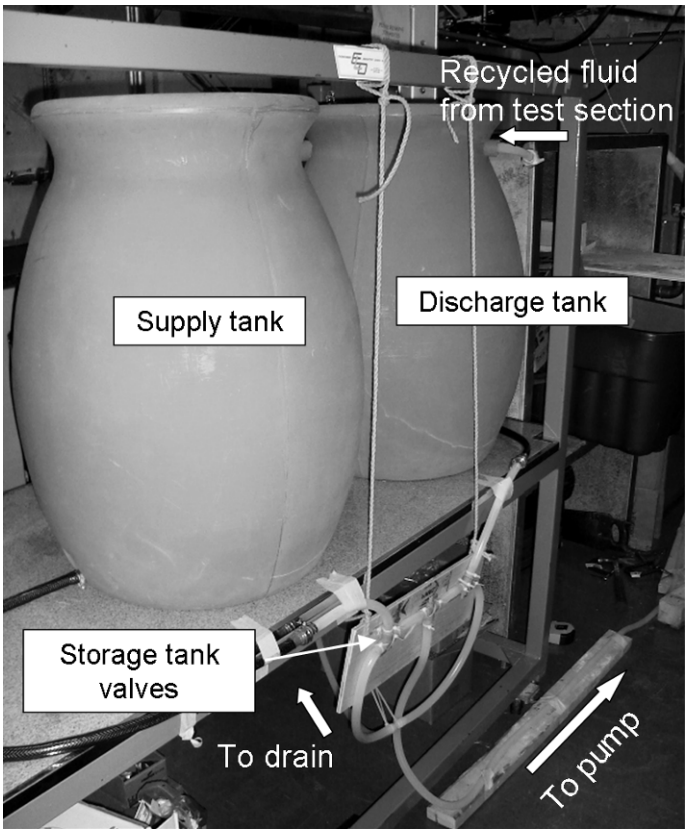

Figure 4.9: Supply and discharge tanks

4.5 Pump and plumbing system

The pump that drives the flow through the fluid column apparatus is a Masterflex® I/P peristaltic pump (see Figure 4.10). A peristaltic pump drives the flow by squeezing the fluid though a flexible tube. The tube is inserted between the housing and three rotating rollers. As the rollers rotate, the tube is occluded (squeezed), forming a “pillow” of fluid

that is pushed through the tube (Cole Parmer, 2006). Since a peristaltic pump creates a pulsating flow, a pulse dampener must be connected after the pump to dampen these pulses and create a smooth, constant flow. Peristaltic pumps deliver a flow rate that is dependent strictly on the rotational speed of the pump (except in the case of highly viscous fluids). Thus, the flow rate may be controlled directly.

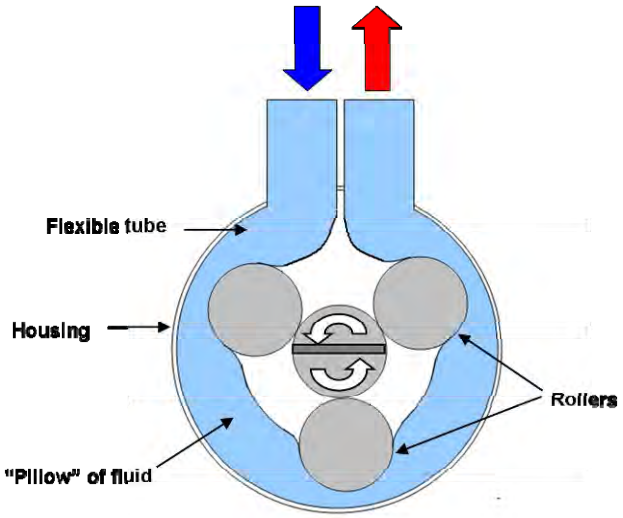

Figure 4.10: Peristaltic pump

A standard I/P pump head was combined with a variable-speed modular digital dispensing pump drive. This combination allows a range of flow rates from 0.45 L/min to 13.0 L/min. In general, it is important to keep flow rates under 3 L/min to avoid excessive air bubbles and pulsations in the flow. Once the pump has been calibrated, the flow rate is controlled directly using the digital controller. A Masterflex® pulse dampener connected after the pump dampens the pulses in the flow.

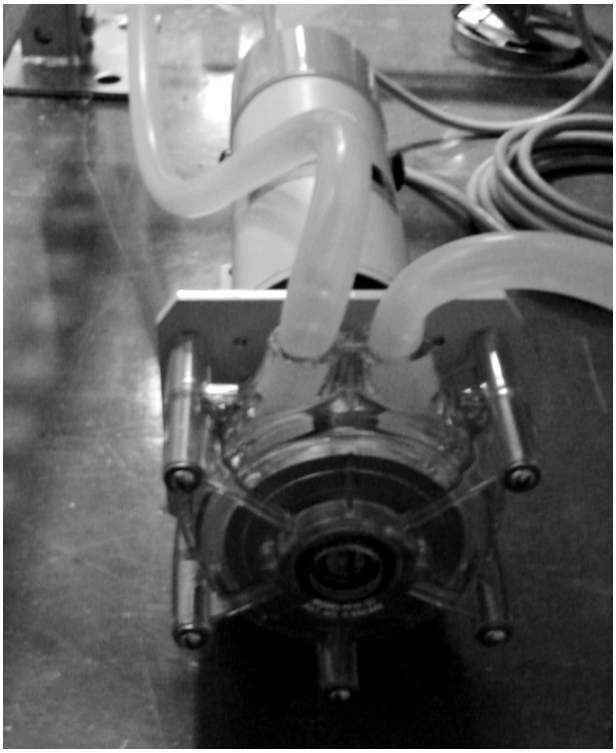

Figure 4.11: Masterflex® I/P variable speed pump drive and pump head

A hydraulic schematic of the plumbing system for the fluid column facility is shown in Figure 4.12. Fluid column ports are labeled P1 through P3; valves are labeled V1 through V8; fittings are labeled F1a and F1b. As mentioned earlier, the system operates in either open-loop or closed-loop mode. Flexible tubing of 1/2 in. (12.7 mm) inner diameter is used throughout most of the system, with a few exceptions: 3/8 in. (9.5 mm) entering and exiting the pulse dampener; 1/4 in. (6.4 mm) from the syringe to the quick disconnect coupling; and 1/4 in. (6.4 mm) from the stopcock (V8) to the test tubes. Table 4.1 describes the plumbing system components and their functions.

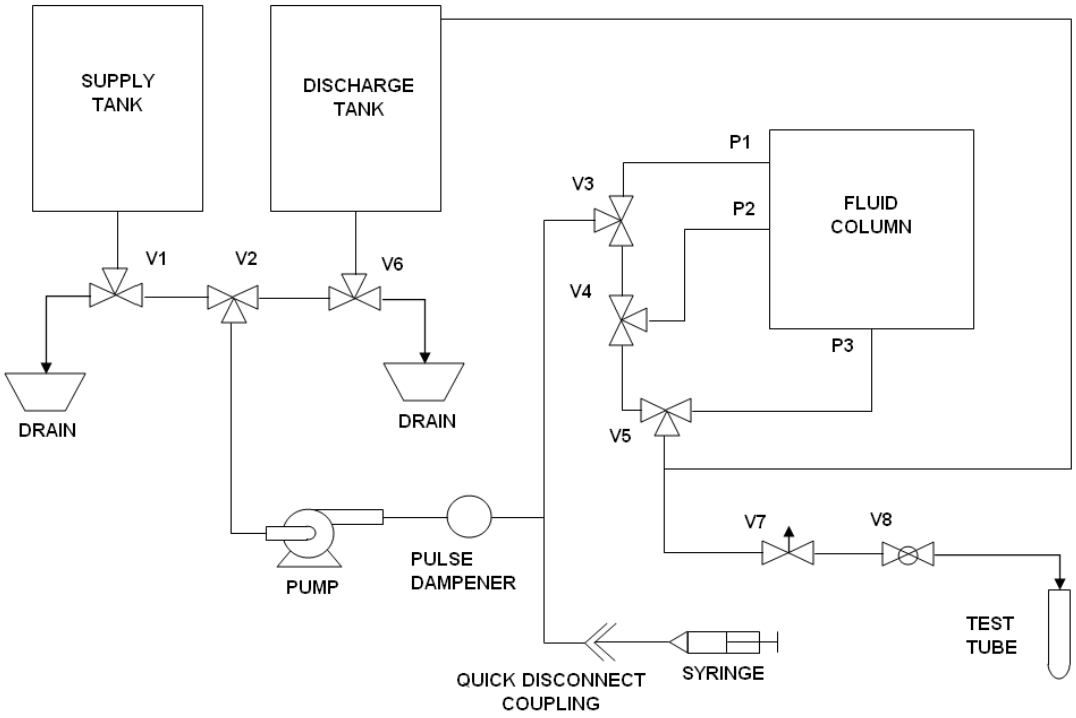

Figure 4.12: Hydraulic schematic of the fluid column facility

Table 4.1: Fluid column plumbing system components

Component	Description	Function
P1	Inlet port	Centre inlet for G1 and G4
P2	Inlet / outlet port	Side inlet for G2 and G3, outlet for G4
P3	Outlet port	Outlet for G1, G2, and G3
V1	Three-way ball valve	Supply tank valve Left to drain / Right to pump via V2
V2	Three-way ball valve	Tank selector valve Left for open loop / Right for closed loop
V3	Three-way ball valve	Inlet selector valve Up to P1 / down to P2
V4	Three-way ball valve	P2 selector valve Up for inlet / down for outlet
V5	Three-way ball valve	Outlet selector valve Left from P2 / Right from P3
V6	Three-way ball valve	Discharge tank valve. Left to pump via V2 / Right to drain
V7	Needle valve	Sampling station flow rate Controls the flow rate to the test tube
V8	Stopcock	Sampling station stopcock

The fluid column is connected to the plumbing system at three ports, labeled P1, P2, and P3. Port P1 delivers the flow to the test section via the centre inlet for geometry #1 (no baffles, centre inlet) and geometry #4 (radial baffles). Port P2 delivers flow through the side inlet for geometry #2 (no baffles, side inlet) and geometry #3 (concentric baffles). P2 also acts as the outlet for geometry #4. P3 acts as the outlet for geometry #1, #2, and #3. Six 3-way ball valves control the flow through the system. Storage tank valves V1, V2, and V3 control flow from the supply and discharge tanks. Valve V2 selects which tank fluid will be drawn from, either the supply tank (open-loop mode) or the discharge tank (closed-loop mode). Valves V1 and V6 allow drainage of the storage tanks. Flow control valves V3, V4, and V5 select the ports through which flow enters and exits the fluid column. Valve V7 is a needle valve that controls the flow rate of fluid to the test tubes at the sampling station. Valve V8 is an on/off stopcock used to fill the test tubes. Tables 4.2 and 4.3 summarize the positions of valves V1 through V6 for all functions of the fluid column system. It is crucial to assure that all valves are in the correct positions before starting the pump to avoid the rupture of water-tight seals.

Table 4.2: Positions of storage tank valves V1, V2, and V6

Valve	Open-loop	Closed-loop	Drain
V1	Right	N/A	Left
V2	Left	Right	N/A
V6	Right	Left	Right

Table 4.3: Positions of flow control valves V3, V4, and V5

Valve	G1	G2	G3	G4	Drain
V3	Up	Down	Down	Up	N/A
V4	N/A	Up	Up	Down	N/A
V5	Right	Right	Right	Left	Right

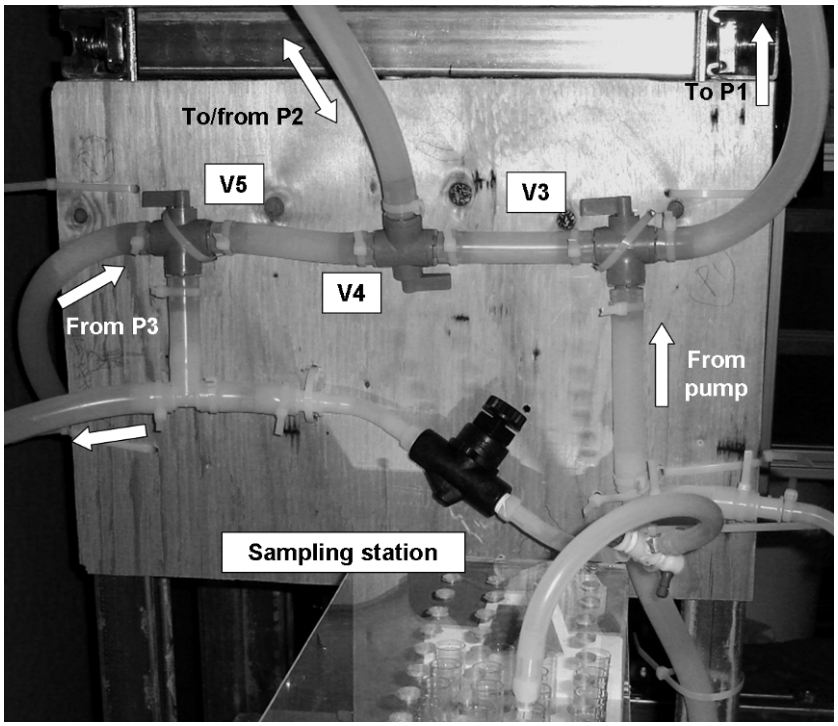

Figure 4.13: Flow control valves

4.6 Tracer dye injection and sampling stations

The RTD experiments involve injecting a florescent dye into the influent flow, and subsequently measuring the concentration of the dye in the fluid exiting the test section as it varies with time. The dye injection station connects with the plumbing system at a T-junction upstream of the inlet selector valve V3 (see Figure 4.14). Syringes are connected/disconnected via a non-spill quick-disconnect coupling. Two 20 mL syringes are used at the start of each test. The first syringe is filled with a 0.5 mg/mL solution of

rhodamine 6B fluorescent dye. Immediately after this syringe is dispensed, a second syringe filled with the working fluid (water or xanthan gum solution) is dispensed to ensure that all the dye enters the influent stream.

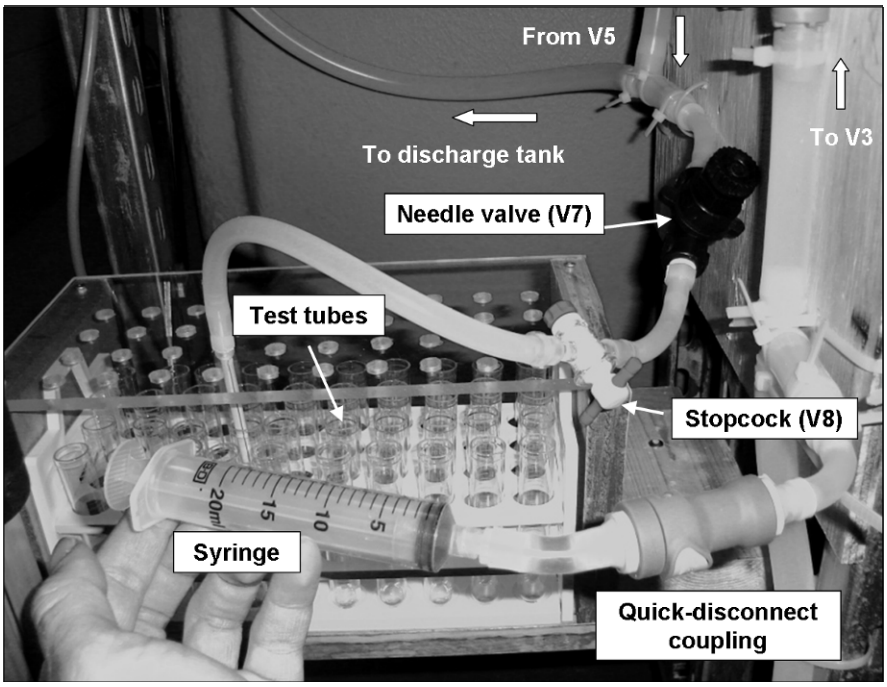

Figure 4.14: Dye injection station and sampling station

The sampling station is located at a T-junction downstream of the fluid column outlet and valve V5. Forty 15 mL test tubes are used for sampling the effluent fluid at regular time intervals. A needle valve is used to control the flow rate of fluid to the test tubes. A glass stopcock turns the flow on or off. The flexible tube used for the sampling station has an inner diameter of ¼ in. (6.4 mm) to reduce the volume of fluid that remains in the tube. The length of the sampling tube is approximately 17 in. (432 mm), so the volume retained by the tube is approximately 13.7 mL.

4.7 PIV system

The PIV system is comprised of four modular components: a PIV laser, a high-speed digital camera, the PIV processor, and software. A Gemini-PIV laser system from New Wave Research Inc. was used to illuminate the particles. This laser is a Class 4 Nd:YAG laser with dual heads. The fundamental frequency of the laser is 1064 nm (New Wave Research, Inc., 1998). A harmonic generator is used to produce a pulse of light at 532 nm, with a power output of 400 mL / 5 ns pulse at this frequency. The two laser heads are contained in one unit, along with the harmonic generator, alignment mirrors, and polarizer assembly. A lens is attached to this unit to focus the laser beam into a sheet of light. Each laser head is attached to its own self-contained power supply via an umbilical hose that contains electrical wires and cooling water tubes. The power supplies run off of a standard 120V AC source; each power supply draws 10A. Two control panels connected to the power supplies are used to fire the lasers and adjust the beam intensity. During PIV tests, the lasers are triggered by the PIV 2000 processor. Emergency shutdown of the PIV laser is triggered by pressing a “panic button” or opening one of the two curtains that enclose the laser hazard zone.

A Kodak Megaplus ES1.0 camera is used in the PIV system (see Figure 4.15). The Kodak Megaplus contains a 1k × 1k format CCD chip and is controlled electronically. This is important for PIV use because it allows fast inter-frame acquisition of two images (Dantec Dynamics, 1998). This camera is an asynchronous or still-frame-type camera, meaning that it will not capture images unless specifically instructed to do so. A Nikon

AF Micro-Nikkor 60 mm 1:28 D lens was used, with a filter to protect the camera against intense laser radiation.

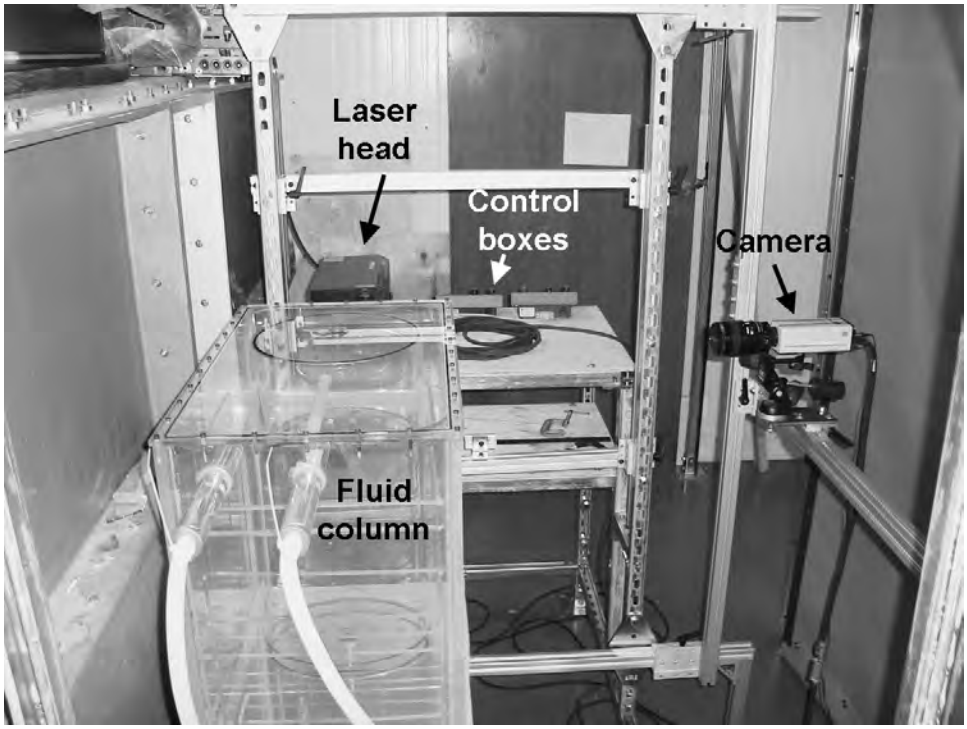

Figure 4.15: PIV laser and camera

The Dantec PIV 2000 Processor is a purpose-built dedicated vector processing unit. The processor has three units: a correlator unit, which produces vector maps quickly and efficiently; an input buffer, which reads the image maps from the camera; and the synchronization unit, which allows the laser system, camera, and software to communicate with each other. The FlowManager software package by Dantec Dynamics controls the PIV process, records the data, and is used to analyze the raw data.

Seeding particles are distributed in the fluid under study, and follow the flow. These seeding particles reflect the laser light, and their motion is used to determine the velocity fields in the 2D plane under study. The seeding particles used are 50 μm polyamide

particles from Dantec Dynamics; the density of these particles is approximately 1030 kg/m^3 (Dantec, 2009).

4.8 Design of support and sliding frames

A steel support frame acts as the rigid skeleton for the fluid column facility. A second, sliding frame is used for precise location of the PIV camera. These two frames are shown in Figure 4.16 as integrated into the fluid column facility.

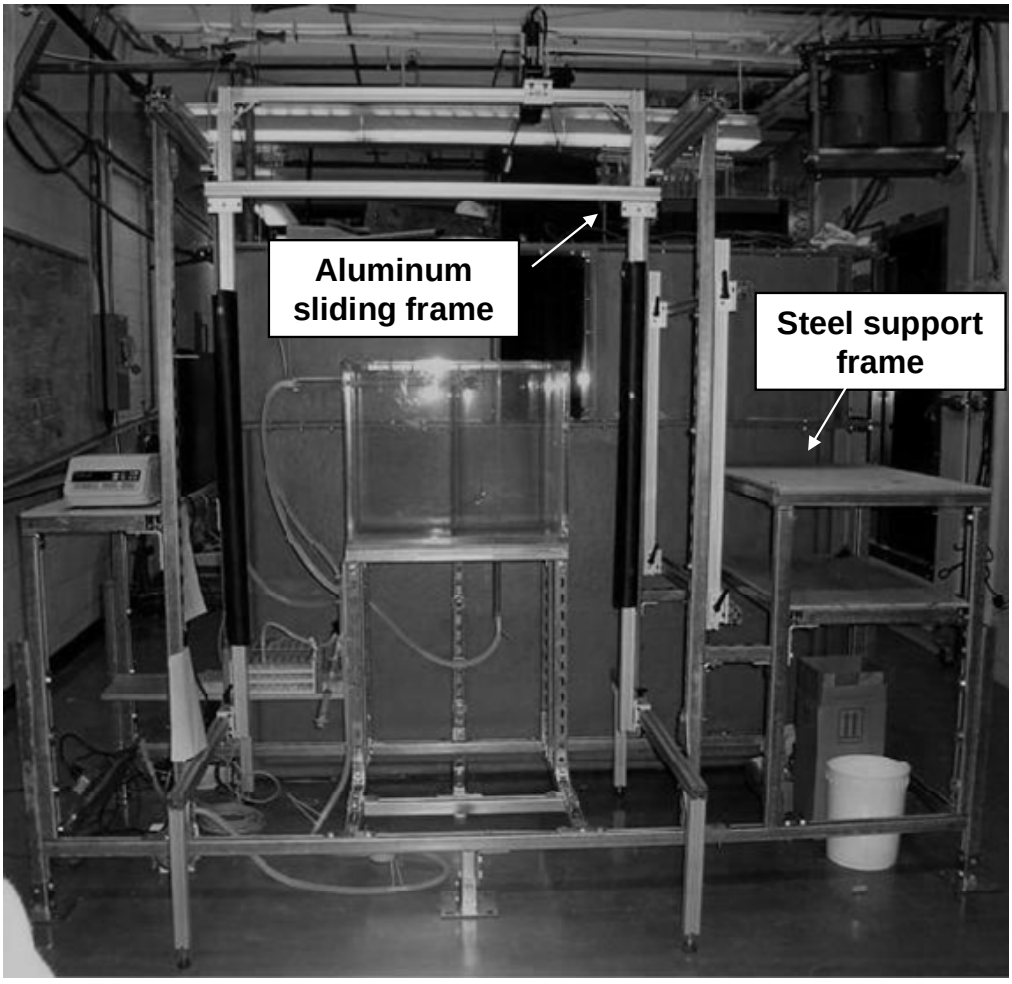

Figure 4.16: Fluid column facility with support and sliding frames

The steel support frame supports the acrylic fluid column, PIV laser, pump controller, flow control valves, and sampling and tracer dye injection stations, as well as the aluminum sliding frame. The frame is designed to contain the bulk of the fluid column facility to a footprint of approximately 3.0 × 0.91 m (120 × 36 in.). Six feet keep the support frame base approximately 150 mm (6 in.) off the floor. Five of these feet are adjustable for levelling purposes; the sixth foot (middle front) is fixed. The acrylic fluid column, weighing over 130 kg when filled, is the heaviest load on the frame. This load is distributed mostly on the two middle feet. The fluid column is situated at about chest-level for ease of observation. This poses a significant concern as a laser safety hazard, since the laser beam is nearly at eye level. Extra precautions, such as beam blockers, are incorporated to mitigate this hazard. In hindsight, the vertical position of the fluid column should have been lowered significantly to avoid this hazard.

The right shelves of the support frame support the laser. The laser may be positioned on either the bottom shelf to illuminate the lower region of the fluid column test section, or the top shelf to illuminate the upper region of the test section. Minor adjustments in laser height are done using blocks or shims. The left shelf of the support frame supports the pump controller. The two vertical sections on either side of the fluid column support the aluminum sliding frame. A drawing of the steel support frame is shown in Figure 4.17.

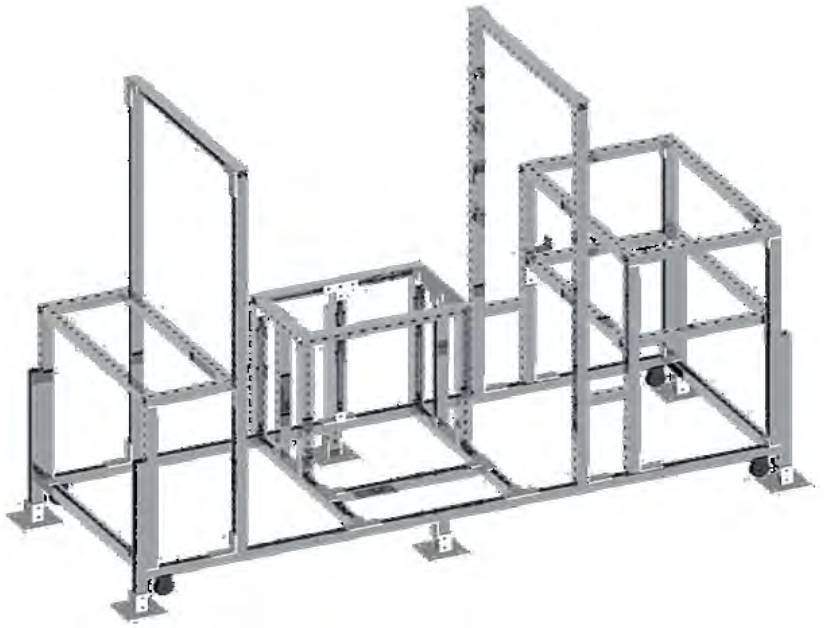

Figure 4.17: 3D rendering of steel support frame

The primary purpose of the aluminum sliding frame is to accurately position the PIV camera within one of two 3D zones, as shown in Figure 4.18. Zone 1 is in front of the fluid column; the camera is positioned in this zone when imaging vertical planes. Zone 2 is above the fluid column; the camera is positioned in this zone when imaging horizontal planes. Within these zones, the camera may be positioned between 152 and 813 mm (6 and 32 in.) away from the fluid column, to allow for the appropriate field of view.

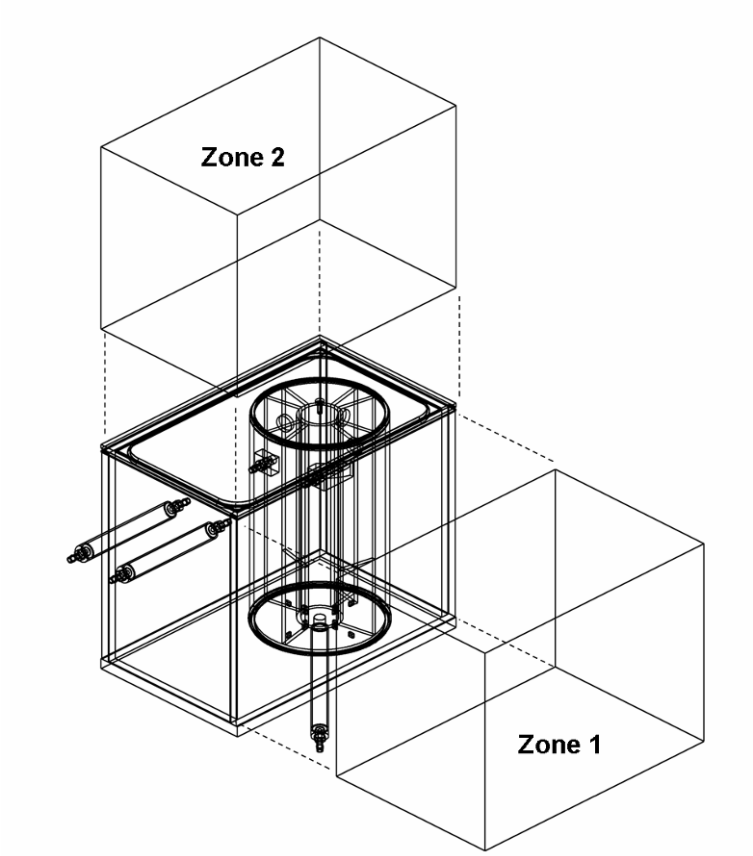

Figure 4.18: PIV Camera zones

The sliding frame is shown isolated from the rest of the fluid column facility in Figure 4.18; it is constructed using a modular t-slot aluminum profile system. The lower guide rails are attached to legs that sit directly on the floor. These guide rails are levelled independently of the support frame using levelling feet before attaching to the support frame. The upper guide rails are connected directly to the vertical members of the support frame. The U-subframe, which consists of two long vertical legs extending downward from a horizontal crossbeam, slides forward and backward on the lower and upper guide rails. The sliding crossbeam slides up and down on the legs of the U-subframe. The camera is normally mounted on the sliding crossbeam using a 3-way pan-tilt head; this

gives the camera six degrees of freedom. Alternatively, the camera may be mounted on the top crossbeam of the U-subframe, to extend the distance from the fluid column, and thus increase the field of view. Note that in certain situations, when the camera is above the fluid column (Zone 2), the right leg of the U-subframe may be removed to provide an unobstructed path for the laser beam.

Two vertical guide rails are located on the right side of the right vertical member of the support frame. Two crossbeams slide up and down on these vertical guide rails. Angled mirrors may be attached to these crossbeams to reflect the laser beam if required. However, since any reflective surfaces increase the hazard of stray beams, the use of these mirrors should be avoided.

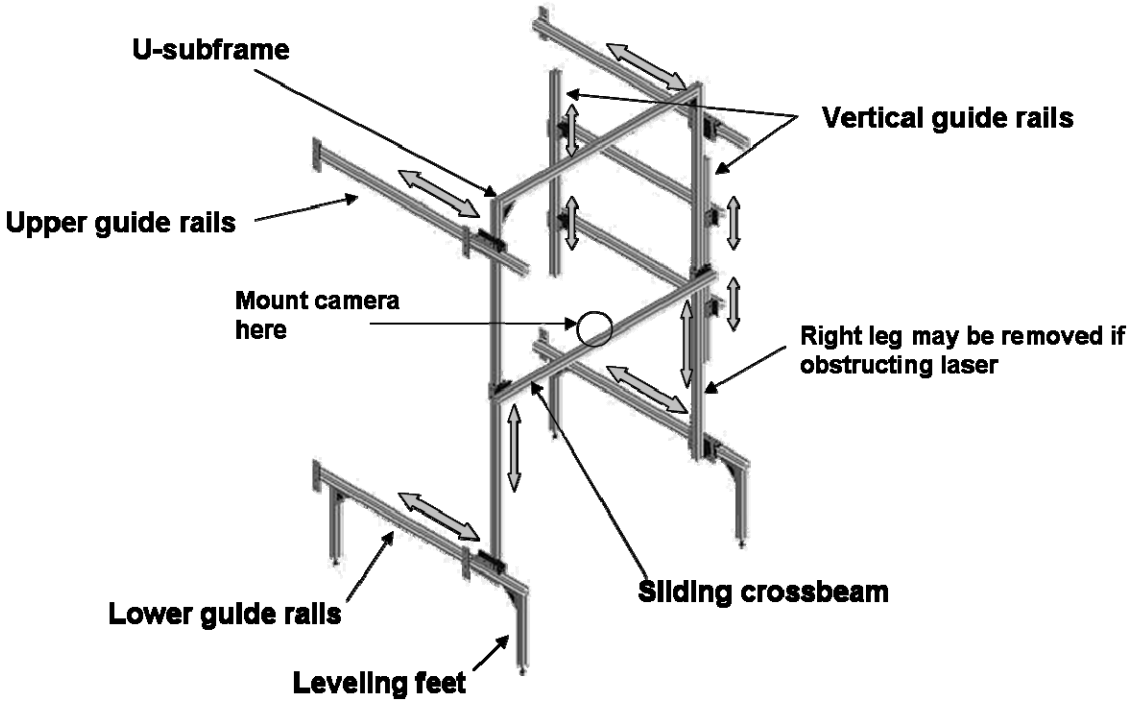

Figure 4.19: Aluminum sliding frame

4.9 Summary

The experimental fluid column facility described in this chapter provides an excellent tool for studying the flow characteristics of anaerobic digesters with various geometrical configurations. This apparatus facilitates tracer-response experiments that can be used to determine the residence time distribution (RTD) of a reactor, as well as PIV experiments to determine velocity fields within the reactor. Chapters 5 and 6 discuss these experiments in detail.

Currently, the fluid column facility is designed to simulate and study the flow characteristics of a continuous-flow anaerobic digester without forced mixing. However, many anaerobic digesters employ mixing in the form of mechanical agitation or bubble mixing. Refer to Appendix H for a description of possible methods of incorporating forced mixing into the fluid column facility.

Chapter 5. Experimental study of residence time distribution

5.1 Introduction

A key parameter in the performance of most chemical reactors or bioreactors is the residence time distribution (RTD). Continuous-flow reactors and semi-batch reactors are designed based on an appropriate hydraulic residence time (HRT). The HRT is the mean time that particles of fluid take as they travel from inlet to outlet; it is calculated by dividing reactor volume by flow rate. If the HRT of a reactor is too small, the fraction of reactants converted to products (percent conversion) will be low. Conversely, if the HRT is too high, the percent conversion will be high, but the reactor volume will be used inefficiently. However, in a real reactor, only a very small fraction of fluid elements will travel from the inlet to the outlet in exactly one HRT; some elements will spend much less time in the reactor, and others will spend much more. This distribution of fluid element residence times, the RTD of a reactor, can be a good indicator of how a reactor will perform.

One of the most common anaerobic digester designs is the continuously stirred tank reactor (CSTR) or complete-mix reactor. Ideally, the CSTR is mixed such that the composition and temperature are uniform through the reactor. While this mixing enhances the reaction, it produces an unfavourable RTD. The RTD of a complete-mix reactor is an exponentially decaying function; thus a large fraction of fluid leaves the reactor well before one HRT, and another large fraction of fluid leaves well after one

HRT. Since unconverted feed is continuously removed from the reactor, a high retention time is required to achieve a reasonable percent conversion (Skiadas and Lyberatos, 1998).

5.1.1 Overview of the RTD study

The objective of this study was to investigate the effects of geometry, flow rate, and viscosity on the flow characteristics of a simulated anaerobic digester, by measuring the residence time distribution. Experimental results were obtained using the fluid column facility described in Chapter 4. The experiments involved a stimulus-response technique in which a fluorescent dye was injected at the inlet of the fluid column test section, and the concentration of the dye was measured with time.

Four different reactor geometries were studied; detailed descriptions of these geometries are given in Chapter 4. All of the geometries involve a vertical cylindrical tank with a single inlet and a single outlet. Geometry #1 (G1) has a horizontal inlet situated near the top of the cylinder, directed towards the centre. Geometry #2 (G2) is similar to G1, but the inlet is directed tangential to the cylinder wall. Geometry #3 (G3) has two concentric cylindrical baffles. All three of these geometries have a vertical outlet located at the centre of the cylinder floor. A fourth geometry, G4, has eight radial baffles that separate the test section into four compartments arranged in a circular manner; each compartment has an upflow and a downflow section. Both inlet and outlet are located near the top of the tank. This geometry is based on a much simplified version of the periodic anaerobic baffled reactor (PABR) described by Skiadas and Lyberatos (1998).

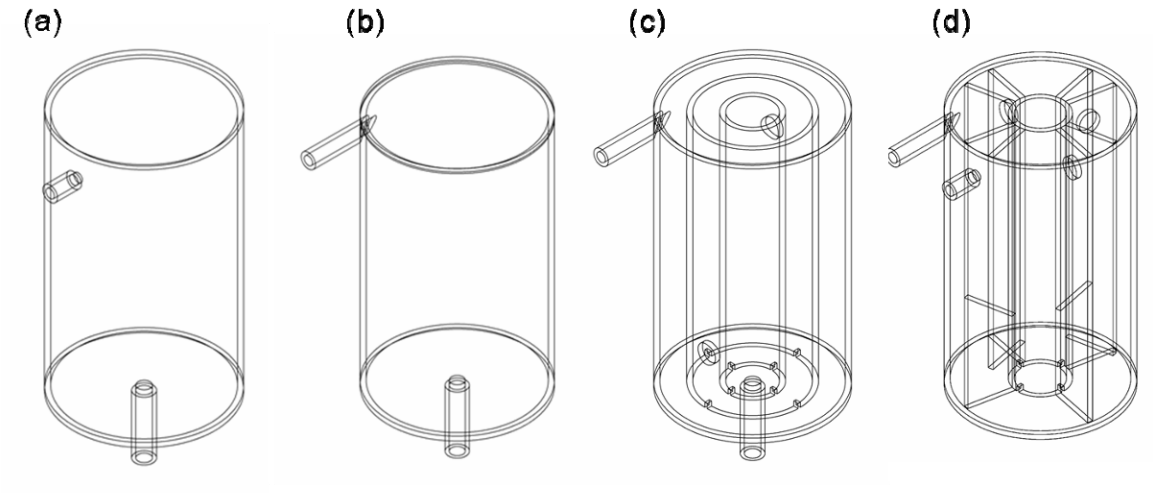

Figure 5.1: Four test geometries. a) G1 centre inlet, b) G2 side inlet, c) G3 concentric baffles, d) G4 radial baffles

Two working fluids were used in the study; water and a 1.0 g/L xanthan gum solution. While water is a Newtonian fluid, the xanthan gum solution exhibits a non-Newtonian behaviour that can be described using the power law. The xanthan gum solution is used to simulate the non-Newtonian properties of liquid manure.

The effect of flow rate on residence time distribution was also studied. The fluid column facility was operated at 0.05 L/s (3.0 L/min) and 0.0125 L/s (0.75 L/min), resulting in hydraulic retention times of approximately 600 s (10 min) and 2400 s (40 min), respectively. The exact HRT was dependent on geometry, since each geometry possessed a slightly different working volume. In total, 12 experimental cases were studied.

Table 5.1: RTD experimental test matrix

Case #	Description	Fluid	Flow rate (L/s)	Target HRT (s)
1	G1: centre inlet	H2O	0.05	600
2	G1: centre inlet	H2O	0.0125	2400
3	G2: side inlet	H2O	0.05	600
4	G2: side inlet	H2O	0.0125	2400
5	G3: concentric baffles	H2O	0.05	600
6	G3: concentric baffles	H2O	0.0125	2400
7	G4: radial baffles	H2O	0.05	600
8	G5: radial baffles	H2O	0.0125	2400
9	G1: centre inlet	XG	0.05	600
10	G2: side inlet	XG	0.05	600
11	G3: concentric baffles	XG	0.05	600
12	G4: radial baffles	XG	0.05	600

5.1.2 Residence time distribution

The residence time distribution of a reactor is the distribution of times that are required for elements of fluid to pass through the reactor (Levenspiel, 1972). The time taken for a fluid element to travel from inlet to outlet is called the exit age of that element. A residence time distribution curve is generally defined such that the area under the curve equals 1 (see Figure 5.2). At any location t on the time axis, the area under the curve to the right of t represents the fraction of fluid at the outlet that has an exit age greater than t. Conversely, the area of the curve to the left of t represents that fraction of fluid leaving the reactor with an exit age less than t. The residence time distribution is also called the exit age distribution, and is represented by the variable E(t).

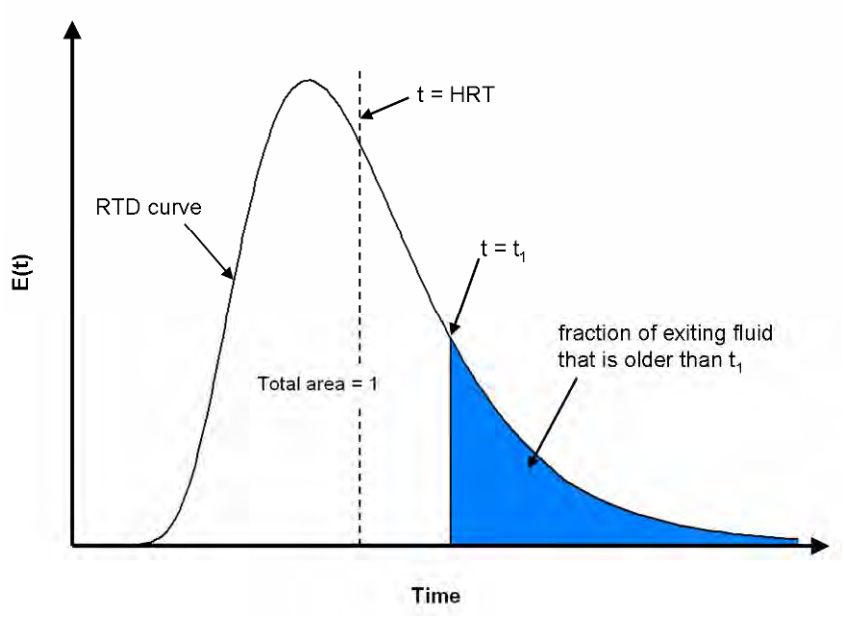

Figure 5.2: The residence time distribution (RTD) curve (Levenspiel, 1972)

The mean time represents the average age of the fluid at the outlet of the reactor. For a closed vessel, this is:

$$t_m = \int_0^\infty tE(t)dt \tag{5.32}$$

In an ideal reactor, the mean time is equal to the hydraulic retention time, or:

$$t_m = HRT = \frac{V}{Q} \tag{5.33}$$

where V is the volume of the reactor and Q is the volume flow rate. However, in non-ideal conditions, this is not necessarily the case, and the value of t_m with respect to the HRT is often useful in diagnosing poor reactor design. For example, if t_m < HRT, this indicates the presence of stagnant zones within the reactor; thus, the effective volume of the reactor is reduced. Another variable used to characterize the RTD of a reactor is the variance, given for a closed vessel as (Levenspiel, 1972):

$$\sigma^2 = \int_0^\infty (t - t_m)^2 E(t) dt = \int_0^\infty t^2 E(t) dt - t_m{}^2 \tag{5.34}$$

There are two types of ideal continuous-flow reactors that will be discussed briefly – the plug flow reactor and the continuously stirred tank reactor (CSTR). A third type of reactor, the batch reactor, is not continuous flow, so it will not be discussed here. In a plug flow reactor, all fluid moves uniformly through the reactor from inlet to outlet (see Figure 5.3). There is no forward or backward mixing or diffusion. Thus, the residence time is the same for all elements of fluid in a plug flow reactor. A CSTR on the other hand, is completely mixed—the contents of the reactor are uniform throughout. Therefore the effluent from a CSTR has the same composition as the fluid within the reactor. The RTD of a CSTR is an exponentially decaying function.

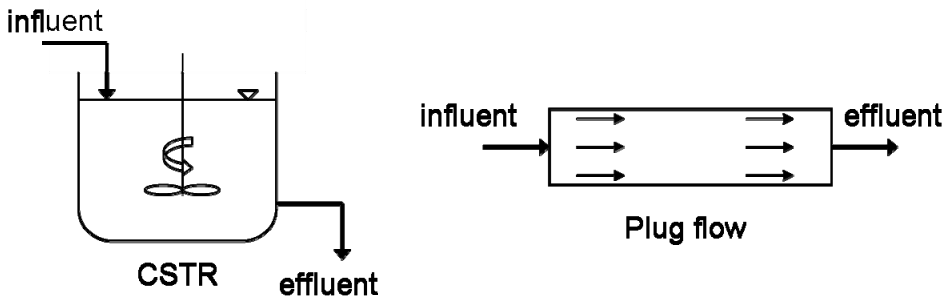

Figure 5.3: Ideal reactors

The RTD curves of both ideal reactors are shown in Figure 5.4 as a function of the normalized time θ, which is calculated as:

$$\theta = \frac{t}{HRT} \tag{5.35}$$

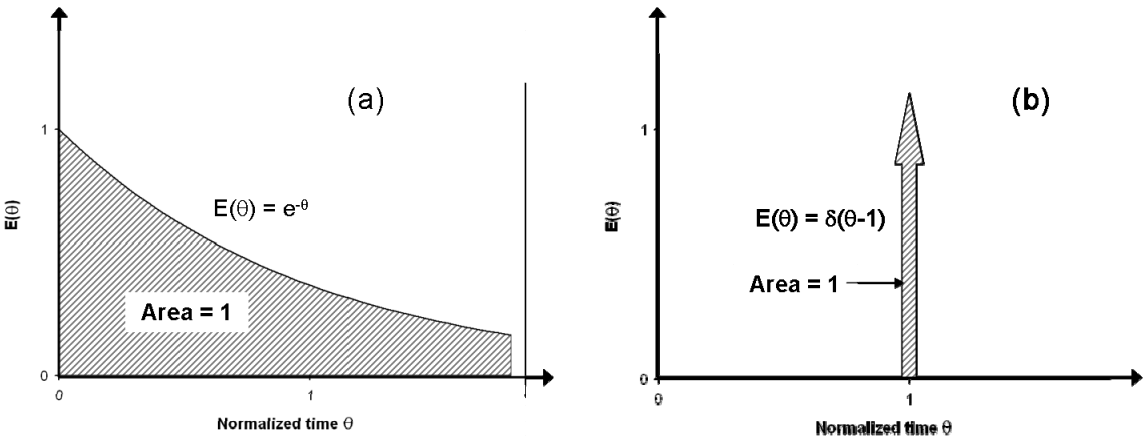

Figure 5.4: RTD curves for ideal reactors. a) CSTR, b) plug flow reactor

The residence time distribution of a reactor is directly related to that reactor's response to an input. The two most common inputs used to determine the RTD of a reactor are a step input and a pulse input of an inert tracer at the inlet of the reactor. The outlet response to a step input is represented by F(t), while the response to a pulse is represented by C(t). For a closed vessel, F(t) and C(t) are related to E(t) as follows (Levenspiel, 1972):

$$E(t) = C(t) = \frac{dF(t)}{dt} \tag{5.36}$$

A variety of single- and multi-parameter models have been used to simulate the performance of reactors. Often, these models are developed by adjusting a set of parameters to fit an experimental RTD curve. The models are then used to predict chemical and biological reactions within the reactor. A widely-used single-parameter model is the tanks-in-series model, which assumes that the reactor can be approximated as a system of complete-mix reactors of equal volume, connected in series. The RTD for N tanks in series is given by (Levenspiel, 1972):

$$E(\theta) = \frac{N(N\theta)^{N-1}}{(N-1)!} e^{-N\theta} \tag{5.37}$$

The parameter N is directly related to the normalized variance of the RTD curve as follows:

$$\sigma_\theta^{\,2} = \frac{\sigma^2}{(HRT)^2} = \frac{1}{N} \tag{5.38}$$

Thus, an RTD curve may be fit to the tanks-in-series model by setting the parameter N to the inverse of the normalized variance. A small value of N (thus, a large variance) indicates that the reactor more closely resembles a CSTR. As the value of N increases, the RTD approaches that of a plug flow reactor.

The residence time distribution of a reactor provides information on the history of fluid as it exits the reactor—that is, the RTD describes how long it has taken for fluid to pass through the reactor. However, the RTD provides little information on mixing, which is an important characteristic of the reactor. The RTD does provide some information on the macromixing; macromixing is how fluid elements of different ages are mixed together. For example, a plug flow digester has no macromixing—fluid elements of different ages are kept separate—but a complete mix digester has infinite macromixing. In general, the variance is a good indicator of macromixing. A large variance indicates a high degree of macromixing, while a small variance indicates a small degree of macromixing. However, the RTD does not indicate how early or late macromixing occurs, called the earliness of mixing. Thus, a reactor in which macromixing occurs very early may have the same RTD as a reactor in which fluid elements of different ages are kept segregated until they are mixed together at the outlet. The RTD also provides no information on micromixing, or the degree to which individual molecules are mixed together. For example, a plug flow

reactor and an infinite series of CSTRs exhibit the same RTD. However, the series of tanks involves vigorous mixing at each stage, whereas the plug flow reactor may have no mixing at all. For these reasons, the current study does not examine the mixing characteristics of anaerobic digesters, only the residence time distribution.

5.2 Literature review

Grobicki and Stuckey (1992) performed RTD studies on the anaerobic baffled reactor (ABR) developed by Bachmann et al. (1983). The ABR is a rectangular reactor with a number of compartments in series, separated by vertical baffles. Each compartment contains an upflow and a downflow section. The RTD was measured on clean reactors using tap water, as well as on reactors inoculated with digester sludge. Four reactors were studied, with working volumes ranging from 7 800 L to 10 400 L; reactors with four, six, and eight compartments were studied. The HRT of the reactors were varied from 1 to 80 hours. They concluded that the ABR could be characterized as a series of well-mixed CSTRs with low dead space. The greater the number of compartments in the reactor, the closer the reactor mimicked a plug-flow reactor.

Li and Choplin (1992) reviewed RTD studies in the literature that involved non-Newtonian fluids. A summary of experimental and theoretical results was presented for a variety of reactor types, such as: the stirred tank reactor, tubular reactor, annular reactor, and scraped-surface heat exchanger. The flow behaviour index n (see Equations 3.3 and 3.4) was noted as an important parameter, and results were given over a range of n covering both pseudoplastic and dilatant fluids. It was also noted that pseudoplastic fluids

($n < 1$) generally influenced the RTD towards a plug-flow distribution, while dilatant fluids ($n > 1$) influenced the RTD towards that of the CSTR case.

Gravilescu and Tudose (1996) measured the RTD of an external-loop airlift bioreactor. This bioreactor incorporated both air-bubble mixing as well as recirculation. They found that the RTD of this reactor oscillated while decaying exponentially; these oscillations corresponded to the recycling of the fluid through the external loop. The RTD was analyzed using the dispersion model and the tanks-in-series model.

A novel reactor design, the periodic anaerobic baffled reactor (PABR), was described by Skiadas and Lyberatos (1998). The PABR can operate as an anaerobic baffled reactor (ABR), upflow sludge blanket reactor (UASBR), or in an intermediate mode. The PABR consists of an annular region separated into four compartments arranged in a circular manner. The order in which fluid flows through the compartments is switched at regular intervals. The performance of the PABR was measured using RTD tests and COD removal studies.

Bello-Mendoza and Sharratt (1999) developed a compartment mixing model based on an RTD study of a simulated anaerobic digester with confined-gas mixing. The digester was experimentally simulated using a 400 L continuous-flow vessel with a centrally-mounted draft tube. Compressed air provided the driving force for the mixing. The RTD studies were performed using tap water and a NaCl tracer. They found that the traditional multiparameter models used to analyze the RTD results lacked physical meaning. They

introduced a compartment-based mixing model composed of an ideally-mixed compartment to represent the area around the draft tube, and two cascades of tanks-in-series to represent the circulating flow on each side of the draft tube. The three model parameters were the ratio of ideally-mixed volume to total volume; the number of tanks in each cascade; and the circulation period.

Batstone et al. (2000) assessed the hydraulic characteristics of a full-scale, two-stage hybrid upflow anaerobic reactor treating pig slaughterhouse effluent. They found that the steady state RTD was very similar to that of a CSTR. A two-tank hydraulic model with a 15:1 tank volume ratio was used to analyze the data.

Liu et al. (2007) measured the RTD of three periodic anaerobic baffled reactors (PABRs) used for treating industrial wastewater from a Chinese traditional medicine production process. The working volume of each reactor was 18 L, and the reactors were operated at a HRT of 2 days. Tests were performed using both tap water and sieved digester sludge. A lithium chloride solution was used as a tracer. Three switching modes were tested: clockwise sequential with a switching period of 4 days; every second compartment with a period of 2 days; and no switching (infinite switching period or ABR mode). It was found that the fraction of dead space was lowest for the “every second” switching mode, while the fraction of dead space was highest for the ABR mode.

Roussinova and Kresta (2008) investigated the relationship between blend time and RTD for a stirred tank. They defined the blend time as the time required for the normalized

tracer concentration variance to decay to within 5% of the final mean concentration. Recommendations were made for the design of a CSTR. These include: a line from the inlet to the outlet should go through the impeller; and the ratio of HRT to blend time should be no less than 10.

5.3 Experimental methods

5.3.1 RTD experimental procedure

To measure residence time distribution, the method described by Levenspiel (1972) was used. In this method, a pulse of tracer fluid is injected at the inlet of the reactor during operation, and its concentration is measured at the outlet over a period of several HRT. The tracer used in the current experiments was a 20 mL pulse of 0.5 mg/mL rhodamine B fluorescent dye. The dye was injected via syringe upstream of valve V3 (see Figure 5.5). A second syringe, filled with 20 mL of the working fluid (either water or xanthan gum) was injected directly after the dye to push the dye into the main fluid stream. A stopwatch was started after the second syringe had been completely dispensed. Forty samples were collected in test tubes at the sampling station downstream of valve V5 over a time period of approximately two to three HRT. The volume of each sample collected was approximately 15 mL. The concentration of rhodamine B in each sample was measured by fluorescence, and a RTD curve was constructed from the relative concentrations of dye measured at each time interval.

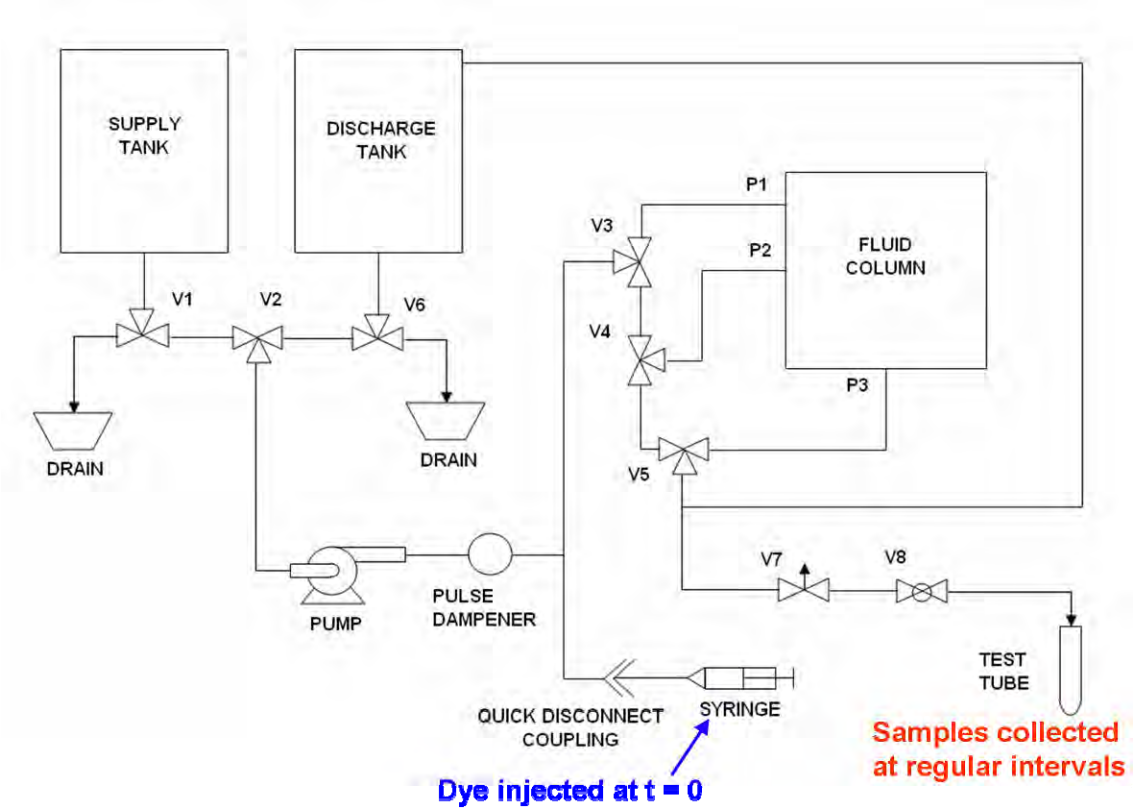

Figure 5.5: System diagram of the fluid column facility, indicating dye injection and sampling stations

For the RTD experiments, the fluid column facility was operated in open-loop mode to prevent the tracer dye from being recycled through the system. If the working fluid to be used was xanthan gum, 150 L of 1.0 g/L xanthan gum solution was prepared prior to the test (see next section for details on the preparation of the solution). Otherwise, the supply tank was filled with 150 L of tap water. The system was operated at a steady flow rate for five to ten minutes before starting the test to ensure steady state conditions. Also prior to starting the test, approximately 100 mL of fluid was drained into a beaker at the sampling station to ensure that residual dye from the previous experiment was removed.

The pump was calibrated by measuring the time taken for 6.0 L of fluid to flow through the system. This volume of fluid was measured by accumulating the fluid in a graduated container. Once calibrated, the flow rate could be controlled directly through the digital pump controller. The flow rate was checked before each series of experiments to ensure the proper flow rate through the system.

5.3.2 Preparation of xanthan gum solution

For each test run involving xanthan gum, 150 L of solution had to be prepared. The solution was prepared in three stages, adding 40 L of tap water and 10 L of a concentrated xanthan gum (5 g/L) solution at each stage. The solution was mixed after each stage using an electric drill and a 135 mm diameter paint mixer. The concentrated solution was prepared 1.0 L at a time using a blender. Each time, five grams of xanthan gum powder was added to 1.0 L of tap water, and the solution was blended on a low setting for 30 s at room temperature. After blending, the consistency of the concentrated solution was uniform with the exception of air bubbles. These bubbles were generally released when the concentrated solution was added to the 1 g/L solution. After the full 150 L was prepared, a 600 mL sample was collected to measure the viscosity of the solution.

5.3.3 Fluorescence analysis

The fluorescent characteristics of rhodamine B were used to measure its concentration at the test section outlet. From each 15 mL sample collected during the experiment, four

200 μL volumes were drawn using a micropipette. These volumes were dispensed on a 96 well plate. Two plates were used for each test (160 volumes in total from 40 samples). A BioTek® Synergy™ 4 Multi-Mode Microplate Reader with the Gen5 software package was used to detect the fluorescence of the samples. An excitation wavelength of 540 nm was used; emissions were detected at 625 nm. Since four measurements were performed for each sample, the average value was used for all calculations. The average standard deviation for these measurements was 5% to 10%.

5.4 Initial calculations

Several initial calculations were performed prior to the analysis of the RTD experimental results. First, the volume of each geometry was calculated; the volume differs between geometries due to the presence of baffles. The hydraulic residence time (HRT) was then calculated based on the reactor volume and volumetric flow rate (Equation 5.33). The inlet and outlet velocities and inlet and outlet Re were also calculated. Other calculations included in this section are: the standard concentration curves for the fluorescence of rhodamine B; the calculation of power law parameters for xanthan gum from experimental data; and overall parameters used for the analysis of RTD curves.

5.4.1 Geometry and volume calculations

The volume of the fluid column test section was calculated based on a cylinder of diameter 0.286 m and height 0.495 m. Since G1 and G2 have no baffles, they have the same volume. For the baffled geometries G3 and G4, the volume of the baffles was

calculated and subtracted from the volume of the cylinder. These volumes are shown in Table 5.2. For the RTD experiments, the entire volume that the fluid must flow through between the tracer injection point and the location of sampling should be included to find an accurate HRT. The volume that is not a part of the test section—inlet and outlet tubes, flexible tubing, and valves—are shown in line 5 of Table 5.2. Since this extra volume accounts for less than 2% of the total working volume, it was neglected. The volume of the sampling tube is also shown; this is also a very small value, and was neglected from all calculations. The volumes of the CFD model geometries are slightly larger than the actual test section volumes because they include the inlet and outlet volumes (see Chapter 6 for further detail). Thus, the actual volumes for G1 to G4 will be used in all subsequent calculations.

Table 5.2: Fluid column volume

Geometry	Volume - actual (m^3)	Volume - CFD (m^3)
G1	0.031764	0.032090
G2	0.031764	0.032103
G3	0.027615	0.027865
G4	0.024662	0.024866
Inlet / outlet tube	0.000551	N/A
Sample tube	0.000014	N/A

5.4.2 Calculation of HRT

The hydraulic retention times were calculated using Equation 5.33, based on the volume and flow rate for each case. The target HRTs of 600 s (10 min) and 2 400 s (40 min) were based on an approximate test section volume of 30 L. For the target HRT of 600 s, the flow rate was set to 0.05 L/s (3.0 L/min); for the target HRT of 2 400 s, the flow rate was

set to 0.0125 L/s (0.75 L/min). The actual values of HRT for all four geometries are shown in Table 5.3.

Table 5.3: Actual hydraulic retention times for each geometry

		Target HRT = 600 s		Target HRT = 2 400 s	
Geometry	**Volume (L)**	**Q (L/s)**	**HRT (s)**	**Q (L/s)**	**HRT (s)**
1	31.764	0.05	635.3	0.0125	2541.1
2	31.764	0.05	635.3	0.0125	2541.1
3	27.615	0.05	552.3	0.0125	2209.2
4	24.662	0.05	493.2	0.0125	1973.0

5.4.3 Inlet and outlet velocities and Reynolds numbers

The inlet and outlet velocities were calculated based on the flow rate, as shown in Table 5.4. These values represent the mean velocities, as given by:

$$u_m = \frac{4Q}{\pi D^2} \quad [m/s] \tag{5.39}$$

where D is the inlet or outlet diameter [m] and Q is the volume flow rate [m^3/s]. The mean velocities give a good indication of the velocity scale found in the test section; generally, the maximum velocity magnitude has an upper limit of approximately $1.5u_{in}$.

Table 5.4: Inlet and outlet mean velocities

			Flow rate = 0.05 L/s		Flow rate = 0.0125 L/s	
Geometry	**D_{in} (m)**	**D_{out} (m)**	**u_{in} (m/s)**	**u_{out} (m/s)**	**u_{in} (m/s)**	**u_{out} (m/s)**
1 – 3	0.0183	0.0254	0.190	0.0987	0.0475	0.0247
4	0.0183	0.0183	0.190	0.190	0.0475	0.0475

The Reynolds numbers at the inlet and outlet were calculated as shown in Table 5.5. Typically, the value of Re_{in} is the most important parameter when comparing to other

data found in the literature. The Reynolds number for a Newtonian fluid (such as water) is defined as:

$$\mathrm{Re}_D = \frac{\rho u_m D}{\mu} \tag{5.40}$$

where ρ is the density of the fluid [kg/m^3], μ is the dynamic viscosity [Pas], D is the characteristic diameter [m], and u_m is the mean velocity [m/s]. In Table 5.5, the inlet and outlet diameters and mean velocities were chosen to calculate Re. Another possible choice would be to use the diameter of the test section and mean velocity through the test section (calculated as flow rate divided by cross-sectional area). However, there are definite shortcomings to this option, since the mean velocity through the test section is in no way representative of the range of velocities produced in the test section. Secondly, the insertion of baffles changes the effective hydraulic diameter; for G3 and G4, the hydraulic diameter varies with position in the test section. Thus, the Reynolds number at the inlet and outlet is the best choice.

Table 5.5: Inlet and outlet Reynolds numbers

		Water		Xanthan gum	
Flow rate	**Geometry**	**Re_{in}**	**Re_{out}**	**Re_{in}**	**Re_{out}**
0.05 L/s	1 - 3	3479	2506	266.6	116.0
0.05 L/s	4	3479	3479	266.6	266.6
0.0125 L/s	1 – 3	869.7	626.6	32.73	14.24
0.0125 L/s	4	869.7	869.7	32.73	32.73

For non-Newtonian fluids, μ is not constant, but varies with flow rate and with position inside the tube. Thus, Equation 5.40 cannot be used for fluids such as xanthan gum solutions. Metzner and Reed (1955) defined the Reynolds number for a power-law fluid as:

$$\mathrm{Re}_{NN} = \frac{\rho u^{2-n} D^n}{8^{n-1} K} \tag{5.41}$$

where K is the consistency coefficient [Pa·s^n] and n is the flow behaviour index [dimensionless]. For a 1.0 g/L xanthan gum solution, K = 0.126 Pa·s^n, while n = 0.487 (Speers and Tung, 1986).

Assuming that the transition from laminar to turbulent flow occurs at Re = 2100, it can be seen that turbulence is most likely encountered for the cases where the working fluid is water and the flow rate is 0.05 L/s (Cases 1, 3, 5, and 7 in Table 5.1). However, turbulent flow was also visually observed from the motion of the tracer dye for the water cases with flow rates of 0.0125 L/s. This is probably due to a number of turbulence triggers within the plumbing system, including the pump, step expansions and contractions, valves, and threads.

5.4.4 Standard curves for rhodamine B

For the fluorescence test data to be useful for RTD analysis, the linearity was tested. Dilutions of rhodamine were prepared using both tap water and xanthan gum, and the fluorescence response was measured. As seen in Table 5.6, the fluorescence response readings are linear over a dye concentration range of approximately 9.8×10^{-6} to 2.5×10^{-3} g/L for water, and 2.4×10^{-5} to 6.25×10^{-3} for xanthan gum. The fluorescence response of rhodamine in water is about twice the response of rhodamine in xanthan gum. The correlation is excellent for both of these curves (above 0.998).

Table 5.6: Fluorescence response for rhodamine B dye in water and xanthan gum

Water		Xanthan Gum	
Concentration (g/L)	**Fluorescence**	**Concentration (g/L)**	**Fluorescence**
4.000E-02	Overflow	5.000E-02	Overflow
2.000E-02	Overflow	2.500E-02	Overflow
1.000E-02	Overflow	1.250E-02	Overflow
5.000E-03	Overflow	6.250E-03	82694
2.500E-03	55113	3.125E-03	45613
1.250E-03	26669	1.563E-03	20826.5
6.250E-04	12008	7.813E-04	9618.75
3.125E-04	6226	3.906E-04	4935
1.563E-04	3482	1.953E-04	2174.5
7.813E-05	1752	9.766E-05	986.5
3.906E-05	749	4.883E-05	562
1.953E-05	434	2.441E-05	263.25
9.766E-06	252		
Slope	2.194E+07		1.3495E+07
R	0.99942		0.99875

5.4.5 Viscosity calculations for xanthan gum

Viscosity measurements were taken for each batch of xanthan gum prepared using a Brookfield DVII+PRO viscometer. 600 mL of xanthan gum were sampled from the large, 150 L batch before starting each RTD experiment. Eleven shear rates between 2.2 and 44.0 s^{-1} were tested in both ascending and descending order. The raw viscosity measurements ranged from an average of 105.4 mPa·s at the lowest shear rate to 22.9 mPa·s at the highest shear rate. This data was then fit to the power law model; the results are given in Table 5.7. See Chapter 3 for more detail on measuring viscosity and viscosity models.

Table 5.7: Empirical power law parameters for xanthan gum, 1.0 g/L

	Ascending			Descending		
Batch	**K (Pa·s^n)**	**n**	**R**	**K (Pa·s^n)**	**N**	**R**
1	0.1535	0.4799	0.9864	0.1486	0.4905	0.9948
2	0.1775	0.4454	0.9893	0.1576	0.4770	0.9975
3	0.1644	0.4681	0.9923	0.1610	0.4708	0.9972
4	0.1419	0.5001	0.9923	0.1601	0.4686	0.9969
Average	0.1593	0.4734		0.1568	0.4767	
St dev	0.01523	0.02285		0.00565	0.00981	

As seen in Table 5.7, the order in which the shear rates were tested (ascending or descending) did not significantly affect the data. Thus, for the 1.0 g/L xanthan gum solution used in the RTD tests, the consistency coefficient K and flow behaviour index n were measured as 0.158 Pa·s^n and 0.475 respectively. These values are very close to the values given by Speers and Tung (1986), as mentioned in Section 5.4.3.

5.5 Results and discussion

5.5.1 Visual observations

Images of the G1 centre inlet test section taken throughout an RTD experiment are shown in Figure 5.6. The flow rate is 0.05 L/s, and the working fluid is water. At this flow rate, the hydraulic retention time is 635 s.

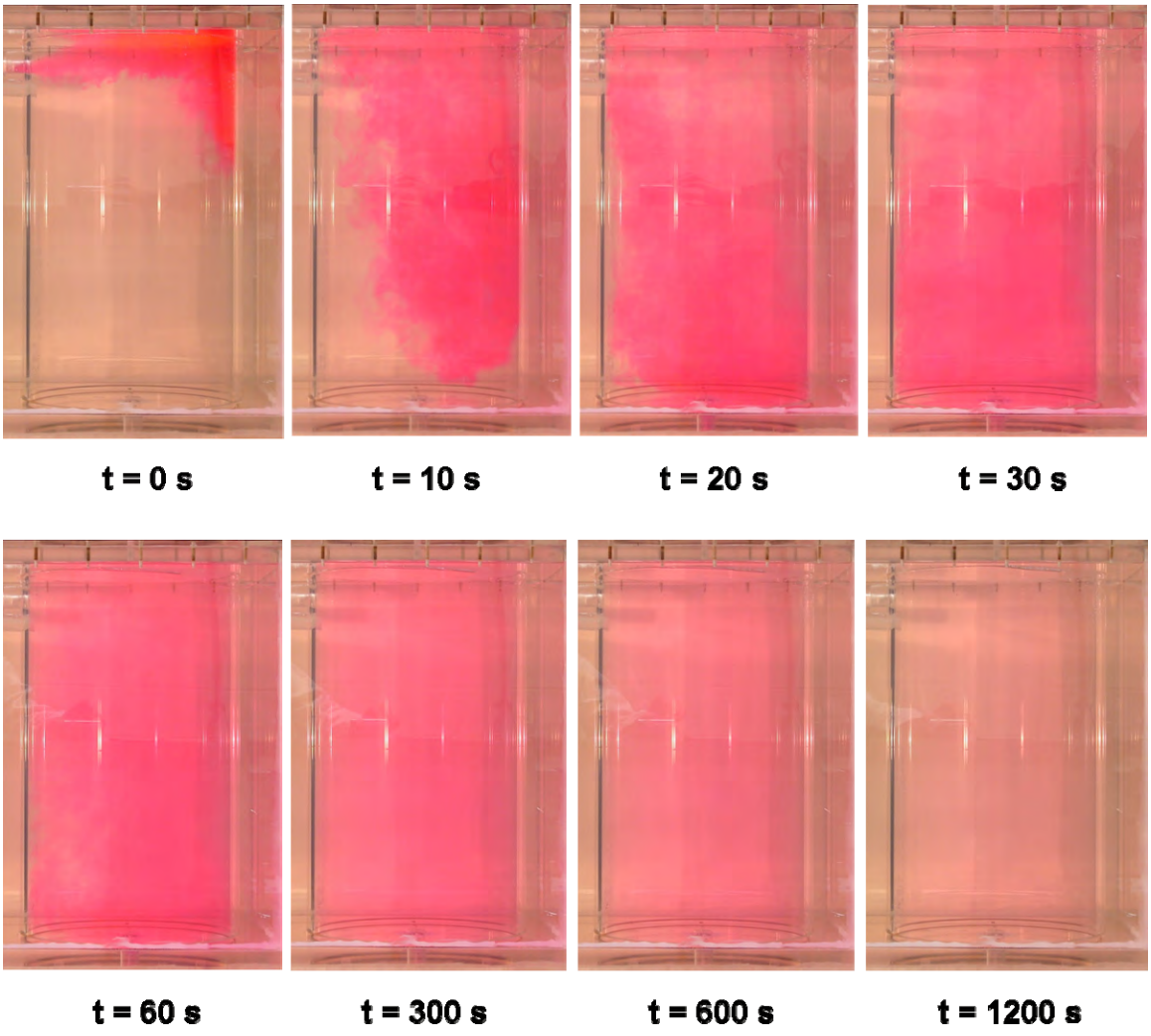

Figure 5.6: Tracer dye flowing through G1 test section, flow rate = 0.05 L/s

As seen in the figure, rhodamine tracer dye enters the test section from the centre inlet in a turbulent jet that impinges against the far wall of the cylinder. The tracer spreads throughout the test section, and is almost fully dispersed by t = 60 s (θ = 0.094). From this point on, the concentration of tracer in the test section is slowly diluted; at t = 1200 s (θ = 1.89) there is still a visible amount of tracer left. From these visual observations, it is expected that the RTD for G1 in water might resemble the exponential decay of a CSTR,

with a small delay of approximately 0.1 HRT. This hypothesis is confirmed in the following subsection.

Figure 5.7 shows images of the G4 radial baffles test section after dye has been injected. The flow rate and working fluid are the same as the previous case; however, the HRT is much smaller (493 s vs. 635 s) due to the volume occupied by the baffles. It is immediately apparent that this geometry behaves very differently than G1. The tracer dye travels through all four compartments in a counter-clockwise direction, entering from the top of each compartment and descending quickly through the first section, then ascending slowly through the second section. The downward section of each compartment has a smaller cross-section than the upward section, so the fluid experiences higher velocities in the former. In an actual digester with suspended solids, these characteristics would increase the retention of solids by promoting settling. As the tracer moves through each compartment, it slowly disperses. The tracer is flushed out of the G4 test section much quicker than the G1 centre inlet case; by t = 900 s (θ = 1.83) almost all of the tracer is gone. It may be surmised that this geometry behaves similar to a dispersed plug flow reactor, with a nearly bell-shaped RTD.

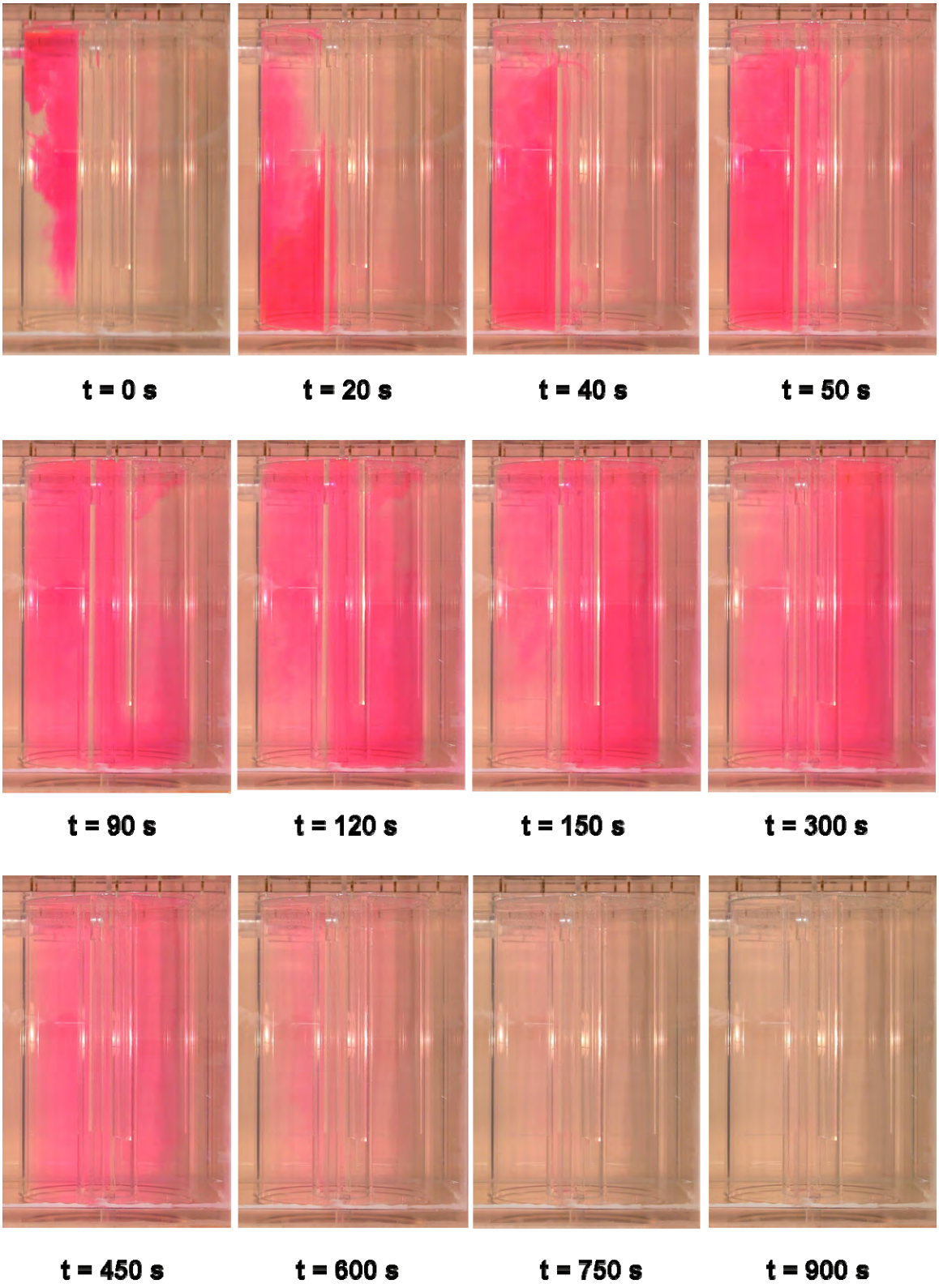

Figure 5.7: Tracer dye flowing through G4 test section, flow rate = 0.05 L/s

5.5.2 Fluorescence response data and interpretation

During the RTD experiment, a 15 mL test tube was filled at each time step. To measure the concentration of rhodamine dye, four fluorescence measurements were taken for each test tube. The average of these values was used to evaluate the concentration at each time step. This data is shown in Figure 5.8 for the G1 centre inlet geometry, with a flow rate of 0.05 L/s and water as the working fluid. Three trials were performed to ensure the repeatability of the experiment.

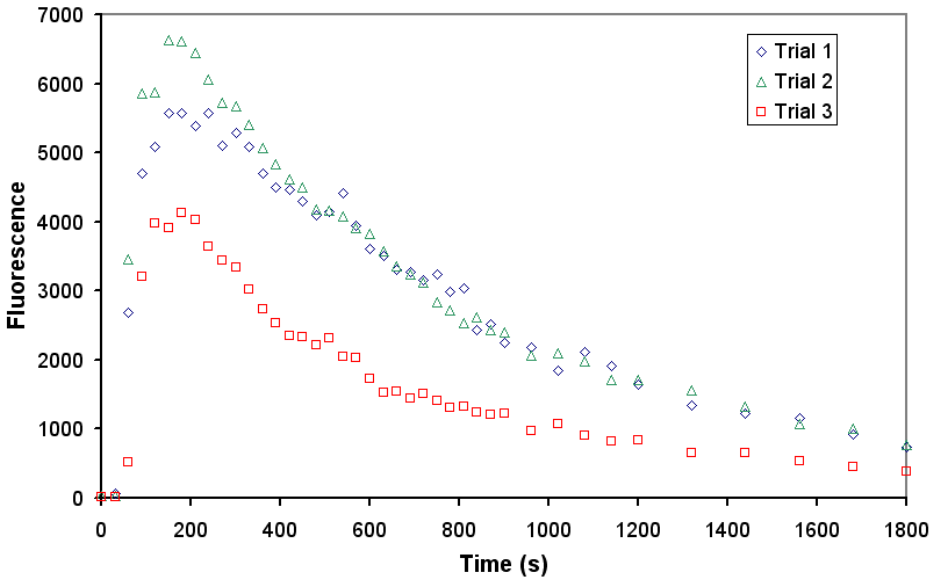

Figure 5.8: Fluorescence data for G1 centre inlet; H_2O; 0.05 L/s

As seen in Figure 5.8, the shape of the RTD curve is similar for all three trials; however, the magnitude differs for each case. The data was normalized by the integrated area under each curve. A significant problem arose when considering the tail of the RTD curves. The linearity of the fluorescence readings is doubtful for readings less than 250; data under this value was therefore rejected. To replace the tail data, the curve was extrapolated using an exponential function:

$$Fls(t > \theta_n) = c_1 \exp(-c_2\theta) \tag{5.42}$$

where *Fls* is the fluorescence reading, θ is the normalized time after tracer injection, θ_n is the cutoff time, and c_1 and c_2 are constants. To determine the constants c_1 and c_2, a linear regression of the last five data points (θ_{n-4} through θ_n) was performed, yielding a slope m and a y-intercept b. Using m and b, c_1 and c_2 were determined as follows:

$$c_2 = -\frac{m}{m\theta_{n-2} + b} \tag{5.43}$$

$$c_1 = \frac{m\theta_{n-2} + b}{\exp(-c_2 + \theta_{n-2})} \tag{5.44}$$

The area under this exponential tail was then calculated by integrating equation 5.42 from θ_n to ∞. This integral was then added to the integrated area under the actual data, as calculated by the trapezoid rule. Figure 5.9 demonstrates these calculations; the normalized time θ is shown on the x axis.

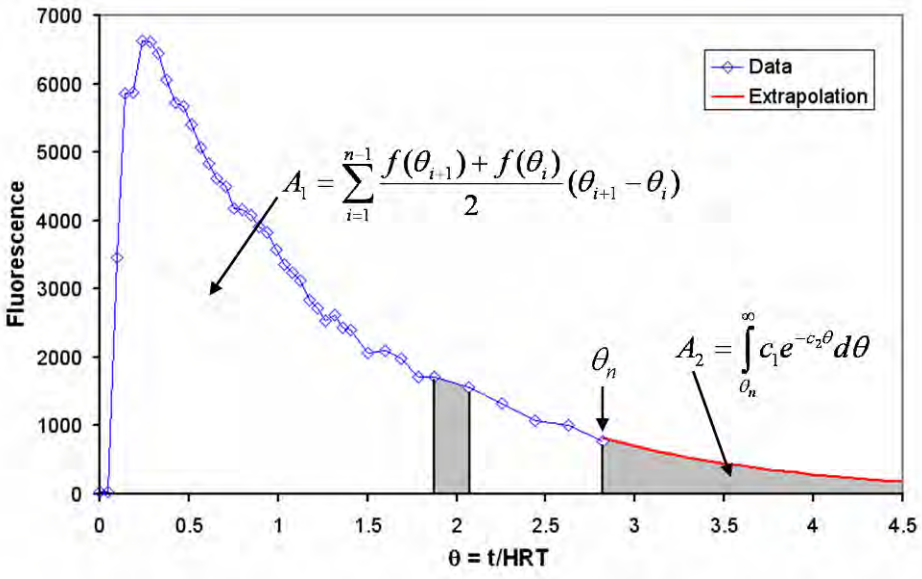

Figure 5.9: Fluorescence data with extrapolation for G1; H_2O; 0.05 L/s

The experimental data was then normalized according to:

$$E(\theta) = \frac{Fls(\theta)}{A_1 + A_2} \tag{5.45}$$

where A_1 and A_2 are the integrated areas under the experimental data and the exponential tail, respectively. Figure 5.10 shows the final normalized E(θ) curves for all three trials. These curves match each other well, with the exception of the height of the peak. This confirms the repeatability of the experiment.

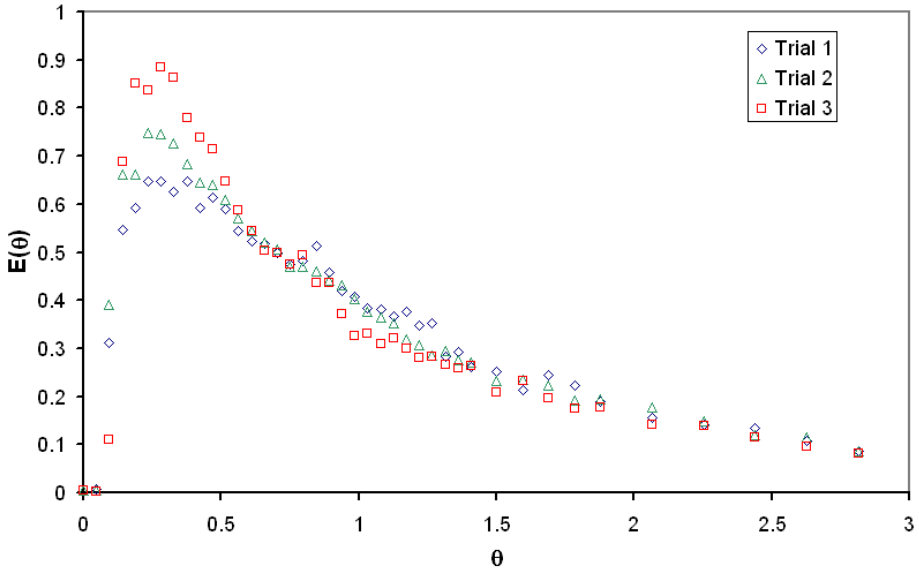

Figure 5.10: Normalized RTD curves for G1 centre inlet; H_2O; 0.05 L/s

5.5.3 Residence time distribution – effect of geometry, flow rate, and fluid viscosity

The geometry of a reactor plays a crucial role in determining its residence time distribution. In the current study, four geometries were investigated, as previously described. The key characteristics of these geometries are: impingement of the inlet jet on the cylinder wall in G1; swirling flow in G2; and the effect of baffles in G3 and G4.

Figures 5.11 to 5.13 compare the RTD for these four geometries when the flow conditions (working fluid and flow rate) are held constant.

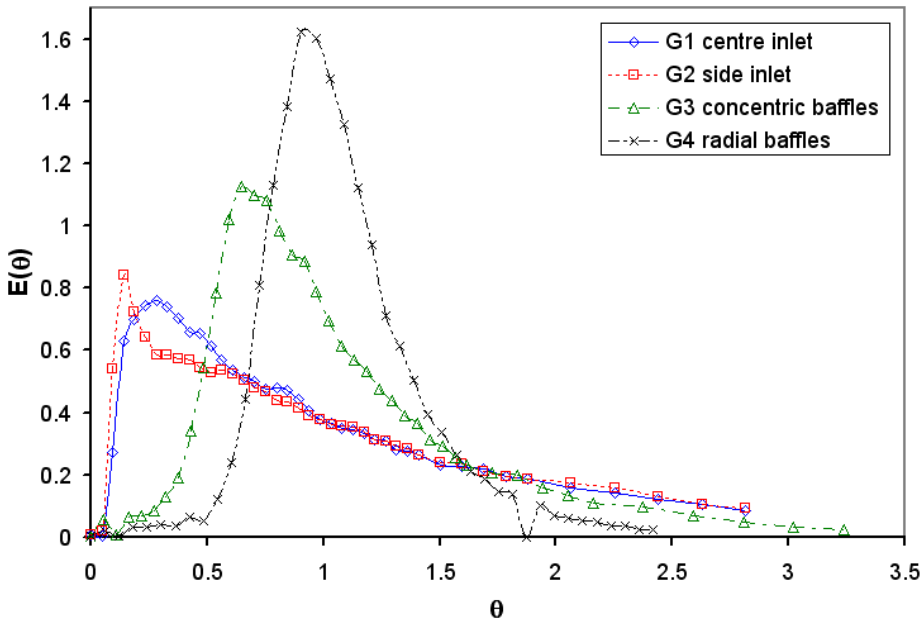

Figure 5.11: RTD for all four geometries; H_2O; 0.05 L/s

The residence time distributions measured with water flowing at 0.05 L/s are shown in Figure 5.11. It is easily seen that each geometry produces a unique RTD curve. Geometries 1 and 2 produce similar RTD curves, with a steep rise to an early peak, then a gradual exponential decay. Although G2 exhibits a sharper peak than G1, these two curves are nearly identical after $\theta = 0.6$. It is important to remember from Figure 5.10 that the region close to the peak is the most sensitive and variable; thus, the small differences in the shape and location of the peak are not of great interest. Geometries 3 and 4 produce very different curves than G1 and G2, with higher, later peaks and much quicker decays. The RTD for G4 is nearly symmetrical, and its peak is close to $\theta = 1$. This means that a

large portion of the fluid resides in the test section for approximately 1 HRT before exiting. The RTD curve for G4 resembles a dispersed plug flow reactor.

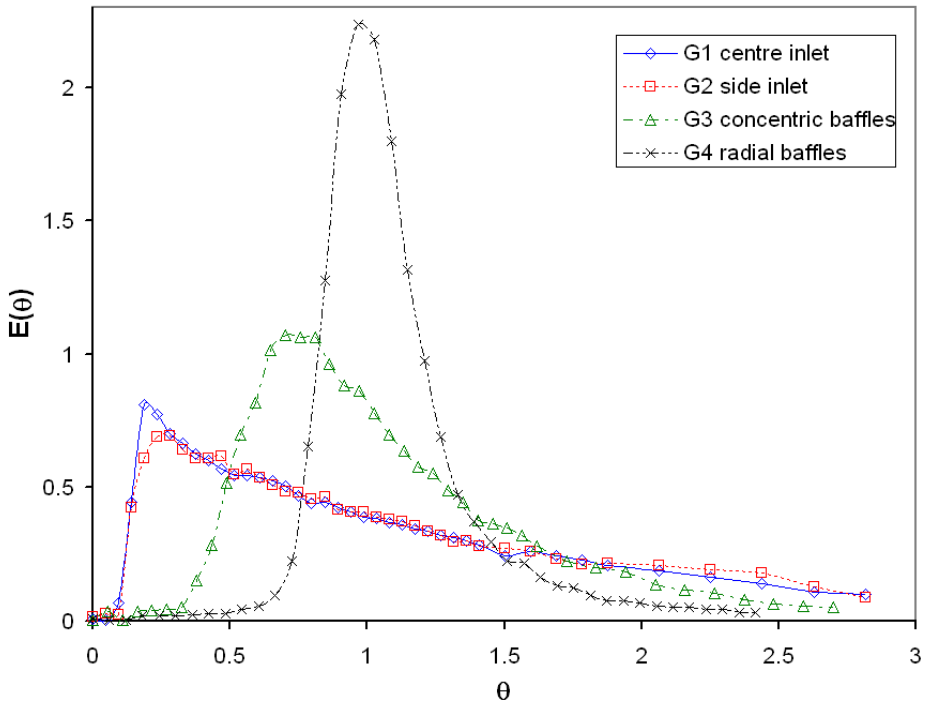

Figure 5.12: RTD for all four geometries; H_2O; 0.0125 L/s

The RTD tests performed with water at a flow rate of 0.0125 L/s are shown in Figure 5.12. Thus, the only difference between Figure 5.12 and Figure 5.11 is a slower flow rate. Comparing these two figures, it can be seen that the shape of the curves do not change significantly with flow rate. There is little difference in the curves of G1, G2, and G3; however, G4 exhibits a dramatically higher peak at the lower flow rate. It can be concluded that as the flow rate decreases, the performance of G4 approaches plug flow. This makes sense, since lower flow rates would tend to produce less mixing in the corners, and the baffles create a series of long, slender conduits for the fluid flow.

However, a slower flow rate does not significantly alter the RTD of reactors that exhibit CSTR-like behaviour, such as G1 and G2.

It is evident that G3 represents an intermediate case between the CSTR-like performance of G1 and G2, and the dispersed plug-flow behaviour of G4. This can be related to the uniformity of flow within a reactor. For example, at any given cross-section in G1 and G2, it is very unlikely that the direction of flow will be uniform across that cross-section. However, in G4, the radial baffles create eight separate sections in which the direction of flow is fairly uniform across any given cross-section. In G3, there is a blend of these two cases. The direction of flow is quite uniform in the innermost compartment that leads to the outlet. However, flow in the two annular sections is not uniform in direction, due to the shape of these sections. Evidence to support this hypothesis is given by the CFD results shown in Chapter 6.

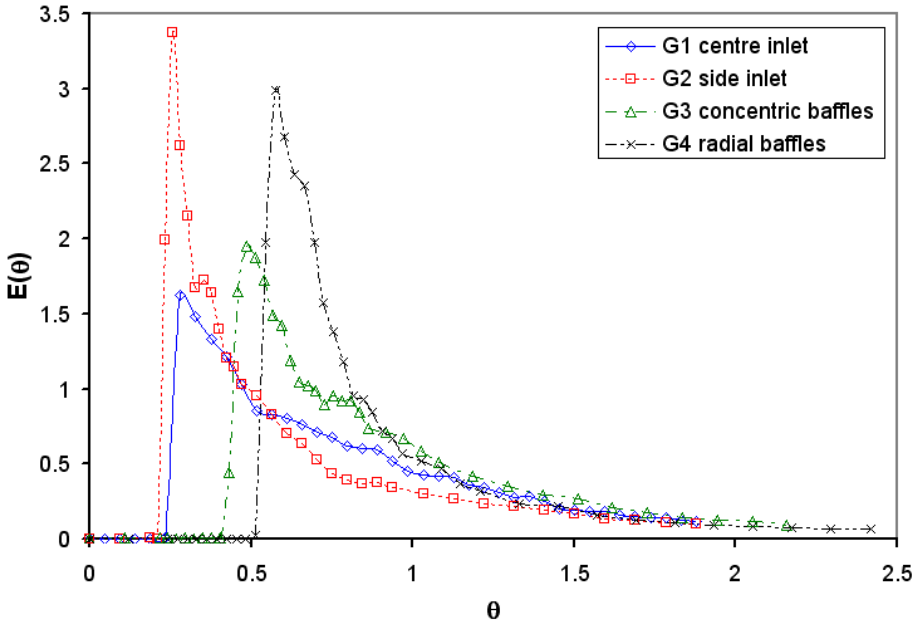

Figure 5.13: RTD for all four geometries; xanthan gum; 0.05 L/s

Figure 5.13 represents the RTD curves for the cases where xanthan gum (K = 0.158 Pa·s^n, n = 0.475) served as the working fluid; the flow rate for these cases was 0.05 L/s. This graph represents a significant change from the water results. All four geometries produce RTD curves with similar shapes—a delayed, sharp rise to the peak value, followed by a long exponential decay. However, the graphs differ in the height of the peak and the length of the delay. Geometries 1 and 2 exhibit shorter delays (between 0.2 and 0.25 HRT), while G3 exhibits a longer delay (approx. 0.4 HRT) and G4 the longest (approx. 0.5). Whereas the RTD curves for G1 and G2 were almost identical in the water experiments, they are very different in the xanthan gum test, especially in the height of the peak. In relation to the water cases, the peak occurs later for G1 and G2, but earlier for G3 and G4. Thus, the change from a Newtonian to a non-Newtonian working fluid pushes G1 and G2 further away from CSTR behaviour, while shifting G3 and G4 in the opposite direction (towards CSTR behaviour).

Table 5.8: Overall RTD parameters for all experimental cases

Geometry	Working fluid	Flow rate (L/s)	Mean θ_m	Variance σ_θ^2	Location of peak	Peak value
1	water	0.05	1.343	1.59	0.2815	0.759
2	water	0.05	1.35	1.52	0.1408	0.840
3	water	0.05	1.14	0.465	0.6477	1.12
4	water	0.05	1.08	0.125	0.9062	1.62
1	water	0.0125	1.29	1.163	0.1877	0.812
2	water	0.0125	1.27	0.952	0.2815	0.695
3	water	0.0125	1.15	0.390	0.7016	1.00
4	water	0.0125	1.13	0.140	0.9666	2.23
1	xanthan gum	0.05	0.999	0.722	0.2815	1.63
2	xanthan gum	0.05	0.789	0.512	0.2581	3.37
3	xanthan gum	0.05	1.03	0.420	0.4858	1.95
4	xanthan gum	0.05	0.973	0.342	0.5739	2.99

Table 5.8 compares the overall parameters for all twelve experimental cases. The mean and variance given in the table were calculated according to Equations 5.32 and 5.34. The integration was performed over the experimental data using the trapezoid rule; the extrapolated tail however was integrated analytically. The mean θ_m represents the centroid of the curve; for ideal reactors such as plug flow reactors or CSTRs, $\theta_m = 1$. A value of less than 1.0 indicates channeling and a decrease in the effective working volume of the digester; however, a value larger than 1.0 indicates that the tracer is delayed in low flow zones (or dead zones) or by adsorption onto the solid surfaces. Nine out of twelve experimental cases show $\theta_m > 1$. The largest mean values occur for the G1 and G2 water cases; this is a result of the large tails present in these curves. In general, θ_m is much smaller for G3 and G4, indicated smaller dead zone volumes in both of these reactors. In the xanthan gum cases, θ_m is very close to one for all cases with the exception of G2 ($\theta_m = 0.79$). The mean is much smaller than 1.0 for this case because of the high, early peak. It can be seen in Figure 5.13 that the tails of all four xanthan gum curves are relatively small, thus the mean is smaller for these cases than for the water cases.

The variance is a measure of the spread of the RTD curve. An ideal plug flow reactor has a variance of $\sigma_\theta^2 = 0$; while a CSTR has a variance of $\sigma_\theta^2 = 1$. The trend in variance is clear for all three sets of flow conditions: σ_θ^2 decreases from G1 to G2 to G3 to G4. The water cases for G1 and G2 have the highest variance ($\sigma_\theta^2 = 0.95$ to 1.6); this of course is largely influenced by the large tails in these cases. In general, the baffled geometries (G3 and G4) have much smaller variances ($\sigma_\theta^2 < 0.5$). The fact that G4 has the smallest variance shows that it is the closest to a plug flow digester. The variance decreases for

G1, G2, and G3 as the flow rate is slowed from 0.05 L/s to 0.0125 L/s; G4 however shows a slight increase in variance. When xanthan gum is used as the working fluid, the variance decreases dramatically for G1 and G2, signifying that the non-Newtonian properties of the xanthan gum cause a shift towards a more plug-flow-like behaviour. However, for G4, the variance is higher for the xanthan gum case, showing that the non-Newtonian fluid actually causes a shift away from plug-flow behaviour. The variance for G3 decreases only slightly when xanthan gum is used.

5.5.4 Comparison to one-parameter RTD models

Two one-parameter RTD models—the tanks-in-series model and the dispersion model—are discussed in Section 5.1.2. These models are fitted to empirical data by matching the variance of the curve. However, not all empirically-determined RTD curves are accurately described by these models. Figure 5.14 compares the empirical RTD curves for the 0.05 L/s water tests for G1 and G3, and the tanks-in-series model for these RTD curves. Using Equation 5.38 to determine the proper N value for both curves, we find that N = 0.63 for G1 and N = 1.47 for G3. To accommodate the factorial function, the number of tanks in series is rounded to the closest integer; both of these N values round to 1. Thus, both G1 and G3 are approximated as single complete-mix tanks when using the tanks-in-series model. As seen in the Figure 5.14, the tanks-in-series model fits the RTD curve for G1 fairly well after approximately 0.3 HRT; however, it does not match the G3 RTD curve at all. For most of the experimental cases, the one-parameter tanks-in-series model provided a poor approximation to the actual results.

As mentioned in Section 5.1.2, the near-plug-flow approximation should not be used for the dispersion model if D/uL > 0.01, or σ_θ^2 > 0.02. The dispersion model becomes mathematically very complex with large vessel dispersion numbers, and can only be solved analytically for one specific set of boundary conditions (Levenspiel, 1972). Since all of the variances measured in the RTD experiments are larger than this value, the dispersion model is not considered further.

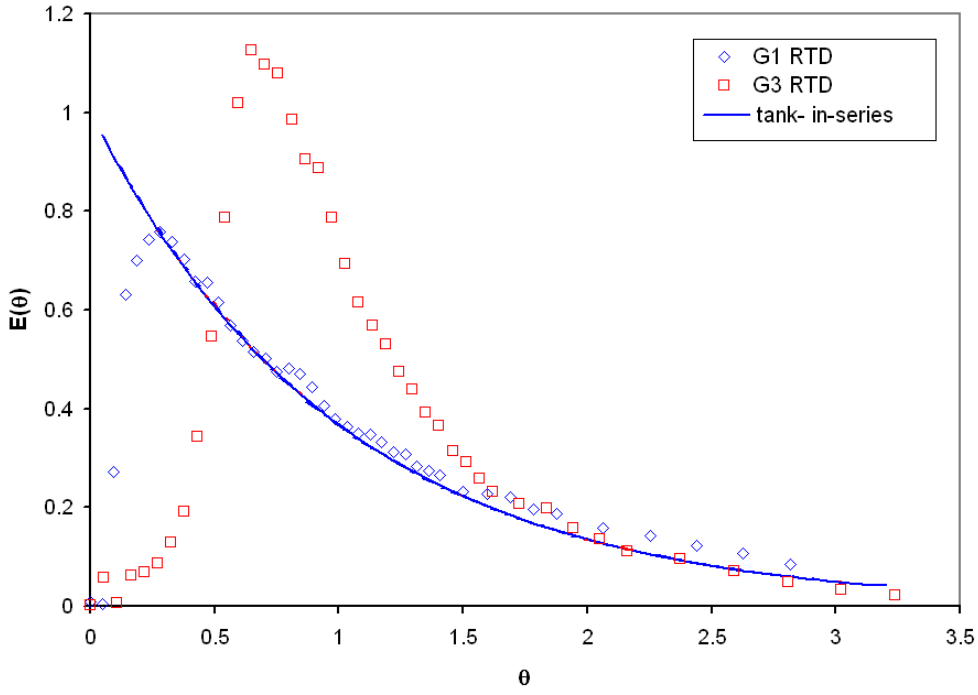

Figure 5.14: Tanks-in-series fit for G1 and G3; H_2O, 0.05 L/s

The values of N and standard error associated for all experimental runs are shown in Table 5.9. The standard error is calculated as the root-mean-square value of the differences. For G1 and G2, all cases are represented by a value of N = 1, with the exception of N = 2 for G2, xanthan gum. N is the highest for G4, showing values of 7 and

8 for the cases involving water. However, N decreases to 3 when xanthan gum is used as the working fluid. In all cases, the standard error is very high, ranging from 0.18 to 0.76, showing that, overall, the tanks-in-series model poorly represents the experimental data. In general, the highest standard error occurs when xanthan gum is the working fluid; thus, the one-parameter tanks-in-series model represents these cases especially poorly.

Table 5.9: One-parameter tanks-in-series model

Geometry	Working fluid	Flow rate (L/s)	Variance σ_θ^2	N	N (integer)	St. error
1	water	0.05	1.59	0.630	1	0.241
1	water	0.0125	1.16	0.860	1	0.263
1	xanthan gum	0.05	0.722	1.39	1	0.431
2	water	0.05	1.52	0.660	1	0.228
2	water	0.0125	0.952	1.05	1	0.268
2	xanthan gum	0.05	0.512	1.95	2	0.761
3	water	0.05	0.465	1.47	1	0.430
3	water	0.0125	0.390	2.57	3	0.181
3	xanthan gum	0.05	0.420	2.38	2	0.499
4	water	0.05	0.125	8.01	8	0.210
4	water	0.0125	0.140	7.15	7	0.426
4	xanthan gum	0.05	0.342	2.92	3	0.748

5.5.5 Comparison to multiparameter RTD models

Two multi-parameter models were investigated with the aim of representing the experimental data with greater accuracy than the one-parameter tanks-in-series model. The first model is an ideal plug-flow reactor connected in series with an ideal continuously stirred tank reactor; this model is labelled the PFR-CSTR series model, and is shown in Figure 5.15. The order in which these reactors are connected has no bearing on the RTD, since the RTD gives no information on the earliness of mixing. The two

parameters used in this model are the mean, θ_m, and the fraction of volume occupied by the plug-flow region, V_p/V. The RTD of the PFR-CSTR series model is given by:

$$E(\theta) = \begin{Bmatrix} 0 & \theta^* < 0 \\ \dfrac{1}{\theta_m[1-(V_P/V)]}\exp(-\theta^*) & \theta^* \geq 0 \end{Bmatrix} \tag{5.46}$$

Where θ^* is the adjusted normalized time, given by:

$$\theta^* = \frac{\theta - (V_P/V)}{\theta_m[1-(V_P/V)]} \tag{5.47}$$

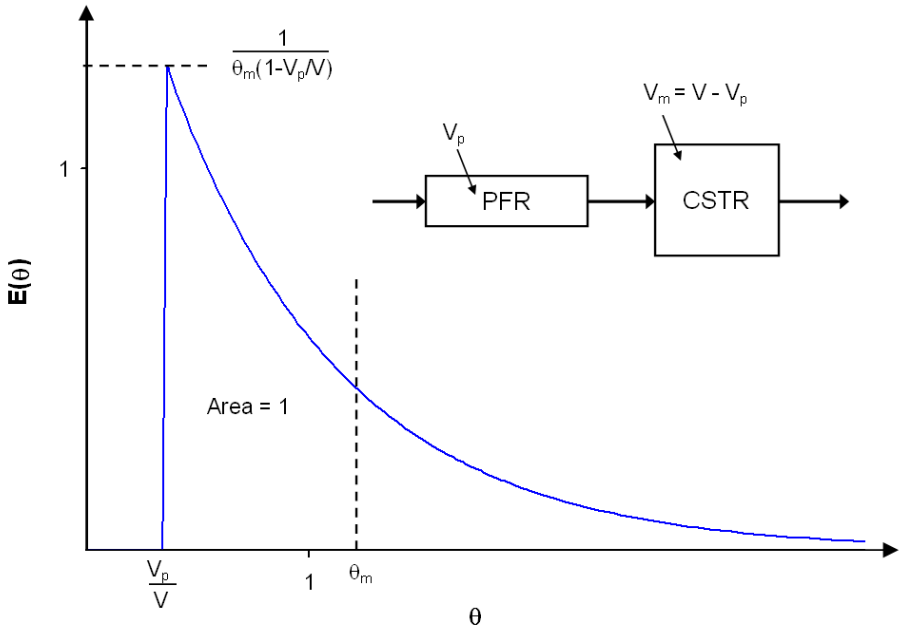

Figure 5.15: PFR-CSTR series model

The mean θ_m is calculated from the experimental data as shown in Table 5.8. The second parameter, V_p/V is related to the delay between $\theta = 0$ and the sharp rise to the peak. The exact value of V_p/V was found by minimizing the standard error by the trial-and-error method. Figure 5.16 shows the PFR-CSTR model used to approximate the RTD of G1

with water and a flow rate of 0.05 L/s. The model does an excellent job of approximating the shape of the experimental curve. The standard error is 0.12131, which represents a 50% reduction in error over the tanks-in-series model for this case.

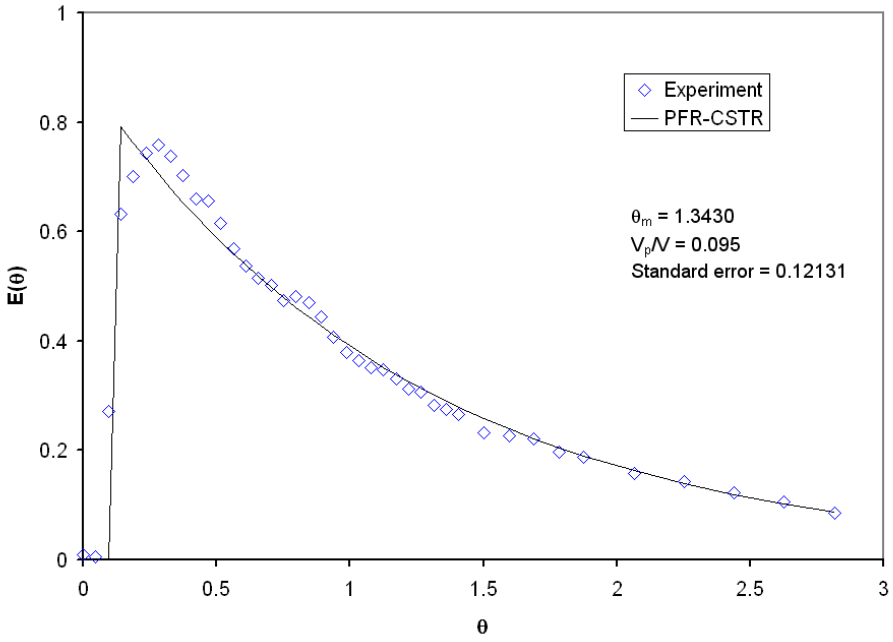

Figure 5.16: PFR-CSTR series model fit to G1; H_2O; 0.05 L/s

The PFR-CSTR series model was used to approximate eight of the twelve experimental cases; only the water experiments for G3 and G4 were not fit to this model. Table 5.10 shows the values of θ_m, V_p/V, and the standard errors for these eight cases. The fraction of plug-flow volume V_p/V is much smaller for the G1 and G2 water experiments than for the xanthan gum experiments: $V_p/V = 0.095$ for G1 and 0.047 for G2. It is interesting to note that both flow rates exhibit the same value of V_p/V for these geometries. The standard errors are significantly lower for the PFR-CSTR series model than for the tanks-in-series model. However, due to the sharp, high peaks found in the RTDs of G2 and G4

with xanthan gum, the standard error for these cases is still quite high (0.50213 and 0.28214 respectively).

Table 5.10: PFR-CSTR series model – parameters and standard error

Geometry	Working fluid	Flow rate (L/s)	Mean θ_m	V_p/V	Standard error
1	water	0.05	1.343	0.095	0.121
1	water	0.0125	1.294	0.095	0.0634
1	xanthan gum	0.05	0.999	0.28	0.0711
2	water	0.05	1.351	0.047	0.0414
2	water	0.0125	1.272	0.047	0.135
2	xanthan gum	0.05	0.789	0.25	0.502
3	xanthan gum	0.05	1.03	0.45	0.122
4	xanthan gum	0.05	0.973	0.54	0.282

The second multi-parameter model is an extension of the PFR-CSTR model; it replaces the complete-mix tank with a series of ideal complete-mix tanks (see Figure 5.17). This modified tanks-in-series model fits the remaining experimental cases quite well. The parameters of the model are the mean θ_m, the fraction of plug flow volume V_p/V, and the number of complete-mix tanks in series, N. The mean is calculated as described above, while the number of tanks N is related to the variance of the curve by:

$$N = \frac{(\theta_m *)^2}{\sigma_\theta^{\,2}} \tag{5.48}$$

where θ_m* is calculated as:

$$\theta_m * = \frac{\theta_m - (V_P/V)}{\theta_m\left[1-(V_P/V)\right]} \tag{5.49}$$

To fit the model to the empirical data, V_p/V was manipulated to minimize the standard error.

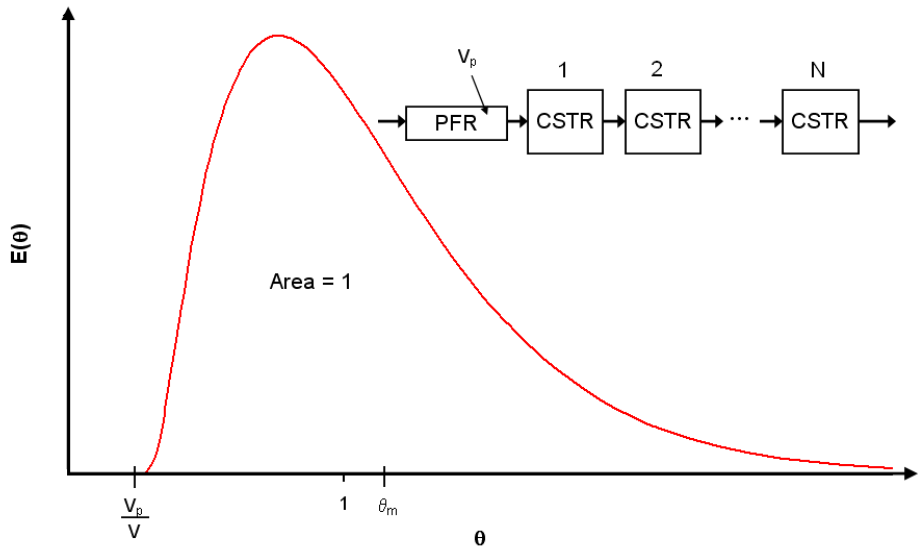

Figure 5.17: Modified tanks-in-series model

The RTD curve for the modified tanks-in-series model is described by the following equation:

$$E(\theta) = \left\{ \begin{array}{ll} 0 & \theta^* < 0 \\ \dfrac{1}{\theta_m[1-(V_P/V)]} \dfrac{N(N\theta^*)^{N-1}}{\Gamma(N)} \exp(-N\theta^*) & \theta^* \geq 0 \end{array} \right\} \tag{5.50}$$

where θ* is the adjusted normalized time as given in Equation 5.49. The function Γ(N) replaces the factorial term to allow non-integer values of N. Γ(N) is given as:

$$\Gamma(N) = \int_0^\infty s^{N-1} e^{-s} ds \tag{5.51}$$

Note that for N = 1, the modified tanks-in-series model reduces to the PFR-CSTR series model. Figure 5.18 shows the modified tanks-in-series model fitted to the RTD data for G3 with water at 0.05 L/s.

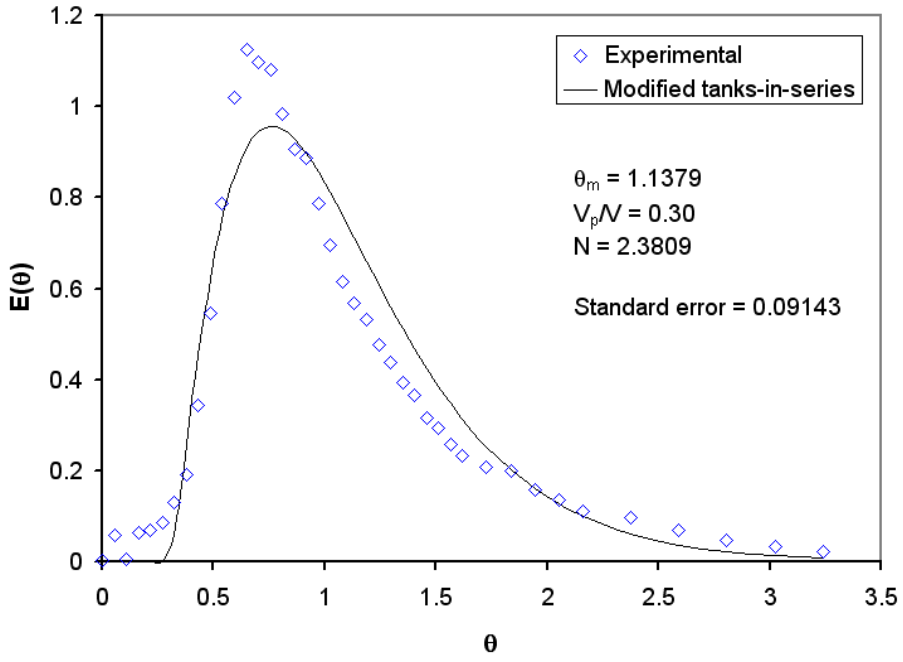

Figure 5.18: Modified tanks-in-series model for G3; H_2O; 0.05 L/s

Table 5.11 shows the parameters and standard error for each of the four cases fit to this model. A very interesting feature of this table is that N corresponds quite well to the actual number of compartments in the reactor geometry. G3 has three concentric, circular sections, and N = 2.38 and 2.83 for the G3 cases; G4 however, has eight straight sections, and N = 8.48 and 8.83 for each of the G4 cases. The standard error between the experimental data and the model is less than 0.11 for all cases.

Table 5.11: Modified tanks-in-series model – parameters and standard error

Geometry	Working fluid	Flow rate (L/s)	Mean θ_m	V_p/V	N	St. error
3	water	0.05	1.14	0.3	2.38	0.0914
3	water	0.0125	1.14	0.28	2.83	0.0711
4	water	0.05	1.08	0.27	8.48	0.0659
4	water	0.0125	1.13	0.5	8.83	0.109

Figures 5.19 through 5.21 compare the experimental data to the multi-parameter models for all twelve cases.

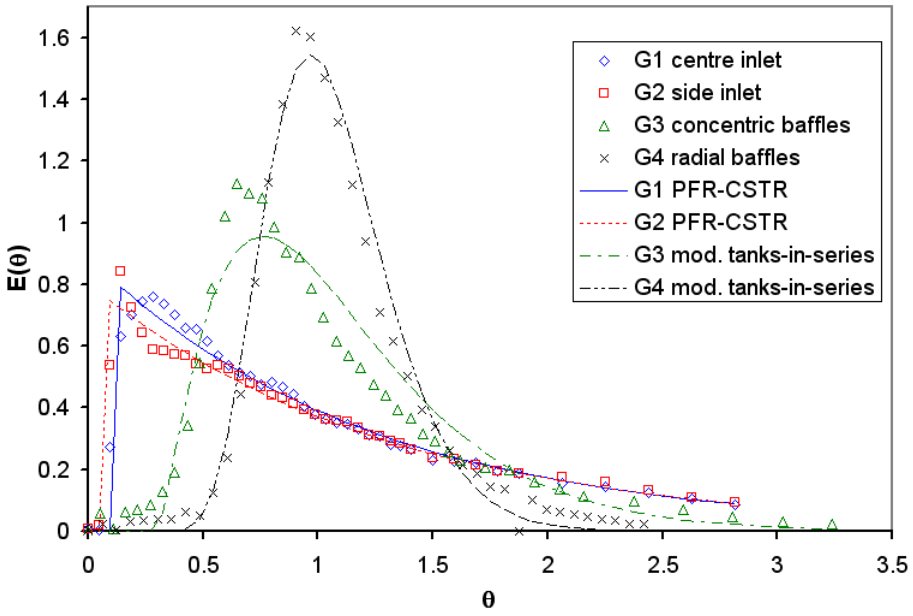

Figure 5.19: Comparison of experimental data and models, H_2O at 0.05 L/s

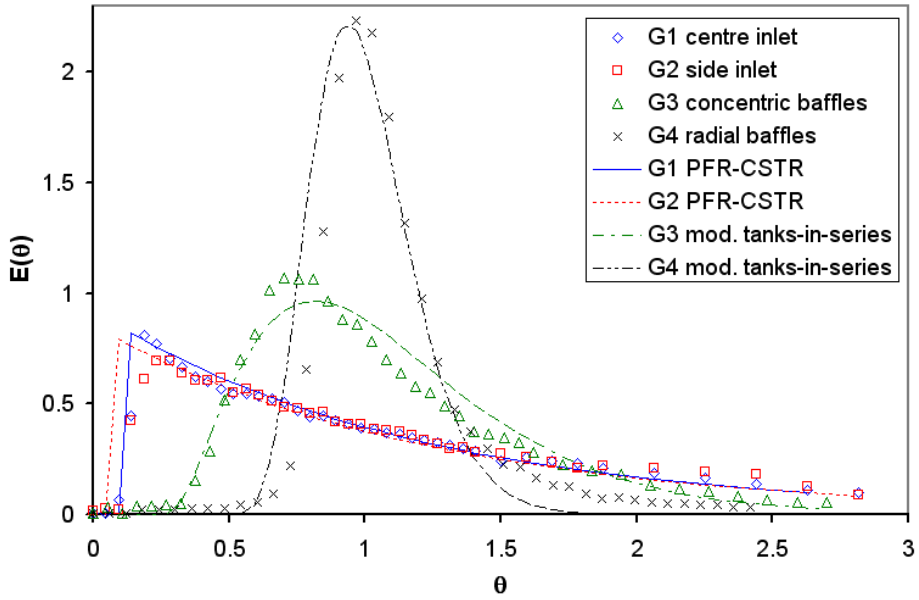

Figure 5.20: Comparison of experimental data and models, H_2O at 0.0125 L/s

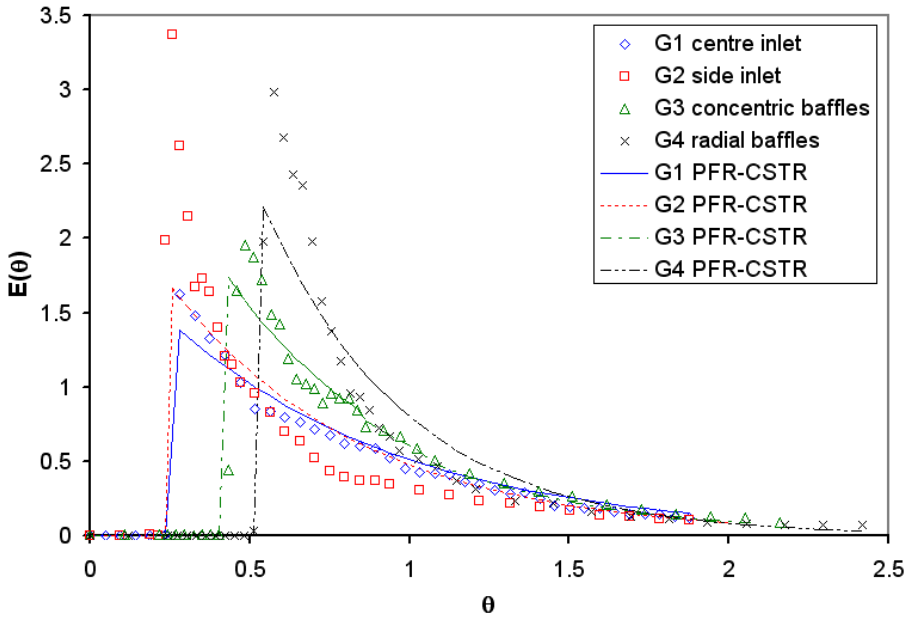

Figure 5.21: Comparison of experimental data and models, xanthan gum at 0.05 L/s

5.5.6 Dead space

The fraction of reactor volume occupied by dead space is a good indicator of reactor performance. Dead space or dead zones are regions within the reactor where flow velocities are relatively low; often fluid will be delayed in these regions. Dead space may decrease the effective volume of the reactor, or may create regions of non-uniform temperature or concentration. Thus, a low fraction of dead space is preferable, and often will lead to increased reactor performance. The tail of the residence time distribution curve indicates the amount of dead space is in the reactor; a large tail signifies a large fraction of dead space. Grobicki and Stuckey (1992) used the following equation to estimate the fraction of dead space based on experimental RTD curves:

$$\frac{V_d}{V} = 1 - \mu_a v_a \tag{5.52}$$

where V_d/V is the volume fraction of dead space, and μ_a and v_a are defined as follows:

$$\mu_a = \frac{\int_0^2 \theta \cdot E(\theta) d\theta}{\int_0^2 E(\theta) d\theta} \tag{5.53}$$

$$v_a = F(2) = \int_0^2 E(\theta) d\theta \tag{5.54}$$

Based on these equations, the volume fraction of dead space was estimated for all experimental cases, as shown in Table 5.12. As expected, the highest fraction of dead space was found for G1 and G2 with water. However, the dead space is higher for G2 under all three sets of flow conditions. This indicates, surprisingly, that the swirling flow in G2 actually increases the dead space in the reactor. The dead space in G3 is consistently much lower than that of G1 and G2. Slowing the flow rate from 0.05 to 0.0125 L/s decreased the dead space for the G1, G2, and G3 water cases. Since $\mu_a v_a > 1$ for the G4 water cases, the equation breaks down and gives negative values for the dead space. This emphasizes the fact that Equation 5.52 is a fairly arbitrary measure of dead space; however, it is still apparent that G4 has very little dead space, as expected. Switching the working fluid to xanthan gum does not significantly alter the dead space fraction for G1 and G2; however G3 and G4 jump dramatically to 17.7% and 19.3% dead space, respectively.

Table 5.12: Estimated volume fraction of dead space

Geometry	Working fluid	Flow rate (L/s)	v_a	μ_a	Dead space V_d/V
1	water	0.05	0.791	0.822	0.350
2	water	0.05	0.736	0.775	0.430
3	water	0.05	0.903	0.965	0.128
4	water	0.05	0.975	1.05	-0.0262
1	water	0.0125	0.787	0.868	0.323
2	water	0.0125	0.733	0.826	0.395
3	water	0.0125	0.916	1.01	0.0800
4	water	0.0125	0.964	1.07	-0.0347
1	xanthan gum	0.05	0.894	0.767	0.314
2	xanthan gum	0.05	0.931	0.640	0.405
3	xanthan gum	0.05	0.925	0.891	0.177
4	xanthan gum	0.05	0.940	0.859	0.193

5.6 Summary of findings

The residence time distribution is often used to predict the performance of a reactor or diagnose problematic flow patterns within the reactor. The RTD of four lab-scale anaerobic digester reactor geometries was determined using a tracer dye experiment. Two of these geometries, G1 and G2, did not include baffles, while G3 contained two concentric, circular baffles and G4 contained eight radial baffles. Forced mixing was not considered in the study. Tests were run with a Newtonian fluid (water) and a non-Newtonian fluid (1 g/L solution of xanthan gum). The RTDs of the baffle-less geometries (G1 and G2) exhibited an exponential decay similar to that of a complete-mix reactor. However, the RTD of G4—with radial baffles directing the flow in a series of parallel vertical channels—resembled a slightly skewed bell curve, similar to that of a dispersed plug flow reactor. The concentric baffle reactor represented an intermediate case. The use of a non-Newtonian working fluid significantly impacted the RTD, shifting G1 and G2 away from complete-mix behaviour, while shifting G4 away from plug flow behaviour.

Consequently, the variances of the G1 and G2 RTD curves decreased dramatically when the working fluid was switched from water to xanthan gum; while the variance of G4 increased significantly. The use of xanthan gum also caused the peak values for G3 and G4 to occur much earlier.

Two multi-parameter ideal reactor models were used to describe the results. The PFR-CSTR series model was the combination of a plug flow reactor and a complete-mix reactor in series. The modified tanks-in-series model connected a plug flow reactor in series with a series of complete-mix reactor.

This knowledge can be extended to the design of anaerobic digesters for liquid hog manure. An optimal reactor would produce an RTD with a small variance and a peak value at 1.0 HRT. From all of the cases studied, the radial baffle G4 geometry provides an excellent RTD with water at a flow rate of 0.0125 L/s. However, liquid hog manure is non-Newtonian, with pseudoplastic properties similar to xanthan gum. By comparing the RTD curves for G4, it can easily be seen that the non-Newtonian properties of xanthan gum would significantly decrease reactor performance, due to the increase in variance and the shift to an earlier peak. The estimated dead space also increases significantly. The reactor with concentric baffles, G3, is the second-best candidate, though its performance is markedly poorer than G4. A positive characteristic of G3 is that is seems much less affected by the switch to a non-Newtonian working fluid, as evidenced by the smaller changes in variance, location of peak, and dead space.

However, the non-baffled geometries (G1 and G2) are poor candidates for an anaerobic digester, due to their high variances, early peaks, and large fractions of dead space.

The application of the concept of residence time distribution to anaerobic digester technology is explored in greater detail in Chapter 6 through the use of numerical simulation.

Chapter 6. CFD study of an anaerobic digester

6.1 Introduction

6.1.1 Overview

The design of an effective and efficient anaerobic digester requires a thorough knowledge of flow patterns within the digester, and how these flow patterns vary with certain design parameters such as size, geometry, and fluid properties. In Chapter 5, an experimental study of the residence time distribution of a lab-scale anaerobic digester was performed, and the effects of geometry, flow rate, and viscosity were examined. This chapter expands on that experimental study by using computational fluid dynamics (CFD) to simulate the fluid flow within lab-scale and pilot-scale reactors. Three-dimensional CFD models give detailed and accurate predictions of the velocity fields within a reactor; by studying the relationship between the boundary conditions, flow patterns, and residence time distribution, a greater knowledge of the operation of an anaerobic digester can be achieved.

Three-dimensional models of continuous-flow reactors were developed using the commercial software package FLUENT®. Four reactor geometries were modeled; these geometries correspond directly to the geometries studied in the RTD experiments. All of the experimental cases were simulated using these models. Additional simulations were performed using the fluid properties of liquid hog manure at 3% and 8% total solids. The viscous properties of manure at these concentrations were determined from the generalized viscosity model described in Chapter 3; according to this model, manure at

3% TS is Newtonian, while manure at 8% TS is a non-Newtonian power-law fluid. The RTD of the reactors was studied by simulating a transient stimulus-response experiment similar to the tracer dye experiments described in Chapter 5. Finally, two geometries (G1 with centre inlet and G4 with radial baffles) were scaled up to simulate a 2000 L reactor with a hydraulic retention time (HRT) of 17 days. The volume and HRT correspond to that of two pilot scale anaerobic digesters built at the University of Manitoba's Glenlea Research Station.

The meshes for all four geometries were tested for grid independence. Validation of the 3D numerical models was performed by comparing the velocity fields for two geometries with the results of a particle image velocimetry (PIV) study performed using the fluid column facility. Further validation of the models is found in Chapter 5, where the experimental RTD results are compared to those produced using CFD.

6.1.2 Governing equations

Computational fluid dynamics (CFD) uses numerical techniques to solve the governing equations of a fluid flow problem in two or three dimensions. The models described in this chapter are three-dimensional, and involve the following equations: continuity, momentum, energy, turbulence, and species transport. The continuity equation and momentum equations, also known as the Navier Stokes equations, are described in vector notation for steady-state, incompressible flow as follows:

Continuity (conservation of mass):

$$\nabla \cdot \vec{v} = 0 \tag{6.55}$$

Navier-Stokes (conservation of momentum):

$$\rho\left[\nabla\cdot(\vec{v}\vec{v})\right] = -\nabla p + \nabla\cdot\left(\bar{\bar{\tau}}\right) + \rho\vec{g} + \vec{F} \tag{6.56}$$

where $\vec{v}$ is the 3D velocity vector, ρ is the fluid density, p is pressure, $\vec{g}$ is the vector of acceleration due to gravity, and $\vec{F}$ is the external body force. The stress tensor, $\bar{\bar{\tau}}$ is defined as follows:

$$\bar{\bar{\tau}} = \mu\left[\left(\nabla\vec{v} + \nabla\vec{v}^{\,\mathrm{T}}\right) - \frac{2}{3}\nabla\cdot\vec{v}I\right] \tag{6.57}$$

where μ is the kinematic viscosity, and I is the unit tensor. For non-Newtonian flows, μ is replaced by η, which is a function of shear rate, as described in Section 6.1.4. For detailed discussion of all the governing equations and their treatment in FLUENT®, refer to Fluent (2005). FLUENT® uses a segregated solver to solve the continuity and Navier-Stokes equations separately.

6.1.3 Modeling assumptions

For the development of the numerical model, the following assumptions were made:

1. The reactor operates under steady-flow conditions.
2. All working fluids used are incompressible.
3. Isothermal conditions are assumed, since the effects of heat transfer are beyond the scope of this study.
4. Uniform fluid properties are assumed, with the exception of viscosity for the non-Newtonian fluid cases. In these cases, viscosity varies with shear rate according to the power law.

5. The density of all fluids is assumed to be 1000 kg/m^3.
6. Chemical reactions are ignored, since the focus of the study is on the fluid flow within the reactor.
7. Multi-phase effects such as the settling of solids and biogas formation and flow are neglected. These effects drastically complicate the model, and would obscure the study of viscous effects.
8. Turbulence is assumed for the lab-scale cases where water is the working fluid. This is because the Reynolds number is relatively high, and turbulent flow was observed during experimentation. Laminar flow is assumed for all other cases due to very low Reynolds numbers.
9. Uniform inlet velocity is assumed.
10. All walls are assumed to be smooth.
11. The tracer is modeled with the same properties of the working fluid. The rate of molecular diffusion is set very low, so that the tracer follows the flow as close as possible.
12. Adsorption of the tracer dye on solid surfaces is neglected, since the extent to which this occurs is unknown.
13. Small features present in the experimental model – such as the locating slots for the baffles and the screw plug in the lid – are not modeled.
14. Inlets and outlets are modeled as straight tubes with the same diameter as the orifice to the test section.

6.1.4 Modeling viscosity

One of the key parameters in this study is the viscosity of the working fluid. Four fluids were simulated in the study – water, xanthan gum, and liquid hog manure at 3% and 8% TS. While water and the 3% TS manure have Newtonian properties, the other two fluids are modeled using the non-Newtonian power law model in Fluent. This power law model is described as follows (Fluent, 2005):

$$\eta_{\min} < \eta = k\left(\frac{d\gamma}{dt}\right)^{n-1} \exp\left(\frac{T_0}{T}\right) < \eta_{\max} \tag{6.58}$$

where η is the apparent viscosity [Pa·s], η_{min} is the lower viscosity limit, η_{max} is the upper viscosity limit, $d\gamma/dt$ is the shear rate [s^{-1}], k is the consistency coefficient [$Pa \cdot s^n$], n is the flow behaviour index [dimensionless], T is the temperature [K], and T_0 is the reference temperature. Since isothermal conditions are assumed, $T = T_0$ everywhere in the reactor, so $\exp(T_0/T) = 1$ everywhere. The viscosity parameters for the fluids used in this study are given in Table 6.1; for the Newtonian fluids, only the value of μ is applicable. The consistency coefficient K and flow behaviour index n for the 1.0 g/L solution of xanthan gum is taken from Speers and Tung (1986). The values for K and n for 8% TS liquid hog manure are determined from Equations 3.29 and 3.30, with T = 308 K (35°C) and TS = 8.0; similarly the value of μ for 3% TS manure is determined from Equation 3.26, T = 308 K and TS = 3.0. These values are calculated at 35°C to reflect mesophilic conditions. The maximum and minimum limits for the apparent viscosity of the non-Newtonian fluids are set rather arbitrarily. The maximum limit for xanthan gum and 8% TS manure are derived from these fluids' respective power law correlations, with the shear rate set to 0.001 and 0.0002 s^{-1}, respectively. At smaller shear rates, the fluid

velocities are generally so low that increasing the apparent viscosity further would not greatly affect the solution. For xanthan gum, the minimum apparent viscosity is derived from the power law correlation with a shear rate of 100 s^{-1}. Since the value obtained (0.0119 Pa·s) is not less than the viscosity of the solvent (water), this is a realistic value. The pseudoplastic properties of xanthan gum solutions are due to the molecular properties of the gum; in contrast, the pseudoplastic properties of liquid manure are due mainly to the interactions between large suspended particles. Thus, it is expected that the lower viscosity limit of 8% TS manure would be much higher than the lower viscosity limit of the xanthan gum solution. The lower viscosity limit was therefore set as 0.486 Pa·s, which is derived from the power law correlation for 8% TS manure with a shear rate of 0.8 s^{-1}. In the numerical solutions for these non-Newtonian cases, the lower viscosity limits only come into play in very small regions of the domain; in some cases, the limits are not reached at all. Thus, it can be assumed that the arbitrary viscosity limits do not significantly affect the solution.

Table 6.1: Power law parameters for the viscosity of working fluids

Working fluid	K (Pa·s^n) / μ (Pa·s)	n	T_0 (K)	η_{min} (Pa·s)	η_{max} (Pa·s)
water	0.00100	N/A	N/A	N/A	N/A
liquid hog manure, 3% TS	0.00931	N/A	N/A	N/A	N/A
1 g/L xanthan gum sol'n	0.126	0.487	298	0.0119	4.359
liquid hog manure, 8% TS	0.439	0.512	298	0.486	29.24

6.1.5 PIV validation

To validate the CFD model, flow field results from the model were compared to experimental data obtained using particle image velocimetry (PIV). PIV is an

instantaneous, two-dimensional, non-invasive flow-mapping technique that has become widely-used for studying flow in transparent media (Gaden, 2007). PIV uses a pulsed laser that illuminates reflective particles in the flow. A high-speed digital camera captures images of these particles as they travel with the flow. Two images are captured in quick succession at regular time intervals. The digital images are divided into small, rectangular interrogation areas for analysis. For each pair of images, each interrogation area within the first image is compared to its corresponding interrogation area in the second image. The PIV software identifies the particles, and calculates the change in their positions within the interrogation area. The velocity of each particle is then calculated as:

$$\vec{u} = u\hat{i} + v\hat{j} = \frac{\Delta x\hat{i} + \Delta y\hat{j}}{\Delta t} \tag{6.59}$$

where u and v are the components of velocity in the x and y directions, $\hat{i}$ and $\hat{j}$ are unit vectors, Δx and Δy are the changes in x and y position of the particle, and Δt is the time between images.

6.2 Literature review

Several researchers have applied CFD to anaerobic digesters and related technologies. Fleming (2002) developed a 3D model of a covered lagoon digester. This complex model incorporated the processes of bulk fluid motion, sedimentation, bubble mixing, bubble entrainment, advection, biological reactions, and heat transfer. The model was validated using performance data from full scale digesters in North Carolina. Forschner et al. (2004) modeled a horizontal mixing vessel operating as a complete stirred tank reactor (CSTR). Vesvikar and al-Dahhan (2005) performed CFD simulations of an internal airlift

loop reactor (ALR); the ALR was cylindrical with a central draft tube. The numerical predictions were compared to experimental results obtained from a lab-scale ALR operating with 5% TS municipal sewage. Vesvikar and Al-Dahhan considered regions with velocities less than 5% of the maximum velocity to be dead or stagnant; according to this definition, they found that dead space occupied 25.0% to 59.7% of the digester volume for flat-bottomed digesters, and 11.02% to 29.57% for conical-bottomed digesters. They stated that the numerical and experimental results were in good agreement, despite the fact that the fluid properties of water were used in the CFD simulations. Wu and Chen (2008) used CFD to simulate fluid flow in a cylindrical continuous flow reactor. The dimensions of a lab-scale digester, five "scale-up" digesters ranging from 1 to 5 m^3, and a 40 m^3 pilot-scale digester were used. Hydraulic retention times studied ranged from approximately 4 s for the lab-scale digester to 4000 s for the pilot-scale digester. The properties of both water and liquid manure were used in the simulations and compared. Terashima et al. (2009) developed a 3D model of a mechanically agitated digester with a centrally-located internal draft tube; the rheological properties of digested sludge were incorporated through empirically-determined power law parameters. Meroney and Colorado (2009) simulated four large, circular anaerobic digester tanks with single and multiple draft tube mixers.

Research into the reactor designs used for other processes is often applicable to the design of anaerobic digesters. For example, the pulp and paper industry uses large reactors for the mixing of non-Newtonian fluids, analogous to a complete-mix anaerobic digester. Ford et al. (2006) used CFD to model the dynamic response of agitated pulp

stock chests to a pseudo-random binary input. The pulp was modeled as a non-Newtonian Bingham Plastic. They found that the reactor designs studied were far from ideal due to a high degree of channeling in the system. Ford et al. (2007) continued this work by studying the effect of impeller speed on degree of channeling.

6.3 Model description

6.3.1 Geometry

The four reactor geometries studied in Chapter 5 were modeled and meshed using the GAMBIT® 2.2 software package. All four reactor geometries are based on a vertical cylindrical tank with a height of 495 mm and a diameter of 286 mm. Geometries 1 and 2 have no baffles; G1 has a centre inlet while G2 has a side inlet. Geometry 3 is divided into three sections by two concentric, cylindrical baffles that extend the full height of the reactor. Geometry 4 is annular with eight radial baffles; four of these baffles extend the full height of the reactor, while the other four leave a gap at the bottom. These four geometries as modeled in GAMBIT® are shown in Figure 6.1.

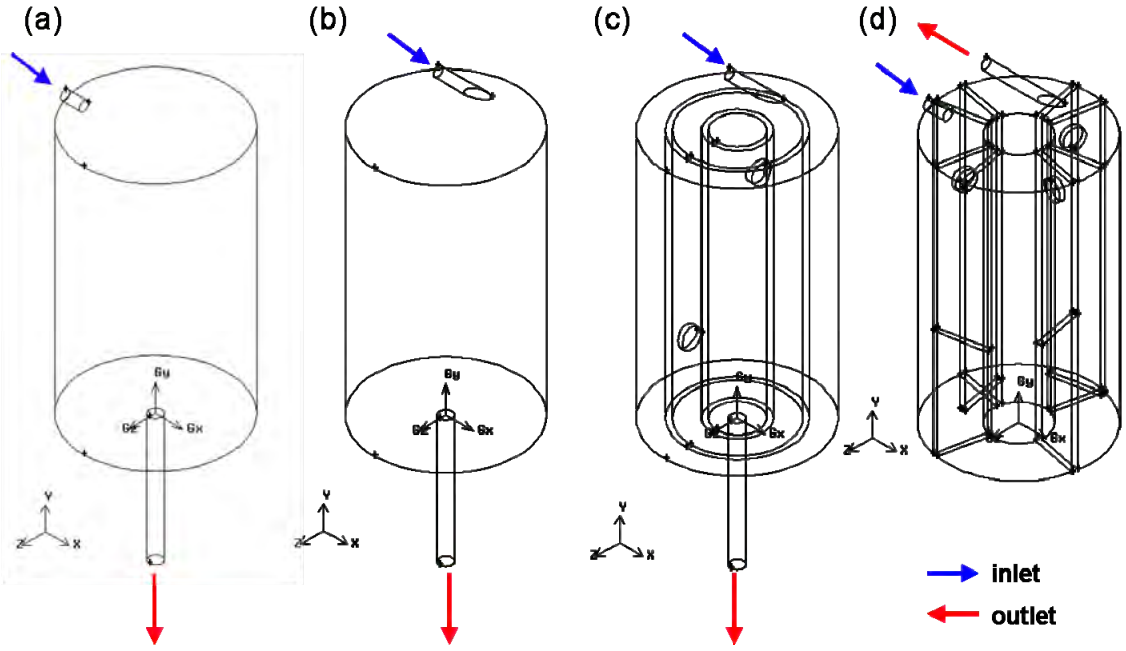

Figure 6.1: Reactor geometries as modeled in GAMBIT® 2.2; a) G1 centre inlet, b) G2 side inlet, c) G3 concentric baffles, d) G4 radial baffles.

6.3.2 Mesh

Meshes were constructed based on the four geometries shown in Figure 6.1. For all geometries except for G4 (radial baffles), a combination of hexahedral and tetrahedral elements was used; the G4 mesh was constructed using only hexahedral elements. In general, the meshes were constructed so that elements were more closely spaced near the reactor walls and in other regions where high velocity gradients were expected. Two or three meshes were created for each geometry to facilitate grid independence tests. The mesh statistics are summarized in Table 6.2.

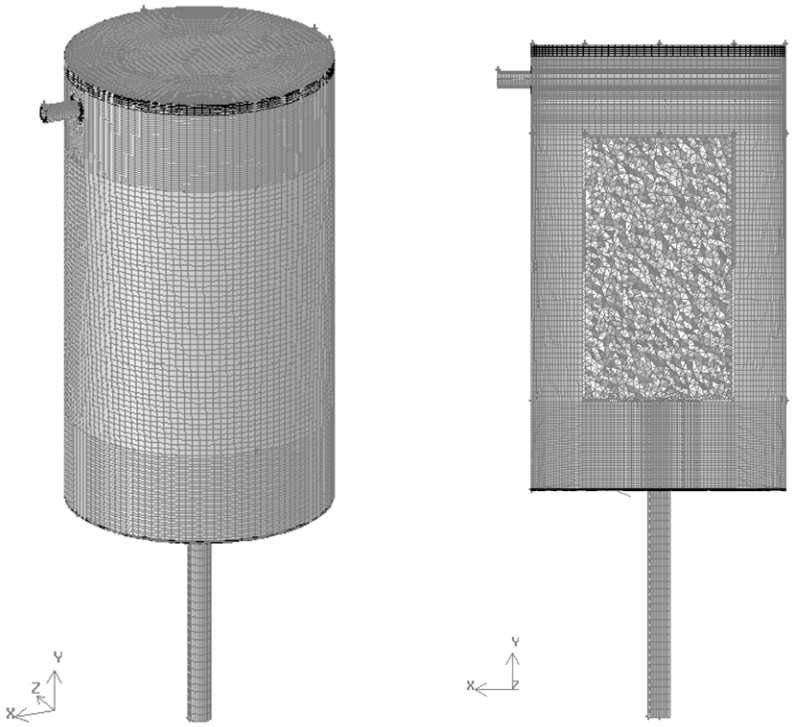

Figure 6.2: Computational mesh for G1 with centre inlet

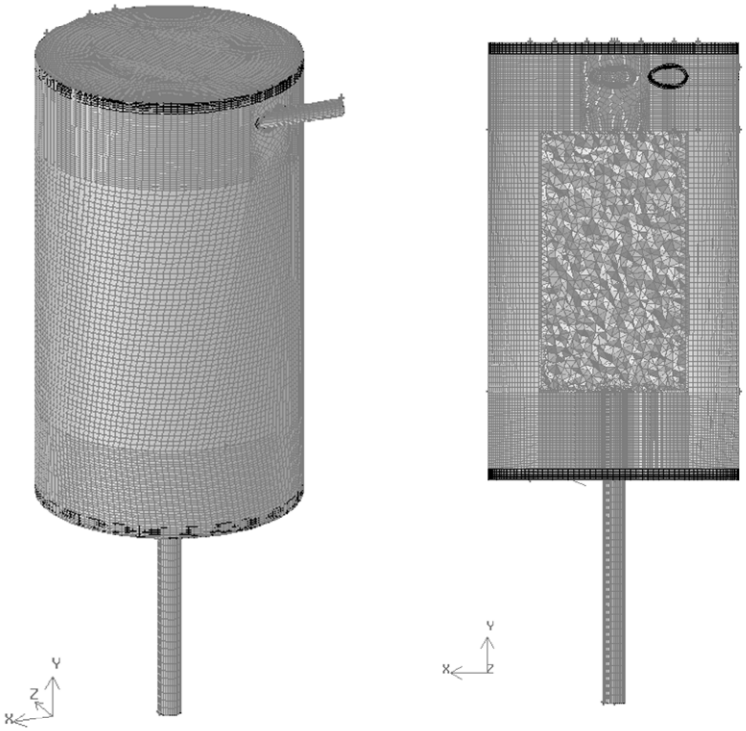

Figure 6.3: Computational mesh for G2 with side inlet

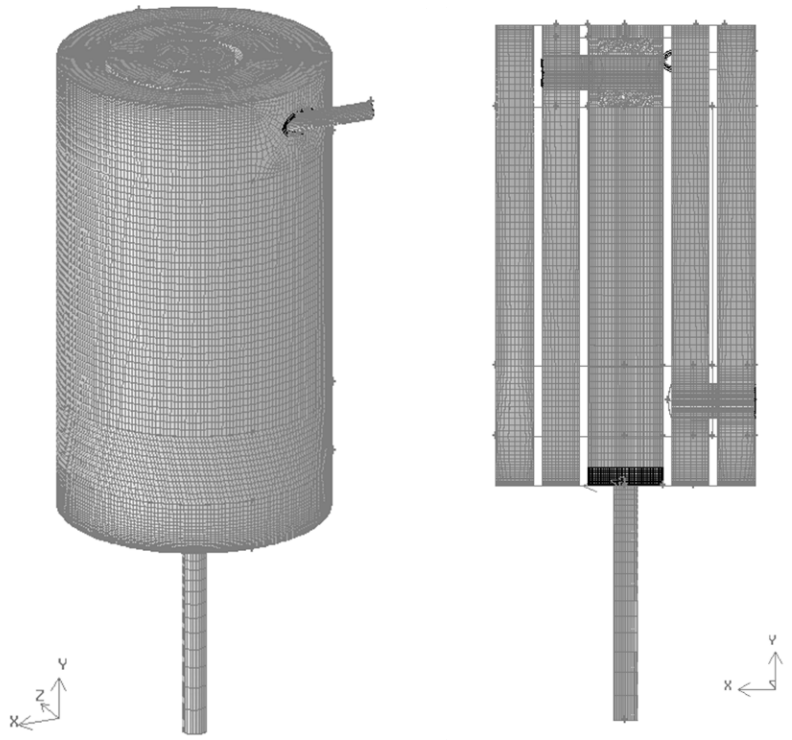

Figure 6.4: Computational mesh for G3 with concentric baffles

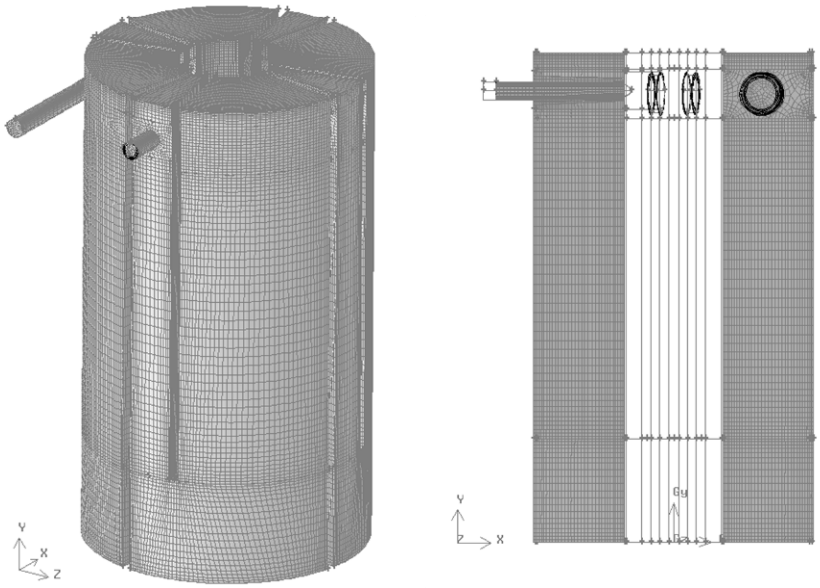

Figure 6.5: Computational mesh for G4 with radial baffles

Table 6.2: Computational mesh statistics

Geometry	Quality	Element type	Elements	Faces	Nodes
G1 centre inlet	coarse	hex / tet	306 193	833 872	249 163
G1 centre inlet	medium	hex / tet	589 390	1 606 294	454 566
G1 centre inlet	fine	hex / tet	1 015 436	2 730 987	781 530
G2 side inlet	medium	hex / tet	603 067	1 677 050	493 032
G2 side inlet	fine	hex / tet	1 393 297	3 712 451	1 003 701
G3 concentric baffles	medium	hex / tet	496 938	1 504 835	514 019
G3 concentric baffles	fine	hex / tet	1 281 915	3 849 273	1 302 190
G4 radial baffles	medium	Hex	661 284	2 032 935	711 392
G4 radial baffles	fine	Hex	1 349 657	4 127 977	1 429 959

6.3.3 Solver

Each simulation was run in two stages – the flow field was first established using the steady-state solver, then the RTD tracer simulation was performed using the transient solver. To establish the flow field, the steady-state Navier-Stokes equations were solved implicitly as segregated equations according to the SIMPLE method developed by Patankar (1980). Momentum, energy, and turbulence equations were discretized using the first-order upwind scheme. Relaxation factors used were as follows: 0.25 for pressure; 0.5 for momentum; 0.8 for turbulent kinetic energy, turbulent dissipation rate, and turbulent viscosity; and 1.0 for density, body forces, species transport, and energy. The normalized convergence criteria were: 10^{-4} for continuity, 10^{-6} for energy, and 10^{-5} for all other equations. The standard k-ε turbulence model with standard wall functions was used only when water was the working fluid, due to its low viscosity and thus, higher Reynolds number. The values of the empirical constants were taken at their default values: $C_\mu = 0.09$; $C_{1\varepsilon} = 1.44$; $C_{2\varepsilon} = 1.92$; $\sigma_k = 1.0$; $\sigma_\varepsilon = 1.3$.

6.3.4 Fluid properties

Since only isothermal conditions were considered, the only relevant fluid properties were density and viscosity. The density for all fluids was set at 1000 kg/m^3. Viscosity was set according to the parameters shown in Table 6.1. For cases that involved the non-Newtonian viscosity model, the energy equation was also required, since temperature influences the viscosity model. For these cases, the thermal properties of water at 298 K were set, though these properties have no real bearing on the model, since temperature is uniform throughout.

6.3.5 Boundary conditions

The inlet boundary conditions varied depending on the case: a detailed summary of these boundary conditions is given in Table 6.3. The mass flow rates were derived from the target volume flow rates, given a density of 1000 kg/m^3. For cases involving turbulence models, k-ε boundary conditions were set according to hydraulic diameter of the inlet and a turbulence intensity of 25%, estimated from initial PIV results. A no slip condition was applied at the walls, with zero heat transfer for cases that required the energy equation.

Table 6.3: Inlet boundary conditions

	H_2O – 0.05 L/s	**H_2O – 0.0125 L/s**	**Other fluids – 0.05 L/s**
Mass flow rate (kg/s)	0.05	0.0125	0.05
Direction vector	Normal to surface	Normal to surface	Normal to surface
Init. gauge pressure (Pa)	0	0	0
Turbulence intensity (%)	25	25	N/A
Hydraulic diameter (m)	0.01826	0.01826	N/A

6.3.6 Transient RTD Studies

To determine the RTD of the reactors, each reactor's transient response to a step tracer input was simulated. All flow conditions were held constant during these transient simulations; only the species transport equation was active to model the flow of tracer through the reactor. The first-order implicit transient solver was used. The species transport equation was turned on, with no volumetric reactions; inlet diffusion, thermal diffusion, and the diffusion energy source term were neglected. A tracer species was created with identical properties to the working fluid. The properties of the mixture were set as identical to the working fluid and tracer species; mass diffusion was set to 2.88×10^{-8} to neglect the effect of diffusion. The concentration of tracer species throughout the reactor was initialized to 0, while the concentration at the inlet was set to 0.1. A user-defined function (UDF) was defined to incorporate a non-uniform time step that increases as the simulation progresses, as shown in Table 6.4. The time step increases based on the flow time relative to the nominal HRT; for cases with Q = 0.05 L/s, HRT_{nom} is 600 s, while cases with Q = 0.0125 L/s, HRT_{nom} is 2400 s. A surface monitor was defined at the outlet to record the mass-averaged concentration of tracer species at each time step. The curve recorded can be translated to the F(t) curve for the reactor dividing by the initial inlet concentration.

Table 6.4: Non-uniform time step

Flow time interval	**Time step**	**HRT_{nom} = 600 s**	**HRT_{nom} = 2400 s**
t_{flow} / HRT < 0.002	HRT / 3000	Δt = 0.2 s	Δt = 0.8 s
0.002 ≤ t_{flow} / HRT < 0.05	HRT / 1200	Δt = 0.5 s	Δt = 2.0 s
0.05 ≤ t_{flow} / HRT < 0.2	HRT / 300	Δt = 2.0 s	Δt = 8.0 s
0.2 ≤ t_{flow} / HRT < 1.5	HRT / 120	Δt = 5.0 s	Δt = 20.0 s
t_{flow} / HRT ≥ 1.5	HRT / 30	Δt = 20.0 s	Δt = 80.0 s

6.4 Grid independence tests

Grid independence tests were conducted to ensure quality of the solution. Water was used as the working fluid, at a flow rate of 0.05 L/s; turbulent conditions were assumed. For G1 centre inlet, three grids were created with coarse, medium, and fine mesh sizes; only medium and fine grids were constructed for the other three geometries. The mesh statistics for these grids are shown in Table 6.2. Figures 6.6 through 6.9 compare the velocity profiles along lines running in the x, y, and z directions. As shown in Figure 6.6, a dominant feature of the velocity field for G1 is the jet produced by the centre inlet (a, c, and d). Figure 6.6b shows how this jet is directed downward after impinging on the far cylinder wall. All three grids produce closely-matched results; the medium and fine grids produce almost identical profiles, agreeing to with 0.5%, relative to an inlet velocity of 0.19 m/s.

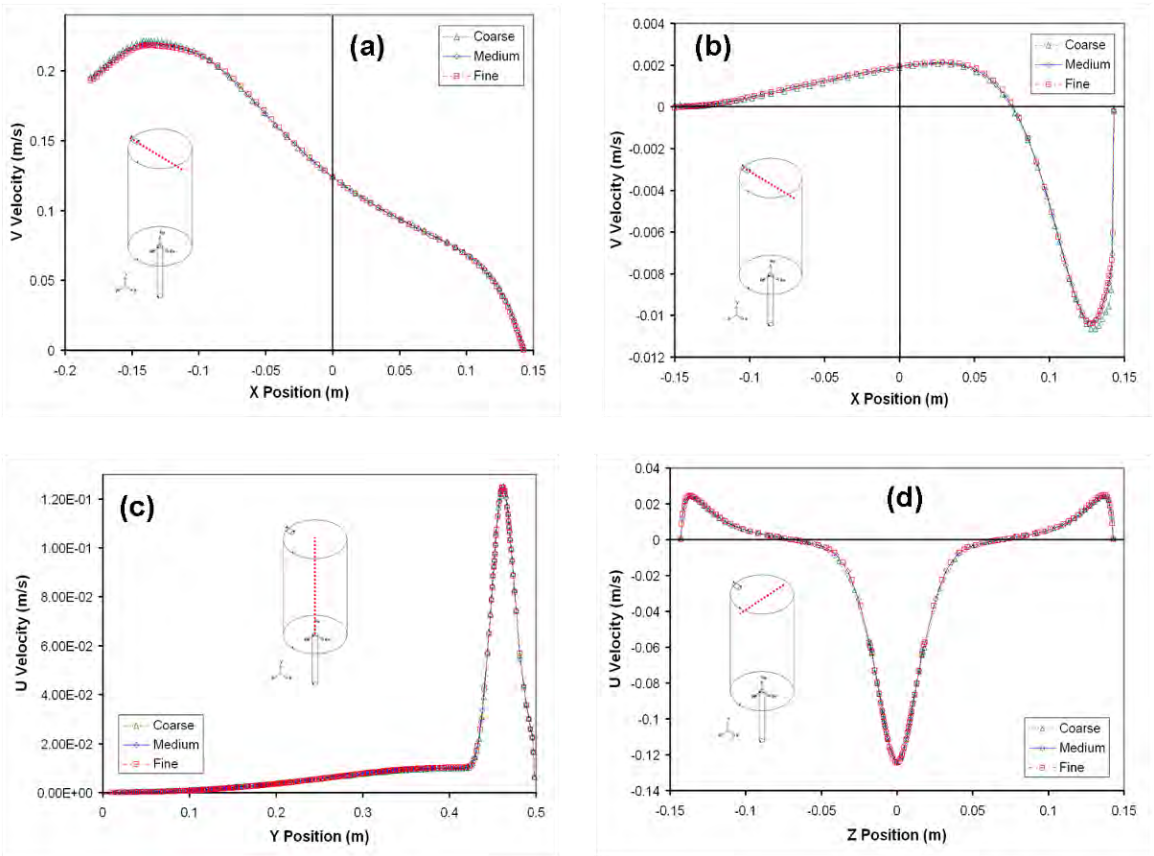

Figure 6.6: Velocity profiles for G1 centre inlet

Selected velocity profiles for the G2 side inlet geometry are shown in Figure 6.7. The U and W velocity profiles (b and d) show the swirling nature of the flow in this geometry, with high tangential velocity components near the cylindrical wall. The centerline profile of V velocity (c) shows a large velocity gradient near the bottom of the reactor, as fluid speeds up towards the outlet. The profiles generated by both medium and fine grids are in excellent agreement with each other. The largest disagreement in the profiles shown is 2.0% in the U velocity vs. z position profile (d). All other profiles have maximum disagreements of less than 0.80%.

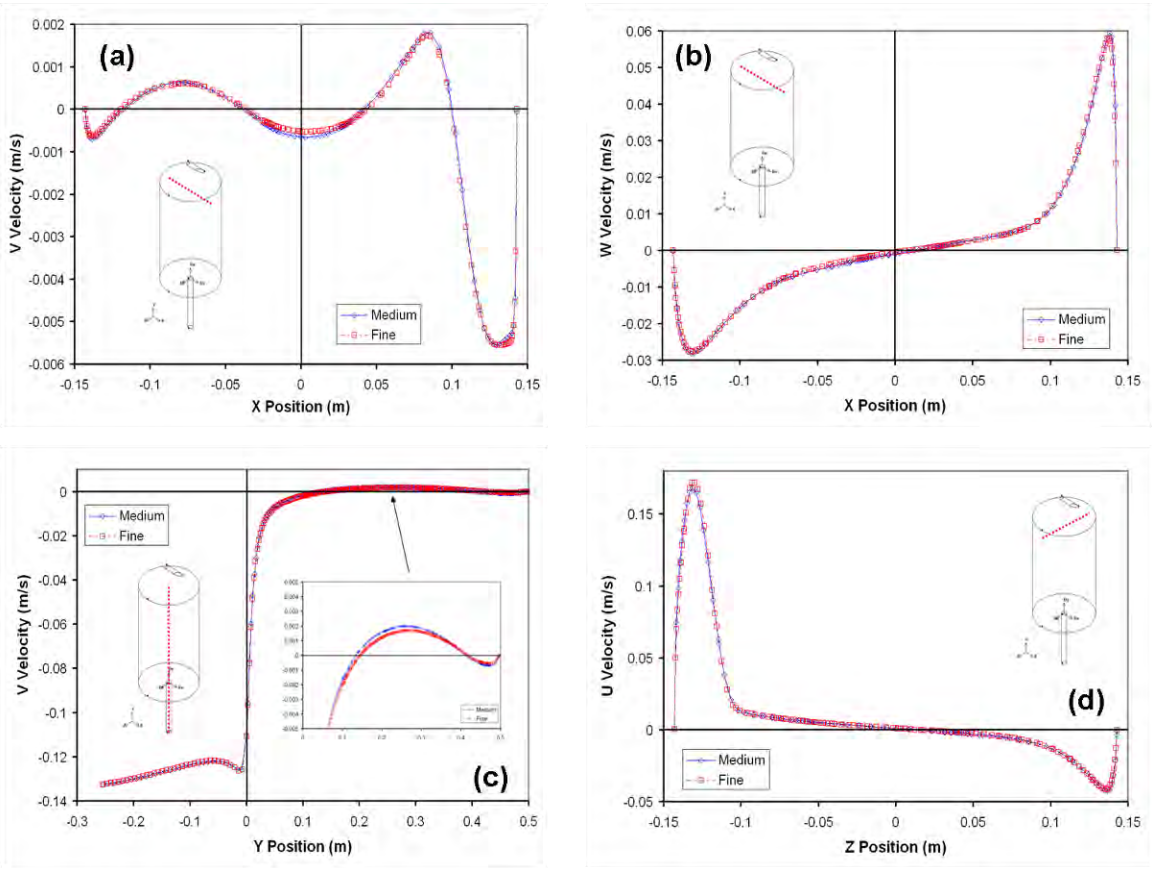

Figure 6.7: Velocity profiles for G2 side inlet

Figure 6.8 shows selected velocity profiles for the G3 concentric baffles geometry. Excellent agreement is evident between the medium and fine meshes for all profiles. These profiles show how the concentric baffles shape the flow. The U velocity profiles (a and c) indicate the presence of a jet that flows through the top hole in the innermost baffle. The V velocity vs. x position profile (b) shows how this jet impinges against the inner wall of the baffle, opposite the hole, and is directed downward toward the outlet. All velocity profiles agree to within 1.0% of the inlet velocity.

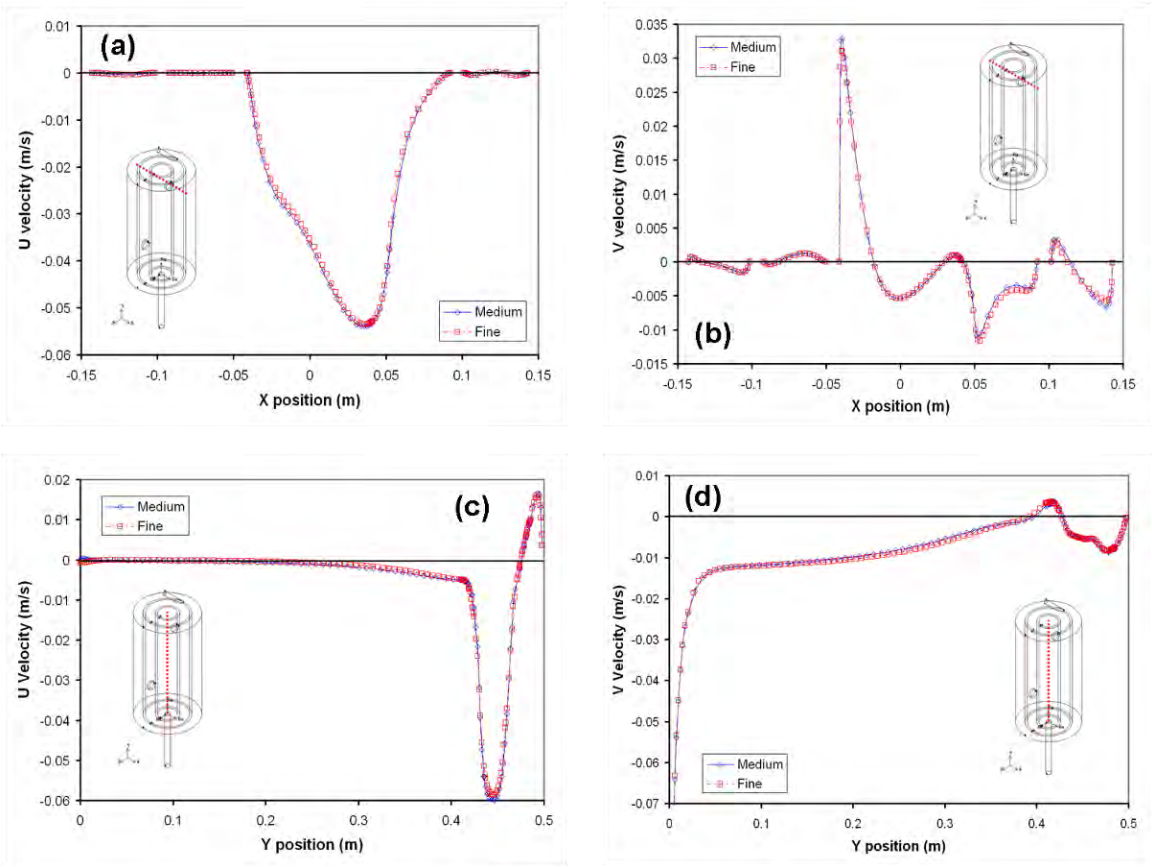

Figure 6.8: Velocity profiles for G3 concentric baffles

Four velocity profiles are shown in Figure 6.8 for vertical lines in the G4 radial baffles geometry. The profile in (a) shows the U velocity along the centreline of the first section (downward flowing) of this reactor. The profiles in (b) through (d) correspond to the centreline of the second section of the reactor; the fluid flows upwards in this section. The U velocity profiles in (a) show a maximum difference of 2.1% between the medium and fine mesh solution; the other profiles agree to within 0.60%. Since all the profiles examined show excellent agreement between medium and fine grids, the medium grids were chosen for all geometries.

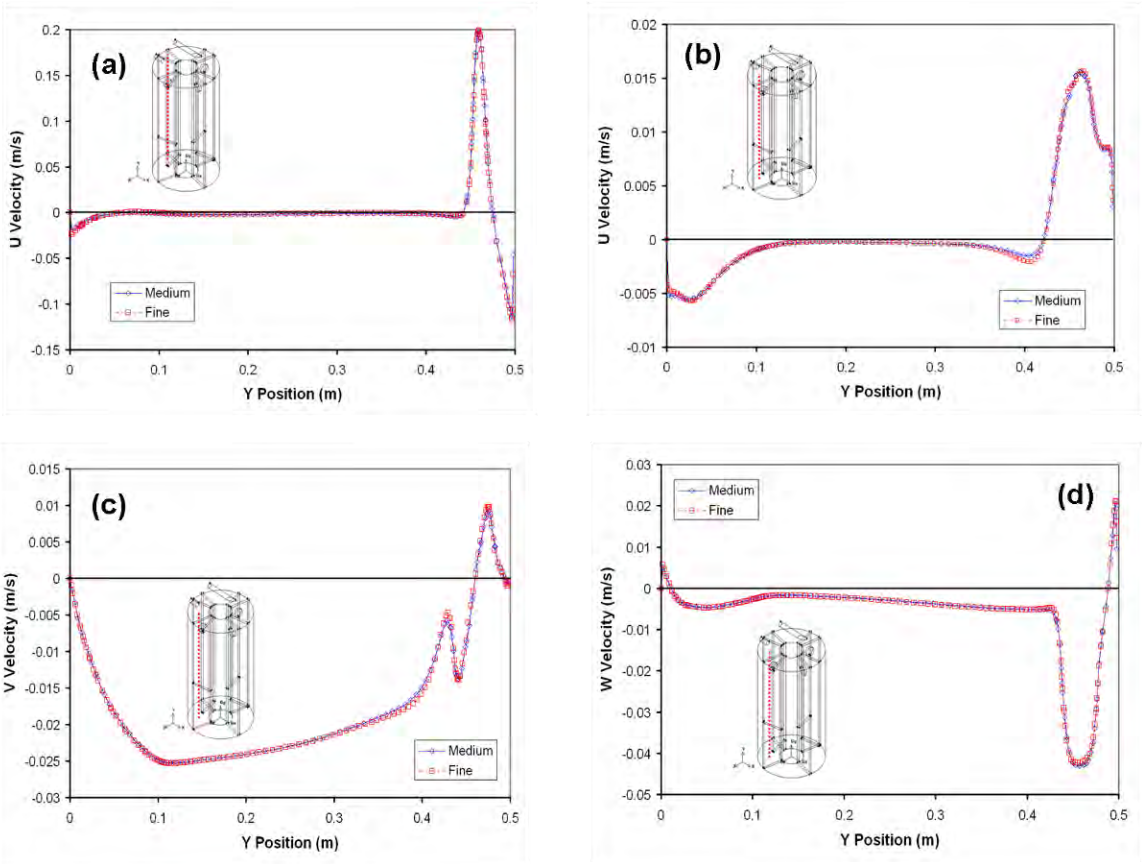

Figure 6.9: Velocity profiles for G4 radial baffles.

6.5 Results and discussion

Twenty-four simulations were performed as a part of this CFD study; these cases are summarized in Table 6.5. In Cases 1 through 20, the dimensions and flow rates used correspond directly to those used in the experimental RTD study described in Chapter 5. For these cases, four fluids were tested; water, a 1 g/L xanthan gum solution, and liquid hog manure at 3% and 8% total solids concentration. The hydraulic retention time for the 0.05 L/s cases varies from 8.2 to 10.2 minutes, depending on geometry; the HRT for the 0.0125 L/s cases varies from 32.9 to 42.4 minutes. The Reynolds number for these lab-scale simulations varies between 98.96 (8% TS manure) and 3479 (water, 0.05 L/s).

Cases 21 through 24 were performed using scaled-up versions of G1 and G4. The size of these pilot-scale reactor geometries was chosen to reflect the scale of the pilot anaerobic digesters at the University of Manitoba Glenlea Research Station. The volume of these reactors is 2000 L, and the HRT is approximately 17 days. Due to the low flow rates for these simulations, Re_{in} is very small.

Table 6.5: Summary of CFD cases

Case	Geometry	Fluid	Flow regime	Q (L/s)	HRT (s)	Re_{in}
1	G1 center inlet	H2O	turbulent	0.05	635	3479
2	G1 center inlet	H2O	turbulent	0.0125	2541	869.7
3	G1 center inlet	XG	laminar	0.05	635	268.1
4	G1 center inlet	Manure 3% TS	laminar	0.05	635	374.5
5	G1 center inlet	Manure 8% TS	laminar	0.05	635	98.96
6	G2 side inlet	H2O	turbulent	0.05	635	3479
7	G2 side inlet	H2O	turbulent	0.0125	2541	869.7
8	G2 side inlet	XG	laminar	0.05	635	268.1
9	G2 side inlet	Manure 3% TS	laminar	0.05	635	374.5
10	G2 side inlet	Manure 8% TS	laminar	0.05	635	98.96
11	G3 concentric baffles	H2O	turbulent	0.05	635	3479
12	G3 concentric baffles	H2O	turbulent	0.0125	2541	869.7
13	G3 concentric baffles	XG	laminar	0.05	635	268.1
14	G3 concentric baffles	Manure 3% TS	laminar	0.05	635	374.5
15	G3 concentric baffles	Manure 8% TS	laminar	0.05	635	98.96
16	G4 radial baffles	H2O	turbulent	0.05	635	3479
17	G4 radial baffles	H2O	turbulent	0.0125	2541	869.7
18	G4 radial baffles	XG	laminar	0.05	635	268.1
19	G4 radial baffles	Manure 3% TS	laminar	0.05	635	374.5
20	G4 radial baffles	Manure 8% TS	laminar	0.05	635	98.96
21	G1: pilot-scale	H2O	laminar	0.00136	1.471×10^6	23.9
22	G1: pilot-scale	Manure 8% TS	laminar	0.00136	1.471×10^6	0.006854
23	G4: pilot-scale	H2O	laminar	0.00136	1.471×10^6	23.9
24	G4: pilot-scale	Manure 8% TS	laminar	0.00136	1.471×10^6	0.006854

6.5.1 Reactor geometry 1, centre inlet

Figures 6.10 and 6.11 show the pathlines of fluid particles for the centre inlet geometry G1, with a flow rate of 0.05 L/s. These figures are coloured according to the velocity

magnitude, on a logarithmic scale. There is a striking difference between the Newtonian cases (Figure 6.10) and the non-Newtonian cases (Figure 6.11). In the Newtonian cases, the inlet jet projects directly across the reactor, impinging on the opposite wall. This jet diffuses quicker in the case where water is the working fluid (a), due to turbulence. After impinging against the wall, the fluid swirls in half-circles towards the outlet. In the non-Newtonian cases (Figure 6.11), the jet diffuses well before it reaches the opposite wall. After leaving the inlet, the pathlines are drawn quickly down towards the outlet. In the case where 8% TS manure is the working fluid (b), the jet barely exists at all. By comparing these four cases, it is evident that viscosity has a profound impact on the behaviour of the fluid within the reactor.

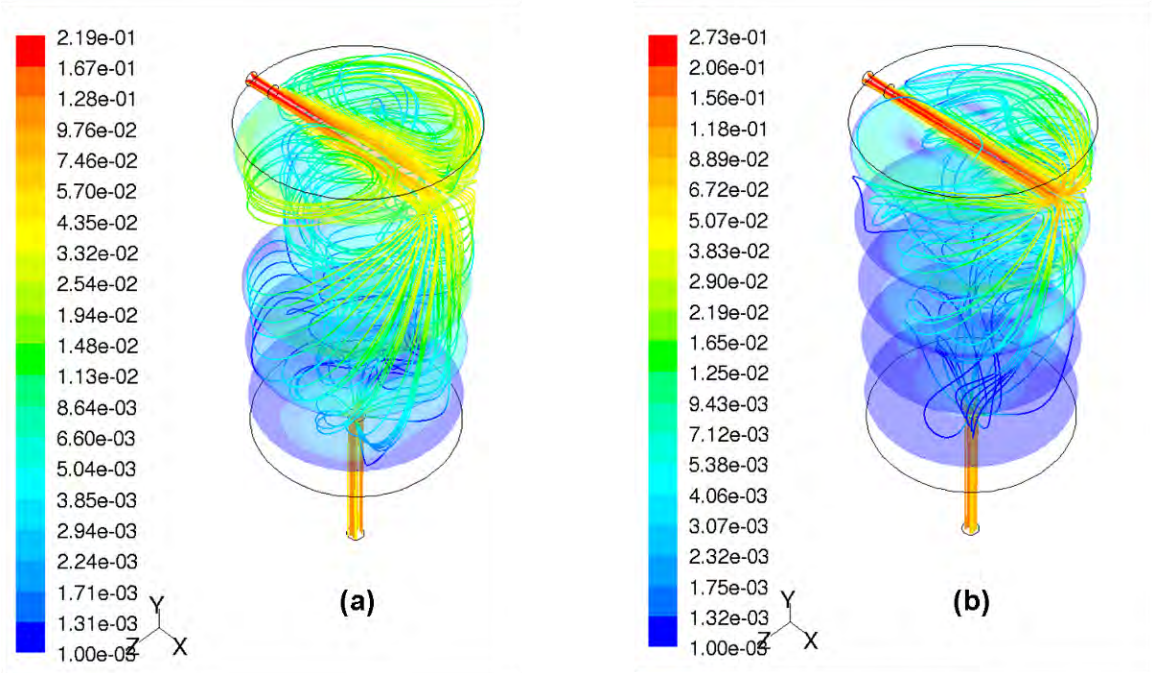

Figure 6.10: Velocity magnitude and pathlines for G1 centre inlet. a) water; b) 3% TS manure

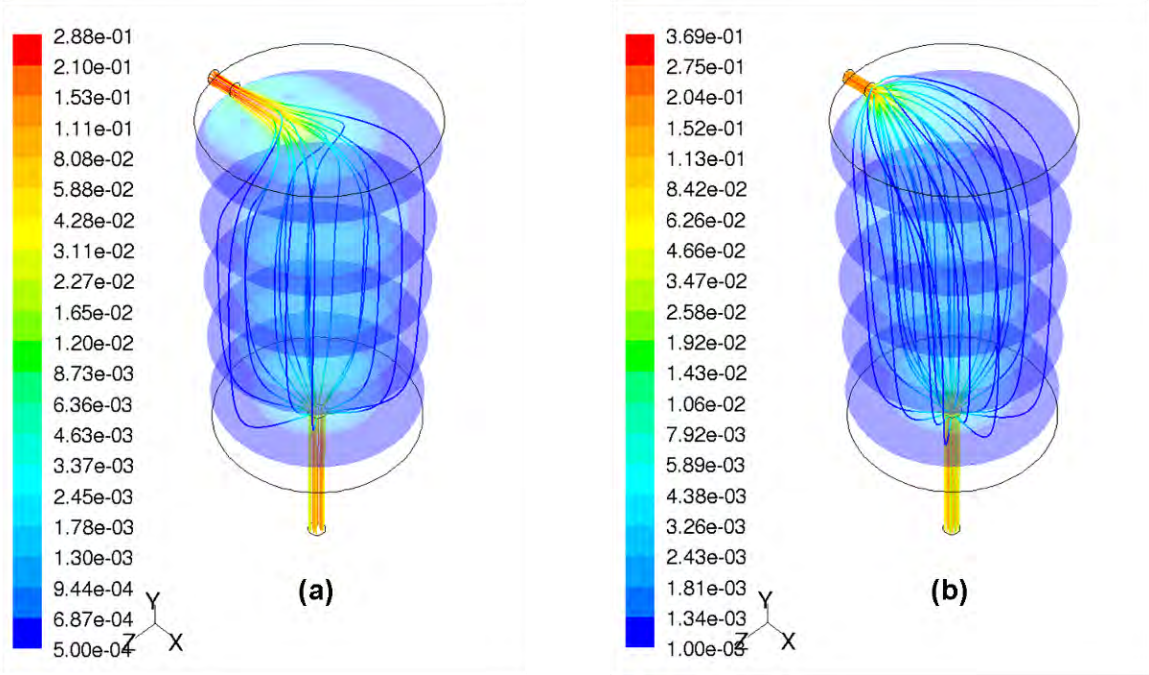

Figure 6.11: Velocity magnitude and pathlines for G1 centre inlet. a) xanthan gum; b) 8% TS manure

The variation of apparent viscosity for the non-Newtonian cases is shown in Figure 6.12. Due to the power law relationship between shear rate and apparent viscosity, apparent viscosity is high in regions with low degrees of shear, and low in regions with high shearing. In both cases, the lowest apparent viscosities occur at the inlet and outlet, while the highest apparent viscosities occur in the centre of the reactor, as well as where the cylindrical wall meets the lid and the floor. In the xanthan gum case, the upper limit of apparent viscosity (4.36 Pa·s) is reached, but not the lower limit (0.0119 Pa·s). The opposite is true for the case of 8% TS manure.

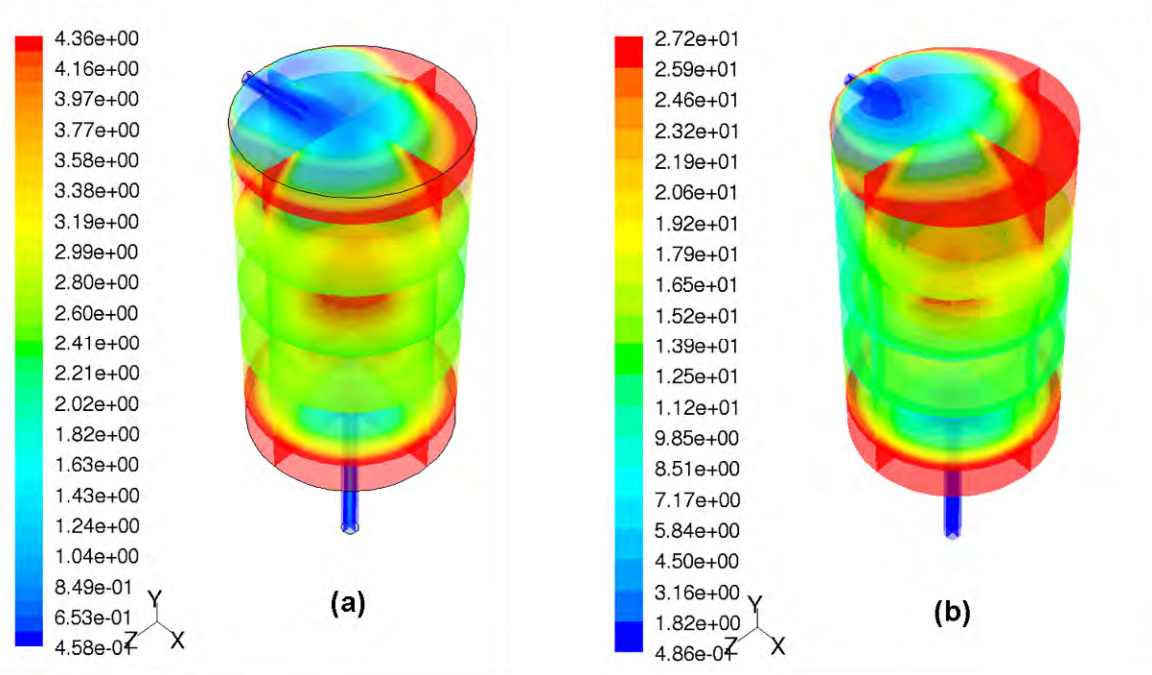

Figure 6.12: Apparent viscosity for G1 centre inlet. a) xanthan gum; b) 8% TS manure

The flow patterns described above can be related to the residence time distributions for G1 as shown in Figure 6.13. The difference in flow patterns between the Newtonian and non-Newtonian fluids is also reflected in the RTD. For water and the 3% TS manure, the value at the peak is relatively low: 0.85 and 0.98, respectively. These curves are more rounded and feature larger exponential tails, indicating a high degree of macromixing and dispersion. In contrast, the non-Newtonian cases shows longer delays, higher and sharper peaks (2.11 and 2.30 for xanthan gum and 8% TS manure, respectively), and quicker decays. For this reactor geometry, the xanthan gum and the high-solids manure produce similar RTD curves. However, there are significant differences between the two Newtonian cases. Compared to water, the low-solids manure has a much later peak; it also shows a secondary peak that occurs at $\theta = 0.15$. This secondary peak indicates a small degree of short-circuiting, however this is difficult to identify from the pathlines

shown in Figure 6.10. In terms of overall parameters, the non-Newtonian cases have smaller variances, but higher fractions of dead space. The non-Newtonian cases also have mean values that fall well short of 1.0; this indicates that the effective volume of the reactor in these cases is greatly reduced. The fact that a significant portion of the digester volume is ineffective can also be concluded by examining Figures 6.11 and 6.12; the large stagnant regions at the outer edges of the reactor, where apparent viscosity is very high, are essentially dead spaces. Thus, it can be concluded that a good reactor design would avoid sharp corners and 90° angles when a non-Newtonian fluid is involved.

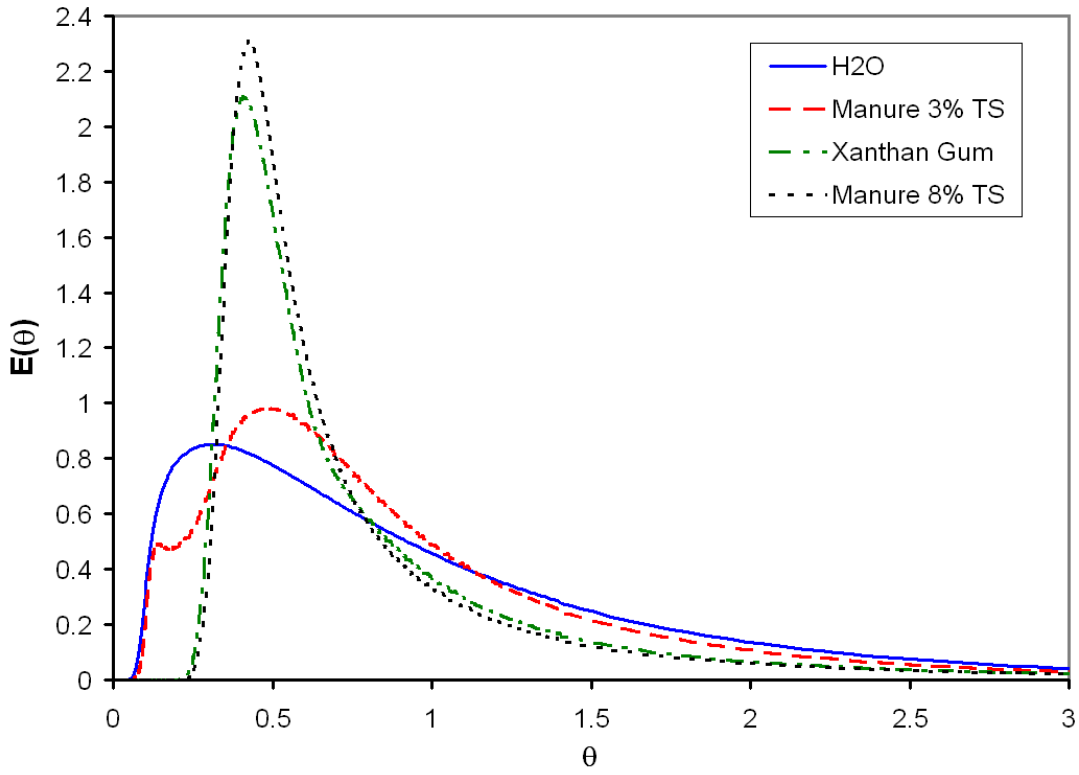

Figure 6.13: Residence time distributions for G1 centre inlet, CFD results

Table 6.6: Overall RTD parameters, G1 centre inlet

Fluid	θ_m	σ_θ^2	Dead space	Peak value	Loc. of peak
H2O	1.010	0.6961	0.3009	0.8516	0.313
Manure 3% TS	0.9460	0.5145	0.2967	0.9809	0.485
Xanthan gum	0.8314	0.4377	0.3668	2.105	0.407
Manure 8% TS	0.8106	0.4192	0.3783	2.304	0.422

6.5.2 Reactor geometry 2, side inlet

The pathlines and velocity contours for the side inlet geometry G2 are shown in Figures 6.14 and 6.15; the flow rate for these cases is 0.05 L/s. As with G1, there are significant differences between the Newtonian and non-Newtonian cases. For water and low-solids manure, there is a high degree of swirl in the clockwise direction (as viewed from the top). The swirl is still present in the xanthan gum case, but only in the top third of the reactor. However, the swirl is lost completely in the high-solids manure case; fluid entering the reactor from the inlet is immediately drawn toward the outlet. In the Newtonian cases, the velocity is low near the centre of the reactor; velocity increases as one moves radially outward. This opposite trend is true for the non-Newtonian cases, where the velocity is low near the wall, and increases towards the centre. The maximum velocity is higher in the non-Newtonian cases than in the Newtonian cases (especially in the case of 8% TS manure), but the region of maximum velocity is much smaller in the non-Newtonian cases.

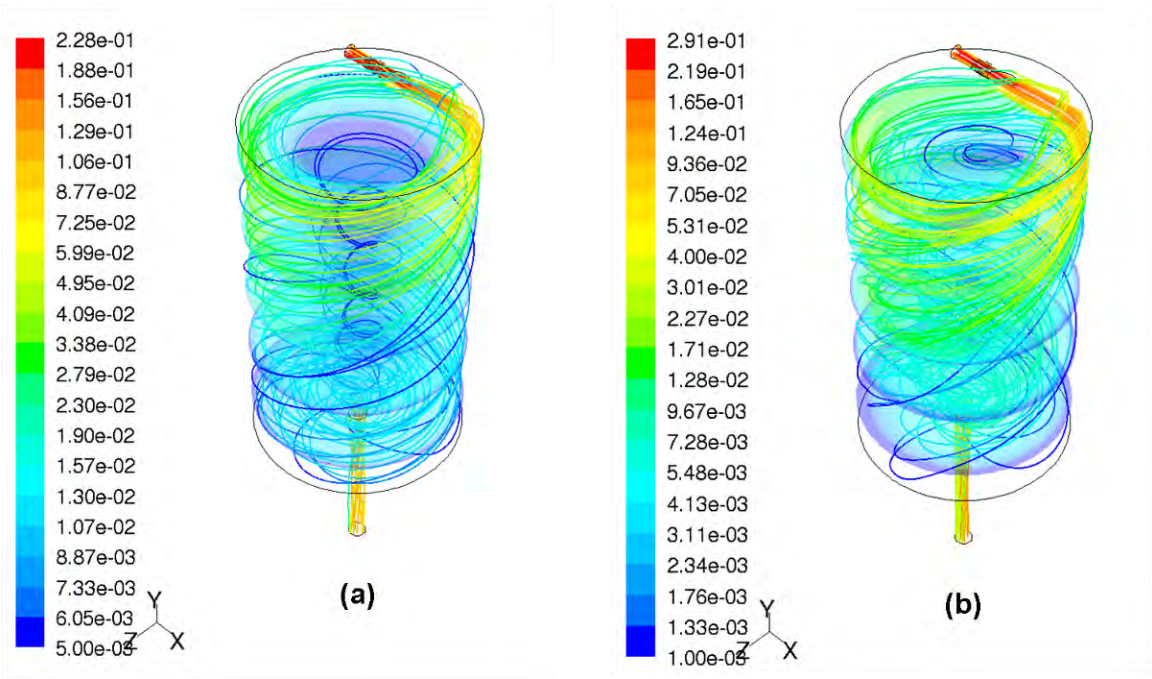

Figure 6.14: Velocity magnitude and pathlines for G2 centre inlet. a) water; b) 3% TS manure

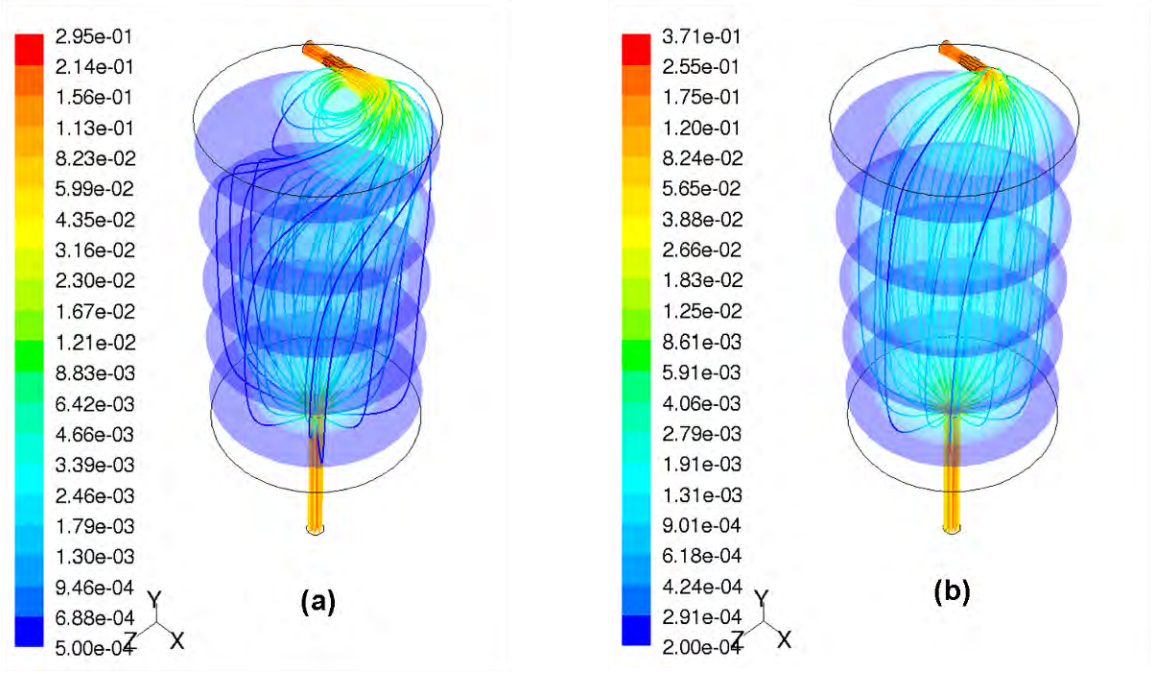

Figure 6.15: Velocity magnitude and pathlines for G2 centre inlet. a) xanthan gum; b) 8% TS manure

Figure 6.16 shows the variation of apparent viscosity within the reactor for xanthan gum (a) and 8% TS manure (b). Similar to G1, the apparent viscosity is lowest near the inlet and outlet, and highest at the edges and in the centre. In the upper part of the reactor, the high-viscosity region is non-axisymmetrical with respect to the y-axis; however, at the bottom of the reactor, the high viscosity region is axisymmetrical. In the case of xanthan gum, the upper viscosity limit is reached (4.36 Pa·s), but not the lower limit; in the case of 8% TS manure, neither limit comes into play.

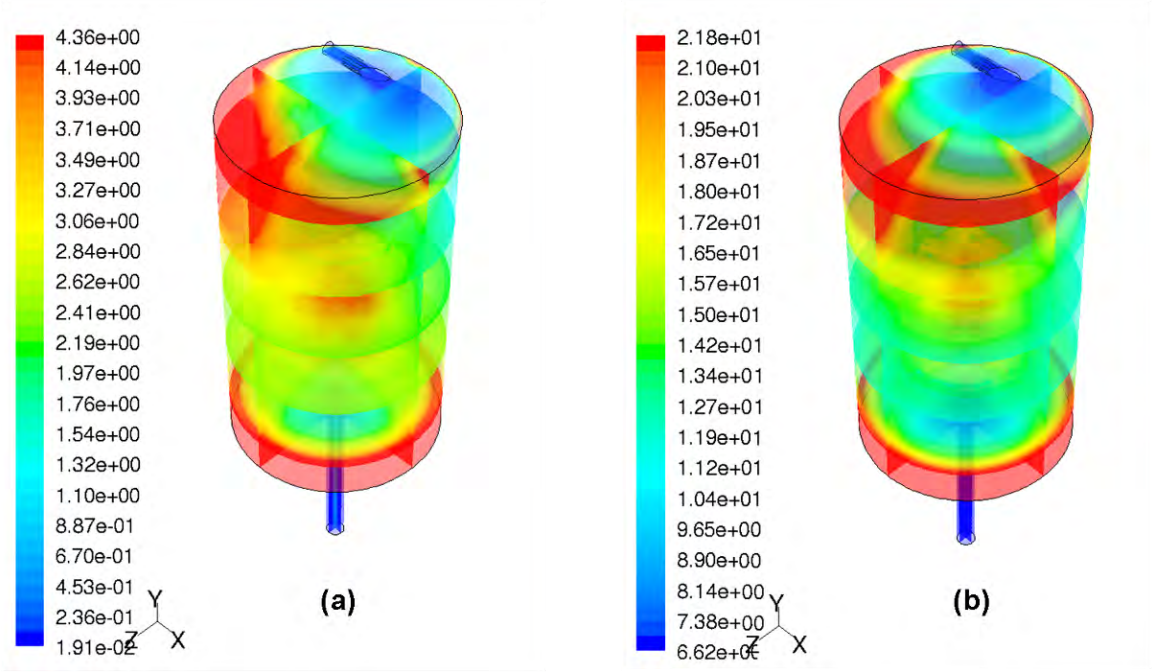

Figure 6.16: Apparent viscosity for G2. a) xanthan gum; b) 8% TS manure

The RTD curves for G2 are shown in Figure 6.17, and the overall parameters are summarized in Table 6.7. Compared to G1, the peaks of the water and low-solids manure cases are higher, sharper, and earlier. As with G1, the 3% TS manure case has a subtle, secondary peak; however, in this case, the primary peak occurs first, and is dramatic,

rising to a value of 1.85. The non-Newtonian RTD curves are similar to the G1 cases. The mean values for all cases are similar to G1; once again, the xanthan gum and high-solids manure fall quite short of 1.0. For the non-Newtonian cases, the variance changes little from G1 to G2; in contrast, the variance decreases moderately for the case of water, and increases dramatically from 0.515 to 0.820 for the case of 3% TS manure. The fraction of dead space is similar to the G1 cases, with the exception of 3% TS manure, where the dead space increases from 0.297 to 0.438.

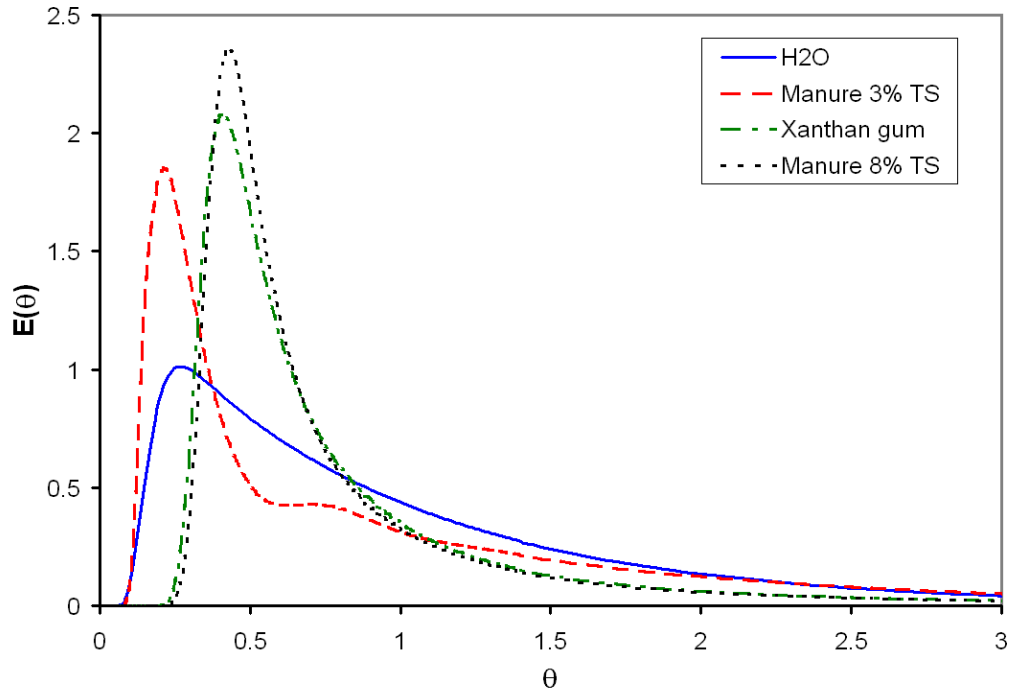

Figure 6.17: Residence time distributions for G2 side inlet, CFD results

Table 6.7: Summary of parameters, G2 side inlet

Fluid	θ_m	σ_θ^2	Dead space	Peak value	Loc. of peak
H2O	0.9862	0.6231	0.3193	1.012	0.274
Manure 3% TS	0.9417	0.8204	0.4380	1.850	0.211
Xanthan Gum	0.8180	0.4306	0.3672	2.081	0.407
Manure 8% TS	0.8037	0.4109	0.3767	2.357	0.430

Figure 6.18 compares the RTD curves for the G1 and G2 manure cases. It is immediately apparent that the RTD curves for 3% TS manure have completely different shapes; however, the 8% manure cases are nearly identical. Thus, the jet flow of G1 and the swirling flow of G2 produce very different RTD characteristics for low-viscosity, laminar flow. However, in high-viscosity, pseudoplastic flow, the jet or swirl is lost, so similar RTD curves are produced for both geometries. In turbulent flow (the water cases), the jet flow and swirling flow still exist, but the turbulent mixing reduces the effect of these flow patterns on the resulting RTD curves.

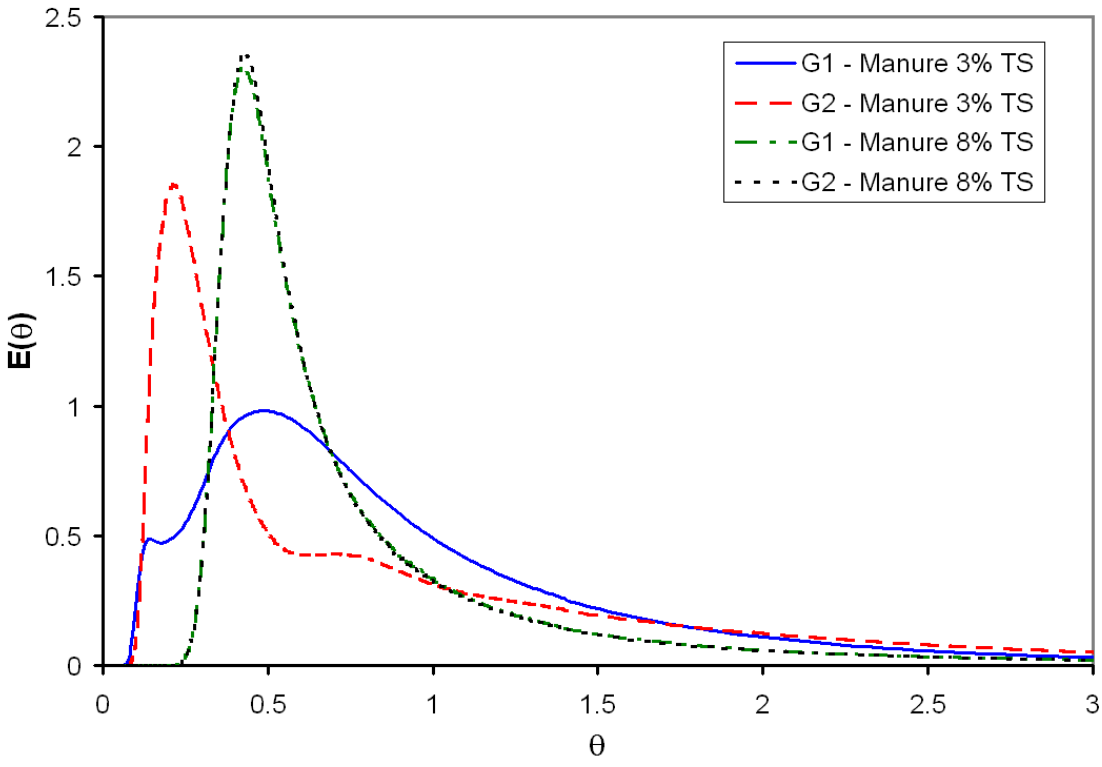

Figure 6.18: Comparison of RTD for simulated manure cases, G1 vs G2

In general, the high variances, early peaks, and large fractions of dead space produced by these first two geometries indicate that they are poor reactor designs. An ideal reactor design produces an RTD curve with a small variance, a small fraction of dead space, and

a peak that occurs at approximately 1 HRT. The introduction of baffles to direct the flow will now be investigated to determine if baffles might have a positive effect on digester performance.

6.5.3 Reactor geometry 3, concentric baffles

Geometry 3, created by adding two concentric baffles to Geometry 2, exhibits different characteristics than the previous two geometries. The velocities and pathlines for G3 are shown in Figures 6.19 and 6.20. This reactor geometry is designed so that fluid flows down through the outer chamber, then up through the intermediate chamber, then down again through the final, inner chamber. When water is the working fluid (Figure 6.19a), the flow in the outer chamber has a strong swirl in the clockwise direction as viewed from the top. Coming up through the intermediate chamber, the flow retains a clockwise motion; however, the tangential component of velocity is much lower than in the previous chamber. In the inner chamber, the swirl is lost completely, as fluid flows straight down towards the outlet. When water is replaced with 3% TS manure (b), the upper half of the outer chamber possesses a strong clockwise swirl; this swirl diminishes in the lower half of the chamber as fluid is drawn towards the entrance to the intermediate chamber (lower hole). There is no clockwise motion at all in the intermediate chamber; the flow branches around the inner baffle as it travels towards the entrance to the third chamber (upper hole). Again, flow in the inner chamber is straight downward.

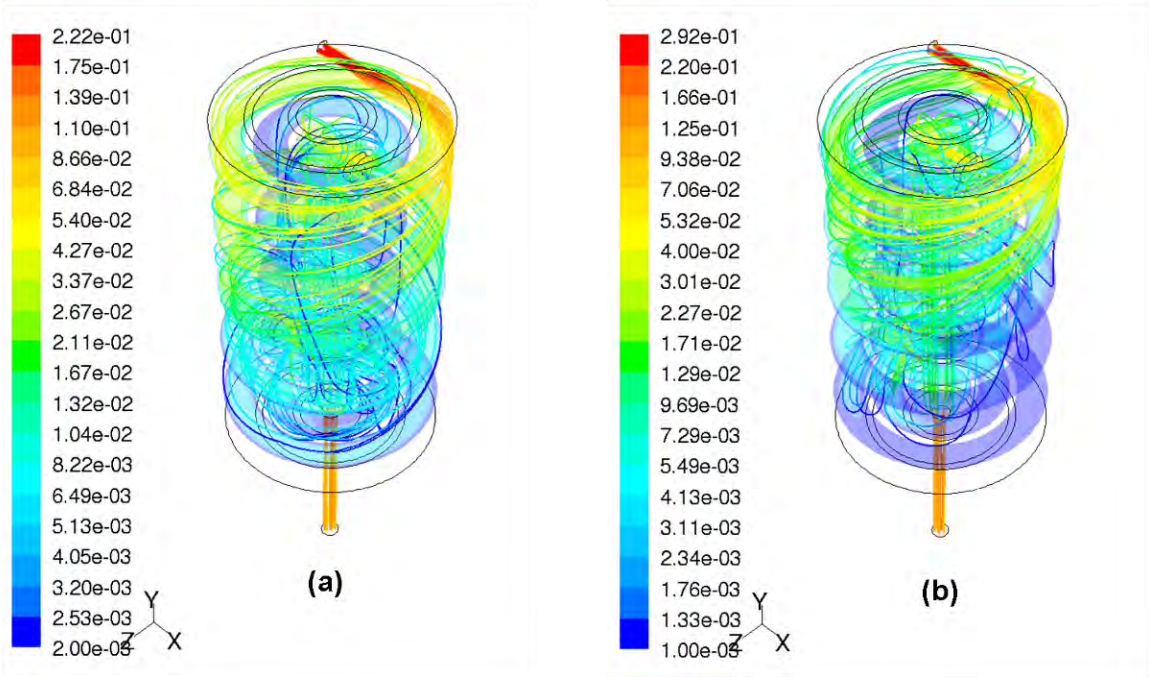

Figure 6.19: Velocity magnitude and pathlines for G3 concentric baffles. a) water; b) 3% TS manure

The xanthan gum case is shown in Figure 6.20a. Fluid in the outer chamber travels almost one full revolution in the clockwise direction as it moves downward from the inlet to the entrance to the intermediate chamber. This represents a significant decrease in swirl from the 3% TS manure case. Finally, in the 8% TS manure case (Figure 6.20b), the fluid actually reverses direction and travels slightly counterclockwise as it flows downwards through the outer chamber. In this case, the portion of the outer chamber that is opposite to the inlet is nearly stagnant.

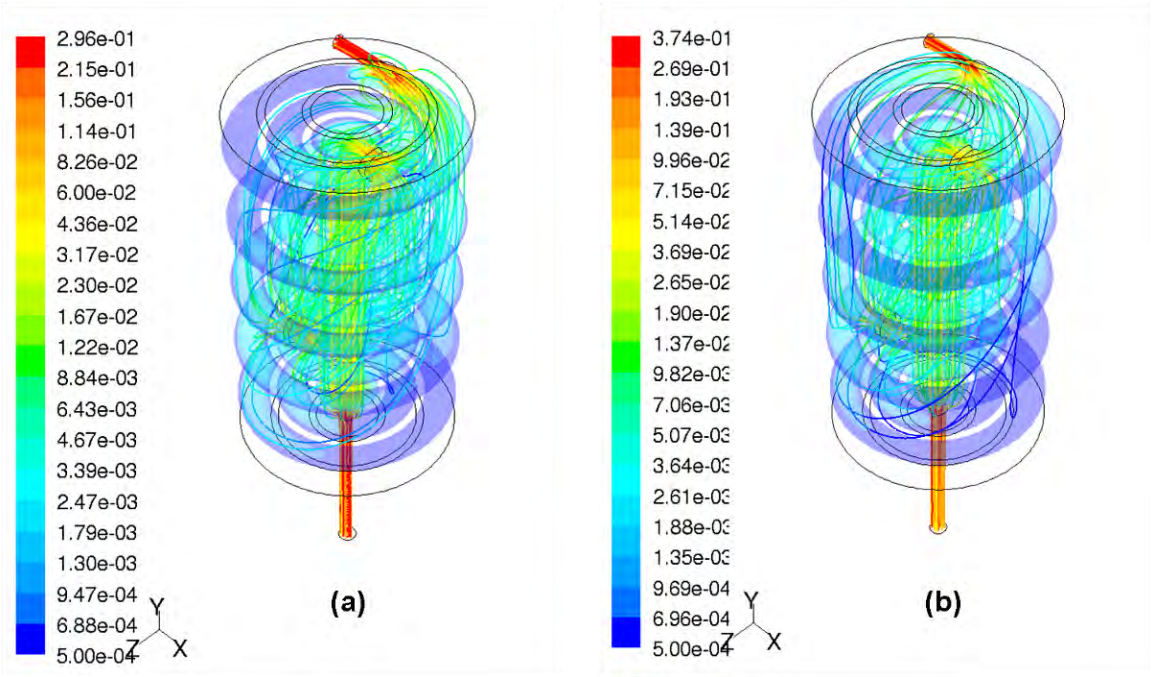

Figure 6.20: Velocity magnitude and pathlines for G3 concentric baffles. a) xanthan gum; b) 8% TS manure

Figure 6.21 depicts the variation of apparent viscosity throughout this reactor geometry for the non-Newtonian cases. In the case of xanthan gum (a), the apparent viscosity is low near the inlet and outlet, as well as in the intermediate and inner chambers. Regions of high viscosity appear in the outer chamber, near the top and bottom. The upper viscosity limit (4.36 Pa·s) comes into play in this case, but the lower limit does not. In the high-solids manure case (b), apparent viscosity is high in the large stagnant region found in the outer chamber, opposite the inlet. Both high and low viscosity limits are reached in this case.

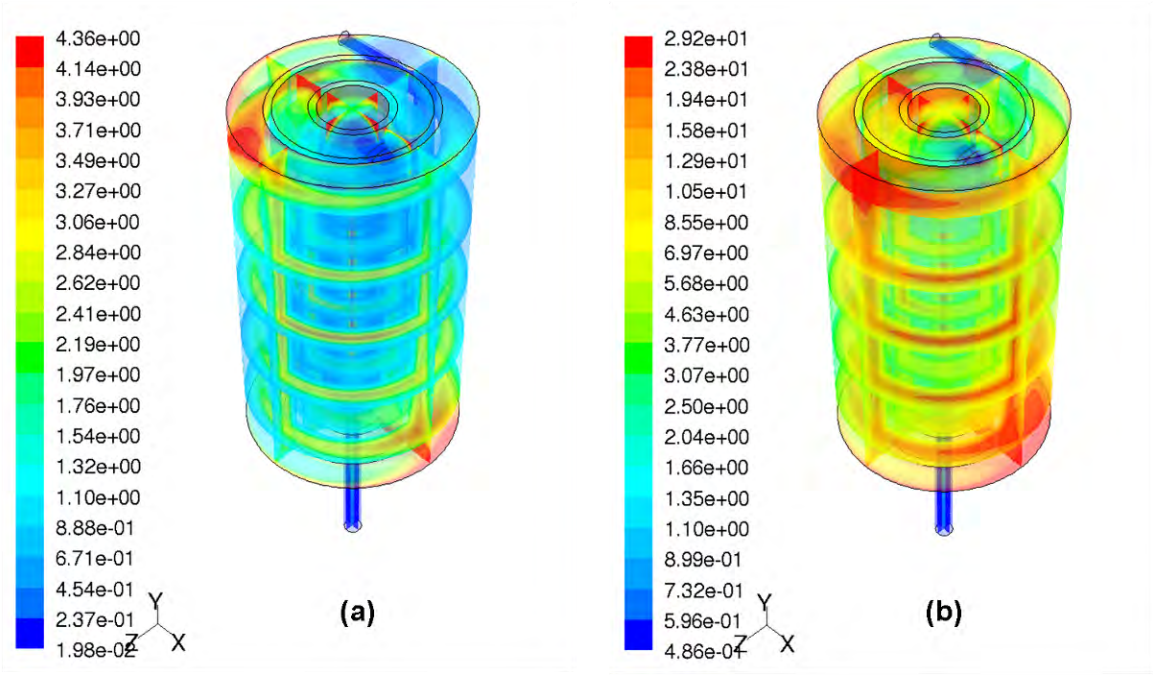

Figure 6.21: Apparent viscosity for G3. a) xanthan gum; b) 8% TS manure

Based on the flow patterns shown above, it is apparent that the full volume of reactor geometry G3 is used most effectively when water is the working fluid. This conclusion is reinforced by the RTD curves for G3, as shown in Figure 6.22. The water case exhibits a relatively low variance of 0.150, a small fraction of dead space, 0.041, and a peak value that occurs at 0.81 (see Table 6.8). This is the most favourable RTD encountered so far. However, the other three fluids possess higher variances, larger fractions of dead space, and earlier peaks, making them much less favourable. Predictably, the 8% manure case shows the highest values for variance and dead space: 0.622 and 0.360, respectively. Considering the variance and dead space, the low-solids manure and xanthan gum cases show definite improvement over the previous two geometries. Overall, geometry G3 is an excellent example of how the viscous properties of the working fluid can significantly affect the performance characteristics of the reactor.

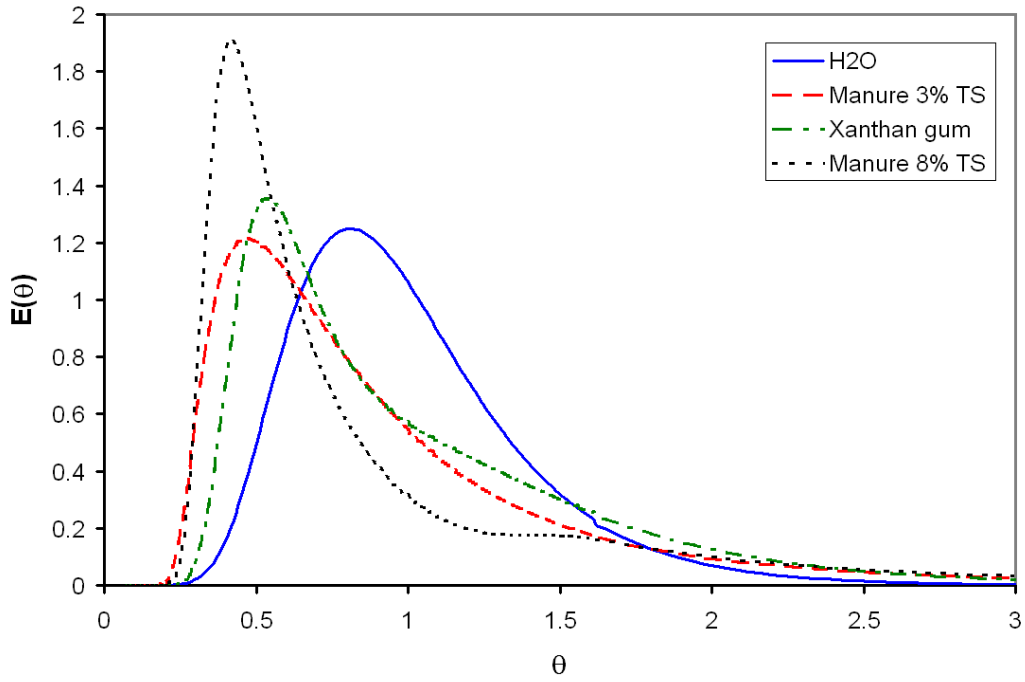

Figure 6.22: Residence time distributions for G3 concentric baffles, CFD results

Table 6.8: Summary of overall parameters, G3 concentric baffles

Fluid	θ_m	σ_θ^2	Dead space	Peak value	Loc. of peak
H2O	1.008	0.1499	0.0414	1.250	0.810
Manure 3% TS	0.9613	0.4781	0.2628	1.215	0.468
Xanthan Gum	1.008	0.3473	0.1729	1.355	0.540
Manure 8% TS	0.9279	0.6221	0.3597	1.906	0.414

6.5.4 Reactor geometry 4, radial baffles

Reactor geometry G4 represents a significant departure from the previous three geometries. The radial baffles introduced in G4 divide the cylindrical tank into eight straight channels. As shown in Figures 6.23 and 6.24, there is significantly less variation in the flow field between the four working fluids, as compared to the previous three reactor geometries. The most significant differences between these four cases relates to

the flow behaviour at the corners. For the Newtonian cases, pathlines come fairly close to the corners; however, for the non-Newtonian cases, large stagnant zones develop in the corners. This is especially evident in at the bottom of the reactor, as fluid passes under the short baffles and is redirected upwards.

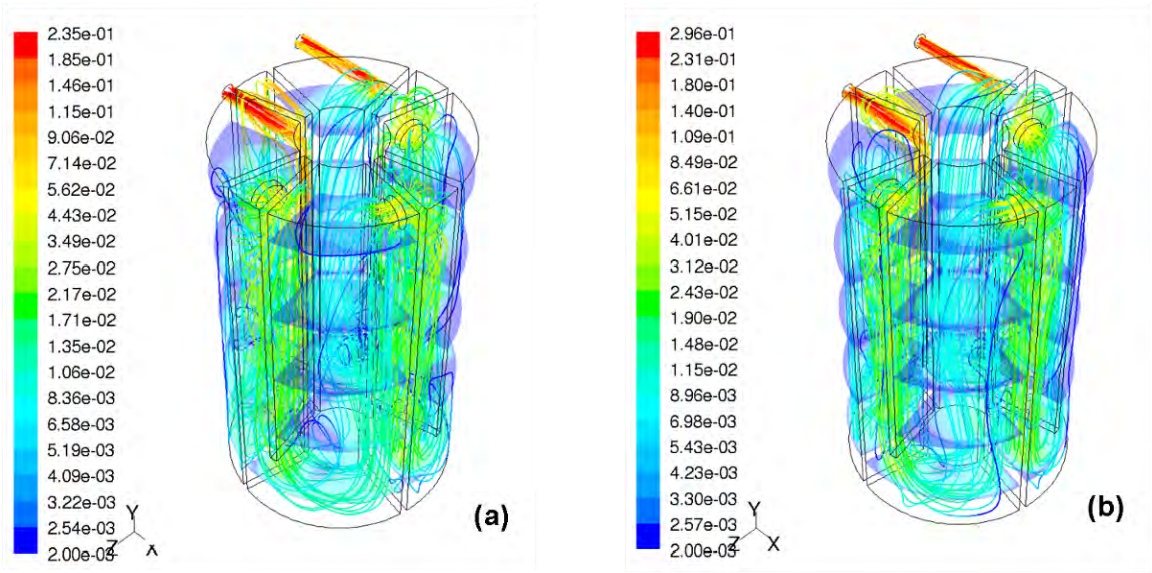

Figure 6.23: Velocity magnitude and pathlines for G4 radial baffles. a) water; b) 3% TS manure

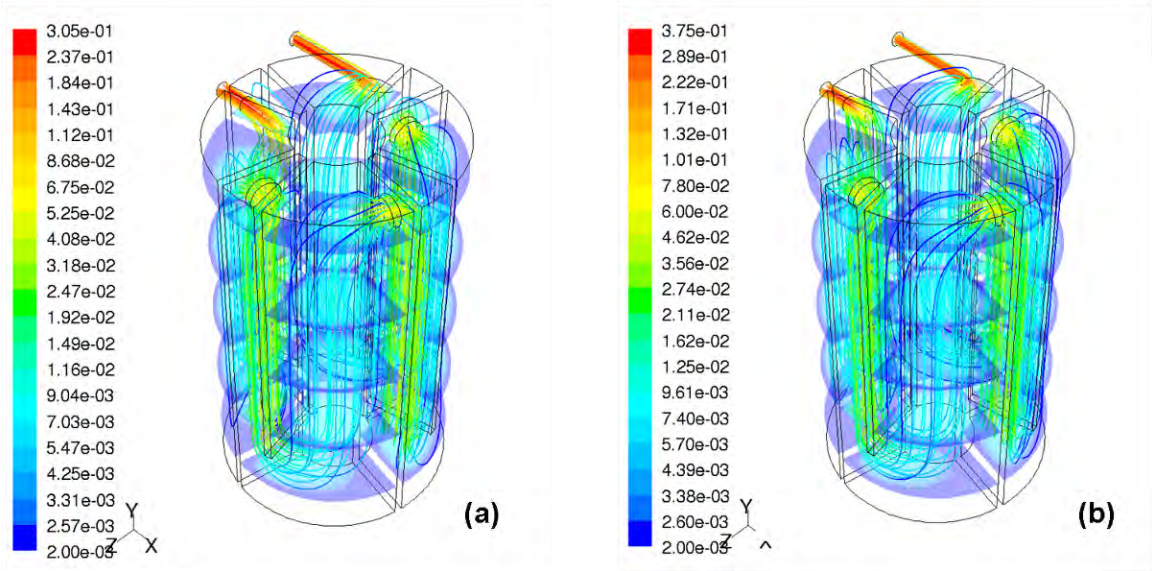

Figure 6.24: Velocity magnitude and pathlines for G4 radial baffles. a) xanthan gum; b) 8% TS manure

Figure 6.25 represents the variation in apparent viscosity for the non-Newtonian fluids; the 1 g/L xanthan gum solution is shown in (a), and the 8% TS liquid manure is shown in (b). As expected, apparent viscosity is lowest at the inlet and outlet, and highest at the corner. The narrow, downward-flowing channels also show low viscosity, due to the high degree of shearing. Smaller regions of high viscosity are found at the centre of each of the wider, upward flowing channels; even though velocity is relatively high in these regions, the velocity gradients are low. Once again, the upper and lower viscosity limits come into play for both cases, with the exception of the lower limit in the xanthan gum case.

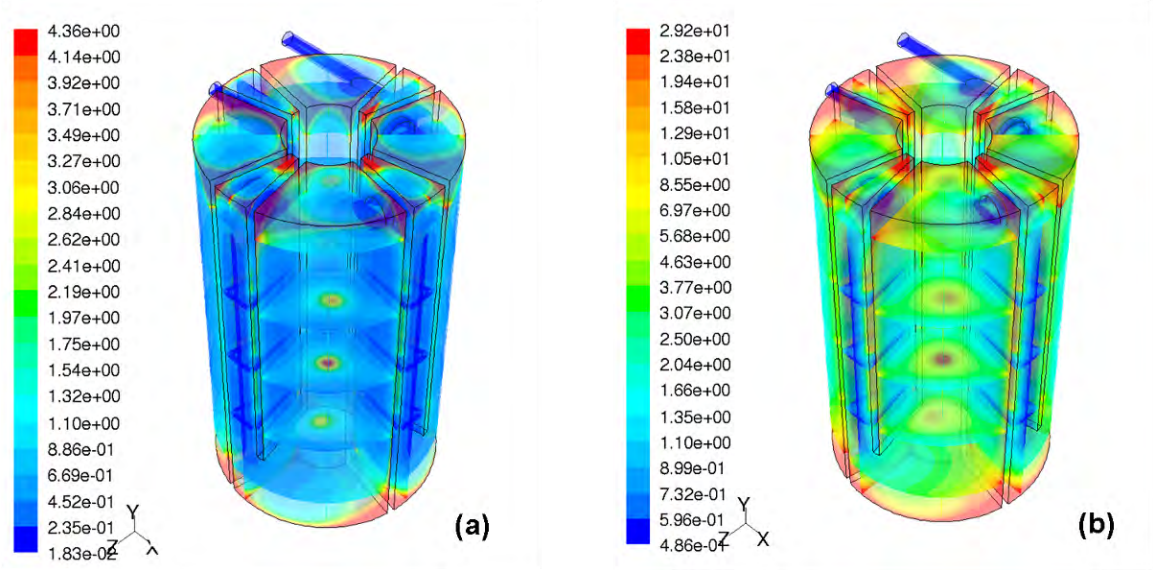

Figure 6.25: Apparent viscosity for G4. a) xanthan gum; b) 8% TS manure

As seen in Figure 6.26, the RTD curves for each of these four cases show a high degree of similarity, especially compared with previous cases. The height of the peak only varies 4.6% between all four cases (see Table 6.9). As viscosity increases, the location of the peak shifts to the left; the non-Newtonian cases peak at about $\theta = 0.6$, while the low-

solids manure peaks at 0.765 and water peaks at 0.876. Variance and dead space are relatively low for all cases; both of these quantities are much higher for the non-Newtonian cases. When water is the working fluid, the estimated dead space is less than 1% of the reactor volume; this quantity is 7.96% for low-solids manure, while the xanthan gum and high-solids manure cases show dead spaces of 18.1% and 18.9% of the reactor volume, respectively. As well, the mean time θ_m is very close to 1.0 for all cases, indicating efficient use of the full reactor volume. With regards to variance and dead space, three out of the four fluids perform best with this geometry; the exception is xanthan gum, which shows slightly smaller values with G3. With regards to location of peak however, all four fluids perform best with G4.

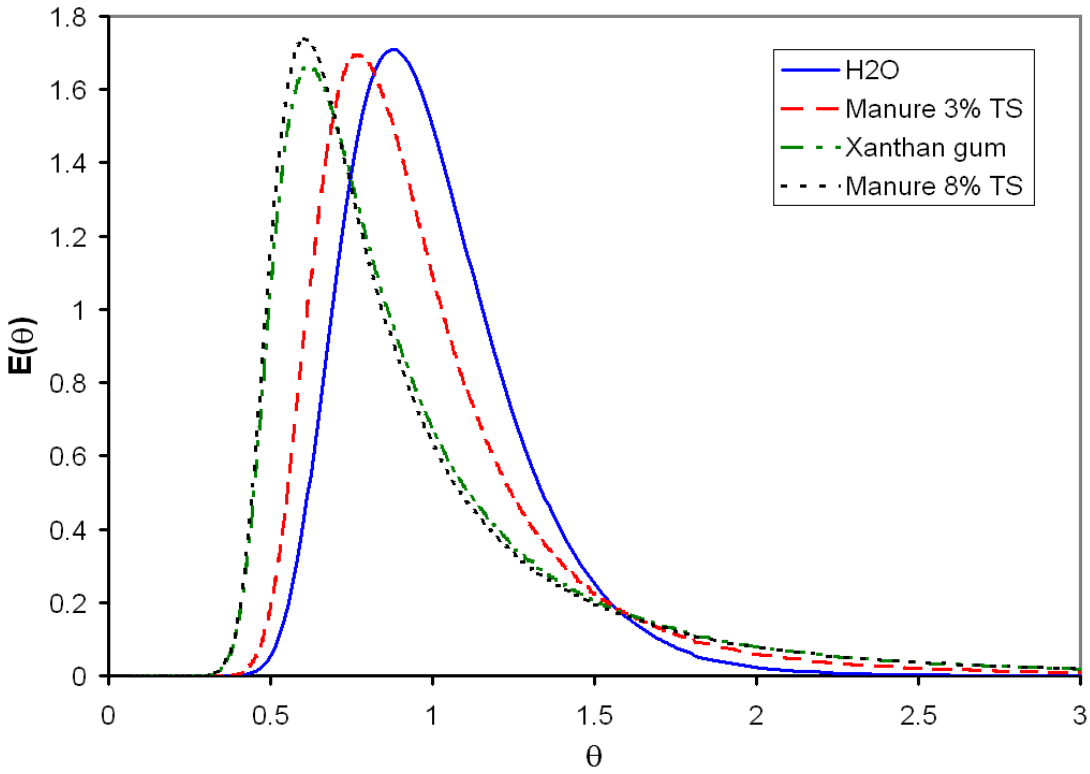

Figure 6.26: Residence time distributions for G4 radial baffles, CFD results

Table 6.9: Summary of overall parameters, G4 radial baffles

Fluid	θ_m	σ_θ^2	Dead space	Peak value	Loc. of peak
H2O	1.007	0.07430	0.003957	1.709	0.8760
Manure 3% TS	1.005	0.1902	0.07955	1.696	0.7652
Xanthan Gum	0.9866	0.3641	0.1814	1.662	0.6142
Manure 8% TS	0.9798	0.3846	0.1898	1.740	0.6041

6.5.5 Effect of flow rate on RTD

To study the effect of a reduced flow rate on the residence time distribution, four simulations were performed at a flow rate of 0.0125 L/s. Water was used as the working fluid. This flow rate represents a reduction in flow rate of 75%, corresponding to four times the initial HRT for each case. The resulting RTD curves are compared with the results from the 0.05 L/s cases in Figure 6.27. The decrease in flow rate has the greatest effect in the case of G3, where the peak is shifted from $\theta = 0.810$ to 0.594, dead space increases from 0.0414 to 0.145, and the variance doubles. These shifts are most likely due to decreased swirl in the outer chamber. The RTD curve of G1 is also significantly affected by decreasing the flow rate; at the lower flow rate, the peak occurs earlier—$\theta = 0.160$ versus 0.313—and rises from 0.852 to 1.04 (see Table 6.10). The dead space also increases from 0.301 to 0.366. These changes are due to changes in the velocity profile of the inlet jet, which diffuses quicker and impinges with less momentum against the cylinder wall. The changes in RTD for G2 and G4 are more subtle; the peak shifts slightly to the right for G2, and rises by 5.7% for G4.

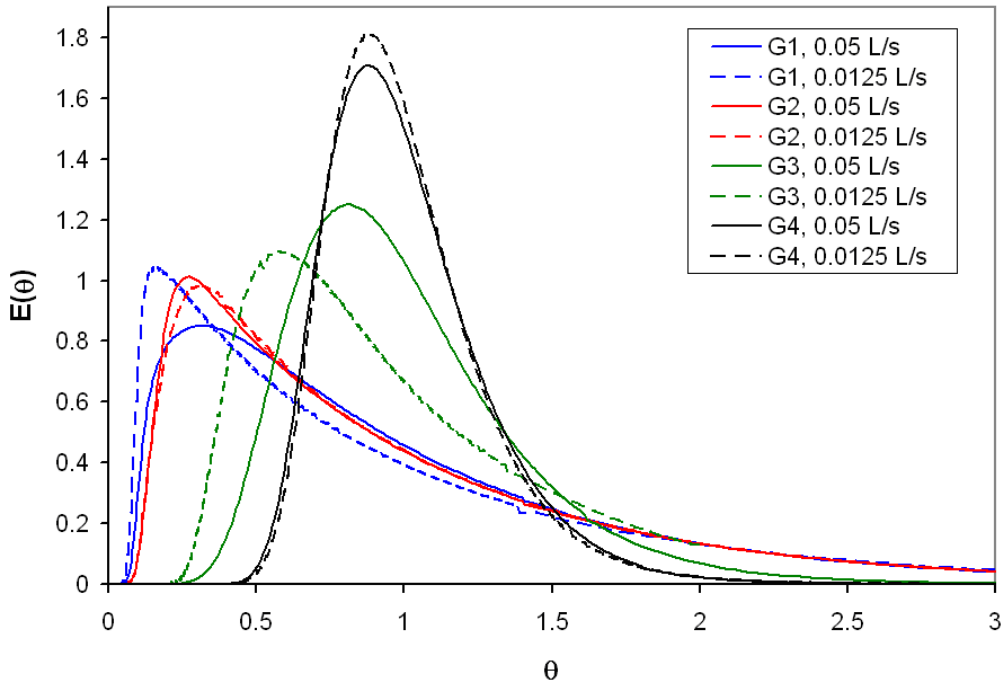

Figure 6.27: RTD comparison, H_2O; 0.05 and 0.0125 L/s

Table 6.10: Comparison of overall parameters, H_2O; 0.05 and 0.0125 L/s

Geometry	Q (L/s)	θ_m	σ_θ^2	Dead space	Peak value	Loc. of Peak
G1	0.05	1.010	0.6961	0.3009	0.8516	0.3128
G1	0.0125	0.9708	0.7102	0.3661	1.039	0.1599
G2	0.05	0.9862	0.6231	0.3278	1.012	0.2737
G2	0.0125	0.9921	0.6196	0.3106	0.9825	0.3131
G3	0.05	1.008	0.1499	0.04142	1.250	0.8096
G3	0.0125	1.006	0.3008	0.1450	1.093	0.5937
G4	0.05	1.007	0.07430	0.003957	1.709	0.8760
G4	0.0125	1.007	0.07399	0.008472	1.809	0.8865

6.5.6 Pilot-scale simulations

The first twenty cases in this study, as described above, simulate flow conditions in a lab-scale reactor of approximately 30 L. When relating the results of these simulations to the design of actual anaerobic digesters, it is important to consider that their scale does not

compare well with that of real-life reactors. To demonstrate the effect of scale on the residence time distribution, four cases were performed on scaled-up versions of the reactor geometries G1 and G4, each with a volume of 2000 L. The linear scaling factors for these two pilot-scale geometries were 3.97 for G1 and 4.33 for G4. The flow rate was also changed to 0.00136 L/s, to produce a hydraulic retention time of approximately 17 days. Each geometry was simulated with water and 8% TS manure. For the pilot-scale G1 geometry (Figure 6.28), the flow field exhibits an inlet jet that does not impinge on the opposite wall, but instead is drawn down towards the outlet about half-way across the reactor (a). This represents an intermediate case between the lab-scale Newtonian cases, where the inlet jet impinges against the wall, and the non-Newtonian cases, where the extent of the inlet jet is very short. When 8% TS manure was simulated in the pilot-scale reactor (b), the flow field is similar to the lab-scale case with the same fluid. In the G4 geometry (Figure 6.29), the flow fields for water (a) and 8% TS manure (b) are very similar, and are also similar to the non-Newtonian lab-scale cases (refer to Figure 6.24).

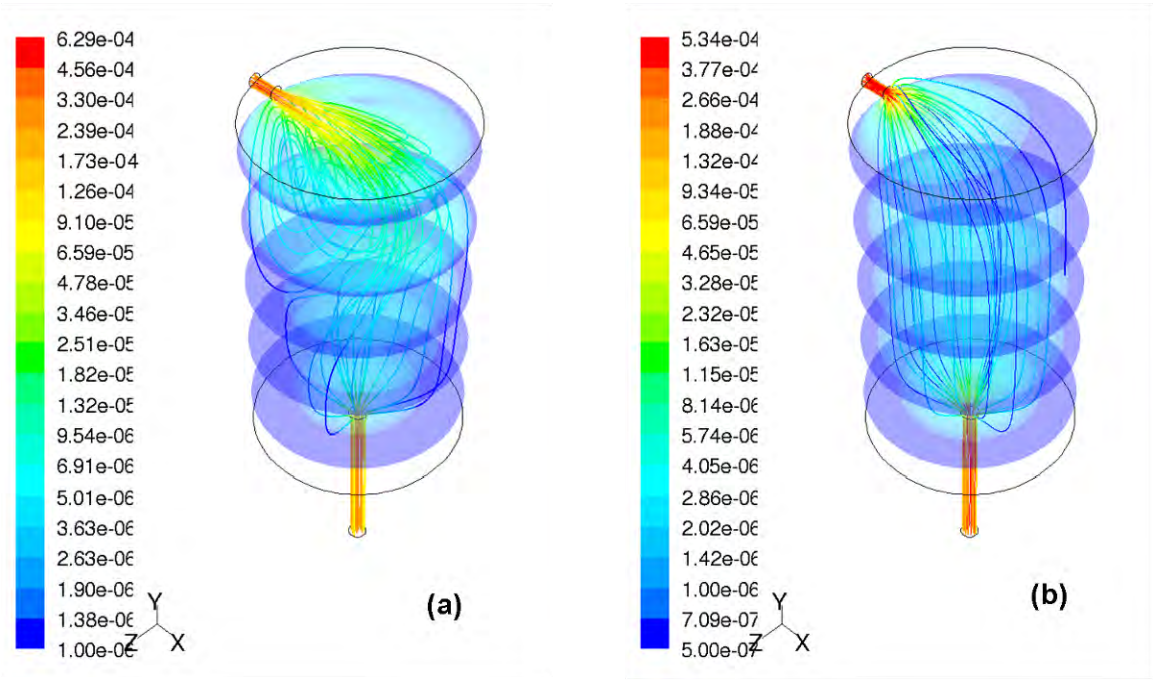

Figure 6.28: Velocity magnitude and pathlines for pilot-scale G1. a) water; b) 8% TS manure

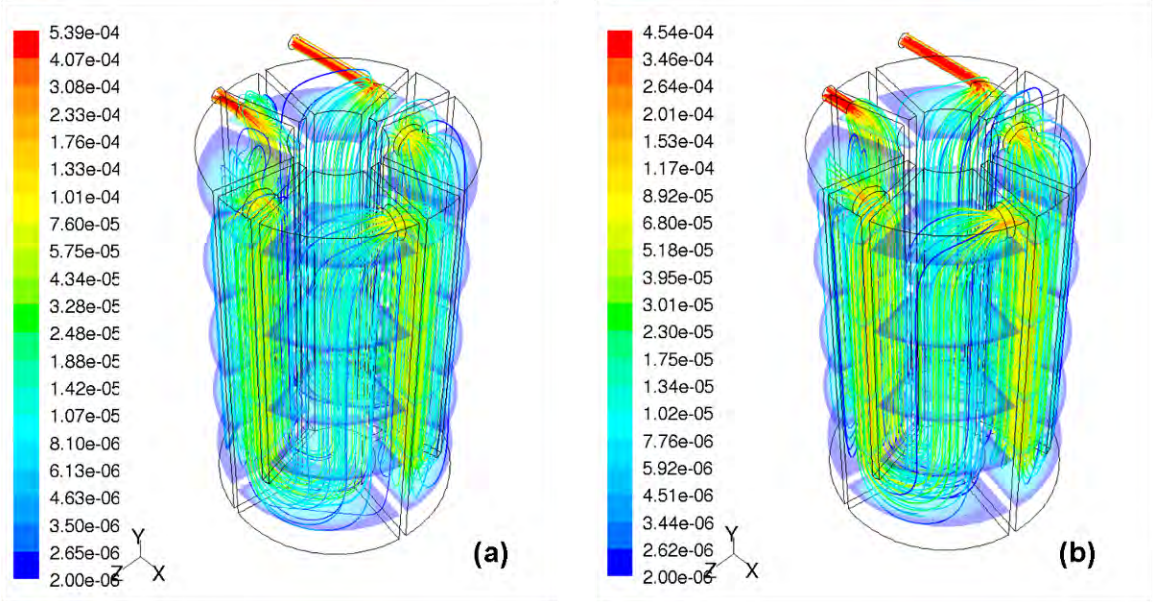

Figure 6.29: Velocity magnitude and pathlines for pilot-scale G4. a) water; b) 8% TS manure

The pilot-scale simulations feature larger volumes and smaller flow rates than the lab-scale cases; thus, the shear rates produced in these simulations are generally very low. This is reflected in Figure 6.30, which depicts the apparent viscosity for the pilot-scale G1 and G4 reactors with 8% TS manure as the working fluid. Throughout both reactors, the apparent viscosity is at the maximum limit (29.24 Pa·s); apparent viscosity only drops in the inlet and outlet pipes, where shear rates are much higher. The lowest viscosities present in these simulations are still much higher than the minimum viscosity limit of 0.486 Pa·s. Thus, the results of these simulations do not accurately represent how a pseudoplastic fluid would flow inside these reactors; instead, they more closely model a fluid with a constant viscosity of 29.24 Pa·s. This is problematic; however, at such low shear rates, a pseudoplastic model may not even properly apply to manure of this solids content.

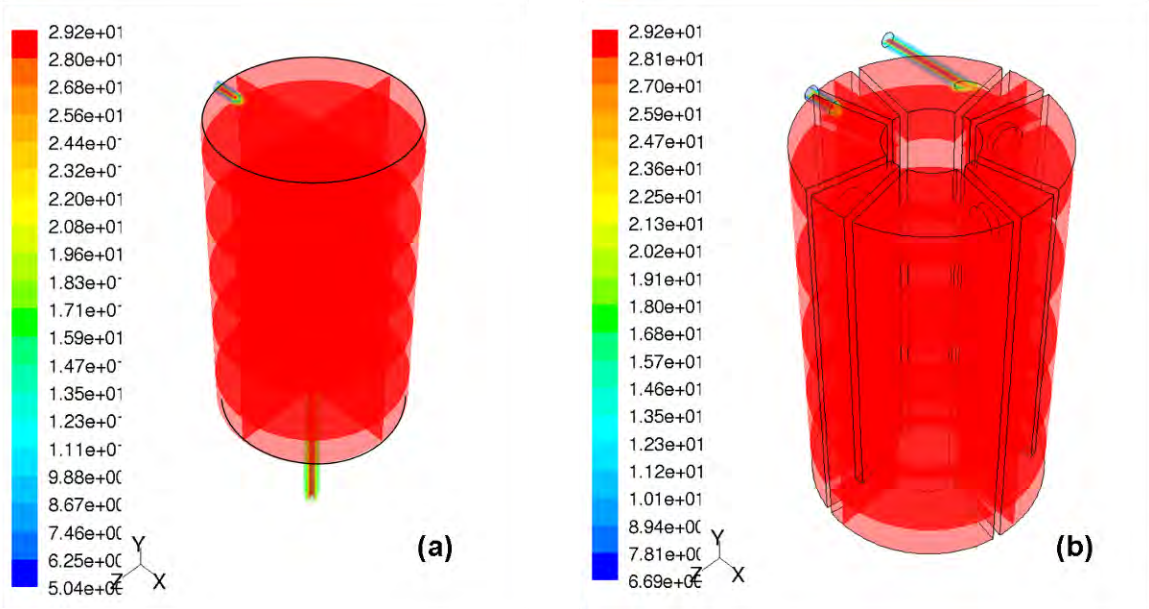

Figure 6.30: Apparent viscosity for pilot-scale reactors with 8% TS manure. a) G1; b) G4

The residence time distributions for the pilot-scale simulations are given in Figure 6.31. It can be seen in this figure that the viscous properties of water and high-solids manure have much less impact on the RTD than was found in the lab-scale simulations. Especially, the G4 simulations produce nearly identical RTD curves for both fluids. There is more contrast between water and 8% TS manure for geometry G1; even so, the variance, dead space fraction, and peak value varies less than 10% between these two cases (see Table 6.11). The shapes of the G1 curves more closely resemble the lab-scale non-Newtonian cases, with sharper peaks that occur later; the pilot-scale cases have much lower peaks, however. In contrast, the G4 results more closely represent the bell-shaped RTD curve produced by water in the lab-scale G4 reactor.

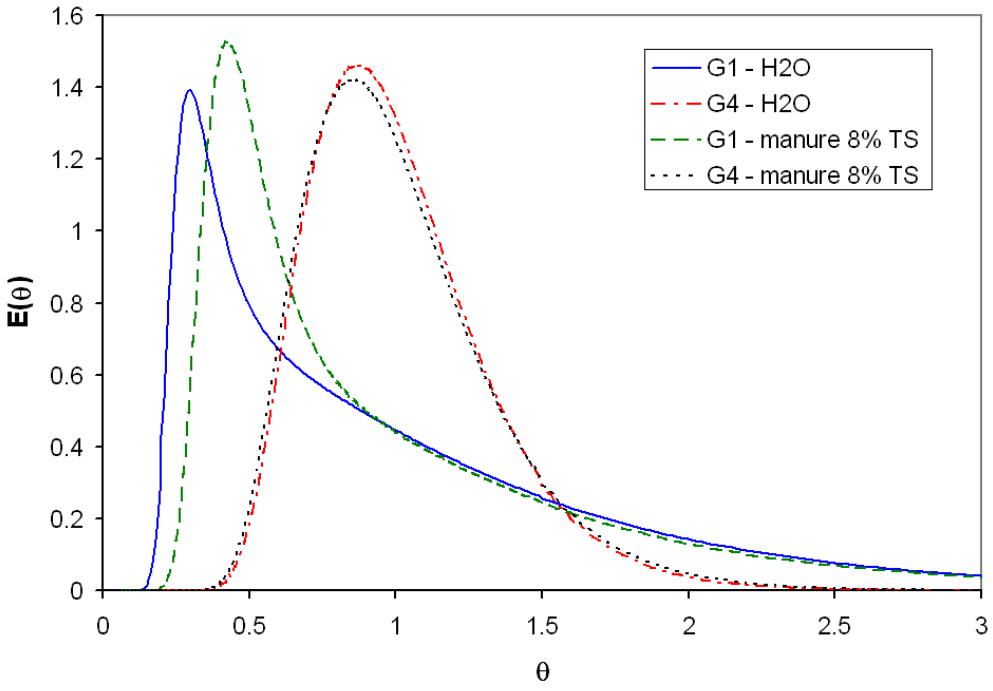

Figure 6.31: Residence time distributions for pilot-scale simulations

Table 6.11: Summary of overall parameters for pilot-scale simulations

Fluid	θ_m	σ_θ^2	Dead space	Peak value	Loc. of peak
G1 – H2O	0.9988	0.5836	0.3334	1.392	0.3000
G1 – 8% TS manure	1.001	0.5357	0.3083	1.527	0.4248
G4 – H2O	1.014	0.09564	0.01693	1.462	0.8743
G4 – 8% TS manure	1.014	0.1064	0.02621	1.421	0.8576

Figure 6.32 and 6.33 compare variance and dead space for the lab-scale and pilot-scale simulations where water and 8% TS manure are the working fluids. The largest discrepancy occurs in the case of G4, with 8% TS manure; in this case, the lab-scale simulation predicts much greater variance and dead space than the pilot-scale simulation. This reflects the fact that in the lab-scale simulations, changing the working fluid greatly affects the RTD curve; whereas in the pilot-scale simulations, the working fluid has a much smaller effect. For the other simulations however, the pilot-scale results are not far different from the lab-scale values. The difference in variance is less than 0.12 for the G1 cases, and approximately 0.021 for G4 with water; dead space changes 0.07 and 0.032 for G1 water and G1 manure, respectively, while the difference is only 0.013 for G4 with water.

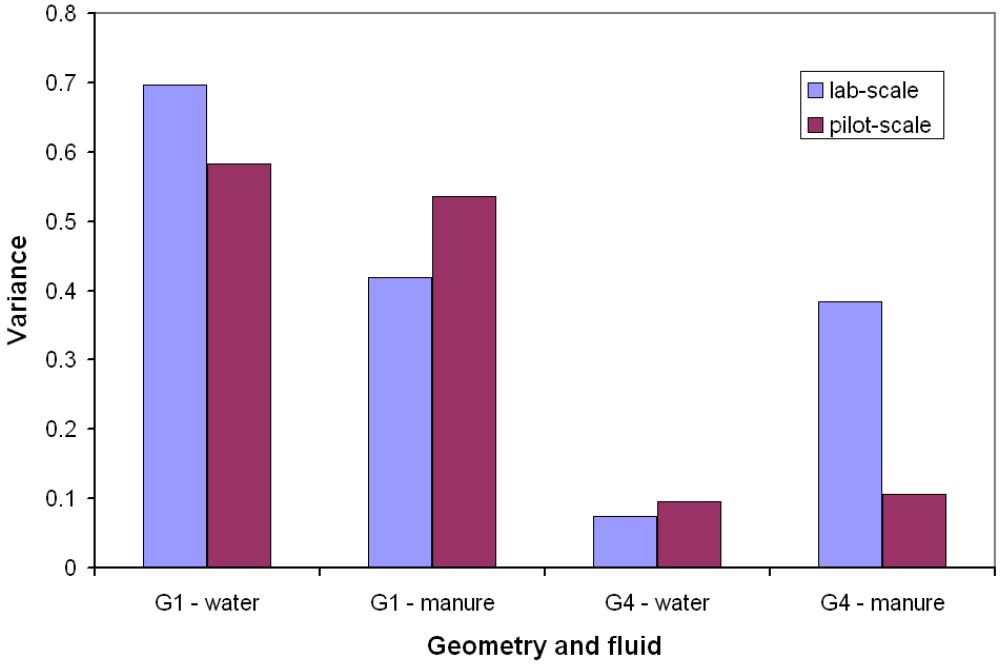

Figure 6.32: Comparison of variance for G1 and G4, lab-scale vs. pilot-scale

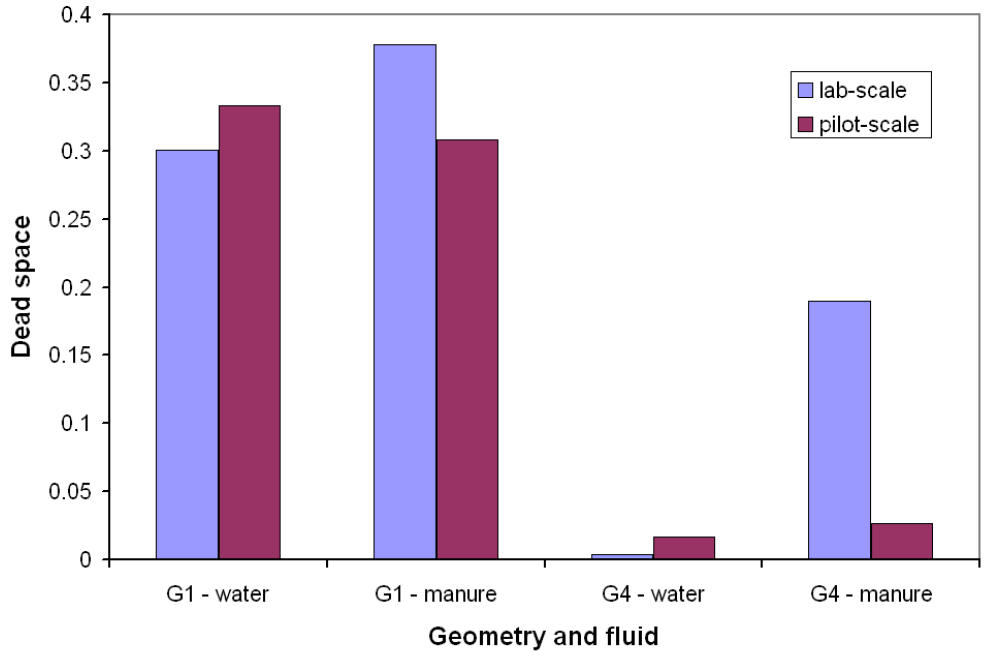

Figure 6.33: Comparison of dead space for G1 and G4, lab-scale vs. pilot-scale

6.5.7 Possible sources of error for CFD simulations

There are several potential sources of error that may affect the accuracy of the CFD simulations. These sources of error are most often related to unknowns in the problem, and include the following:

Turbulence modeling – The inlet boundary condition for turbulence was based on an estimated value, with the assumption that this boundary condition would not greatly affect the solution. A different value for this boundary condition might produce a different solution.

Viscosity modeling – the upper and lower viscosity limits for the power law model were estimated, and most likely do not accurately reflect the actual viscous behaviour of the non-Newtonian fluids under study. However, collecting viscosity data at extreme shear ranges is very difficult, and this data rarely exists in the literature. For the lab-scale simulations, the limits are only reaches in small regions of the domain; however, in the pilot-scale simulations, the upper viscosity limit dominates the domain. To properly simulate the flow of liquid manure in the pilot-scale reactor, reliable rheological data at very low shear rates would first have to be obtained.

Inlet geometry and velocity profile – the inlet geometry in the numerical model is very simple: a short, straight tube entering the reactor. This however, may not reflect the true inlet geometry in an actual digester. Furthermore, the uniform velocity boundary condition at the inlet most likely does not reflect the actual velocity profile.

Transient simulation – the effect of choosing a different scheme for time step was not investigated in this study. Choosing smaller time steps may produce a different RTD

curve, though it is most likely that this difference would be small, since the transient solution converged quickly (within 10 iterations) for each time step.

Most of these potential sources of error have only a minor impact on the final solutions. This is especially the case since the key dependent variable in this study—the RTD—is an overall parameter that is generally not very sensitive to small changes in the velocity field.

6.6 Validation of CFD model using PIV

6.6.1 PIV experimental procedure

To validate the CFD model used in this chapter, flow field results from the model were compared to experimental data obtained using particle image velocimetry (PIV). The PIV system used was supplied by Dantec Dynamics, and is described in Chapter 4. Two CFD cases were replicated experimentally for this comparison: reactor geometries G1 (centre inlet) and G2 (side inlet) with water flowing at 0.0125 L/s. This flow rate was chosen because at a flow rate of 0.05 L/s, small bubbles became entrained in the fluid stream, and accumulated under the test section lid; at the lower flow rate, these bubbles were avoided. PIV experiments could not be performed with the xanthan gum solution due its opaque nature at a concentration of 1 g/L. The PIV experiment was conducted on the horizontal plane that is at the same height as the inlet. This plane was selected because of the large range of velocities within this plane, and the characteristic differences between G1 and G2 that are most evident on this plane. To allow for an appropriate field of view,

the camera was mounted on the top crossbar of the movable U-subframe (see Figure 3.34)

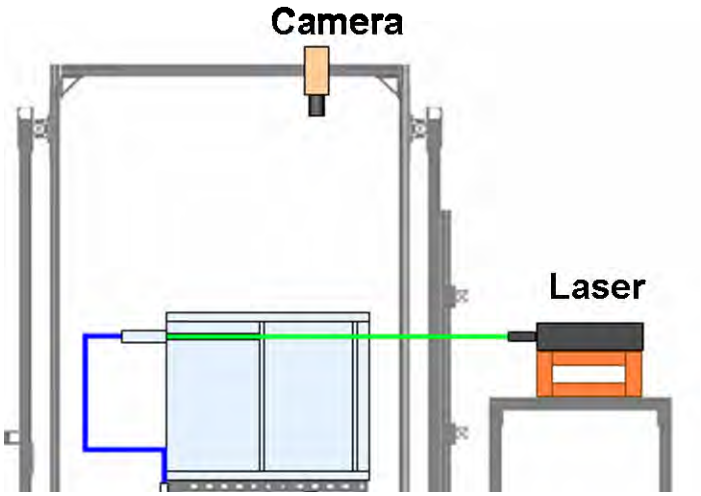

Figure 6.34: Setup for PIV experiment

Due to the large size of the area under study, multiple camera positions were used to capture the full flow field. The horizontal plane was divided into nine square sectors of equal size, as shown in Figure 6.35. Since the flow in G1 is symmetrical, only the top six sectors were used (A through F); all nine sectors were used for G2. The size of each sector was approximately 95 mm x 95 mm. Figure 6.35 shows how a template was used to accurately locate the camera and determine the coordinates of the centre of the field of view. Nine square holes were cut in the template as shown. The camera was positioned so that all four edges of the appropriate square were in view. An initial image was captured so that the exact location of the field of view could be determined. The template was then removed so that the full field of view would be available for the PIV experiment.

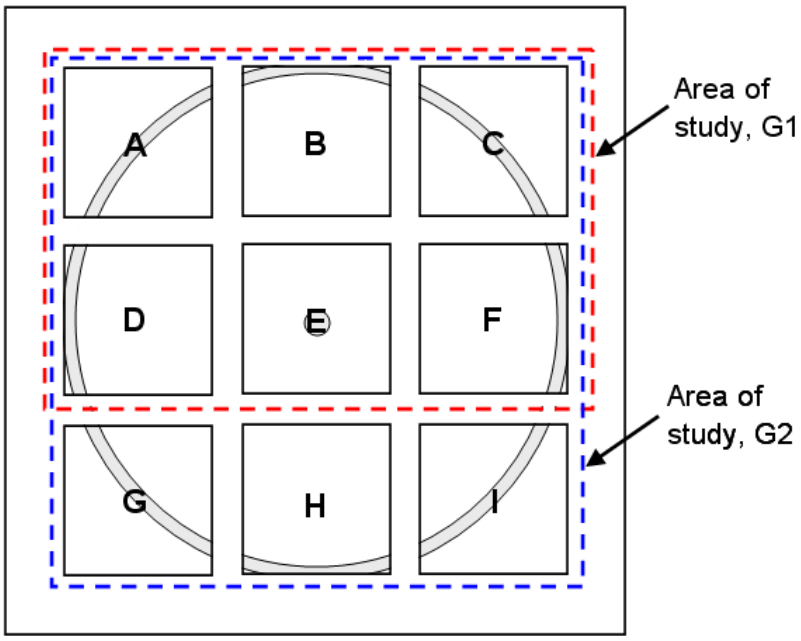

Figure 6.35: Template used to accurately position the PIV camera

The fluid column system was filled with filtered tap water for the PIV experiments. Reflective 50 μm polyamide particles were dispersed throughout the system until an appropriate uniform concentration was achieved. The system was run in closed-loop mode to recycle the particles. Before each experiment, the fluid column test section was mechanically mixed to bring settled particles back into suspension. To allow the swirl to die down, five to ten minutes was elapsed before turning on the pump to circulate the water at 0.0125 L/s. The system was run for ten minutes before beginning the PIV test to ensure steady-state conditions.

The FlowManager software package by Dantec Dynamics was used to control the PIV system and collect the data. For each sector, 1000 recordings were captured (each recording consists of two frames). Table 6.12 shows the input parameters for the PIV

experiment. Approximately 6 to 12 particles were visible within each 32 x 32 pixel interrogation area. The time between frames was set so that particles traveled no more than 1/3 of an interrogation area (ie. 1.23 mm) in the time elapsed between frames. Close to the inlet, the time between frames was set to 8 000 ns, while for low-velocity sectors, this time was increased up to 24 000 ns. Velocity vectors were calculated using the adaptive correlation tool.

Table 6.12: Input parameters for PIV experiment

Parameter	Value
Laser pulse frequency	4 Hz
Time between frames	8000 to 24000 ns
Pulses between each recording	1
Recordings per burst	1000
Number of bursts	1
Image size	1008 X 1016 pixels 116.1 X 117.0 mm
Interrogation area	32 X 32 pixels 3.69 X 3.69 mm
Interrogation area overlap	50%
Scale factor	12.799

6.6.2 PIV calculations

Once the velocity vector maps were produced, FlowManager's statistics tool was used to post-process the results. For this study, only the mean flow values were used for comparison to the CFD model; turbulence data was not considered. This data was then imported into MATLAB® for further processing. The initial images, taken with the template in view, were used to calculate the offset coordinates for each of the vector maps. This calculation is demonstrated in Figure 6.36 and Equations 6.60 and 6.61.

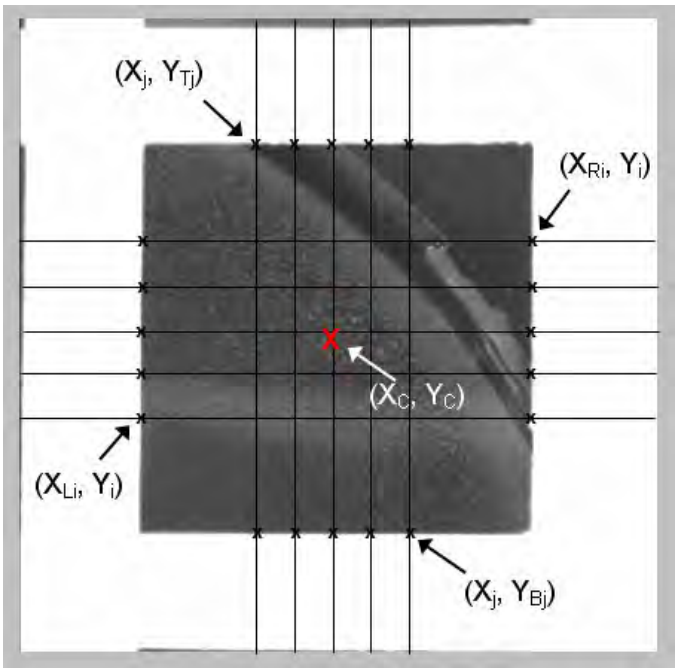

Figure 6.36: Calculating the location of the centre of the template square

$$X_C = \frac{1}{2}\left(\frac{1}{n}\sum_{i=1}^{n} X_{R,i} + \frac{1}{n}\sum_{j=1}^{n} X_{L,j}\right) \tag{6.60}$$

$$Y_C = \frac{1}{2}\left(\frac{1}{n}\sum_{i=1}^{n} Y_{T,i} + \frac{1}{n}\sum_{j=1}^{n} Y_{B,j}\right) \tag{6.61}$$

where $X_{R,i}$ and $X_{L,i}$ are where each horizontal line intersects the right and left edges of the template square, and $Y_{T,j}$ and $Y_{B,j}$ are where each vertical line intersects the top and bottom edges of the template square. The values of X_c and Y_c were then used to offset the x and y coordinates of the vector maps. The individual vector maps were then concatenated to produce one vector map describing the velocity field of the entire plane.

6.6.3 PIV results and comparison to CFD model

Figures 6.37 through 6.42 compare the results from the PIV experiments and CFD simulations for G1 and G2. The CFD contours were generated in FLUENT®, while the

PIV contours were generated in MATLAB®. These two software packages have slightly different colour schemes, so the colours do not match exactly; however, the range and spacing of contours is the same for both. For the PIV results, the area outside the test section appears as near-zero velocity regions; these regions occur in the top right and left corners of the G1 plots, and in all four corners of the G2 plots. In all PIV plots, a "dead zone" appears at the centre of the test section; this dead zone is due to the presence of an acrylic plug that obscures that portion of the image, and must be ignored. This is most noticeable in the G1 plots, where the inlet jet passes directly underneath the plug.

Figure 6.37 compares the velocity magnitude and velocity vectors for G1. Six vector maps are concatenated to produce the PIV plot. Qualitatively, the contours match fairly well, especially in the area of the jet (Sectors D, E, and F). Sector A (top left corner) however, does not match well. In this sector, the PIV results show higher velocities than the CFD results; there is also a significant discontinuity between Sector A and the sector below, Sector D. Thus, Sector A contains a high degree of error, for some unknown reason.

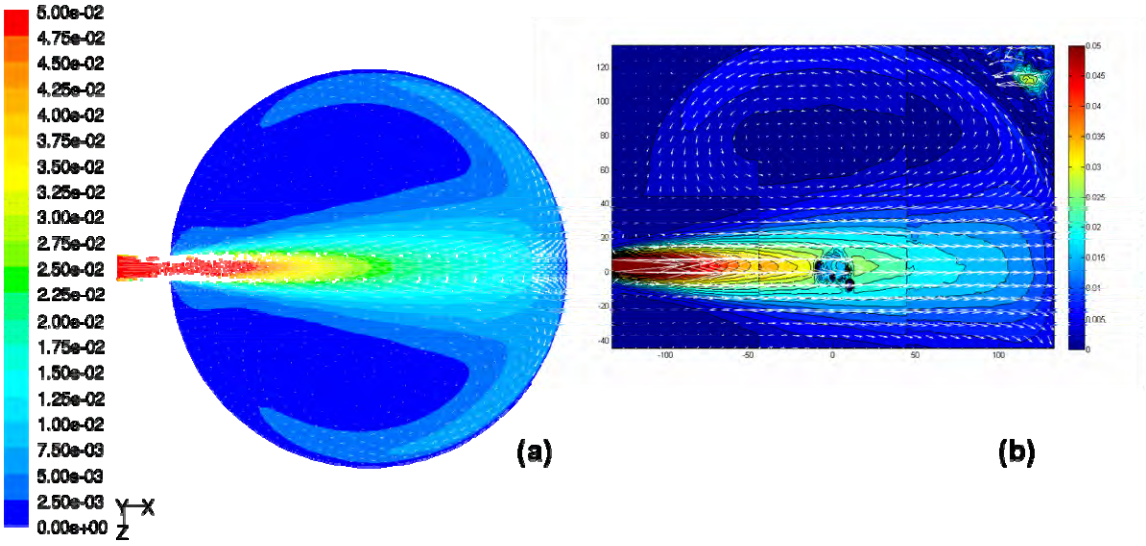

Figure 6.37: Comparison of PIV and CFD results – G1, velocity magnitude and vectors. a) CFD; b) PIV

The U component of velocity for G1 is shown in Figure 6.38. These contours match very well, with the exception of slight discontinuities at the boundaries between PIV sectors. These slight discontinuities are evident in all of the PIV results. Figure 6.39 shows the W component of velocity. As in Figure 6.37b, the velocity in Sector A of the PIV results is too high, and there is a major discontinuity between Sector A and Sector D. Thus, the error in velocity magnitude found in Figure 6.37b is mostly due to the W component.

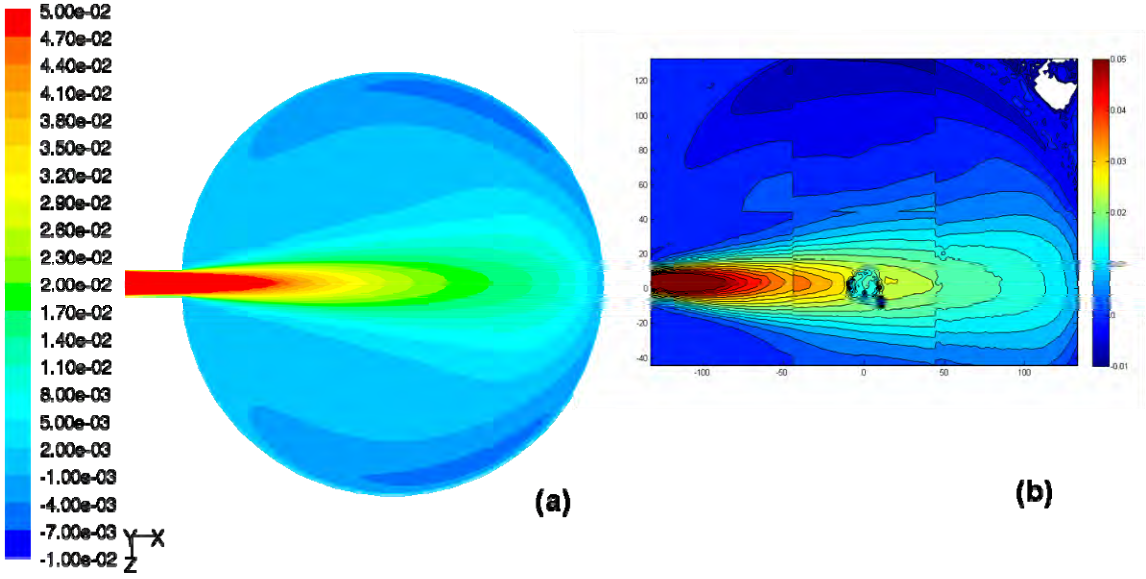

Figure 6.38: Comparison of PIV and CFD results – G1, U velocity. a) CFD; b) PIV

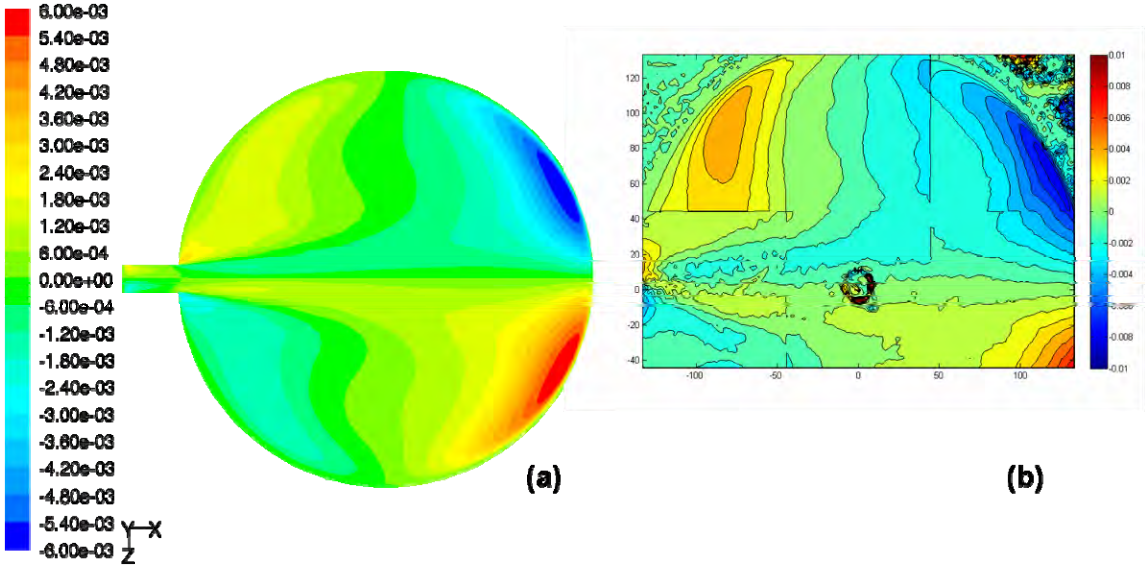

Figure 6.39: Comparison of PIV and CFD results – G1, W velocity. a) CFD; b) PIV

Figure 6.40 compares the velocity magnitude and velocity contours for G2. The swirling pattern is evident in both. The immediate area of the jet compares well for both PIV and CFD results. However, further from the jet, the PIV results show that the velocity is highest close to the wall, and decreases quickly as one moves away from the wall; the

CFD results, however, predict a region of high velocity that extends further from the wall. Sector F (middle right) in the PIV results is discontinuous with its neighbouring sectors.

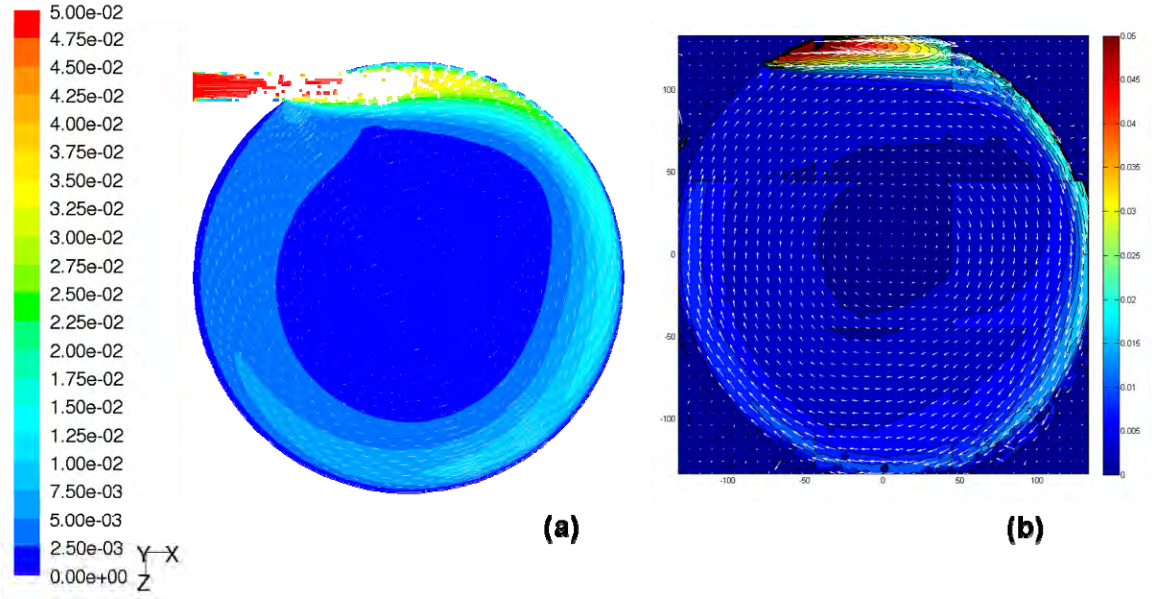

Figure 6.40: Comparison of PIV and CFD results – G2, velocity magnitude and vectors. a) CFD; b) PIV

The U and W components of velocity are compared in Figures 6.41 and 6.42. For the most part, the CFD and PIV results compare well. In general, contours match better in areas of high velocity than in areas of low velocity. As in the previous figure, Sector F of the PIV results is discontinuous with its neighbouring sectors.

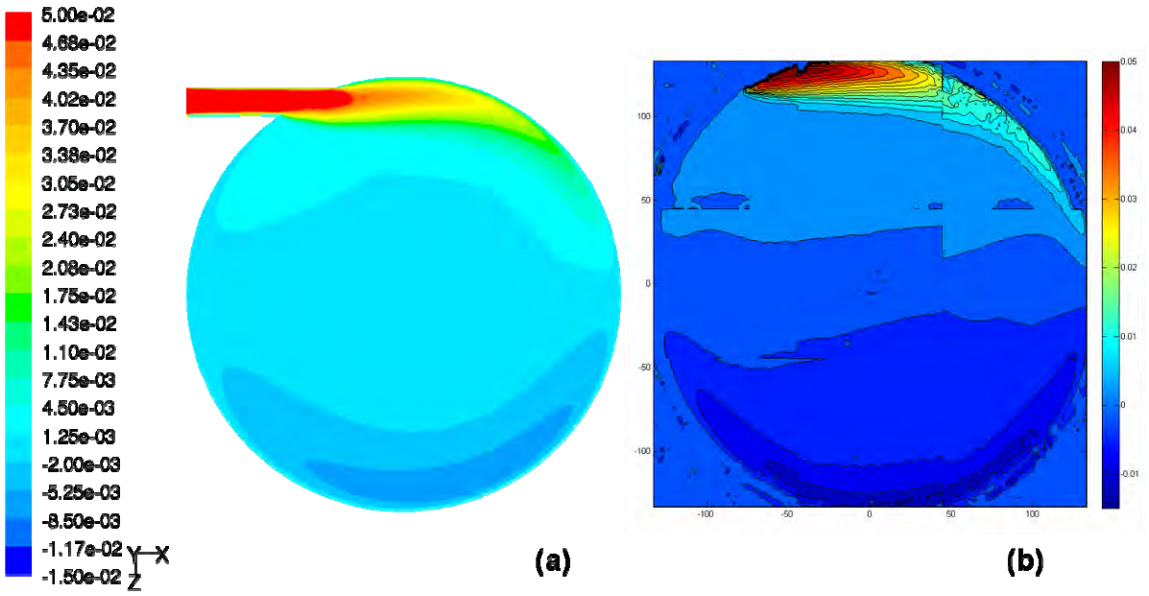

Figure 6.41: Comparison of PIV and CFD results – G2, U velocity. a) CFD; b) PIV

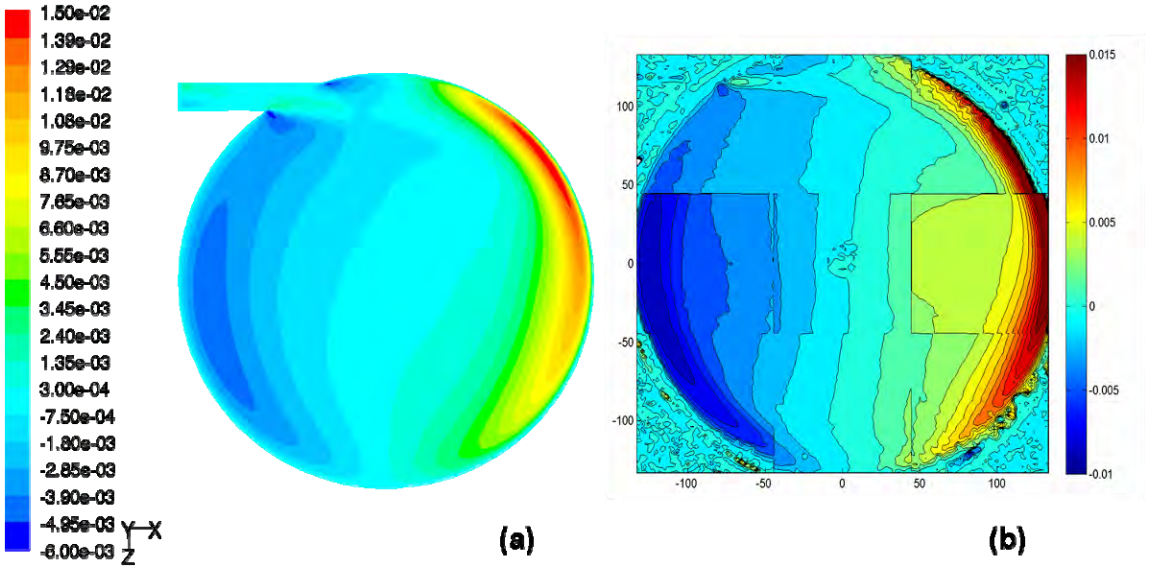

Figure 6.42: Comparison of PIV and CFD results – G2, W velocity. a) CFD; b) PIV

A more precise comparison can be made by examining the velocity profiles at selected locations. Figure 6.43 presents the U velocity profiles for G1 at x = -0.0369 m and x = 0.0369 m for both PIV and CFD results. The profile at x = 0 could not be compared,

since the presence of the plug in the centre obscures the PIV results. At both locations, the two sets of results compare well, though the CFD results underpredict the peak velocities by 5.46% and 8.04% for x = -0.0369 m and x = 0.0369 m, as shown in Table 6.12. Percent difference values are relative to an average inlet velocity of 0.0475 m/s. Profiles of U velocity at the same locations were compared for G2, as shown in Figure 6.44. The profiles at x = -0.0369 m (a) match exceptionally well, with a difference in peak velocity of only 0.4%. There is more disagreement at x = 0.0369 m, where the difference in peak values is 12.65%.

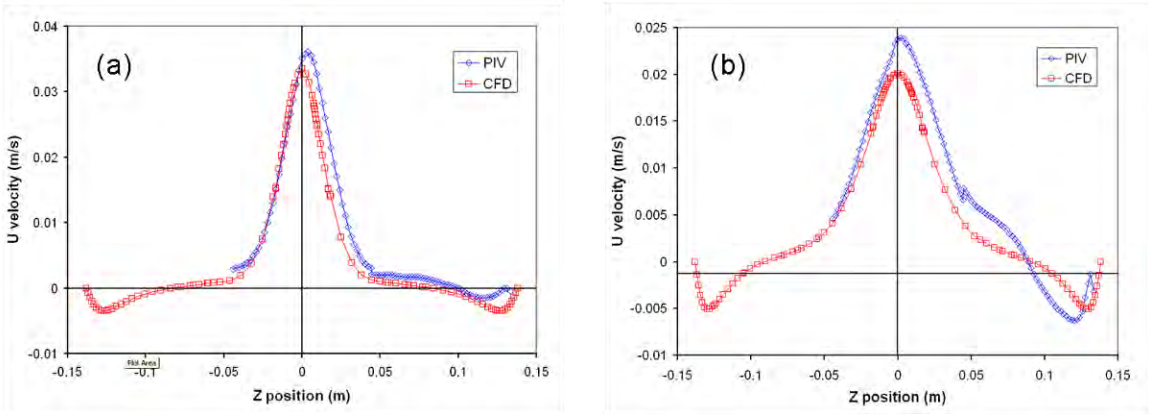

Figure 6.43: U velocity profiles for G1. a) x = -0.0368 m; b) x = 0.0368 m

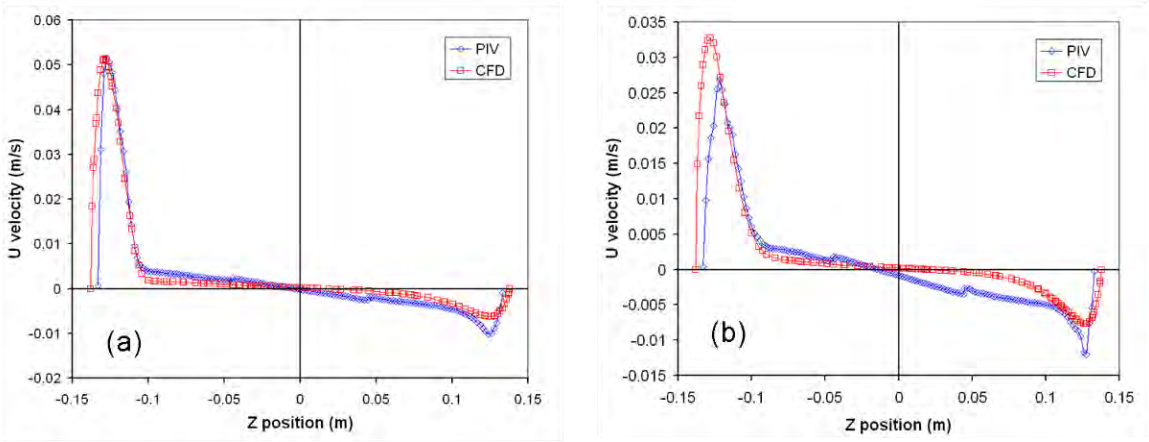

Figure 6.44: U velocity profiles for G2. a) x = -0.0368 m; b) x = 0.0368 m

Table 6.12: Comparison of maximum U velocity for selected profiles, PIV vs. CFD

Geometry	x location (m)	U - PIV (m/s)	U - CFD (m/s)	% difference
G1	-0.0369	0.03612	0.03352	5.46
G1	0.0369	0.02393	0.02011	8.04
G2	-0.0369	0.05155	0.05136	0.398
G2	0.0369	0.02675	0.03276	12.65

6.6.4 Possible sources of error for PIV experiments

There are numerous possible sources of error in a PIV experiment. These include:

Laser misalignment – though care was taken to ensure proper alignment of the laser, it is difficult to match the correct horizontal plane exactly. Due to the 3D nature of the flow field, if the laser plane is a few millimeters too high or two low, the results will vary from the expected values.

Scaling errors – if the PIV images were not scaled correctly, the velocities may be higher or lower than expected.

Wall errors – PIV may not give accurate results very near a wall. Objects such as walls often cause erroneous vectors. As well, an interrogation area 3.7 mm square may be too large to accurately capture the velocity gradients at the wall.

Reflections – Laser reflections off of various surfaces may cause erroneous vectors. In general, much effort was made to minimize these reflections.

Edge of the field of view – often, PIV results become skewed near the edge of the camera's field of view. Overlapping sectors allowed for the deletion of most of these edges; however, this effect may still be responsible for the slight discontinuities present at the boundaries between sectors.

Low velocity – at any given Δt, there is a limit to the minimum velocity that the PIV can measure, based on the resolution of the image. The resolution used in this study was approximately 0.115 mm. For Δt = 8000 ns, a particle must be travelling at 0.014 m/s to completely traverse the pixel in the time elapsed between frames; for Δt = 24000 ns, this minimum velocity decreases to 0.0048 m/s. This is why contours match better in high-velocity regions than in low-velocity regions.

Inlet turbulence – the degree of turbulence at the inlet is unknown, which may affect how well CFD and PIV results match. In the CFD simulations, a value of 25% was given for inlet turbulence intensity, based on a hydraulic diameter of 0.01826 m. Turbulence scales however, were not taken into account when performing the PIV experiment, so any turbulence parameters that may be derived from the PIV data are not reliable.

Given this list of possible sources of error, it is apparent that both the CFD and PIV results have inherent uncertainty intervals that are difficult to assess quantitatively.

6.7 Comparison of CFD results to RTD experiments

Figures 6.45 through 6.47 compare the experimental RTD results with the CFD predictions. In general, the shapes of the predicted curves match up well with those determined by the experiments, especially for the water cases. However, there are significant differences between the simulations and the experiments as well, most notably the magnitude of the peaks and the size of the tails. For the water cases, the CFD models

predict slightly higher peaks and tails that decay more rapidly. The exception is G4, 0.0125 L/s, where the experimental peak rises to 2.23, but the simulation predicts a peak of only 1.81. The differences between the xanthan gum experiments and simulations are more significant. With the exception of G1, the simulated peak values are on average 38% lower than the experimental peaks. The RTD curves from the CFD models are also smoother, and rise and fall more gradually than the experimental results. The experimental RTD curve for G1 does not seem to fit; according to the 3D model, it should match the G2 curve fairly closely. This discrepancy may be in part due to a difference in sampling frequency in the area of the peak. For the G2 experiment, samples were collected every 15 s between 120 and 300 s; for the G1 experiments, samples were collected every 30 s in this range.

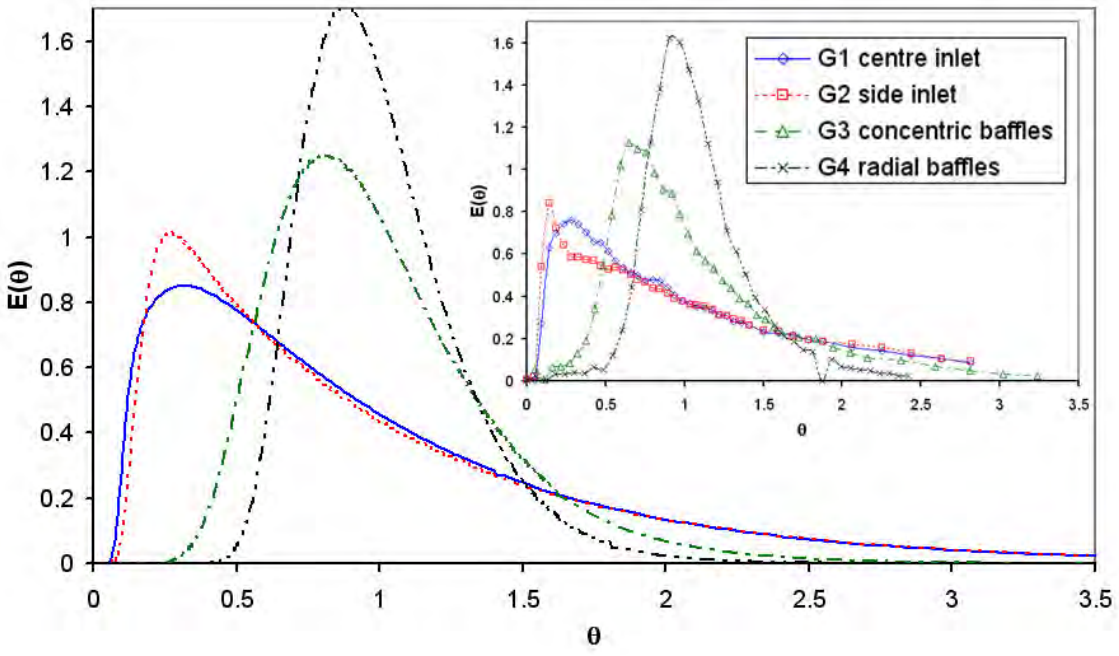

Figure 6.45: CFD results for water at 0.05 L/s (experimental results inset)

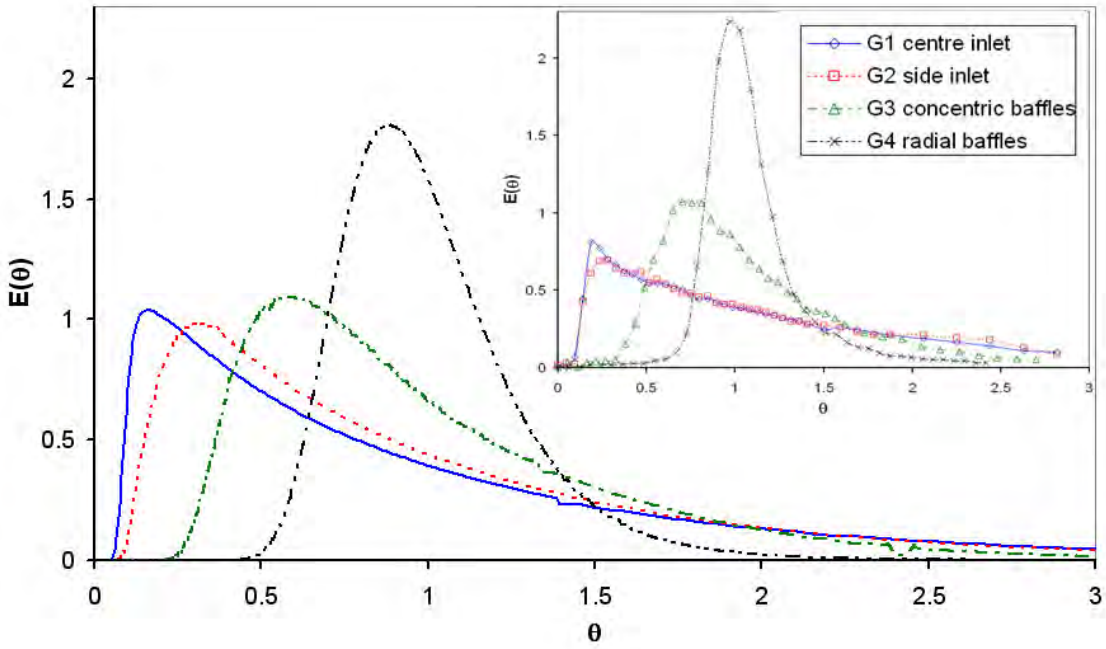

Figure 6.46: CFD results for water at 0.0125 L/s (experimental results inset)

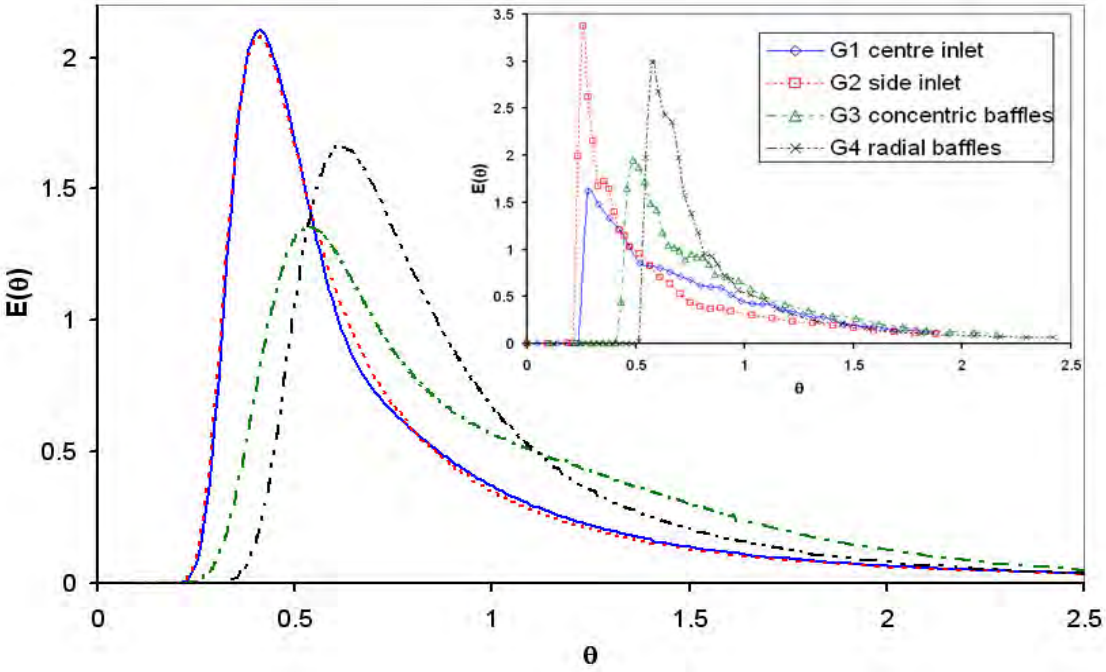

Figure 6.47: CFD results for xanthan gum at 0.05 L/s (experimental results inset)

The mean, variance, and location of peak for the experimental and numerical RTD curves are compared in Figures 6.48 through 6.50. There is a significant discrepancy between

the CFD and experimental mean and variance in cases where the experiments showed heavy tails; this discrepancy is especially large for the G1 and G2 water experiments. The mean and variance for the xanthan gum cases all match quite well, with the exception of the G1 mean value. The locations of the peak value are consistently well-matched, with an average difference of 0.081 HRT between the CFD and the experimental results.

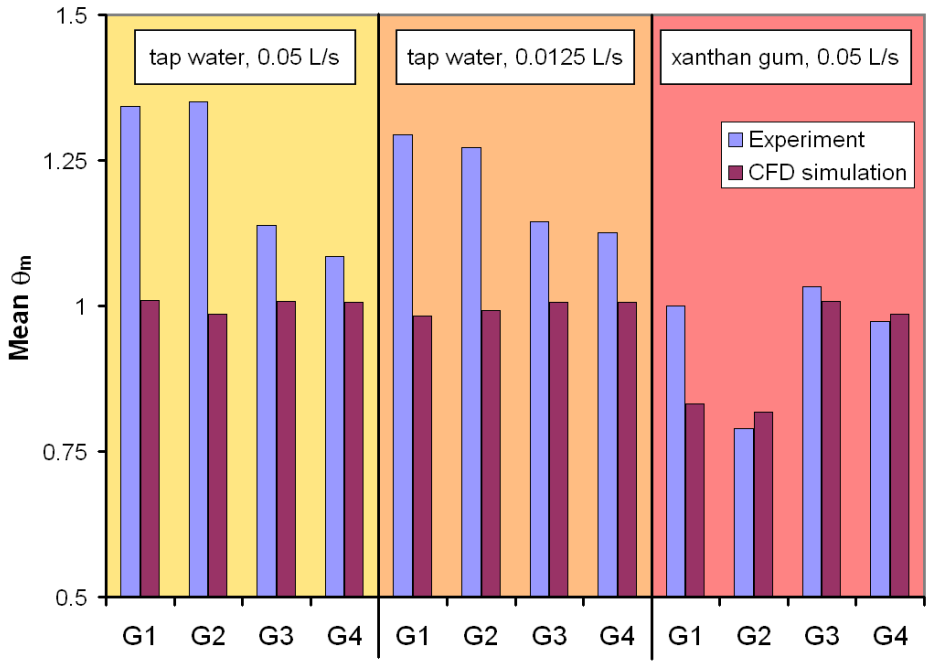

Figure 6.48: Comparison of mean values, θ_m

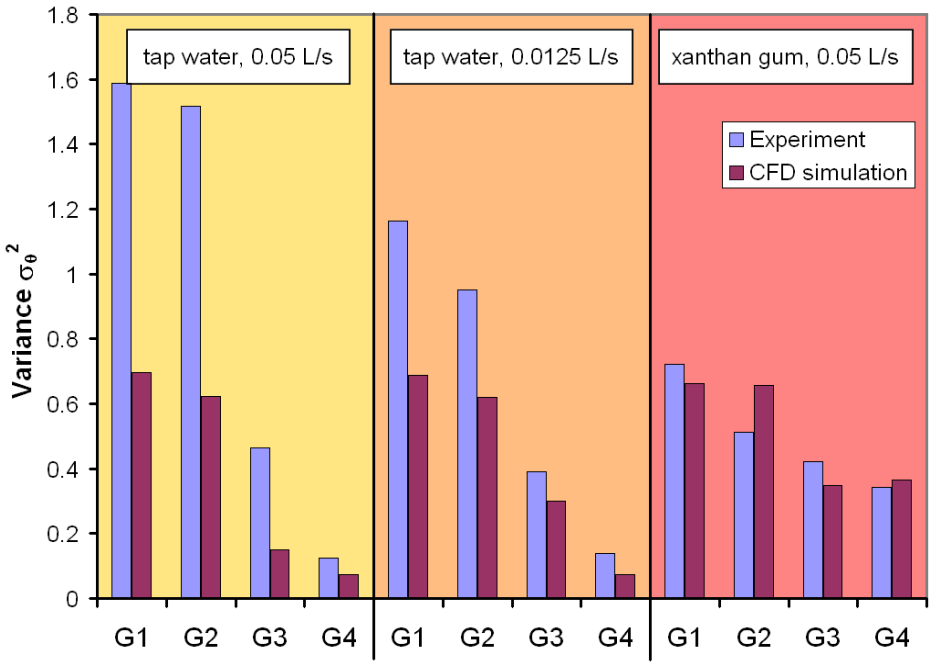

Figure 6.49: Comparison of variances, σ_θ^2

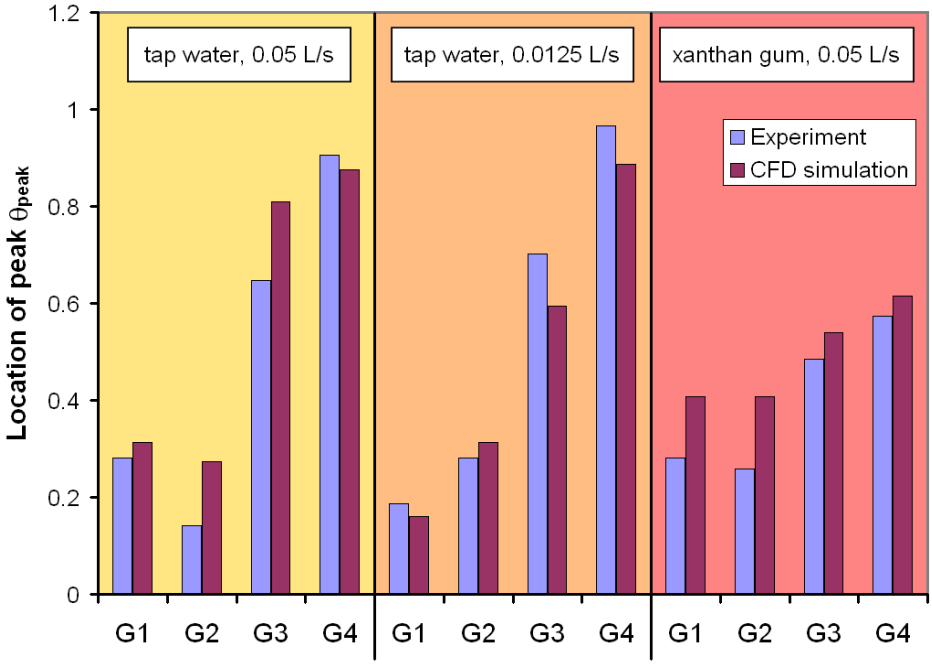

Figure 6.50: Comparison of the location of peak values, θ_{peak}

All empirical investigations are prone to experimental error from a variety of sources. Some of the possible sources of error that may have affected the data collected from the current experiments are as follows:

diffusion of the tracer dye – the rate of molecular diffusion of the tracer dye is unknown. A tracer that diffuses quickly will generally increase the variance of the RTD. Also, the diffusion of the tracer dye may differ between water and xanthan gum.

effect of tracer dye injection on inlet velocity – the inlet velocity increases by a certain amount when the tracer dye is injected, due to the increased mass flow. If each 20 mL syringe is dispensed over a period of 2 s, the volume flow rate increases by 0.01 L/s; this is very significant compared with the steady state inlet velocity (0.05 or 0.0125 L/s). How sensitive the system is to this momentary increased inflow is unknown.

mixing before and after test section – the inlet and outlet tubes may allow for a significant amount of mixing directly before and after entry to the fluid column. How this affects the RTD readings is unknown.

adsorption of tracer dye to solid surfaces – it was observed that the tracer dye has a sort of affinity to the inner surfaces of the flexible hose. Adsorption of the dye onto the hose may increase the measured RTD variance.

6.8 Summary of findings

Computational fluid dynamics (CFD) was employed to simulate the flow of fluid in a continuous-flow anaerobic digester. Twenty-four simulations were performed in total, not

including grid independence tests. Twelve of these cases were numerical recreations of the residence time distribution (RTD) experiments performed using lab-scale reactor geometries as described in Chapter 5. The simulation of liquid manure at two solids concentrations flowing through these lab-scale reactors comprised another eight cases. The remaining four cases were performed on a pilot-scale reactor with a volume of 2000 L and a hydraulic retention time of 17 days. The study focused on general flow patterns and RTD, and how these were affected by geometry, viscosity, and flow rate.

Comparing the RTD curves of the baffled reactor geometries (G3 and G4) to the geometries without baffles (G1 and G2), the baffled geometries exhibit lower fractions dead space, especially where water is the working fluid. The baffled geometries also exhibit later peaks—ie. peaks that occur closer to 1 HRT—and smaller variances in most cases when compared to the non-baffled geometries.

Studying the effect of non-Newtonian flow within the reactors, the peak value of the RTD curve is generally higher than in the corresponding Newtonian cases. In the non-Newtonian cases, the peaks occur later in the non-baffles geometries, and earlier in the baffled geometries when compared to the Newtonian cases. Also, in most cases, the fraction of dead space is higher in non-Newtonian cases.

Lowering the flow rate of water from 0.05 L/s to 0.0125 L/s produces fairly subtle differences in RTD, with the exception of the G3 concentric baffles geometry. For this

geometry, decreasing the flow rate causes the peak to shift left by 0.216 HRT, and increases the dead space fraction from 0.0414 to 0.145.

In the pilot-scale simulations, the RTD peaks occur later (closer to 1 HRT) than in the lab-scale simulations. In general, different fluids produce similar RTD curves for a given geometry. The G4 radial baffles geometry produces nearly identical RTD curves for water and 8% TS manure. The difference between these two fluids is more noticeable in the G1 centre inlet geometry; 8% TS manure exhibits a later peak and a slightly smaller dead space fraction and variance than water for this geometry. The fact that the RTD curves of the Newtonian and non-Newtonian fluids are largely similar can be explained by the extremely low shear rates involved in these cases. Comparing lab-scale to pilot scale cases, the inlet Reynolds numbers for the pilot-scale simulations are 2 or more orders of magnitude smaller than the lab-scale simulations. If forced mixing were incorporated into these simulations, shear rates would be much higher, and thus, significant differences would be apparent between the water and 8% TS manure cases. However, forced mixing is outside the scope of this study.

The use of CFD allows easy comparison of different fluids, flow rates, scales, and geometries when studying residence time distributions.

Chapter 7. Conclusions and recommendations

7.1 Objective

The objective of this thesis was to study how the non-Newtonian properties of liquid hog manure affect the flow characteristics within an anaerobic digester. This objective was accomplished in three stages:

1. The physical properties of liquid hog manure sampled from outdoor storage lagoons were determined experimentally. Density, total solids, particle size distribution, and viscosity were measured and correlated.
2. Residence time distribution (RTD) experiments were performed to compare Newtonian and non-Newtonian flows within four different anaerobic digestion reactor geometries.
3. Flow conditions within lab-scale and pilot-scale anaerobic digester reactors were simulated using three-dimensional modelling techniques. The effect of flow rate, working fluid, and geometry were studied.

7.2 Physical and properties of hog manure

Hog manure was collected from several depths and locations within two outdoor storage lagoons. Samples collected ranged from 0.67% to 37.1% TS, and represented three different zones within the lagoon; a surface zone containing dilute manure under 3.6% TS; below that, a transition zone with TS between 3.6% and 6.5%; and at the bottom of

the lagoon, a sludge zone with TS > 6.5%. The depth of the transition zone varied within the lagoons depending on proximity to the lagoon banks and inlet/outlet.

Particle size distribution of the manure samples was measured based on mass fraction and particle count. Two experimental techniques were used to measure the particle size distribution: microscopic image analysis and wet sieve tests. Due to the settling of solids within the lagoon, the largest particles were found in samples collected from the sludge zone. The results of these tests were well-described by Rosin-Rammler distribution.

The viscosity of liquid manure samples between 0.67% and 12.9% TS were measured using a Brookfield DV-II+Pro rotational viscometer. Measurements were taken at 15°C, 25°C, 40°C, and 60°C, and at shear rates ranging from 0.0066 to 44 s^{-1}. Surface samples (TS < 3.6%) exhibited Newtonian viscosity; viscosity increased exponentially with increasing solids concentration, but decreased with increasing temperature. Two samples within the transition zone (TS = 5.09% and 5.51% TS) were pseudoplastic, and were fit to the non-Newtonian power law. Samples collected from the sludge zone (TS > 6.5%) exhibited non-Newtonian and time-dependent characteristics. Power law parameters were determined based on the steady-state apparent viscosity of these samples. The consistency coefficient K was correlated to temperature and total solids using an exponential relation. Flow behaviour index n was scattered between 0.31 and 0.91 for these sludge-zone samples.

7.3 Experimental residence time distribution study

An experimental fluid column facility was designed and constructed to perform RTD experiments using four lab-scale anaerobic digester reactor geometries. Two of these geometries were unbaffled—the difference between these two geometries was the location of the inlet, with G1 have a centre inlet and G2 having a side inlet. The other two geometries were baffled—G3 contained two concentric cylindrical baffles, while G4 contained eight radial baffles. The conditions used for the experiments were continuous flow with no forced mixing. All geometries were tested with water (representing a Newtonian fluid) flowing at 0.05 and 0.0125 L/s, and a xanthan gum solution (representing a non-Newtonian fluid) at a 0.05 L/s

The unbaffled geometries, operating under Newtonian flow conditions, exhibited RTDs with early peaks and long, exponentially decaying tails. The RTDs for G4 (radial baffles) however were nearly bell-shaped, with peaks between 0.90 and 1.0 HRT. The RTD for G3 (concentric baffles) represented an intermediate case, with peaks at 0.65 and 0.7 HRT for the 0.05 L/s and 0.0125 L/s cases, respectively. Replacing water with a non-Newtonian fluid severely impacted the RTD curves of the four reactors. All four geometries exhibited a delay followed by a steep rise to a sharp peak, then an exponential decay. For the non-baffled geometries, the peaks were shifted later, and the variance of the RTD curves decreased; for G4 (radial baffles), the peak shifted earlier, while variance increased. For G3 (concentric baffles), the peak shifted earlier in time, but variance decreased. Comparing the estimated dead space fractions, the unbaffled geometries possessed the highest fractions of dead space for all flow conditions, while G4 (radial

baffles) possessed the lowest. However, the fraction of dead space for G4 rose dramatically when the non-Newtonian fluid was used.

Multi-parameter models were developed to fit the measured RTD curves. Two models were used: the PFR-CSTR model, which represents an ideal plug flow reactor and an ideal CSTR (continuously stirred tank reactor or complete mix reactor) in series; and the modified tanks-in-series model, which represents an ideal plug flow reactor followed in series by a finite number of ideal CSTRs. These models fit the experimental curves to within a normalized standard error of 0.15, with the exception of xanthan gum flowing in G4.

7.4 CFD simulation of flow conditions in anaerobic digester reactors

Twenty-four 3D simulations of flow in anaerobic digester reactors were performed using computational fluid dynamics (CFD). Twelve of these simulations recreated the RTD experiments described in Chapter 5; eight incorporated the properties of liquid manure at 3% and 8% TS, using correlations developed in Chapter 3; and the final four simulations represented water and 8% TS manure flowing through two pilot-scale reactor geometries. Results were compared to the experimentally-determined RTD curves, and the model was validated using particle image velocimetry (PIV) data collected using the experimental fluid column facility.

The CFD simulations compared well with the experimental results, exhibiting similar RTD curve shapes, and confirming the trends suggested by the experimental study. However, some discrepancies existed between the experimental and numerical RTD curves. For the water cases, the experimental results showed larger tails than the corresponding CFD simulations; meanwhile, the xanthan gum experiments exhibited higher and sharper peaks than those indicated by the simulations.

Pilot-scale simulations were performed using two geometries (G1 centre inlet and G4 radial baffles) and two fluids (water and 8% TS manure). In these simulations, the RTD peaks occurred later (closer to 1 HRT) than in the lab-scale simulations. In general, different fluids produced similar RTD curves for a given geometry. The similarity between the RTD curves of the Newtonian and non-Newtonian fluids can be explained by the extremely low shear rates involved in these cases. If forced mixing were incorporated into these simulations, shear rates would be much higher, and thus, significant differences would be apparent between the water and 8% TS manure cases. However, forced mixing was outside the scope of this study.

7.5 Recommendations

In this thesis, the investigation of non-Newtonian flow within an anaerobic digester was subjected to several limitations. These limitations were imposed due to time constraints, as well as in order to limit the scope of the project. Limitations in the experimental investigation of the physical properties of hog manure included the following: the number of samples studied; the physical properties that were measured; and the range of shear

rates under which the viscosity was measured. Collecting and studying more samples would be beneficial, especially samples with solids concentrations greater than 3.6% TS. More data points in this range would give better correlations, especially for the viscous characteristics. Also, the properties of fresh hog manure diluted to target concentrations could be measured and compared to the data collected in this study. Testing a greater range of physical properties, including thermal conductivity, specific heat, and composition, would also supplement the findings of this thesis. Furthermore, testing the viscosity at a greater range of shear rates would have provided a more complete representation of the rheology of liquid hog manure; however, a more sophisticated viscometer or rheometer would be needed for these tests.

Several simplifying assumptions were used in the RTD studies and CFD simulations. These assumptions included: continuous flow, no forced mixing, uniform properties, constant volume, and constant and uniform temperature. Also, the effects of microbial and chemical reactions, bubbling, and settling were neglected. Removing these assumptions would create a more complex and realistic system, and merits further study. Introducing forced mixing, in the form of an impeller, external agitation loop, or gas bubbling, would be a natural next step. This thesis identified the important effects of non-Newtonian behaviour on the flow within an unmixed reactor; these non-Newtonian effects will become even more significant in the presence of forced mixing. Another opportunity for study is the study of settling mechanisms in an anaerobic digester, using the particle size distribution results given in this thesis. Ultimately, a sophisticated model

that realistically incorporates all of the mechanisms present in anaerobic digesters could be produced to aid in the design of efficient and cost-effective systems.

Chapter 8. Bibliography

Achkari-Begdouri, A and P.R. Goodrich. 1992. Rheological properties of Moroccan dairy cattle manure. *Bioresour. Technol.* 40(2): 149-156.

Axapoulos, P., P. Panagakis, A. Tsavdaris, and D. Georgakakis. 2001. Simulation and experimental performance of a solar-heated anaerobic digester. *Solar Energy*. 70(2):155-164.

Bachmann, A., et al. 1982. Comparison of fixed-film reactors with a modified sludge blanket reactor. In *Proc. 1st International Conference on Fixed-Film Biological Processes*, 2, 1192- 1211.

Barker, J.C. and L.B. Driggers. 1981. Design criteria for alternative swine waste flushing systems. In *Livestock Waste: A Renewable Resource – Proceedings 4th International Symposium on Livestock Wastes – 1980*. St. Joseph, Mich.: ASAE.

Bello-Medoza, R., P. N. Sharrat. 1999. Analysis of retention time distribution (RTD) curves in an anaerobic digester with confined-gas mixing using a compartment model. *Wat. Sci. Technol.* 40(8): 49-56.

Benali, M. and T. Kudra. 2002. Thermal dewatering of diluted organic suspensions: process mechanism and drying kinetics. *Drying Technol.* 20(4&5): 935-951.

Bio-Terre. 2009. Achievements – Cook Feeder Farm. Bio-Terre Systems Inc. Available online at: http://www.bioterre.com/cook-feeder-farm.php. Accessed 2 May 2009.

Brookfield. 2006. "More Solutions to Sticky Problems." Middleboro, Mass.: Brookfield Engineering Labs., Inc.

CEC. 2007. A Report on Current Knowledge of Key Environmental Issues related to Hog Production in Manitoba. Clean Environment Commission.

Chen, T. H. and W. H. Shyu. 1996. Performance of four types of anaerobic reactors in treating very dilute dairy wastewater. *Biomass and Bioenergy*. 11(5): 431-441.

Chen, Y. R. 1986. Rheological properties of sieved beef-cattle manure slurry: rheological model and effect of temperature and solids concentration. *Agric. Wastes* 15(1): 17-33.

Cicek, N., S. Lambert, H.D. Venema, K. R. Snelgrove, E. L. Bibeau, and R. Grosshans. 2006. Nutrient removal and bio-energy production from Netley-Libau Marsh at Lake Winnipeg through annual biomass harvesting. *Biomass and Bioenergy*, 30, 529-536.

Dantec Dynamics. 2009. http://www.dantecdynamics.com/Default.aspx?ID=731.

DEA. 2003. Renewable Energy – Danish Solutions. ISBN 87-7844-404-7. Copenhagen, Denmark: Danish Energy Authority.

Dugba, P. N., R. H. Zhang, T. R. Rumsey, T. G. Ellis. 1999. Computer simulation of a two-stage anaerobic sequential batch reactor system for anaerobic wastewater treatment. *Trans. ASAE*. 42(2): 471-477.

Einstein, A. 1905. Über die von der molekularkinetishen Theorie der Wärme geforderte Bewegung von in ruhenden flüssigkeiten suspendierten Teilchen. *Annalen der Physik*. 17: 549-560.

El-Mashad, H.M., W.K.P van Loon, G. Zeeman, and G.P.A. Bot. 2005. Rheological properties of dairy cattle manure. *Bioresour. Technol.* 96(5): 531-535.

Environment Canada. 2008. Canada's greenhouse gas emissions: understanding the trends, 1990-2006. Cat. No. En81-4/2006-2E.

Fleming, J. G. 2002. Novel simulation of anaerobic digestion using computational fluid dynamics. Ph.D. diss. Raleigh, N.C.: North Carolina State University, Department of Mechanical Engineering.

Fluent. 2005. *Fluent 6.2 User's Guide*. Lebanon, N.H.: Fluent Inc.

Ford, C. C., F. Ein-Mozaffari, C. P. J. Bennington, and F. Taghipour. 2006. Simulation of mixing dynamics in agitated pulp stock chests using CFD. *AIChE*. 52(1): 3562 – 3569.

Ford, C. C., C. P. J. Bennington, and F. Taghipour. 2007. Modeling of a pilot-scale pulp mixing chest using CFD. *PAPTAC 93rd Annual Meeting 2007 – Preprints A*. 229 – 234. Pulp and Paper Technical Association of Canada.

Forshner, P., et al. 2004. Design of horizontal vessels operated as CSTR - basic mixing tasks, RTD, productivity. *Chem. Eng. Technol*. 27(3): 282-286.

Fox, R.W., A.T. McDonald, and P.J. Pritchard. 2004. *Introduction to Fluid Mechanics*. 6th ed. New York, N.Y.: John Wiley & Sons.

Gaden, D. L. F. 2007. An investigation of river kinetic turbines: performance enhancements, turbine modeling techniques, and an assessment of turbulence models. M. Sc. thesis. Winnipeg, Manitoba: University of Manitoba, Department of Mechanical and Manufacturing Engineering.

Gebremedhin, K. G., B. Wu, C. Gooch, P. Wright, and S. Inglis. 2005. Heat transfer model for plug-flow anaerobic digesters. *Trans. ASAE*. 48(2):777-785.

Gebremedhin, K. G. and S. Inglis. 2007. Validation of a biogas production model and determination of thermal energy from plug-flow anaerobic digesters. *Trans. ASABE*. 50(3): 975-979.

Grevilescu, M. R. Z. Tudose. 1996. Residence time distribution of liquid phase in an external-loop airlift bioreactor. *Bioprocess Eng.* 183-193.

Grobicki, A., D. C. Stuckey. 1992. Hydrodynamic characteristics of the anaerobic baffled reactor. *Wat. Res.* 26(3), 371-378.

Hashimoto, A.G. and Y.R. Chen. 1976. Rheology of livestock waste slurries. *Trans. ASAE* 19(5): 930-934.

Hughes, D. 2007. The energy sustainability dilemma: powering the future in a finite world. In *PHEV2007 Conference Proceedings*. Winnipeg, MB: Centre for Sustainable Transportation and Plugin Highway Network. Available at: http://www.pluginhighway.ca/proceedings.php#papers. Accessed 10 April 2009.

IPCC. 2001. *Climate Change 2001: A Scientific Basis, Intergovernmental Panel on Climate Change*. Cambridge, U.K.: Cambridge University Press.

IPCC. 2007. *Climate Change 2007: Synthesis Report*. Valencia, Spain: Intergovernmental Panel on Climate Change.

Karim, K., K. T. Klasson, R. Hoffman, S. R. Drescher, D. W. DePaoli, M. H. Al-Dahhan. 2005. Anaerobic digestion of animal waste: effect of mixing. *Bioresource Technol*. 96: 1607-1612.

Keener, H.M., J.J. Hoorman, and M.H. Klingman. 2006. Rheology and flowability properties of liquid dairy and swine manure. ASABE Paper No. 064072. St. Joseph, Mich.: ASABE.

Kumar, M., H.D. Bartlett, and N.N. Mohsenin. 1972. Flow properties of animal waste slurries. *Trans. ASAE* 15(4): 718-722.

Landry, H., C. Laguë, and M. Roberge. 2004. Physical and rheological properties of manure products. *Applied Eng. in Agric.*, 20(3): 277-288.

Levin, D. B., H. Zhu, M. Beland, N. Cicek, and B. E. Holbein. 2007. Potential for hydrogen and methane production from biomass residues in Canada. *Bioresource Technol*. 98: 654-660.

Levenspiel, O. 1972. *Chemical Reaction Engineering.* 2nd Ed. New York, N.Y., John Wiley and Sons.

Li, H. Z., L. Choplin. 1992. Residence time distribution (RTD) in rheologically complex fluids. *Proc. of the 4th international workshop on polymer reaction engineering*, 22-29. Berlin, Germany: VCH Publishers.

Lusk, P. 1998. Methane recovery from animal manures: The current opportunities casebook. SR-580-25145. Golden, Colorado.: USDE National Renewable Energy Laboratory.

MacLeod, C. 2004. Harnessing the Power of Anaerobic Digestion: Part I. Canadian Pork Council.

Manitoba Clean Environment Commission. 2007. Environmental sustainability and hog production in Manitoba. Winnipeg, MB: Manitoba Clean Environment Commission.

Massé L., D.I. Massé, V. Beaudette, and M. Muir. 2004. Particle size distribution and characteristics of raw and anaerobically digested swine manure slurry. ASAE Paper No. 044085. St. Joseph, Mich. ASAE.

Metzer, A. B., J. C. Reed. 1955. Flow of non-newtonian fluids - correlation of the laminar, transition, and turbulent-flow regions. *Amer. Industr. Chem. Eng. J.* 1(4): 434-440.

MLA. 2008. *The Environmental Amendment Act (Permanent Ban on Building or Expanding Hog Facilities).* The Manitoba Legislative Assembly, Bill 17, 2nd Session, 39th Legislature. Available online at: http://web2.gov.mb.ca/bills/39-2/b017e.php. Accessed 25 April 2009.

MoEEC and MoE. 2009. Climate and energy policy for a sustainable future. Memorandum. Ministry of Enterprise, Energy and Communications and Ministry of Environment. Sweden. Available at: http://www.sweden.gov.se/content/1/c6/12/32/52/b03e9aa8.pdf. Accessed 25 April 2009.

Morrison, F.A. 2001. *Understanding Rheology*. New York, N.Y: Oxford University Press.

NCLE. 2008. National Centre for Livestock and the Environment Research Update, May 2008. Available at: http://www.umanitoba.ca/afs/ncle/NCLE_activities_May_2008.pdf. Accessed 2 May 2009.

Nelson, C. and J. Lamb, 2002. Final Report: Haubenschild Farms Anaerobic Digester Updated! St. Paul, MN: The Minnesota Project.

NRCan. 2006. Canada's Energy Outlook – The Reference Case 2006. Natural Resources Canada, Analysis and Modeling Division. Cat. No. M144-126/2006E-PDF.

NRCan. 2007. Biomass and Bioenergy. CETC #2008-43 / 2007-07-09. Ottawa, OT: Natural Resources Canada. Available online at: http://canmetenergy.nrcan.gc.ca/eng/publications.html?2008-43. Accessed 25 April 2009.

O'Neil, D. J. 1985. Rheology and mass/heat transfer aspects of anaerobic reactor design. *Biomass.* 8: 205-216.

Patankar, S. V. 1980. *Numerical Heat Transfer and Fluid Flow*. Washington, D.C.: Hemisphere.

Pontes, R. F. F. and J. M Pinto. 2006. Analysis of integrated kinetic and flow models for anaerobic digesters. *Chem. Eng. J*. 122:65-80.

Roussinova, V. S. M. Kresta. 2008. Comparison of continuous blend time and residence time distribution models for a stirred tank. *Ind. Chem. Eng.* 47: 3532-3539.

Skiadas, I. V., G. Lyberatos. 1998. The periodic anaerobic baffled reactor. *Wat. Sci. Technol*. 38(8,9): 401-408.

Speers, R. A., M. A. Tung. 1986. Concentration and temperature dependence of flow behaviour of xanthan gum dispersions. *J. Food Sci*. 51(1): 96-98.

Statistics Canada. 2007. *2006 Census of Agriculture*.

Statistics Canada. 2009. Hog Statistics: Fourth Quarter, 2008. Statistics Canada cat. #23-010-X, vol. 8, no. 1.

U.S. EPA. 2006. Global Mitigation of non-CO_2 Greenhouse Gases. EPA 430-R-06-005, Washington, D.C.: US EPA Office of Atmospheric Programs.

Vesvikar, M. S. and M. Al-Dahhan. 2005. Flow pattern visualization in a mimic anaerobic digester using CFD. *Bioeng. and Biotechnol.* 89(6): 719 – 732.

Wen, Z. and S. Chen. 2006. Development of a sequential continuous stirred tank reactor (CSTR) system for anaerobic digestion of liquid dairy manure. In *2006 ASABE Annual International Meeting*. Portland, Oregon: ASABE.

Wilkie, A. C. 1998. Anaerobic digestion of livestock waste: a suitable approach to odour abatement. In *The North Carolina 1998 Pork Conference and Beef Symposium*, 5-16. Raleigh, N.C.: North Carolina Pork Council.

Wu, B. and S. Chen. 2008. CFD simulation of non-Newtonian fluid flow in anaerobic digesters. *Bioeng. and Biotechnol*. 99(3): 700 – 711.

Zhang, R. H., J. Tao, and P. N. Dugba. 2000. Evaluation of a two-stage anaerobic sequential batch reactor system for anaerobic wastewater treatment. Trans. ASAE. 43(6): 1795-1801.

Zupancic, G. D. and M. Ros. 2003. Heat and energy requirements in thermophilic anaerobic sludge digestion. *Renewable Energy*. 28: 2255-2267.

8.1 Graphic References

Bio-Terre. 2009. Achievements – Cook Feeder Farm. Bio-Terre Systems Inc. Available online at: http://www.bioterre.com/cook-feeder-farm.php. Accessed 2 May 2009. Used with permission.

NCLE. 2008. National Centre for Livestock and the Environment Research Update, May 2008. Available at: http://www.umanitoba.ca/afs/ncle/NCLE_activities_May_2008.pdf. Accessed 2 May 2009. Used with permission.

Nelson, C. and J. Lamb, 2002. Final Report: Haubenschild Farms Anaerobic Digester Updated! St. Paul, MN: The Minnesota Project. Used with permission.

Appendix A. Hog manure viscosity results: full data set

Viscosity of manure samples with TS < 3.6%

Operation	% T.S.	Temp. (°C)	μ (Pa·s)	+/- μ (Pa·s)	Shear rates (s^{-1})
1	0.672	15	5.876E-03	1.19E-03	8.8 to 44
1	0.672	25	5.413E-03	1.26E-03	8.8 to 44
1	0.686	15	6.336E-03	1.08E-03	8.8 to 44
1	0.686	25	5.608E-03	1.21E-03	8.8 to 44
1	0.686	40	4.670E-03	1.06E-03	8.8 to 44
1	0.686	60	4.087E-03	9.82E-04	8.8 to 44
1	0.716	15	5.923E-03	1.17E-03	8.8 to 44
1	0.716	25	5.330E-03	1.15E-03	8.8 to 44
1	0.716	40	4.543E-03	1.02E-03	8.8 to 44
1	0.741	15	6.433E-03	1.19E-03	8.8 to 44
1	0.741	25	5.689E-03	1.14E-03	8.8 to 44
1	0.741	40	4.791E-03	1.05E-03	8.8 to 44
1	0.741	60	4.136E-03	7.89E-04	8.8 to 44
1	0.747	15	6.346E-03	1.20E-03	8.8 to 44
1	0.747	25	5.591E-03	1.12E-03	8.8 to 44
1	0.747	40	4.771E-03	1.09E-03	8.8 to 44
1	0.747	60	3.990E-03	8.82E-04	8.8 to 44
1	0.777	15	5.910E-03	1.21E-03	8.8 to 44
1	0.777	25	5.292E-03	1.11E-03	8.8 to 44
1	0.777	40	4.472E-03	1.05E-03	8.8 to 44
1	0.903	15	6.357E-03	1.26E-03	8.8 to 44
1	0.903	25	5.397E-03	1.20E-03	8.8 to 44
1	0.903	40	4.652E-03	1.14E-03	8.8 to 44
1	0.903	60	3.945E-03	9.49E-04	8.8 to 44
1	1.36	15	8.196E-03	8.59E-04	8.8 to 44
1	1.36	40	5.892E-03	9.55E-04	8.8 to 44
1	1.36	60	4.694E-03	8.13E-04	8.8 to 44
1	1.54	15	7.200E-03	9.57E-04	8.8 to 44
1	1.54	25	6.120E-03	9.47E-04	8.8 to 44
1	1.54	40	5.171E-03	8.89E-04	8.8 to 44
1	1.54	60	4.165E-03	9.46E-04	8.8 to 44
1	2.25	15	8.561E-03	6.72E-04	8.8 to 44
1	2.25	25	7.391E-03	7.03E-04	8.8 to 44
1	2.25	40	5.854E-03	8.35E-04	8.8 to 44
1	2.25	60	4.511E-03	7.95E-04	8.8 to 44
2	2.05	15	8.511E-03	1.12E-03	8.8 to 44
2	2.05	25	7.447E-03	1.33E-03	8.8 to 44
2	2.05	40	6.276E-03	1.17E-03	8.8 to 44
2	2.05	60	5.096E-03	1.08E-03	8.8 to 44
2	2.07	15	8.466E-03	1.06E-03	8.8 to 44

(Table 3.6 continued)

Operation	% T.S.	Temp. (°C)	μ (Pa·s)	+/- μ (Pa·s)	Shear rates (s^{-1})
2	2.07	40	6.109E-03	1.25E-03	8.8 to 44
2	2.07	60	5.066E-03	1.07E-03	8.8 to 44
2	2.34	15	9.028E-03	1.11E-03	8.8 to 44
2	2.34	25	8.225E-03	1.36E-03	8.8 to 44
2	2.34	40	6.650E-03	1.25E-03	8.8 to 44
2	2.34	60	5.366E-03	1.20E-03	8.8 to 44
2	2.97	15	1.270E-02	4.80E-04	8.8 to 44
2	2.97	25	1.086E-02	6.05E-04	8.8 to 44
2	2.97	40	8.889E-03	8.21E-04	8.8 to 44
2	2.97	60	7.387E-03	9.28E-04	8.8 to 44
2	3.33	15	1.375E-02	6.12E-04	8.8 to 44
2	3.33	25	1.198E-02	5.73E-04	8.8 to 44
2	3.33	40	9.808E-03	6.05E-04	8.8 to 44
2	3.33	60	8.021E-03	8.16E-04	8.8 to 44
2	3.37	15	1.309E-02	6.58E-04	8.8 to 44
2	3.37	25	1.154E-02	5.49E-04	8.8 to 44
2	3.37	40	9.522E-03	6.43E-04	8.8 to 44
2	3.37	60	7.549E-03	9.53E-04	8.8 to 44
2	3.55	15	1.602E-02	1.11E-03	8.8 to 44
2	3.55	25	1.442E-02	1.14E-03	8.8 to 44
2	3.55	40	1.181E-02	8.81E-04	8.8 to 44
2	3.55	60	9.009E-03	5.96E-04	8.8 to 44

Consistency coefficient K and flow behaviour index n for Operation 1, TS = 5.09% and 5.51%

% T.S.	Temp (°C)	K ($Pa·s^n$)	± K ($Pa·s^n$)	n	± n	Corr. Coeff.	Shear rates (s^{-1})		
5.09	15	0.1767	2.28E-04	0.5230	1.59E-02	0.9968	8.8	To	44
5.09	25	0.1407	2.62E-04	0.5516	1.91E-02	0.9959	8.8	To	44
5.09	40	0.1112	4.33E-04	0.5304	2.76E-02	0.9907	8.8	To	44
5.09	60	0.02335	2.76E-04	0.9121	4.80E-02	0.9904	8.8	To	44
5.51	15	0.2172	1.88E-04	0.4731	1.33E-02	0.9976	8.8	To	44
5.51	25	0.1908	1.46E-04	0.4778	1.22E-02	0.9977	8.8	To	44
5.51	40	0.1382	4.18E-04	0.4978	2.43E-02	0.9918	8.8	To	44
5.51	60	0.06012	3.55E-04	0.6053	3.40E-02	0.9892	8.8	To	44

Power law parameters for high-TS samples

Oper.	% T.S.	Temp (°C)	K ($Pa \cdot s^n$)	n	Corr. Coeff.	Shear rates (s^{-1})			Data pts.
1	9.45	15	2.054	0.4322	0.9926	0.0066	to	0.198	3
1	9.45	40	1.349	0.3112	0.9834	0.011	to	0.264	3
1	9.45	60	1.245	0.5217	0.9962	0.11	to	0.66	4
2	6.49	15	0.3075	0.5894	0.9802	1.1	to	13.2	5
2	6.49	25	0.3139	0.5392	0.9863	1.1	to	22	7
2	6.49	40	0.2478	0.5909	0.9918	1.1	to	22	7
2	6.49	60	0.1622	0.5673	0.9413	1.1	to	22	7
2	12.9	15	6.154	0.6116	0.9998	0.011	to	0.044	3
2	12.9	25	3.900	0.5798	0.9837	0.011	to	0.066	4
2	12.9	40	3.470	0.6080	0.9585	0.011	to	0.11	6

Appendix B. GAMBIT journal files for CFD meshes

```
************************** GEOMETRY #1 **************************

/ Journal File for GAMBIT 2.2.30, Database 2.2.14, ntx86 BH04110220
/ Identifier "FluidCol-G1-medhex3"
/ File opened for write Thu Oct 02 09:58:43 2008.
identifier name "FluidCol-G1-medhex3" new nosaveprevious

/ Variables

$cyl_r = 5.625
$cyl_h = 19.625
$out_r = 0.5
$out_h = 10.0
$in_r = 0.3595
$in_h = 2.0
$in_y = 18.125
$in_x = $cyl_r - 0.5

$gridsize = 0.3
$gridcount = 80
$BL_size = 0.1

$step = 3
/Geometry
IF COND ($step .gt. 0)
volume create "Cylinder" height $cyl_h radius1 $cyl_r radius2 $cyl_r
radius3 \
  $cyl_r offset 0 (0.5*$cyl_h) 0 yaxis frustum
volume create "Outlet" height $out_h radius1 $out_r radius2 $out_r
radius3 $out_r \
  offset 0 (-$out_h/2) 0 yaxis frustum
volume create "Inlet" height $in_h radius1 $in_r radius2 $in_r radius3
$in_r \
  offset ($in_h/2 + $in_x) $in_y 0 xaxis frustum
volume unite volumes "Cylinder" "Outlet" "Inlet"
ENDIF

/Splitting
IF COND ($step .gt. 1)
volume create "Inner-Cyl" height (2*$cyl_h) radius1 (0.6*$cyl_r)
radius2 \
  (0.6*$cyl_r) radius3 (0.6*$cyl_r) offset 0 0 0 yaxis frustum
face create "splitplane1" width (2*$cyl_r) height (2*$cyl_r) zxplane
rectangle \
  offset 0 (0.2*$cyl_h) 0
face create "splitplane2" width (2*$cyl_r) height (2*$cyl_r) zxplane
rectangle \
  offset 0 (0.8*$cyl_h) 0
face create "splitplane3" width (2*$cyl_r) height $cyl_h xyplane
rectangle \
  offset 0 ($cyl_h/2) (2*$in_r)
```

```
face create "splitplane4" width (2*$cyl_r) height $cyl_h xyplane
rectangle \
  offset 0 ($cyl_h/2) (-2*$in_r)

/face move "splitplane3" dangle -15 vector 0 1 0 origin 0 0 0
/face move "splitplane4" dangle 15 vector 0 1 0 origin 0 0 0

volume split "Cylinder" connected face "splitplane2"
volume split "Cylinder" connected face "splitplane1"
face split "face.3" connected face "face.12" keeptool
volume split "volume.4" connected volume "Inner-Cyl" keeptool
volume split "Cylinder" connected volume "Inner-Cyl"
volume split "volume.3" connected face "splitplane3"
volume split "volume.3" connected face "splitplane4"

face create "splitplane5" width ($cyl_r) height (2*$cyl_h) xyplane
rectangle \
  offset (0.5*$cyl_r) 0 0
face split "face.5" connected face "splitplane5" keeptool
face split "face.18" connected face "splitplane5" keeptool
face split "face.19" connected face "splitplane5"

ENDIF

/ Meshing
IF COND ($step .gt. 2)

edge mesh "edge.43" successive ratio1 1 intervals 10
edge mesh "edge.2" "edge.58" successive ratio1 1 intervals 25
edge mesh "edge.59" successive ratio1 1 intervals 50
edge mesh "edge.28" "edge.46" successive ratio1 1 intervals 5
edge mesh "edge.6" successive ratio1 1 intervals 20
edge mesh "edge.71" "edge.29" successive ratio1 1 intervals 5


blayer create "BL1" first 0.05 growth 1.2 total 0.496496 rows 6
transition 1 \
  trows 0
blayer attach "BL1" face "face.38" edge "edge.43" add
blayer create "BL2" first 0.05 growth 1.2 total 0.496496 rows 6
transition 1 \
  trows 0
blayer attach "BL2" face "face.30" "face.2" "face.2" edge "edge.59"
"edge.2" \
  "edge.58" add
blayer create "BL3" first 0.02 growth 1.2 rows 4 transition 1 \
  trows 0
blayer attach "BL3" face "face.9" edge "edge.6" add
blayer create "BL4" first 0.03 growth 1.2 rows 6 transition 1 \
  trows 0
blayer attach "BL4" face "face.38" edge "edge.8" add

face mesh "face.9" pave
face mesh "face.10" map intervals 10
face mesh "face.38" pave size 0.1
face mesh "face.30" "face.2" map
```

```
edge mesh "edge.70" "edge.54" successive ratio1 1.1 intervals 20
edge mesh "edge.52" "edge.68" successive ratio1 0.90909091 intervals 20

face mesh "face.32" "face.3" submap

edge mesh "edge.69" "edge.53" successive ratio1 1 intervals 24

face mesh "face.33" "face.21" pave

edge mesh "edge.49" "edge.65" successive ratio1 0.90909091 intervals 20
edge mesh "edge.47" "edge.63" successive ratio1 1.1 intervals 20
edge mesh "edge.48" "edge.64" successive ratio1 1 intervals 24

face mesh "splitplane2" "face.36" map

volume mesh "volume.3" cooper source "face.33" "face.37" "face.32"
"face.36"
volume mesh "volume.8" cooper source "face.35" "face.21" "splitplane2"
\
  "face.3"
volume mesh "volume.9" cooper source "face.38" "face.9" "face.40"

edge mesh "edge.90" successive ratio1 1 intervals 50
face mesh "face.18" map

volume mesh "volume.4" cooper source "face.31" "face.36" "face.39" \
  "splitplane2" "splitplane1" size 1

edge mesh "edge.1" successive ratio1 1 intervals 90
edge mesh "edge.92" successive ratio1 1 intervals 30

blayer create "BL3" first 0.05 growth 1.2 total 0.496496 rows 6
transition 1 \
  trows 0
blayer attach "BL3" face "face.19" "face.19" edge "edge.1" "edge.92"
add

edge mesh "edge.91" successive ratio1 1 intervals 35
face mesh "face.19" map
volume mesh "Cylinder" cooper source "splitplane1" "face.1" size 1

face mesh "face.4" pave size .1
edge mesh "edge.84" successive ratio1 1 intervals 30
face mesh "face.5" map
face mesh "face.29" pave

volume mesh "Inner-Cyl" cooper source "face.29" "face.26" "face.4"
volume mesh "volume.5" tetrahedral size 0.5

ENDIF

/ Meshing
IF COND ($step .gt. 3)
physics create "tank" ctype "FLUID" volume "Inner-Cyl" "volume.3"
"volume.5" \
```

```
  "volume.4" "Cylinder" "volume.8" "volume.9"
physics create "inlet" btype "MASS_FLOW_INLET" face "face.9"
physics create "outlet" btype "OUTFLOW" face "face.4"
ENDIF
```

```
  *************************** GEOMETRY #2 ***************************

/ Journal File for GAMBIT 2.2.30, Database 2.2.14, ntx86 BH04110220
/ Identifier "FluidCol-G2-med"
/ File opened for write Thu Oct 02 09:58:43 2008.
identifier name "FluidCol-G2-med69" new nosaveprevious

/ Variables

$cyl_r = 5.625
$cyl_h = 19.625
$out_r = 0.5
$out_h = 10.0
$in_r = 0.3595
$in_h = 6.0
$in_y = 18.125
$in_x = -$cyl_r
$in_z = -5.0

$gridsize = 0.3
$gridcount = 80
$BL_size = 0.1

$step = 3
/Geometry
IF COND ($step .gt. 0)
volume create "Cylinder" height $cyl_h radius1 $cyl_r radius2 $cyl_r
radius3 \
  $cyl_r offset 0 (0.5*$cyl_h) 0 yaxis frustum
volume create "Outlet" height $out_h radius1 $out_r radius2 $out_r
radius3 $out_r \
  offset 0 (-$out_h/2) 0 yaxis frustum
volume create "Inlet" height $in_h radius1 $in_r radius2 $in_r radius3
$in_r \
  offset ($in_h/2 + $in_x) $in_y $in_z xaxis frustum
volume unite volumes "Cylinder" "Outlet" "Inlet"
ENDIF

/Splitting
IF COND ($step .gt. 1)
volume create "Inner-Cyl" height (2*$cyl_h) radius1 (0.6*$cyl_r)
radius2 \
  (0.6*$cyl_r) radius3 (0.6*$cyl_r) offset 0 0 0 yaxis frustum
face create "splitplane1" width (2*$cyl_r) height (2*$cyl_r) zxplane
rectangle \
  offset 0 (0.2*$cyl_h) 0
face create "splitplane2" width (2*$cyl_r) height (2*$cyl_r) zxplane
rectangle \
  offset 0 (0.8*$cyl_h) 0
face create "splitplane3" width (2*$cyl_r) height $cyl_h xyplane
rectangle \
  offset 0 ($cyl_h/2) (4*$in_r)
face create "splitplane4" width (2*$cyl_r) height $cyl_h xyplane
rectangle \
  offset 0 ($cyl_h/2) (-4*$in_r)
```

```
face move "splitplane3" dangle -62.73 vector 0 1 0 origin 0 0 0
face move "splitplane4" dangle -62.73 vector 0 1 0 origin 0 0 0

volume split "Cylinder" connected face "splitplane2"
volume split "Cylinder" connected face "splitplane1"
face split "face.3" connected face "face.12" keeptool
volume split "volume.4" connected volume "Inner-Cyl" keeptool
volume split "Cylinder" connected volume "Inner-Cyl"
volume split "volume.3" connected face "splitplane3"
volume split "volume.3" connected face "splitplane4"

face create "splitplane5" width ($cyl_r) height (2*$cyl_h) xyplane
rectangle \
  offset (0.5*$cyl_r) 0 (-4*$in_r)
face move "splitplane5" dangle -62.73 vector 0 1 0 origin 0 0 0
face split "face.18" connected face "splitplane5" keeptool
face split "face.19" connected face "splitplane5"
face create "splitplane6" width ($cyl_r) height (2*$cyl_h) xyplane
rectangle \
  offset (0.5*$cyl_r) 0 0
face split "face.5" connected face "splitplane6"

ENDIF

/ Meshing
IF COND ($step .gt. 2)

edge mesh "edge.60" "edge.61" successive ratio1 1 intervals 20
edge mesh "edge.2" successive ratio1 1 intervals 4
edge mesh "edge.53"  successive ratio1 1 intervals 46
edge mesh "edge.65" successive ratio1 1 intervals 50

blayer create "BL1" first 0.05 growth 1.2 total 0.496496 rows 6
transition 1 \
  trows 0
blayer attach "BL1" face "face.36" edge "edge.61" add
blayer create "BL2" first 0.05 growth 1.2 total 0.496496 rows 6
transition 1 \
  trows 0
blayer attach "BL2" face "face.30" "face.2" "face.2" edge "edge.65"
"edge.2" \
  "edge.53" add
blayer create "BL3" first 0.02 growth 1.2 rows 4 transition 1 \
  trows 0
blayer attach "BL3" face "face.7" edge "edge.5" add
blayer create "BL4" first 0.03 growth 1.2 rows 6 transition 1 \
  trows 0
blayer attach "BL4" face "face.38" edge "edge.8" add

face mesh "face.7" pave intervals 20
face mesh "face.10" map intervals 10

blayer create "BL5" first 0.02 growth 1.2 rows 6 transition 1 \
  trows 0
blayer attach "BL5" face "face.36" edge "edge.8" add
```

```
face mesh "face.36" pave size 0.1
face mesh "face.30" "face.2" map

edge mesh "edge.45" "edge.63" successive ratio1 0.90909091 intervals 20
edge mesh "edge.44" "edge.62" successive ratio1 1.1 intervals 20
edge mesh "edge.56" "edge.72" successive ratio1 0.90909091 intervals 20
edge mesh "edge.57" "edge.73" successive ratio1 1.1 intervals 20

face mesh "face.35" "face.3" submap

edge mesh "edge.68" "edge.51" successive ratio1 1 intervals 24

face mesh "face.32" "face.21" pave

edge mesh "edge.50" "edge.67" successive ratio1 1 intervals 24

face mesh "splitplane4" "face.33" map

volume mesh "volume.3" cooper source "face.35" "face.32" "face.39"
"face.40"
volume mesh "volume.8" cooper source "face.3" "face.21" "splitplane2" \
  "face.34"
volume mesh "volume.9" cooper source "face.36" "face.7" "face.43"

edge mesh "edge.84" successive ratio1 1 intervals 50
face mesh "face.18" map

volume mesh "volume.4" cooper source "face.31" "face.37" "face.39" \
  "splitplane2" "splitplane1" size 1

edge mesh "edge.1" successive ratio1 1 intervals 120
edge mesh "edge.86" successive ratio1 1 intervals 20

blayer create "BL6" first 0.05 growth 1.2 total 0.496496 rows 6
transition 1 \
  trows 0
blayer attach "BL6" face "face.19" "face.19" edge "edge.1" "edge.86"
add

edge mesh "edge.85" successive ratio1 1 intervals 35
face mesh "face.19" map
volume mesh "Cylinder" cooper source "splitplane1" "face.1" size 1

blayer create "BL7" first 0.02 growth 1.2 rows 4 transition 1 \
  trows 0
blayer attach "BL7" face "face.4" "face.4" edge "edge.3" "edge.93" add

face mesh "face.4" pave size .1
edge mesh "edge.92" successive ratio1 1 intervals 30
face mesh "face.5" map

blayer create "BL8" first 0.04 growth 1.2 rows 6 transition 1 \
  trows 0
blayer attach "BL8" face "face.29" "face.29" edge "edge.7" "edge.91"
add
```

```
face mesh "face.29" pave

volume mesh "Inner-Cyl" cooper source "face.29" "face.26" "face.4"
volume mesh "volume.5" tetrahedral size 0.5

ENDIF

/ Meshing
IF COND ($step .gt. 3)
physics create "tank" ctype "FLUID" volume "Inner-Cyl" "volume.3"
"volume.5" \
  "volume.4" "Cylinder" "volume.8" "volume.9"
physics create "inlet" btype "MASS_FLOW_INLET" face "face.7"
physics create "outlet" btype "OUTFLOW" face "face.4"
ENDIF
```

```
  *************************** GEOMETRY #3 ***************************

/ Journal File for GAMBIT 2.2.30, Database 2.2.14, ntx86 BH04110220
/ Identifier "FluidCol-G3"
/ File opened for write Thu Nov 20 09:58:43 2008.
identifier name "FluidCol-G3-med" new nosaveprevious

/ Variables

$cyl_r = 5.625
$cyl_h = 19.625
$cyl2_rout = 4.0
$cyl2_rin = 3.625
$cyl3_rout = 2
$cyl3_rin = 1.625
$out_r = 0.5
$out_h = 10.0
$in_r = 0.3595
$in_h = 6.0
$in_y = 18.125
$in_z = -5.0
$in_x = -($cyl_r)

$hole1_r = 0.75
$hole1_h = 5.0
$hole1_y = 3.625
$hole2_r = 0.75
$hole2_h = 3.0
$hole2_y = 17.625


$gridsize = 0.3
$gridcount = 80
$BL_size = 0.1

$step = 6
$otherParameter = 1
/Geometry
IF COND ($step .gt. 0)
volume create "Cylinder" height $cyl_h radius1 $cyl_r radius2 $cyl_r
radius3 \
  $cyl_r offset 0 (0.5*$cyl_h) 0 yaxis frustum
volume create "Outlet" height $out_h radius1 $out_r radius2 $out_r
radius3 $out_r \
  offset 0 (-$out_h/2) 0 yaxis frustum
volume create "Inlet" height $in_h radius1 $in_r radius2 $in_r radius3
$in_r \
  offset ($in_h/2 + $in_x) $in_y $in_z xaxis frustum
volume unite volumes "Cylinder" "Outlet" "Inlet"

volume create "Cylinder2" height $cyl_h radius1 $cyl2_rout radius2
$cyl2_rout \
  radius3 $cyl2_rout offset 0 (0.5*$cyl_h) 0 yaxis frustum
volume create "Cylinder2in" height $cyl_h radius1 $cyl2_rin radius2
$cyl2_rin \
  radius3 $cyl2_rin offset 0 (0.5*$cyl_h) 0 yaxis frustum
```

```
volume subtract "Cylinder2" volumes "Cylinder2in"
volume create "Hole1" height $hole1_h radius1 $hole1_r radius2 $hole1_r
\
  radius3 $hole1_r offset -(0.5*$hole1_h) $hole1_y 0 xaxis frustum
volume subtract "Cylinder2" volumes "Hole1"

volume create "Cylinder3" height $cyl_h radius1 $cyl3_rout radius2
$cyl3_rout \
  radius3 $cyl3_rout offset 0 (0.5*$cyl_h) 0 yaxis frustum
volume create "Cylinder3in" height $cyl_h radius1 $cyl3_rin radius2
$cyl3_rin \
  radius3 $cyl3_rin offset 0 (0.5*$cyl_h) 0 yaxis frustum
volume subtract "Cylinder3" volumes "Cylinder3in"
volume create "Hole2" height $hole2_h radius1 $hole2_r radius2 $hole2_r
\
  radius3 $hole2_r offset (0.5*$hole2_h) $hole2_y 0 xaxis frustum
volume subtract "Cylinder3" volumes "Hole2"

volume subtract "Cylinder" volumes "Cylinder2"
volume subtract "Cylinder" volumes "Cylinder3"

ENDIF

/Splitting
IF COND ($step .gt. 1)
volume create "SplitCyl1" height (2*$cyl_h) radius1 $cyl2_rout radius2
\
 $cyl2_rout radius3 $cyl2_rout offset 0 0 0 yaxis frustum
volume create "SplitCyl2" height (2*$cyl_h) radius1 $cyl2_rin radius2 \
 $cyl2_rin radius3 $cyl2_rin offset 0 0 0 yaxis frustum
volume create "SplitCyl3" height (2*$cyl_h) radius1 $cyl3_rout radius2
\
 $cyl3_rout radius3 $cyl3_rout offset 0 0 0 yaxis frustum
volume create "SplitCyl4" height (2*$cyl_h) radius1 $cyl3_rin radius2 \
 $cyl3_rin radius3 $cyl3_rin offset 0 0 0 yaxis frustum

face create "splitplane1" width (2*$cyl_r) height (2*$cyl_r) zxplane
rectangle \
  offset 0 ($hole2_y - 1.5) 0
face create "splitplane2" width $cyl_r height $cyl_h xyplane rectangle
\
  offset (-$cyl_r/2) ($cyl_h/2) 0
face create "splitplane3" width $cyl_r height $cyl_h xyplane rectangle
\
  offset (-$cyl_r/2) ($cyl_h/2) 0

face move "splitplane2" dangle -40 vector 0 1 0 origin 0 0 0
face move "splitplane3" dangle -90 vector 0 1 0 origin 0 0 0

volume split "Cylinder" volume "SplitCyl1" connected
volume split "SplitCyl1" volume "SplitCyl2" connected
volume split "SplitCyl2" volume "SplitCyl3" connected
volume split "SplitCyl3" volume "SplitCyl4" connected
volume modify "Cylinder" label "Annulus1"
volume modify "SplitCyl2" label "Annulus2"
volume modify "SplitCyl4" label "Annulus3"
```

```
volume modify "SplitCyl1" label "LowHole"
volume modify "SplitCyl3" label "HighHole"

volume split "Annulus1" face "splitplane1" connected
volume split "volume.10" face "splitplane2" connected
volume split "volume.10" face "splitplane3" connected
volume modify "volume.10" label "Annulus1Top"
volume modify "volume.11" label "Inlet"

volume create "Tube1" height (2*$hole1_h) radius1 $hole1_r radius2
$hole1_r \
  radius3 $hole1_r offset -($hole1_h) $hole1_y 0 xaxis frustum
volume split "Annulus1" volume "Tube1" connected keeptool
volume split "Annulus2" volume "Tube1" connected
volume create "Tube2" height (3.2*$hole2_h) radius1 $hole2_r radius2
$hole2_r \
  radius3 $hole2_r offset $hole2_h $hole2_y 0 xaxis frustum
volume split "Annulus2" volume "Tube2" connected keeptool
volume split "Annulus3" volume "Tube2" connected

face create "splitplane4" width (2*$cyl_r) height (2*$cyl_r) zxplane
rectangle \
  offset 0 ($hole1_y + 1.5) 0
face create "splitplane5" width (2*$cyl_r) height (2*$cyl_r) zxplane
rectangle \
  offset 0 ($hole1_y - 1.5) 0
face create "splitplane6" width (2*$cyl_r) height (2*$cyl_r) zxplane
rectangle \
  offset 0 ($hole2_y + 1.5) 0
face create "splitplane7" width (2*$cyl_r) height (2*$cyl_r) zxplane
rectangle \
  offset 0 ($hole2_y - 1.5) 0
face create "splitplane8" width $cyl_r height $cyl_h xyplane rectangle
\
  offset (-$cyl_r/2) ($cyl_h/2) 0
face create "splitplane9" width $cyl_r height $cyl_h xyplane rectangle
\
  offset (-$cyl_r/2) ($cyl_h/2) 0
face create "splitplane10" width $cyl_r height $cyl_h xyplane rectangle
\
  offset ($cyl_r/2) ($cyl_h/2) 0
face create "splitplane11" width $cyl_r height $cyl_h xyplane rectangle
\
  offset ($cyl_r/2) ($cyl_h/2) 0
face create "splitplane12" width $cyl_r height $cyl_h xyplane rectangle
\
  offset (-$cyl_r/2) ($cyl_h/2) 0
face create "splitplane13" width $cyl_r height $cyl_h xyplane rectangle
\
  offset (-$cyl_r/2) ($cyl_h/2) 0

face move "splitplane8" dangle -20 vector 0 1 0 origin 0 0 0
face move "splitplane9" dangle 20 vector 0 1 0 origin 0 0 0
face move "splitplane10" dangle -35 vector 0 1 0 origin 0 0 0
face move "splitplane11" dangle 35 vector 0 1 0 origin 0 0 0
face move "splitplane12" dangle -35 vector 0 1 0 origin 0 0 0
```

```
face move "splitplane13" dangle 35 vector 0 1 0 origin 0 0 0

volume split "Annulus1" face "splitplane4" connected keeptool
volume split "Annulus1" face "splitplane5" connected keeptool
volume split "Annulus2" face "splitplane4" connected
volume split "Annulus2" face "splitplane5" connected
volume split "volume.22" face "splitplane6" connected keeptool
volume split "volume.22" face "splitplane7" connected keeptool

volume split "volume.21" face "splitplane8" connected
volume split "volume.21" face "splitplane9" connected
volume split "volume.25" face "splitplane10" connected
volume split "volume.25" face "splitplane11" connected
volume split "volume.23" face "splitplane12" connected
volume split "volume.23" face "splitplane13" connected

volume split "Annulus3" face "splitplane6" connected
volume split "Annulus3" face "splitplane7" connected

volume unite volumes "LowHole" "Tube1" "volume.13"
volume unite volumes "HighHole" "volume.17" "Tube2"

face create "splitplane14" width $cyl_r height $cyl_r zxplane rectangle
\
  offset (-$cyl_r/2) ($hole1_y) (-$cyl_r/2)
face create "splitplane15" width $cyl_r height $cyl_r zxplane rectangle
\
  offset ($cyl_r/2) ($hole2_y) (-$cyl_r/2)
face create "splitplane16" width $cyl_r height $cyl_r zxplane rectangle
\
  offset 0 ($hole2_y) (-$cyl_r/2)
face split "face.19" face "splitplane14" connected keeptool
face split "face.62" face "splitplane14" connected keeptool
face split "face.64" face "splitplane14" connected
face split "face.28" face "splitplane15" connected keeptool
face split "face.72" face "splitplane15" connected
face split "face.74" face "splitplane16" connected

face create "splitplane17" width $cyl_h height $cyl_r yzplane rectangle
\
  offset 0 ($cyl_h/2) (-$cyl_r/2)
volume split "volume.20" face "splitplane17" connected keeptool
face split "face.93" face "splitplane17" connected keeptool
face split "face.105" face "splitplane17" connected keeptool
face split "face.99" face "splitplane17" connected keeptool
face split "face.15" face "splitplane17" connected keeptool
face split "face.121" face "splitplane17" connected keeptool

face create "splitplane18" width $cyl_h height $cyl_r yzplane rectangle
\
  offset 0 (-$cyl_h/2) ($cyl_r/2)
face split "face.5" face "splitplane18" connected


volume modify "Annulus1" label "Annulus1Bot"
volume modify "volume.20" label "Annulus1"
```

```
volume modify "volume.21" label "Ann1Sec"
volume modify "volume.26" label "Ann1Ring"

volume modify "Annulus2" label "Annulus2Bot"
volume modify "volume.22" label "Annulus2"
volume modify "volume.23" label "Ann2Sec1"
volume modify "volume.24" label "Annulus2Top"
volume modify "volume.25" label "Ann2Ring2"
volume modify "volume.27" label "Ann2Sec2"
volume modify "volume.28" label "Ann2Ring1"

volume modify "volume.29" label "Annulus3Top"
volume modify "volume.30" label "Ann3Sec"

face create "splitplane19" width $cyl_r height $cyl_h xyplane rectangle
\
  offset (-$cyl_r/2) ($cyl_h/2) 0
face move "splitplane19" dangle -20 vector 0 1 0 origin 0 0 0
volume split "Annulus1" face "splitplane19" connected
volume modify "volume.31" label "Annulus1_2"

face split "face.92" face "splitplane17" connected keeptool
face split "face.21" face "splitplane17" connected keeptool
face split "face.98" face "splitplane17" connected

face create "splitplane20" width $cyl_r height $cyl_h xyplane rectangle
\
  offset ($cyl_r/2) ($cyl_h/2) 0
face create "splitplane21" width $cyl_r height $cyl_h xyplane rectangle
\
  offset (-$cyl_r/2) ($cyl_h/2) 0

face move "splitplane20" dangle -35 vector 0 1 0 origin 0 0 0
face move "splitplane21" dangle -35 vector 0 1 0 origin 0 0 0

face split "face.31" face "splitplane21" connected
face split "face.32" face "splitplane20" connected

face create "splitplane22" width $cyl_r height $cyl_h xyplane rectangle
\
  offset ($cyl_r/2) ($cyl_h/2) 0
face create "splitplane23" width $cyl_r height $cyl_h xyplane rectangle
\
  offset (-$cyl_r/2) ($cyl_h/2) 0

face move "splitplane22" dangle 35 vector 0 1 0 origin 0 0 0
face move "splitplane23" dangle 35 vector 0 1 0 origin 0 0 0

face split "face.31" face "splitplane23" connected
face split "face.32" face "splitplane22" connected

face create "splitplane24" width $cyl_h height $cyl_r yzplane rectangle
\
  offset 0 ($cyl_h/2) ($cyl_r/2)
face split "face.24" face "splitplane24" connected
```

```
volume create "SplitCyl5" height (4*$cyl_h) radius1 ($cyl3_rin*0.75)
radius2 \
 ($cyl3_rin*0.75) radius3 ($cyl3_rin*0.75) offset 0 0 0 yaxis frustum
volume split "Annulus3" volumes "SplitCyl5" connected keeptool
volume split "Ann3Sec" volumes "SplitCyl5" connected
volume modify "volume.33" label "Out"

ENDIF

/ Meshing outer cylinder
IF COND ($step .gt. 2)

/Inlet
edge mesh "edge.65" "edge.72" "edge.73" "edge.64" bellshape ratio1 \
      0.75 intervals 12
edge mesh "edge.57" "edge.71" successive ratio1 1 intervals 28
edge mesh "edge.70" "edge.63" successive ratio1 1.1 intervals 20
edge mesh "edge.66" "edge.74" successive ratio1 0.90909091 intervals 20
edge mesh "edge.5" "edge.8" successive ratio1 1 intervals 32
blayer create "BL1" first 0.03 growth 1.2 rows 3 transition 1 \
  trows 0
blayer attach "BL1" face "face.7" edge "edge.5" add
face mesh "face.7" pave
face mesh "face.10" map intervals 10
blayer create "BL4" first 0.04 growth 1.2 rows 4 transition 1 \
  trows 0
blayer attach "BL4" face "face.52" edge "edge.8" add
face mesh "face.52" pave
volume mesh "Inlet" cooper source "face.52" "face.7" "face.12"

/Ann1Sec
edge mesh "edge.168" "edge.143" "edge.169" "edge.134" successive \
      ratio1 1 intervals 14
edge mesh "edge.164" "edge.175" successive ratio1 1 intervals 12
edge mesh "edge.173" "edge.174" "edge.165" "edge.166" bellshape \
      ratio1 0.75 intervals 12
edge mesh "edge.80" successive ratio1 1 intervals 48
edge mesh "edge.233" bellshape ratio1 0.75 intervals 12
face mesh "face.89" pave
volume mesh "Ann1Sec" cooper source "face.89" "face.109"
edge mesh "edge.228" successive ratio1 1 intervals 4
face mesh "face.19" map

/Ann2Sec1
edge mesh "edge.200" "edge.201" successive ratio1 1 intervals 28
edge mesh "edge.194" "edge.209" successive ratio1 1 intervals 12
edge mesh "edge.205" "edge.206" "edge.197" "edge.198" bellshape \
      ratio1 0.75 intervals 12
edge mesh "edge.234" bellshape ratio1 0.75 intervals 12
face mesh "face.96" pave
volume mesh "Ann2Sec1" cooper source "face.96" "face.118"


/LowHole
blayer create "BL2" first 0.05 growth 1.2 rows 4 transition 1 \
  trows 0
```

```
blayer attach "BL2" face "face.63" edge "edge.80" add
volume mesh "LowHole" cooper source "face.63" "face.65"

/Ann2Sec2
edge mesh "edge.178" "edge.179" successive ratio1 1 intervals 28
edge mesh "edge.185" "edge.188" successive ratio1 1 intervals 12
edge mesh "edge.183" "edge.184" "edge.189" "edge.190" bellshape \
      ratio1 0.75 intervals 12
edge mesh "edge.240" bellshape ratio1 0.75 intervals 12
edge mesh "edge.86" successive ratio1 1 intervals 40
face mesh "face.101" pave
volume mesh "Ann2Sec2" cooper source "face.101" "face.114"
edge mesh "edge.239" successive ratio1 1 intervals 4
face mesh "face.28" map size 0.1

/HighHole
blayer create "BL3" first 0.05 growth 1.2 rows 4 transition 1 \
  trows 0
blayer attach "BL3" face "face.73" edge "edge.86" add
edge mesh "edge.350" successive ratio1 1 intervals 14
edge mesh "edge.241" successive ratio1 0.833333 intervals 6
edge mesh "edge.351" successive ratio1 1.2 intervals 6
volume mesh "HighHole" cooper source "face.73" "face.75"


IF COND ($otherParameter .lt. 2)

/Annulus1Top
edge mesh "edge.2" successive ratio1 1 intervals 118
edge mesh "edge.69" successive ratio1 1 intervals 84
face mesh "face.2" map
volume mesh "Annulus1Top" map

/Annulus1
edge mesh "edge.292" "edge.294" successive ratio1 1 intervals 36
face mesh "face.51" "face.129" map
volume mesh "Annulus1" map
volume mesh "Annulus1_2" map

/Ann1Ring
face mesh "face.111" map
volume mesh "Ann1Ring" map

/Annulus1Bot
edge mesh "edge.257" successive ratio1 1.1 intervals 20
edge mesh "edge.300" successive ratio1 0.90909091 intervals 20
face mesh "face.92" "face.93" map
volume mesh "Annulus1Bot" cooper source "face.29" "face.91" "face.110"

ENDIF
ENDIF

/ Meshing outer cylinder
IF COND ($step .gt. 3)

IF COND ($otherParameter .lt. 3)
```

```
/Annulus2
edge mesh "edge.187" successive ratio1 1 intervals 22
edge mesh "edge.155" successive ratio1 1 intervals 94
face mesh "face.112" map
edge mesh "edge.263" successive ratio1 1 intervals 36
face mesh "face.105" map
volume mesh "Annulus2" cooper source "face.94" "face.107" "face.113"
"face.117"

/Ann2Ring2
volume mesh "Ann2Ring2" cooper source "face.113" "face.102"

/Annulus2Top
edge mesh "edge.274" successive ratio1 0.90909091 intervals 6
edge mesh "edge.306" successive ratio1 1.1 intervals 6
edge mesh "edge.322" "edge.336" bellshape ratio1 0.75 intervals 12
volume mesh "Annulus2Top" cooper source "face.115" "face.102" "face.32"
"face.133"

/Ann2Ring1
volume mesh "Ann2Ring1" cooper source "face.117" "face.97"

/Annulus2Bot
edge mesh "edge.268" successive ratio1 1.1 intervals 20
edge mesh "edge.308" successive ratio1 0.90909091 intervals 20
edge mesh "edge.319" "edge.333" bellshape ratio1 0.75 intervals 12
volume mesh "Annulus2Bot" cooper source "face.119" "face.97" "face.31"
"face.132"

ENDIF
ENDIF

IF COND ($step .gt. 4)

/Ann3Sec
edge mesh "edge.211" successive ratio1 1 intervals 60
edge mesh "edge.210" "edge.342" successive ratio1 1 intervals 30
blayer create "BL5" first 0.045 growth 1.2 rows 5 transition 1 \
  trows 0
blayer attach "BL5" face "splitplane7" edge "edge.211" add
blayer create "BL6" first 0.045 growth 1.2 rows 5 transition 1 \
  trows 0
blayer attach "BL6" face "splitplane6" "splitplane6" edge "edge.210" \
  "edge.342" add
face mesh "splitplane7" map
face mesh "face.120" triangle
volume mesh "Ann3Sec" cooper source "face.120" "face.143"


/Annulus3
edge mesh "edge.281" "edge.35" successive ratio1 1 intervals 30
blayer create "BL7" first 0.05 growth 1.1 rows 10 transition 1 \
  trows 0
blayer attach "BL7" face "face.121" "face.121" edge "edge.35" \
  "edge.281" add
edge mesh "edge.280" successive ratio1 1 intervals 60
```

```
face mesh "face.121" map
blayer create "BL8" first 0.045 growth 1.2 rows 5 transition 1 \
  trows 0
blayer attach "BL8" face "face.1" "face.1" edge "edge.281" \
  "edge.35" add
face mesh "face.1" map
blayer attach "BL7" face "face.140" edge "edge.348" add
volume mesh "Annulus3" cooper source "face.1" "splitplane7"

/Annulus3Top
face mesh "face.146" pave
edge mesh "edge.343" successive ratio1 1.1 intervals 6
volume mesh "Annulus3Top" cooper source "splitplane6" "face.146"
"face.3"

/Out
edge mesh "edge.286" successive ratio1 1.1 intervals 20
edge mesh "edge.7" successive ratio1 1 intervals 24
face mesh "face.141" pave
volume mesh "Out" cooper source "face.141" "face.142" "face.4"


/SplitCyl5
volume mesh "SplitCyl5" tetrahedral


ENDIF


/ Meshing
IF COND ($step .gt. 5)
physics create "tank" ctype "FLUID" volume "LowHole" "HighHole"
"Annulus1Top" "Inlet" \
  "Annulus1Bot" "Annulus2Bot" "Out" "Annulus1" "Ann1Sec" "Annulus2" \
  "Ann2Sec1" "Annulus2Top" "Ann2Ring2" "Ann1Ring" "Ann2Sec2"
"Ann2Ring1" \
  "Annulus3Top" "SplitCyl5" "Annulus1_2" "Annulus3" "Ann3Sec"
physics create "inlet" btype "MASS_FLOW_INLET" face "face.7"
physics create "outlet" btype "OUTFLOW" face "face.4"
ENDIF
```

```
*************************** GEOMETRY #4 ***************************

/ Journal File for GAMBIT 2.2.30, Database 2.2.14, ntx86 BH04110220
/ Identifier "FluidCol-G4"
/ File opened for write Thu Nov 20 09:58:43 2008.
identifier name "FluidCol-G4-med" new nosaveprevious

/ Variables

$cyl_r = 5.625
$cyl_h = 19.625
$cyl2_r = 2
$out_r = 0.3595
$out_h = 8.0
$out_y = 18.125
$out_z = -5.0
$out_x = -($cyl_r + 2.0)

$in_r = 0.3595
$in_h = 2.0
$in_y = 18.125
$in_x = -($cyl_r - 0.5)

$baffle_t = 0.375
$short_baffle_h = 15.5

$hole_r = 0.75
$hole_h = 5.0
$hole_y = 18.0
$hole_x = $cyl_r - 2.0
$hole_z = $cyl_r - 2.0

$gridsize = 0.3
$gridcount = 80
$BL_size = 0.1

$step = 10
$otherParameter = 1
/Geometry
IF COND ($step .gt. 0)
volume create "Cylinder" height $cyl_h radius1 $cyl_r radius2 $cyl_r
radius3 \
  $cyl_r offset 0 (0.5*$cyl_h) 0 yaxis frustum
volume create "Outlet" height $out_h radius1 $out_r radius2 $out_r
radius3 $out_r \
  offset ($out_h/2 + $out_x) $out_y $out_z xaxis frustum
volume create "Inlet" height $in_h radius1 $in_r radius2 $in_r radius3
$in_r \
  offset (-$in_h/2 + $in_x) $in_y 0 xaxis frustum
volume unite volumes "Cylinder" "Outlet" "Inlet"

volume create "Cylinder2" height $cyl_h radius1 $cyl2_r radius2 $cyl2_r
radius3 \
  $cyl2_r offset 0 (0.5*$cyl_h) 0 yaxis frustum
volume create "Baffle1"  width (2*$cyl_r) depth $cyl_h height $baffle_t
\
```

```
  offset 0 ($cyl_h/2) 0 brick
volume create "Baffle2"  width $baffle_t depth $cyl_h height (2*$cyl_r)
\
  offset 0 ($cyl_h/2) 0 brick
volume create "Baffle-s1"  width (2*$cyl_r) depth $short_baffle_h
height \
  $baffle_t offset 0 ($cyl_h - $short_baffle_h/2) 0 brick
volume create "Baffle-s2"  width $baffle_t depth $short_baffle_h height
\
  (2*$cyl_r) offset 0 ($cyl_h - $short_baffle_h/2) 0 brick

volume create "Hole1" height $hole_h radius1 $hole_r radius2 $hole_r
radius3 \
  $hole_r offset $hole_x $hole_y 0 zaxis frustum
volume create "Hole2" height $hole_h radius1 $hole_r radius2 $hole_r
radius3 \
  $hole_r offset 0 $hole_y $hole_z xaxis frustum
volume create "Hole3" height $hole_h radius1 $hole_r radius2 $hole_r
radius3 \
  $hole_r offset 0 $hole_y (-$hole_z) xaxis frustum

volume subtract "Baffle1" volume "Hole1"
volume subtract "Baffle2" volume "Hole2"
volume subtract "Baffle2" volume "Hole3"

volume move "Baffle-s1" dangle 22.5 vector 0 1 0 origin 0 0 0
volume move "Baffle-s2" dangle 22.5 vector 0 1 0 origin 0 0 0

volume unite volumes "Cylinder2" "Baffle1" "Baffle2" "Baffle-s1"
"Baffle-s2"
volume move "Cylinder2" dangle -11.25 vector 0 1 0 origin 0 0 0
volume subtract "Cylinder" volume "Cylinder2"

ENDIF

/Splitting
IF COND ($step .gt. 1)
face create "splitplane1" width (2*$cyl_r) height (2*$cyl_r) zxplane
rectangle \
  offset 0 ($cyl_h - $short_baffle_h) 0

face create "splitplane2" width (2*$cyl_r) height ($cyl_h) xyplane
rectangle \
  offset 0 ($cyl_h/2) ($baffle_t/2)
face create "splitplane3" width (2*$cyl_r) height ($cyl_h) xyplane
rectangle \
  offset 0 ($cyl_h/2) (-$baffle_t/2)
face create "splitplane4" width ($cyl_h) height (2*$cyl_r) yzplane
rectangle \
  offset ($baffle_t/2) ($cyl_h/2) 0
face create "splitplane5" width ($cyl_h) height (2*$cyl_r) yzplane
rectangle \
  offset (-$baffle_t/2) ($cyl_h/2) 0

face create "splitplane6" width (2*$cyl_r) height (2*$cyl_r) zxplane
rectangle \
```

```
  offset 0 ($in_y - 0.75) 0
face create "splitplane7" width (2*$cyl_r) height (2*$cyl_r) zxplane
rectangle \
  offset 0 ($in_y + 0.75) 0
face create "splitplane8" width (4*$cyl_r) height (4*$cyl_r) zxplane
rectangle \
  offset 0 $in_y 0

face move "splitplane2" dangle -11.25 vector 0 1 0 origin 0 0 0
face move "splitplane3" dangle -11.25 vector 0 1 0 origin 0 0 0
face move "splitplane4" dangle -11.25 vector 0 1 0 origin 0 0 0
face move "splitplane5" dangle -11.25 vector 0 1 0 origin 0 0 0

volume split "Cylinder" connected face "splitplane1"
volume split "volume.3" connected face "splitplane4" keeptool
volume split "volume.3" connected face "splitplane5" keeptool
volume split "volume.5" connected face "splitplane2"
volume split "volume.5" connected face "splitplane3"
volume split "volume.7" connected face "splitplane4"
volume split "volume.7" connected face "splitplane5"

volume split "Cylinder" connected face "splitplane7" keeptool
volume split "volume.9" connected face "splitplane7"
volume split "Cylinder" connected face "splitplane6" keeptool
volume split "volume.9" connected face "splitplane6"

face split "face.10" connected face "splitplane8" keeptool
face split "face.11" connected face "splitplane8" keeptool
face split "face.48" connected face "splitplane8" keeptool
face split "face.49" connected face "splitplane8" keeptool
face split "face.50" connected face "splitplane8"


volume modify "Cylinder" label "Sec1a"
volume modify "volume.2" label "Sec1b"
volume modify "volume.3" label "Sec1c"
volume modify "volume.10" label "Sec2a"
volume modify "volume.4" label "Sec2b"
volume modify "volume.12" label "Sec2c"
volume modify "volume.5" label "Sec3a"
volume modify "volume.6" label "Sec3b"
volume modify "volume.14" label "Sec3c"
volume modify "volume.7" label "Sec4a"
volume modify "volume.8" label "Sec4b"
volume modify "volume.9" label "Sec4c"

volume modify "volume.11" label "Hole1"
volume modify "volume.13" label "Hole2"
volume modify "volume.15" label "Hole3"

volume modify "volume.16" label "Sec1aTop"
volume modify "volume.17" label "Sec4cTop"
volume modify "volume.18" label "Inlet"
volume modify "volume.19" label "Outlet"
```

```
face create "splitplane9" width (2*$cyl_r) height (2*$cyl_r) zxplane
rectangle \
  offset 0 ($hole_y + 1.0) 0
face create "splitplane10" width (2*$cyl_r) height (2*$cyl_r) zxplane
rectangle \
  offset 0 ($hole_y - 1.0) 0

volume split "Sec1c" connected face "splitplane9" keeptool
volume split "Sec2a" connected face "splitplane9" keeptool
volume split "Sec2c" connected face "splitplane9" keeptool
volume split "Sec3a" connected face "splitplane9" keeptool
volume split "Sec3c" connected face "splitplane9" keeptool
volume split "Sec4a" connected face "splitplane9"
volume split "Sec1c" connected face "splitplane10" keeptool
volume split "Sec2a" connected face "splitplane10" keeptool
volume split "Sec2c" connected face "splitplane10" keeptool
volume split "Sec3a" connected face "splitplane10" keeptool
volume split "Sec3c" connected face "splitplane10" keeptool
volume split "Sec4a" connected face "splitplane10"

volume modify "volume.20" label "Sec1cTop"
volume modify "volume.21" label "Sec2aTop"
volume modify "volume.22" label "Sec2cTop"
volume modify "volume.23" label "Sec3aTop"
volume modify "volume.24" label "Sec3cTop"
volume modify "volume.25" label "Sec4aTop"
volume modify "volume.26" label "Sec1cMid"
volume modify "volume.27" label "Sec2aMid"
volume modify "volume.28" label "Sec2cMid"
volume modify "volume.29" label "Sec3aMid"
volume modify "volume.30" label "Sec3cMid"
volume modify "volume.31" label "Sec4aMid"

ENDIF

/ Meshing
IF COND ($step .gt. 2)

/******************* Inlet Section
*********************************************

/Inlet
edge mesh "edge.327" successive ratio1 1 intervals 16
edge mesh "edge.5" "edge.329" successive ratio1 1 intervals 8
edge mesh "edge.330" successive ratio1 1 intervals 10

blayer create "BL1" first 0.02 growth 1.2 rows 4 transition 1 \
  trows 0
blayer attach "BL1" face "face.7" "face.7" "face.7" edge \
  "edge.327" "edge.5" "edge.329" add
face mesh "face.7" pave
face mesh "face.11" "face.170" map

edge mesh "edge.275" "edge.304" successive ratio1 1 intervals 12
edge mesh "edge.281" "edge.302" successive ratio1 .8333333 intervals 8
edge mesh "edge.277" "edge.298" successive ratio1 1.2 intervals 8
```

```
face mesh "face.151" pave

edge mesh "edge.282" "edge.276" "edge.297" "edge.303" bellshape ratio1
\
  0.55 intervals 32
edge mesh "edge.279" "edge.300" bellshape ratio1 0.6 intervals 16

volume mesh "Inlet" cooper source "face.7" "face.151" "face.161"

/Sec1aTop
edge mesh "edge.154" "edge.155" bellshape ratio1 0.6 intervals 16
edge mesh "edge.283" "edge.280" successive ratio1 .8333333 intervals 8
edge mesh "edge.149" "edge.78" successive ratio1 1.2 intervals 8
edge mesh "edge.152" "edge.159" bellshape ratio1 0.55 intervals 32

volume mesh "Sec1aTop" map

/Sec1a
edge mesh "edge.296" "edge.162" "edge.299" "edge.101" bellshape ratio1
\
  0.6 intervals 48
edge mesh "edge.251" successive ratio1 .8333333 intervals 8
edge mesh "edge.245" successive ratio1 1.2 intervals 8
edge mesh "edge.104" "edge.244" bellshape ratio1 0.55 intervals 32
edge mesh "edge.248" bellshape ratio1 0.6 intervals 16

volume mesh "Sec1a" map


/******************************* Outlet Section
**********************************

/Outlet
edge mesh "edge.319" successive ratio1 1 intervals 16
edge mesh "edge.3" "edge.320" successive ratio1 1 intervals 8
edge mesh "edge.317" "edge.321" successive ratio1 1 intervals 16

face mesh "face.4" pave
face mesh "face.10" "face.168" map

edge mesh "edge.284" "edge.310" "edge.287" "edge.312" successive ratio1
\
  1 intervals 12
edge mesh "edge.306" "edge.285" "edge.288" "edge.309" bellshape ratio1
\
  0.55 intervals 40
face mesh "face.154" pave

edge mesh "edge.307" "edge.311" "edge.286" "edge.290" bellshape ratio1
\
  0.55 intervals 32

volume mesh "Outlet" cooper source "face.4" "face.154" "face.165"

/Sec4cTop
edge mesh "edge.127" "edge.138" bellshape ratio1 0.55 intervals 40
```

```
edge mesh "edge.289" "edge.291" successive ratio1 .8333333 intervals 8
edge mesh "edge.125" "edge.113" successive ratio1 1.2 intervals 8
edge mesh "edge.133" "edge.147" bellshape ratio1 0.55 intervals 32

volume mesh "Sec4cTop" map

/Sec4c
edge mesh "edge.240" "edge.243" "edge.305" "edge.308" bellshape ratio1
\
  0.6 intervals 48
edge mesh "edge.109" "edge.241" bellshape ratio1 0.55 intervals 32
edge mesh "edge.231" "edge.238" bellshape ratio1 0.6 intervals 40

volume mesh "Sec4c" map

ENDIF

/************************** Holes
*************************************
IF COND ($step .gt. 3)

/Hole1
edge mesh "edge.347" successive ratio1 1 intervals 12
edge mesh "edge.67" "edge.349" successive ratio1 1 intervals 6
edge mesh "edge.350" successive ratio1 1 intervals 6
blayer create "BL2" first 0.03 growth 1.3 rows 3 transition 1 \
  trows 0
blayer attach "BL2" face "face.144" "face.144" "face.144" edge \
  "edge.347" "edge.67" "edge.349" add

volume mesh "Hole1" cooper source "face.142" "face.144"

/Hole2
edge mesh "edge.339" successive ratio1 1 intervals 11
edge mesh "edge.340" successive ratio1 1 intervals 12
edge mesh "edge.338" successive ratio1 1 intervals 6
blayer create "BL3" first 0.03 growth 1.3 rows 3 transition 1 \
  trows 0
blayer attach "BL3" face "face.145" "face.145" "face.145" edge \
  "edge.339" "edge.340" "edge.66" add

volume mesh "Hole2" cooper source "face.145" "face.146"

/Hole3
edge mesh "edge.354" successive ratio1 1 intervals 12
edge mesh "edge.70" "edge.352" successive ratio1 1 intervals 6
edge mesh "edge.351" successive ratio1 1 intervals 6
blayer create "BL3" first 0.03 growth 1.3 rows 3 transition 1 \
  trows 0
blayer attach "BL3" face "face.147" "face.147" "face.147" edge \
  "edge.70" "edge.352" "edge.354" add

volume mesh "Hole3" cooper source "face.147" "face.148"

ENDIF
```

```
/************************** Midsections
********************************

IF COND ($step .gt. 4)

/Sec1cMid
edge mesh "edge.445" "edge.374" "edge.441" "edge.370" bellshape ratio1
0.55 \
  intervals 32
edge mesh "edge.446" "edge.443" "edge.372" "edge.375" bellshape ratio1
0.55 \
  intervals 40
edge mesh "edge.444" "edge.447" "edge.369" "edge.371" successive ratio1
1 \
  intervals 16
blayer create "BL4" first 0.03 growth 1.3 rows 3 transition 1 \
  trows 0
blayer attach "BL4" face "face.181" "face.181" "face.181" edge \
  "edge.347" "edge.67" "edge.349" add
face mesh "face.181" pave

volume mesh "Sec1cMid" cooper source "face.181" "face.144" "face.208"

/Sec2aMid
edge mesh "edge.455" "edge.384" "edge.456" "edge.385" bellshape ratio1
0.55 \
  intervals 32
edge mesh "edge.459" "edge.388" successive ratio1 1.2 intervals 8
edge mesh "edge.389" "edge.460" successive ratio1 0.83333333 intervals
8
edge mesh "edge.454" "edge.383" bellshape ratio1 0.6 intervals 16
edge mesh "edge.458" "edge.453" "edge.381" "edge.386" successive ratio1
1 \
  intervals 16
blayer create "BL5" first 0.03 growth 1.3 rows 3 transition 1 \
  trows 0
blayer attach "BL5" face "face.215" "face.215" "face.215" edge \
  "edge.348" "edge.68" "edge.346" add
face mesh "face.215" pave

volume mesh "Sec2aMid" cooper source "face.98" "face.142" "face.215"

/Sec2cMid
edge mesh "edge.466" "edge.395" "edge.470" "edge.399" bellshape ratio1
0.55 \
  intervals 32
edge mesh "edge.471" "edge.468" "edge.400" "edge.397" bellshape ratio1
0.55 \
  intervals 40
edge mesh "edge.465" "edge.467" "edge.398" "edge.401" successive ratio1
1 \
  intervals 16
blayer create "BL6" first 0.03 growth 1.3 rows 3 transition 1 \
  trows 0
blayer attach "BL6" face "face.189" "face.189" "face.189" edge \
  "edge.339" "edge.340" "edge.66" add
```

```
face mesh "face.181" pave

volume mesh "Sec2cMid" cooper source "face.189" "face.145" "face.220"

/Sec3aMid
edge mesh "edge.407" "edge.413" "edge.478" "edge.484" bellshape ratio1
0.55 \
  intervals 32
edge mesh "edge.483" "edge.412" successive ratio1 1.2 intervals 8
edge mesh "edge.408" "edge.479" successive ratio1 0.83333333 intervals
8
edge mesh "edge.410" "edge.481" bellshape ratio1 0.6 intervals 16
edge mesh "edge.414" "edge.411" "edge.477" "edge.480" successive ratio1
1 \
  intervals 16
blayer create "BL7" first 0.03 growth 1.3 rows 3 transition 1 \
  trows 0
blayer attach "BL7" face "face.226" "face.226" "face.226" edge \
  "edge.335" "edge.65" "edge.336" add
face mesh "face.226" pave

volume mesh "Sec3aMid" cooper source "face.86" "face.146" "face.226"

/Sec3cMid
edge mesh "edge.421" "edge.425" "edge.492" "edge.496" bellshape ratio1
0.55 \
  intervals 32
edge mesh "edge.420" "edge.423" "edge.491" "edge.494" bellshape ratio1
0.55 \
  intervals 40
edge mesh "edge.424" "edge.426" "edge.490" "edge.493" successive ratio1
1 \
  intervals 16
blayer create "BL8" first 0.03 growth 1.3 rows 3 transition 1 \
  trows 0
blayer attach "BL8" face "face.200" "face.200" "face.200" edge \
  "edge.70" "edge.352" "edge.354" add
face mesh "face.200" pave

volume mesh "Sec3cMid" cooper source "face.200" "face.147" "face.231"

/Sec4aMid
edge mesh "edge.502" "edge.503" "edge.431" "edge.432" bellshape ratio1
0.55 \
  intervals 32
edge mesh "edge.428" "edge.499" successive ratio1 1.2 intervals 8
edge mesh "edge.498" "edge.427" successive ratio1 0.83333333 intervals
8
edge mesh "edge.504" "edge.433" bellshape ratio1 0.6 intervals 16
edge mesh "edge.429" "edge.501" "edge.506" "edge.434" successive ratio1
1 \
  intervals 16
blayer create "BL9" first 0.03 growth 1.3 rows 3 transition 1 \
  trows 0
blayer attach "BL9" face "face.233" "face.233" "face.233" edge \
  "edge.69" "edge.353" "edge.355" add
```

```
face mesh "face.233" pave

volume mesh "Sec4aMid" cooper source "face.233" "face.148" "face.77"

ENDIF


/************************** Topsections
*********************************
IF COND ($step .gt. 5)

/Sec1cTop
edge mesh "edge.185" "edge.172" bellshape ratio1 0.55 intervals 40
edge mesh "edge.376" "edge.373" successive ratio1 0.8333333 intervals 8
edge mesh "edge.171" "edge.103" successive ratio1 1.2 intervals 8
edge mesh "edge.165" "edge.179" bellshape ratio1 0.55 intervals 32

volume mesh "Sec1cTop" map

/Sec2aTop
edge mesh "edge.194" "edge.175" bellshape ratio1 0.6 intervals 16
edge mesh "edge.387" "edge.382" successive ratio1 0.8333333 intervals 8
edge mesh "edge.94" "edge.192" successive ratio1 1.2 intervals 8
edge mesh "edge.184" "edge.183" bellshape ratio1 0.55 intervals 32

volume mesh "Sec2aTop" map

/Sec2cTop
edge mesh "edge.186" "edge.173" bellshape ratio1 0.55 intervals 40
edge mesh "edge.394" "edge.396" successive ratio1 0.8333333 intervals 8
edge mesh "edge.116" "edge.189" successive ratio1 1.2 intervals 8
edge mesh "edge.166" "edge.180" bellshape ratio1 0.55 intervals 32

volume mesh "Sec2cTop" map

/Sec3aTop
edge mesh "edge.156" "edge.157" bellshape ratio1 0.6 intervals 16
edge mesh "edge.406" "edge.409" successive ratio1 0.8333333 intervals 8
edge mesh "edge.75" "edge.161" successive ratio1 1.2 intervals 8
edge mesh "edge.160" "edge.153" bellshape ratio1 0.55 intervals 32

volume mesh "Sec3aTop" map

/Sec3cTop
edge mesh "edge.128" "edge.139" bellshape ratio1 0.55 intervals 40
edge mesh "edge.419" "edge.422" successive ratio1 0.8333333 intervals 8
edge mesh "edge.98" "edge.141" successive ratio1 1.2 intervals 8
edge mesh "edge.148" "edge.134" bellshape ratio1 0.55 intervals 32

volume mesh "Sec3cTop" map

/Sec4aTop
edge mesh "edge.136" "edge.119" bellshape ratio1 0.6 intervals 16
edge mesh "edge.430" "edge.435" successive ratio1 0.8333333 intervals 8
edge mesh "edge.120" "edge.87" successive ratio1 1.2 intervals 8
edge mesh "edge.130" "edge.131" bellshape ratio1 0.55 intervals 32
```

```
volume mesh "Sec4aTop" map

ENDIF


/*************************** Sections a and c
*****************************
IF COND ($step .gt. 6)

/Sec1c
edge mesh "edge.442" "edge.440" "edge.260" "edge.267" bellshape ratio1
\
  0.6 intervals 48
edge mesh "edge.164" "edge.263" bellshape ratio1 0.55 intervals 32
edge mesh "edge.258" "edge.265" bellshape ratio1 0.6 intervals 40

volume mesh "Sec1c" map

/Sec2a
edge mesh "edge.457" "edge.452" "edge.118" "edge.193" bellshape ratio1
\
  0.6 intervals 48
edge mesh "edge.270" successive ratio1 .8333333 intervals 8
edge mesh "edge.269" successive ratio1 1.2 intervals 8
edge mesh "edge.264" "edge.182" bellshape ratio1 0.55 intervals 32
edge mesh "edge.262" bellshape ratio1 0.6 intervals 16

volume mesh "Sec2a" map

/Sec2c
edge mesh "edge.254" "edge.257" "edge.469" "edge.472" bellshape ratio1
\
  0.6 intervals 48
edge mesh "edge.178" "edge.256" bellshape ratio1 0.55 intervals 32
edge mesh "edge.259" "edge.266" bellshape ratio1 0.6 intervals 40

volume mesh "Sec2c" map

/Sec3a
edge mesh "edge.482" "edge.485" "edge.100" "edge.150" bellshape ratio1
\
  0.6 intervals 48
edge mesh "edge.246" successive ratio1 .8333333 intervals 8
edge mesh "edge.252" successive ratio1 1.2 intervals 8
edge mesh "edge.253" "edge.97" bellshape ratio1 0.55 intervals 32
edge mesh "edge.249" bellshape ratio1 0.6 intervals 16

volume mesh "Sec3a" map

/Sec3c
edge mesh "edge.230" "edge.237" "edge.495" "edge.497" bellshape ratio1
\
  0.6 intervals 48
edge mesh "edge.146" "edge.234" bellshape ratio1 0.55 intervals 32
edge mesh "edge.232" "edge.239" bellshape ratio1 0.6 intervals 40
```

```
volume mesh "Sec3c" map

/Sec4a
edge mesh "edge.111" "edge.121" "edge.500" "edge.505" bellshape ratio1
\
  0.6 intervals 48
edge mesh "edge.227" successive ratio1 .8333333 intervals 8
edge mesh "edge.228" successive ratio1 1.2 intervals 8
edge mesh "edge.107" "edge.233" bellshape ratio1 0.55 intervals 32
edge mesh "edge.235" bellshape ratio1 0.6 intervals 16

volume mesh "Sec4a" map

ENDIF

/************************** Section b's ****************************
IF COND ($step .gt. 7)
/Sec1b
edge mesh "edge.151" "edge.177" bellshape ratio1 0.55 intervals 32
edge mesh "edge.168" "edge.176" bellshape ratio1 0.6 intervals 60
edge mesh "edge.102" successive ratio1 1 intervals 4
edge mesh "edge.167" "edge.169" successive ratio1 1 intervals 2
edge mesh "edge.93" "edge.188" "edge.242" "edge.247" bellshape ratio1 \
  0.6 intervals 20

volume mesh "Sec1b" map

/Sec2b
edge mesh "edge.163" "edge.181" bellshape ratio1 0.55 intervals 32
edge mesh "edge.174" "edge.187" bellshape ratio1 0.6 intervals 60
edge mesh "edge.117" successive ratio1 1 intervals 4
edge mesh "edge.190" "edge.191" successive ratio1 1 intervals 2
edge mesh "edge.79" "edge.170" "edge.261" "edge.268" bellshape ratio1 \
  0.6 intervals 20

volume mesh "Sec2b" map

/Sec3b
edge mesh "edge.158" "edge.132" bellshape ratio1 0.55 intervals 32
edge mesh "edge.135" "edge.143" bellshape ratio1 0.6 intervals 60
edge mesh "edge.99" successive ratio1 1 intervals 4
edge mesh "edge.142" "edge.144" successive ratio1 1 intervals 2
edge mesh "edge.88" "edge.124" "edge.250" "edge.255" bellshape ratio1 \
  0.6 intervals 20

volume mesh "Sec3b" map

/Sec4b
edge mesh "edge.129" "edge.145" bellshape ratio1 0.55 intervals 32
edge mesh "edge.126" "edge.137" bellshape ratio1 0.6 intervals 60
edge mesh "edge.112" successive ratio1 1 intervals 4
edge mesh "edge.122" "edge.123" successive ratio1 1 intervals 2
edge mesh "edge.74" "edge.140" "edge.229" "edge.236" bellshape ratio1 \
  0.6 intervals 20
```

```
volume mesh "Sec4b" map

ENDIF

/ physics
IF COND ($step .gt. 10)
physics create "inlet" btype "MASS_FLOW_INLET" face "face.7"
physics create "outlet" btype "OUTFLOW" face "face.4"
physics create "tank" ctype "FLUID" volume "Sec1a" "Sec1b" "Sec1c"
"Sec2b" \
  "Sec3a" "Sec3b" "Sec4a" "Sec4b" "Sec4c" "Sec2a" "Hole1" "Sec2c"
"Hole2" \
  "Sec3c" "Hole3" "Sec1aTop" "Sec4cTop" "Inlet" "Outlet" "Sec1cTop" \
  "Sec2aTop" "Sec2cTop" "Sec3aTop" "Sec3cTop" "Sec4aTop" "Sec1cMid" \
  "Sec2aMid" "Sec2cMid" "Sec3aMid" "Sec3cMid" "Sec4aMid"ENDIF
```

Appendix C. CFD model parameters and mesh characteristics

CFD Mesh Characteristics

Geometry G1
Mesh size medium

```
Grid Size

Level    Cells    Faces    Nodes   Partitions
    0   589390  1606294   454566            1

 1 cell zone, 5 face zones.

Memory Usage
                      cells    faces    nodes    objps    edges
                      -----    -----    -----    -----    -----
Number Used:         589390  1606294   454566        7        0
Mbytes Used:            189      151       24        0        0
Number Allocated:    589390  1606294   454566     1024        0
Mbytes Allocated:       189      151       24        0        0

Array Memory Used:              0 Mbytes
Array Memory Allocated:         0 Mbytes

Zone sizes on domain 1:
  589390 mixed cells, zone  2.
   20573 quadrilateral wall faces, zone  3.
    3204 quadrilateral wall faces, zone  4.
      89 quadrilateral outflow faces, zone  5.
     120 quadrilateral mass-flow-inlet faces, zone  6.
 1582308 mixed interior faces, zone  8.
  454566 nodes.

>> 1 Partitions:
       P   Cells I-Cells Cell Ratio   Faces I-Faces Face Ratio Neighbors
       0  589390       0      0.000 1606294       0      0.000         0

   ------------------------------------------------------------------------
   Collective Partition Statistics:        Minimum   Maximum   Total
   ------------------------------------------------------------------------
   Cell count                              589390    589390    589390
   Mean cell count deviation               0.0%      0.0%
   Partition boundary cell count           0         0         0
   Partition boundary cell count ratio     0.0%      0.0%      0.0%

   Face count                              1606294   1606294   1606294
   Mean face count deviation               0.0%      0.0%
   Partition boundary face count           0         0         0
   Partition boundary face count ratio     0.0%      0.0%      0.0%

   Partition neighbor count                0         0
   ------------------------------------------------------------------------
   Partition Method                        Principal Axes
   Stored Partition Count                  1

   Connected region count      = 1
```

Geometry G1
Mesh size fine

```
Grid Size

Level    Cells    Faces    Nodes   Partitions
    0  1015436  2765603   781530            1

 1 cell zone, 4 face zones.

Memory Usage

                      cells    faces    nodes    objps    edges
                      -----    -----    -----    -----    -----
Number Used:       1015436  2765603   781530        6        0
Mbytes Used:           342      260       42        0        0
Number Allocated:  1015436  2765603   781530     1024        0
Mbytes Allocated:      342      260       42        0        0

Array Memory Used:              0 Mbytes
Array Memory Allocated:         0 Mbytes

Zone sizes on domain 1:
 1015436 mixed cells, zone  2.
   34303 quadrilateral wall faces, zone  3.
     153 quadrilateral outflow faces, zone  4.
     160 quadrilateral mass-flow-inlet faces, zone  5.
 2730987 mixed interior faces, zone  7.
  781530 nodes.

>> 1 Partitions:
       P   Cells I-Cells Cell Ratio   Faces I-Faces Face Ratio Neighbors
       0 1015436       0      0.000 2765603       0      0.000         0

   ------------------------------------------------------------------------
   Collective Partition Statistics:        Minimum   Maximum   Total
   ------------------------------------------------------------------------
   Cell count                              1015436   1015436   1015436
   Mean cell count deviation               0.0%      0.0%
   Partition boundary cell count           0         0         0
   Partition boundary cell count ratio     0.0%      0.0%      0.0%

   Face count                              2765603   2765603   2765603
   Mean face count deviation               0.0%      0.0%
   Partition boundary face count           0         0         0
   Partition boundary face count ratio     0.0%      0.0%      0.0%

   Partition neighbor count                0         0
   ------------------------------------------------------------------------
   Partition Method                        Principal Axes
   Stored Partition Count                  1

Computing connected regions; type ^C to interrupt.
   Connected region count      = 1
Done.
```

Geometry G1
Mesh size coarse

```
Grid Size

Level    Cells    Faces    Nodes   Partitions
    0   306193   849993   249163            1
```

```
 1 cell zone, 4 face zones.

Memory Usage

                     cells    faces    nodes    objps    edges
                     -----    -----    -----    -----    -----
Number Used:        306193   849993   249163        6        0
Mbytes Used:           103       80       13        0        0
Number Allocated:   306193   849993   249163     1024        0
Mbytes Allocated:      103       80       13        0        0

Array Memory Used:              0 Mbytes
Array Memory Allocated:         0 Mbytes

Zone sizes on domain 1:
  306193 mixed cells, zone  2.
   15936 quadrilateral wall faces, zone  3.
      89 quadrilateral outflow faces, zone  4.
      96 quadrilateral mass-flow-inlet faces, zone  5.
  833872 mixed interior faces, zone  7.
  249163 nodes.

>> 1 Partitions:
       P   Cells I-Cells Cell Ratio   Faces I-Faces Face Ratio Neighbors
       0  306193       0      0.000  849993       0      0.000         0

   ------------------------------------------------------------------------
   Collective Partition Statistics:        Minimum   Maximum   Total
   ------------------------------------------------------------------------
   Cell count                              306193    306193    306193
   Mean cell count deviation               0.0%      0.0%
   Partition boundary cell count           0         0         0
   Partition boundary cell count ratio     0.0%      0.0%      0.0%

   Face count                              849993    849993    849993
   Mean face count deviation               0.0%      0.0%
   Partition boundary face count           0         0         0
   Partition boundary face count ratio     0.0%      0.0%      0.0%

   Partition neighbor count                0         0
   ------------------------------------------------------------------------
   Partition Method                        Principal Axes
   Stored Partition Count                  1

Computing connected regions; type ^C to interrupt.
   Connected region count      = 1
Done.
```

Geometry G2
Mesh size medium

```
Grid Size

Level    Cells    Faces    Nodes   Partitions
    0   603067  1677050   493032            1

 1 cell zone, 4 face zones.

Memory Usage

                      cells    faces    nodes    objps    edges
                      -----    -----    -----    -----    -----
Number Used:         603067  1677050   493032        6        0
Mbytes Used:            212      159       26        0        0
Number Allocated:    603067  1677050   493032     1024        0
Mbytes Allocated:       212      159       26        0        0

Array Memory Used:              0 Mbytes
Array Memory Allocated:         0 Mbytes

Zone sizes on domain 1:
  603067 mixed cells, zone  2.
   26584 quadrilateral wall faces, zone  3.
     217 quadrilateral outflow faces, zone  4.
     120 quadrilateral mass-flow-inlet faces, zone  5.
 1650129 mixed interior faces, zone  7.
  493032 nodes.

>> 1 Partitions:
       P   Cells I-Cells Cell Ratio   Faces I-Faces Face Ratio Neighbors
       0  603067       0      0.000 1677050       0      0.000         0

   ------------------------------------------------------------------------
   Collective Partition Statistics:        Minimum   Maximum   Total
   ------------------------------------------------------------------------
   Cell count                              603067    603067    603067
   Mean cell count deviation               0.0%      0.0%
   Partition boundary cell count           0         0         0
   Partition boundary cell count ratio     0.0%      0.0%      0.0%

   Face count                              1677050   1677050   1677050
   Mean face count deviation               0.0%      0.0%
   Partition boundary face count           0         0         0
   Partition boundary face count ratio     0.0%      0.0%      0.0%

   Partition neighbor count                0         0
   ------------------------------------------------------------------------
   Partition Method                        Principal Axes
   Stored Partition Count                  1

Computing connected regions; type ^C to interrupt.
   Connected region count      = 1
Done.
```

Geometry G2
Mesh size fine

```
Grid Size

Level    Cells    Faces    Nodes   Partitions
    0  1393297  3712451  1003701            1

 1 cell zone, 4 face zones.

Memory Usage

                      cells    faces    nodes    objps    edges
                      -----    -----    -----    -----    -----
Number Used:         1393297  3712451  1003701        6        0
Mbytes Used:             469      348       54        0        0
Number Allocated:    1393297  3712451  1003701     1024        0
Mbytes Allocated:        469      348       54        0        0

Array Memory Used:              0 Mbytes
Array Memory Allocated:         0 Mbytes

Zone sizes on domain 1:
 1393297 mixed cells, zone  2.
   42250 quadrilateral wall faces, zone  3.
     292 quadrilateral outflow faces, zone  4.
     219 quadrilateral mass-flow-inlet faces, zone  5.
 3669690 mixed interior faces, zone  7.
 1003701 nodes.

>> 1 Partitions:
       P   Cells I-Cells Cell Ratio   Faces I-Faces Face Ratio Neighbors
       0 1393297       0      0.000 3712451       0      0.000         0

   ------------------------------------------------------------------------
   Collective Partition Statistics:        Minimum   Maximum   Total
   ------------------------------------------------------------------------
   Cell count                              1393297   1393297   1393297
   Mean cell count deviation               0.0%      0.0%
   Partition boundary cell count           0         0         0
   Partition boundary cell count ratio     0.0%      0.0%      0.0%

   Face count                              3712451   3712451   3712451
   Mean face count deviation               0.0%      0.0%
   Partition boundary face count           0         0         0
   Partition boundary face count ratio     0.0%      0.0%      0.0%

   Partition neighbor count                0         0
   ------------------------------------------------------------------------
   Partition Method                        Principal Axes
   Stored Partition Count                  1

Computing connected regions; type ^C to interrupt.
   Connected region count      = 1
Done.
```

Geometry G3
Mesh size medium

```
Grid Size

Level    Cells    Faces    Nodes   Partitions
    0   661284  2032935   711392            1

 1 cell zone, 4 face zones.

Memory Usage

                     cells    faces    nodes    objps    edges
                     -----    -----    -----    -----    -----
Number Used:        661284  2032935   711392        6        0
Mbytes Used:           223      199       38        0        0
Number Allocated:   661284  2032935   711392     1024        0
Mbytes Allocated:      223      199       38        0        0

Array Memory Used:              0 Mbytes
Array Memory Allocated:         0 Mbytes

Zone sizes on domain 1:
  661284 hexahedral cells, zone  2.
   97860 quadrilateral wall faces, zone  3.
      89 quadrilateral outflow faces, zone  4.
     217 quadrilateral mass-flow-inlet faces, zone  5.
 1934769 quadrilateral interior faces, zone  7.
  711392 nodes.

>> 1 Partitions:
       P   Cells I-Cells Cell Ratio   Faces I-Faces Face Ratio Neighbors
       0  661284       0      0.000 2032935       0      0.000         0

   ------------------------------------------------------------------------
   Collective Partition Statistics:        Minimum   Maximum   Total
   ------------------------------------------------------------------------
   Cell count                              661284    661284    661284
   Mean cell count deviation               0.0%      0.0%
   Partition boundary cell count           0         0         0
   Partition boundary cell count ratio     0.0%      0.0%      0.0%

   Face count                              2032935   2032935   2032935
   Mean face count deviation               0.0%      0.0%
   Partition boundary face count           0         0         0
   Partition boundary face count ratio     0.0%      0.0%      0.0%

   Partition neighbor count                0         0
   ------------------------------------------------------------------------
   Partition Method                        Principal Axes
   Stored Partition Count                  1

Computing connected regions; type ^C to interrupt.
   Connected region count      = 1
Done.
```

Geometry G3
Mesh size fine

```
Grid Size

Level    Cells    Faces    Nodes   Partitions
    0  1281915  3859273  1302190            1

 1 cell zone, 4 face zones.

Memory Usage

                     cells    faces    nodes    objps    edges
                     -----    -----    -----    -----    -----
Number Used:       1281915  3859273  1302190        6        0
Mbytes Used:           432      376       70        0        0
Number Allocated:  1281915  3859273  1302190     1024        0
Mbytes Allocated:      432      376       70        0        0

Array Memory Used:              0 Mbytes
Array Memory Allocated:         0 Mbytes

Zone sizes on domain 1:
 1281915 mixed cells, zone  2.
  162390 mixed wall faces, zone  3.
     119 quadrilateral outflow faces, zone  4.
     185 quadrilateral mass-flow-inlet faces, zone  5.
 3696579 mixed interior faces, zone  7.
 1302190 nodes.

>> 1 Partitions:
       P   Cells I-Cells Cell Ratio   Faces I-Faces Face Ratio Neighbors
       0 1281915       0      0.000 3859273       0      0.000         0

   ------------------------------------------------------------------------
   Collective Partition Statistics:        Minimum   Maximum   Total
   ------------------------------------------------------------------------
   Cell count                              1281915   1281915   1281915
   Mean cell count deviation               0.0%      0.0%
   Partition boundary cell count           0         0         0
   Partition boundary cell count ratio     0.0%      0.0%      0.0%

   Face count                              3859273   3859273   3859273
   Mean face count deviation               0.0%      0.0%
   Partition boundary face count           0         0         0
   Partition boundary face count ratio     0.0%      0.0%      0.0%

   Partition neighbor count                0         0
   ------------------------------------------------------------------------
   Partition Method                        Principal Axes
   Stored Partition Count                  1

Computing connected regions; type ^C to interrupt.
   Connected region count      = 1
Done.
```

Geometry G4
Mesh size medium

```
Grid Size

Level    Cells    Faces    Nodes   Partitions
    0   661284  2032935   711392            1

 1 cell zone, 4 face zones.

Memory Usage

                      cells    faces    nodes    objps    edges
                      -----    -----    -----    -----    -----
Number Used:         661284  2032935   711392        6        0
Mbytes Used:            223      199       38        0        0
Number Allocated:    661284  2032935   711392     1024        0
Mbytes Allocated:       223      199       38        0        0

Array Memory Used:              0 Mbytes
Array Memory Allocated:         0 Mbytes

Zone sizes on domain 1:
  661284 hexahedral cells, zone  2.
   97860 quadrilateral wall faces, zone  3.
      89 quadrilateral outflow faces, zone  4.
     217 quadrilateral mass-flow-inlet faces, zone  5.
 1934769 quadrilateral interior faces, zone  7.
  711392 nodes.

>> 1 Partitions:
       P   Cells I-Cells Cell Ratio   Faces I-Faces Face Ratio Neighbors
       0  661284       0      0.000 2032935       0      0.000         0

   ------------------------------------------------------------------------
   Collective Partition Statistics:        Minimum   Maximum   Total
   ------------------------------------------------------------------------
   Cell count                              661284    661284    661284
   Mean cell count deviation               0.0%      0.0%
   Partition boundary cell count           0         0         0
   Partition boundary cell count ratio     0.0%      0.0%      0.0%

   Face count                              2032935   2032935   2032935
   Mean face count deviation               0.0%      0.0%
   Partition boundary face count           0         0         0
   Partition boundary face count ratio     0.0%      0.0%      0.0%

   Partition neighbor count                0         0
   ------------------------------------------------------------------------
   Partition Method                        Principal Axes
   Stored Partition Count                  1

Computing connected regions; type ^C to interrupt.
   Connected region count      = 1
Done.
```

Geometry G4
Mesh size fine

```
Grid Size

Level    Cells    Faces    Nodes   Partitions
    0  1349657  4127977  1429959            1

 1 cell zone, 4 face zones.

Memory Usage

                      cells    faces    nodes    objps    edges
                      -----    -----    -----    -----    -----
Number Used:        1349657  4127977  1429959        6        0
Mbytes Used:            454      400       76        0        0
Number Allocated:   1349657  4127977  1429959     1024        0
Mbytes Allocated:       454      400       76        0        0

Array Memory Used:              0 Mbytes
Array Memory Allocated:         0 Mbytes

Zone sizes on domain 1:
 1349657 hexahedral cells, zone  2.
  157603 quadrilateral wall faces, zone  3.
     256 quadrilateral mass-flow-inlet faces, zone  4.
     153 quadrilateral outflow faces, zone  5.
 3969965 quadrilateral interior faces, zone  7.
 1429959 nodes.

>> 1 Partitions:
       P   Cells I-Cells Cell Ratio   Faces I-Faces Face Ratio Neighbors
       0 1349657       0      0.000 4127977       0      0.000         0

   ------------------------------------------------------------------------
   Collective Partition Statistics:        Minimum   Maximum   Total
   ------------------------------------------------------------------------
   Cell count                              1349657   1349657   1349657
   Mean cell count deviation               0.0%      0.0%
   Partition boundary cell count           0         0         0
   Partition boundary cell count ratio     0.0%      0.0%      0.0%

   Face count                              4127977   4127977   4127977
   Mean face count deviation               0.0%      0.0%
   Partition boundary face count           0         0         0
   Partition boundary face count ratio     0.0%      0.0%      0.0%

   Partition neighbor count                0         0
   ------------------------------------------------------------------------
   Partition Method                        Principal Axes
   Stored Partition Count                  1

Computing connected regions; type ^C to interrupt.
   Connected region count      = 1
Done.
```

CFD model parameters

The following are reports generated by Fluent for representative CFD simulations.

Report #1

Geometry G1
Fluid water
Flow rate 0.05 L/s

```
FLUENT
Version: 3d, dp, segregated, ske (3d, double precision, segregated,
standard k-epsilon)
Release: 6.2.5
Title:

Models
------

   Model                         Settings
   ------------------------------------------------------------------
   Space                         3D
   Time                          Steady
   Viscous                       Standard k-epsilon turbulence model
   Wall Treatment                Standard Wall Functions
   Heat Transfer                 Disabled
   Solidification and Melting    Disabled
   Species Transport             Disabled
   Coupled Dispersed Phase       Disabled
   Pollutants                    Disabled
   Soot                          Disabled

Boundary Conditions
-------------------

   Zones

      name               id   type
      ---------------------------------------
      tank               2    fluid
      wall               3    wall
      top_surf           4    wall
      outlet             5    outflow
      inlet              6    mass-flow-inlet
      default-interior   8    interior
```

```
Boundary Conditions

      tank

         Condition                                                  Value
         ------------------------------------------------------------
         Material Name                                              water-
liquid
         Specify source terms?                                      no

         Source Terms                                               ((mass
      (inactive . #f) (constant . 0) (profile  )) (x-momentum (inactive
      . #f) (constant . 0) (profile  )) (y-momentum (inactive . #f)
      (constant . 0) (profile  )) (z-momentum (inactive . #f) (constant
      . 0) (profile  )) (k (inactive . #f) (constant . 0) (profile  ))
      (epsilon (inactive . #f) (constant . 0) (profile  )))

         Specify fixed values?                                      no
         Local Coordinate System for Fixed Velocities               no

         Fixed Values                                               ((x-
velocity (inactive . #f) (constant . 0) (profile  )) (y-velocity
(inactive . #f) (constant . 0) (profile  )) (z-velocity (inactive . #f)
(constant . 0) (profile  )) (k (inactive . #f) (constant . 0) (profile
)) (epsilon (inactive . #f) (constant . 0) (profile  )))

         Motion Type                                                0
         X-Velocity Of Zone                                         0
         Y-Velocity Of Zone                                         0
         Z-Velocity Of Zone                                         0
         Rotation speed                                             0
         X-Origin of Rotation-Axis                                  0
         Y-Origin of Rotation-Axis                                  0
         Z-Origin of Rotation-Axis                                  0
         X-Component of Rotation-Axis                               0
         Y-Component of Rotation-Axis                               0
         Z-Component of Rotation-Axis                               1
         Deactivated Thread                                         no
         Laminar zone?                                              no
         Set Turbulent Viscosity to zero within laminar zone?       no
         Porous zone?                                               no
         Conical porous zone?                                       no
         X-Component of Direction-1 Vector                          1
         Y-Component of Direction-1 Vector                          0
         Z-Component of Direction-1 Vector                          0
         X-Component of Direction-2 Vector                          0
         Y-Component of Direction-2 Vector                          1
         Z-Component of Direction-2 Vector                          0
         X-Coordinate of Point on Cone Axis                         1
         Y-Coordinate of Point on Cone Axis                         0
         Z-Coordinate of Point on Cone Axis                         0
         Half Angle of Cone Relative to its Axis                    0
         Direction-1 Viscous Resistance                             0
         Direction-2 Viscous Resistance                             0
         Direction-3 Viscous Resistance                             0
         Direction-1 Inertial Resistance                            0
         Direction-2 Inertial Resistance                            0
         Direction-3 Inertial Resistance                            0
         C0 Coefficient for Power-Law                               0
         C1 Coefficient for Power-Law                               0
         Porosity                                                   1

      wall
```

```
         Condition                                                Value
         ---------------------------------------------------------------
         Enable shell conduction?                                 no
         Wall Motion                                              0
         Shear Boundary Condition                                 0
         Define wall motion relative to adjacent cell zone?       yes
         Apply a rotational velocity to this wall?                no
         Velocity Magnitude                                       0
         X-Component of Wall Translation                          1
         Y-Component of Wall Translation                          0
         Z-Component of Wall Translation                          0
         Define wall velocity components?                         no
         X-Component of Wall Translation                          0
         Y-Component of Wall Translation                          0
         Z-Component of Wall Translation                          0
         Wall Roughness Height                                    0
         Wall Roughness Constant                                  0.5
         Discrete Phase BC Type                                   2
         Normal
((polynomial angle 1))
         Tangent
((polynomial angle 1))
         Discrete Phase BC Function                               none
         Impact Angle Function
((polynomial angle 1))
         Diameter Function
((polynomial 1.8e-09))
         Velocity Exponent Function
((polynomial 0))
         Rotation Speed                                           0
         X-Position of Rotation-Axis Origin                       0
         Y-Position of Rotation-Axis Origin                       0
         Z-Position of Rotation-Axis Origin                       0
         X-Component of Rotation-Axis Direction                   0
         Y-Component of Rotation-Axis Direction                   0
         Z-Component of Rotation-Axis Direction                   1
         X-component of shear stress                              0
         Y-component of shear stress                              0
         Z-component of shear stress                              0
         Specularity Coefficient                                  0
```

```
top_surf

         Condition                                                  Value
         -----------------------------------------------------------------
         Enable shell conduction?                                   no
         Wall Motion                                                0
         Shear Boundary Condition                                   0
         Define wall motion relative to adjacent cell zone?         yes
         Apply a rotational velocity to this wall?                  no
         Velocity Magnitude                                         0
         X-Component of Wall Translation                            1
         Y-Component of Wall Translation                            0
         Z-Component of Wall Translation                            0
         Define wall velocity components?                           no
         X-Component of Wall Translation                            0
         Y-Component of Wall Translation                            0
         Z-Component of Wall Translation                            0
         Wall Roughness Height                                      0
         Wall Roughness Constant                                    0
         Discrete Phase BC Type                                     2
         Normal
((polynomial angle 1))
         Tangent
((polynomial angle 1))
         Discrete Phase BC Function                                 none
         Impact Angle Function
((polynomial angle 1))
         Diameter Function
((polynomial 1.8e-09))
         Velocity Exponent Function
((polynomial 0))
         Rotation Speed                                             0
         X-Position of Rotation-Axis Origin                         0
         Y-Position of Rotation-Axis Origin                         0
         Z-Position of Rotation-Axis Origin                         0
         X-Component of Rotation-Axis Direction                     0
         Y-Component of Rotation-Axis Direction                     0
         Z-Component of Rotation-Axis Direction                     1
         X-component of shear stress                                0
         Y-component of shear stress                                0
         Z-component of shear stress                                0
         Specularity Coefficient                                    0

      outlet

         Condition                    Value
         ---------------------------------
         Flow rate weighting          1
         Discrete Phase BC Type       4
         Discrete Phase BC Function   none
```

```
inlet

         Condition                                Value
         -----------------------------------------------
         Mass Flow Specification Method           0
         Mass Flow-Rate                           0.050000001
         Mass Flux                                1
         Average Mass Flux                        1
         Upstream Torque Integral                 1
         Upstream Total Enthalpy Integral         1
         Supersonic/Initial Gauge Pressure        0
         Direction Specification Method           1
         Reference Frame                          0
         Coordinate System                        0
         X-Component of Flow Direction            1
         Y-Component of Flow Direction            0
         Z-Component of Flow Direction            0
         X-Component of Axis Direction            1
         Y-Component of Axis Direction            0
         Z-Component of Axis Direction            0
         X-Coordinate of Axis Origin              0
         Y-Coordinate of Axis Origin              0
         Z-Coordinate of Axis Origin              0
         Turbulence Specification Method          3
         Turb. Kinetic Energy                     1
         Turb. Dissipation Rate                   1
         Turbulence Intensity                     0.25
         Turbulence Length Scale                  1
         Hydraulic Diameter                       0.01826
         Turbulent Viscosity Ratio                10
         Discrete Phase BC Type                   4
         Discrete Phase BC Function               none
         is zone used in mixing-plane model?      no

      default-interior

         Condition   Value
         -----------------

Solver Controls
---------------

   Equations

      Equation     Solved
      -------------------
      Flow         yes
      Turbulence   yes

   Numerics

      Numeric                            Enabled
      -------------------------------------
      Absolute Velocity Formulation      yes

   Relaxation

      Variable                        Relaxation Factor
      ---------------------------------------------
      Pressure                        0.25
      Density                         1
      Body Forces                     1
      Momentum                        0.5
      Turbulence Kinetic Energy       0.80000001
```

```
      Turbulence Dissipation Rate   0.80000001
      Turbulent Viscosity           1

   Linear Solver

                                    Solver     Termination   Residual
Reduction
      Variable                      Type       Criterion     Tolerance
      ------------------------------------------------------------------
-------
      Pressure                      V-Cycle    0.1
      X-Momentum                    Flexible   0.1           0.7
      Y-Momentum                    Flexible   0.1           0.7
      Z-Momentum                    Flexible   0.1           0.7
      Turbulence Kinetic Energy     Flexible   0.1           0.7
      Turbulence Dissipation Rate   Flexible   0.1           0.7

   Discretization Scheme

      Variable                      Scheme
      ------------------------------------------------
      Pressure                      Standard
      Momentum                      First Order Upwind
      Turbulence Kinetic Energy     First Order Upwind
      Turbulence Dissipation Rate   First Order Upwind

   Solution Limits

      Quantity                          Limit
      ------------------------------------
      Minimum Absolute Pressure         1
      Maximum Absolute Pressure         5e+10
      Minimum Temperature               1
      Maximum Temperature               5000
      Minimum Turb. Kinetic Energy      1e-14
      Minimum Turb. Dissipation Rate    1e-20
      Maximum Turb. Viscosity Ratio     100000
```

```
Material Properties
-------------------

   Material: anthracite (inert-particle)

      Property               Units    Method     Value(s)
      ------------------------------------------------
      Density                kg/m3    constant   1550
      Cp (Specific Heat)     j/kg-k   constant   1680
      Thermal Conductivity   w/m-k    constant   0.0454

   Material: water-liquid (fluid)

      Property                          Units      Method     Value(s)
      ------------------------------------------------------------------
      Density                           kg/m3      constant   1000
      Cp (Specific Heat)                j/kg-k     constant   4182
      Thermal Conductivity              w/m-k      constant   0.6
      Viscosity                         kg/m-s     constant   0.001
      Molecular Weight                  kg/kgmol   constant   18.0152
      L-J Characteristic Length         angstrom   constant   0
      L-J Energy Parameter              k          constant   0
      Thermal Expansion Coefficient     1/k        constant   0
      Degrees of Freedom                           constant   0
      Speed of Sound                    m/s        none       #f
```

Report #2

Geometry G1
Fluid TS3-manure (3% TS hog manure)
Flow rate 0.05 L/s

```
FLUENT
Version: 3d, dp, segregated, lam (3d, double precision, segregated,
laminar)
Release: 6.2.5
Title:

Models
------

   Model                         Settings
   ------------------------------------
   Space                         3D
   Time                          Steady
   Viscous                       Laminar
   Heat Transfer                 Disabled
   Solidification and Melting    Disabled
   Species Transport             Disabled
   Coupled Dispersed Phase       Disabled
   Pollutants                    Disabled
   Soot                          Disabled

Boundary Conditions
-------------------

   Zones

      name               id   type
      ---------------------------------------
      tank               2    fluid
      wall               3    wall
      top_surf           4    wall
      outlet             5    outflow
      inlet              6    mass-flow-inlet
      default-interior   8    interior

   Boundary Conditions

      tank

         Condition                                          Value
         ------------------------------------------------------------
         Material Name                                      manure-ts3
         Specify source terms?                              no

         Source Terms                                       ((mass (inactive
. #f) (constant . 0) (profile  )) (x-momentum (inactive . #f) (constant
. 0) (profile  )) (y-momentum (inactive . #f) (constant . 0) (profile
)) (z-momentum (inactive . #f) (constant . 0) (profile  )))

         Specify fixed values?                              no
         Local Coordinate System for Fixed Velocities       no

         Fixed Values                                       ((x-velocity
(inactive . #f) (constant . 0) (profile  )) (y-velocity (inactive . #f)
```

```
(constant . 0) (profile  )) (z-velocity (inactive . #f) (constant . 0)
(profile  )))

         Motion Type                                    0
         X-Velocity Of Zone                             0
         Y-Velocity Of Zone                             0
         Z-Velocity Of Zone                             0
         Rotation speed                                 0
         X-Origin of Rotation-Axis                      0
         Y-Origin of Rotation-Axis                      0
         Z-Origin of Rotation-Axis                      0
         X-Component of Rotation-Axis                   0
         Y-Component of Rotation-Axis                   0
         Z-Component of Rotation-Axis                   1
         Deactivated Thread                             no
         Porous zone?                                   no
         Conical porous zone?                           no
         X-Component of Direction-1 Vector              1
         Y-Component of Direction-1 Vector              0
         Z-Component of Direction-1 Vector              0
         X-Component of Direction-2 Vector              0
         Y-Component of Direction-2 Vector              1
         Z-Component of Direction-2 Vector              0
         X-Coordinate of Point on Cone Axis             1
         Y-Coordinate of Point on Cone Axis             0
         Z-Coordinate of Point on Cone Axis             0
         Half Angle of Cone Relative to its Axis        0
         Direction-1 Viscous Resistance                 0
         Direction-2 Viscous Resistance                 0
         Direction-3 Viscous Resistance                 0
         Direction-1 Inertial Resistance                0
         Direction-2 Inertial Resistance                0
         Direction-3 Inertial Resistance                0
         C0 Coefficient for Power-Law                   0
         C1 Coefficient for Power-Law                   0
         Porosity                                       1

      wall

         Condition                                                Value
         ---------------------------------------------------------------
         Enable shell conduction?                                 no
         Wall Motion                                              0
         Shear Boundary Condition                                 0
         Define wall motion relative to adjacent cell zone?       yes
         Apply a rotational velocity to this wall?                no
         Velocity Magnitude                                       0
         X-Component of Wall Translation                          1
         Y-Component of Wall Translation                          0
         Z-Component of Wall Translation                          0
         Define wall velocity components?                         no
         X-Component of Wall Translation                          0
         Y-Component of Wall Translation                          0
         Z-Component of Wall Translation                          0
         Discrete Phase BC Type                                   2
         Normal
((polynomial angle 1))
         Tangent
((polynomial angle 1))
         Discrete Phase BC Function                               none
         Impact Angle Function
((polynomial angle 1))
         Diameter Function
((polynomial 1.8e-09))
```

```
         Velocity Exponent Function
((polynomial 0))
         Rotation Speed                                  0
         X-Position of Rotation-Axis Origin              0
         Y-Position of Rotation-Axis Origin              0
         Z-Position of Rotation-Axis Origin              0
         X-Component of Rotation-Axis Direction          0
         Y-Component of Rotation-Axis Direction          0
         Z-Component of Rotation-Axis Direction          1
         X-component of shear stress                     0
         Y-component of shear stress                     0
         Z-component of shear stress                     0
         Specularity Coefficient                         0

      top_surf

         Condition                                       Value
         ------------------------------------------------------------
         Enable shell conduction?                        no
         Wall Motion                                     0
         Shear Boundary Condition                        0
         Define wall motion relative to adjacent cell zone?   yes
         Apply a rotational velocity to this wall?       no
         Velocity Magnitude                              0
         X-Component of Wall Translation                 1
         Y-Component of Wall Translation                 0
         Z-Component of Wall Translation                 0
         Define wall velocity components?                no
         X-Component of Wall Translation                 0
         Y-Component of Wall Translation                 0
         Z-Component of Wall Translation                 0
         Discrete Phase BC Type                          2
         Normal
((polynomial angle 1))
         Tangent
((polynomial angle 1))
         Discrete Phase BC Function                      none
         Impact Angle Function
((polynomial angle 1))
         Diameter Function
((polynomial 1.8e-09))
         Velocity Exponent Function
((polynomial 0))
         Rotation Speed                                  0
         X-Position of Rotation-Axis Origin              0
         Y-Position of Rotation-Axis Origin              0
         Z-Position of Rotation-Axis Origin              0
         X-Component of Rotation-Axis Direction          0
         Y-Component of Rotation-Axis Direction          0
         Z-Component of Rotation-Axis Direction          1
         X-component of shear stress                     0
         Y-component of shear stress                     0
         Z-component of shear stress                     0
         Specularity Coefficient                         0

      outlet

         Condition                    Value
         ----------------------------------
         Flow rate weighting          1
         Discrete Phase BC Type       4
         Discrete Phase BC Function   none

      inlet
```

```
         Condition                                  Value
         -----------------------------------------------
         Mass Flow Specification Method             0
         Mass Flow-Rate                             0.050000001
         Mass Flux                                  1
         Average Mass Flux                          1
         Upstream Torque Integral                   1
         Upstream Total Enthalpy Integral           1
         Supersonic/Initial Gauge Pressure          0
         Direction Specification Method             1
         Reference Frame                            0
         Coordinate System                          0
         X-Component of Flow Direction              1
         Y-Component of Flow Direction              0
         Z-Component of Flow Direction              0
         X-Component of Axis Direction              1
         Y-Component of Axis Direction              0
         Z-Component of Axis Direction              0
         X-Coordinate of Axis Origin                0
         Y-Coordinate of Axis Origin                0
         Z-Coordinate of Axis Origin                0
         Discrete Phase BC Type                     4
         Discrete Phase BC Function                 none
         is zone used in mixing-plane model?        no

      default-interior

         Condition   Value
         -----------------

Solver Controls
---------------

   Equations

      Equation   Solved
      -----------------
      Flow       yes

   Numerics

      Numeric                            Enabled
      ---------------------------------------
      Absolute Velocity Formulation      yes

   Relaxation

      Variable      Relaxation Factor
      -------------------------------
      Pressure      0.25
      Density       1
      Body Forces   1
      Momentum      0.5

   Linear Solver

                    Solver     Termination   Residual Reduction
      Variable      Type       Criterion     Tolerance
      ------------------------------------------------------------
      Pressure      V-Cycle    0.1
      X-Momentum    Flexible   0.1           0.7
      Y-Momentum    Flexible   0.1           0.7
      Z-Momentum    Flexible   0.1           0.7
```

```
   Discretization Scheme

      Variable   Scheme
      ----------------------------
      Pressure   Standard
      Momentum   First Order Upwind

   Solution Limits

      Quantity                    Limit
      --------------------------------
      Minimum Absolute Pressure   1
      Maximum Absolute Pressure   5e+10
      Minimum Temperature         1
      Maximum Temperature         5000

Material Properties
-------------------

   Material: anthracite (inert-particle)

      Property               Units    Method     Value(s)
      ------------------------------------------------
      Density                kg/m3    constant   1550
      Cp (Specific Heat)     j/kg-k   constant   1680
      Thermal Conductivity   w/m-k    constant   0.0454

   Material: manure-ts3 (fluid)

      Property                          Units      Method     Value(s)
      ------------------------------------------------------------------
      Density                           kg/m3      constant   1000
      Cp (Specific Heat)                j/kg-k     constant   4182
      Thermal Conductivity              w/m-k      constant   0.6
      Viscosity                         kg/m-s     constant   0.009309
      Molecular Weight                  kg/kgmol   constant   18.0152
      L-J Characteristic Length         angstrom   constant   0
      L-J Energy Parameter              k          constant   0
      Thermal Expansion Coefficient     1/k        constant   0
      Degrees of Freedom                           constant   0
      Speed of Sound                    m/s        none       #f
```

Report #3

Geometry G1
Fluid XG (1.0 g/L xanthan gum solution)
Flow rate 0.05 L/s

```
FLUENT
Version: 3d, dp, segregated, lam (3d, double precision, segregated,
laminar)
Release: 6.2.5
Title:

Models
------

   Model                         Settings
   ------------------------------------
   Space                         3D
   Time                          Steady
   Viscous                       Laminar
   Heat Transfer                 Enabled
   Solidification and Melting    Disabled
   Radiation                     None
   Species Transport             Disabled
   Coupled Dispersed Phase       Disabled
   Pollutants                    Disabled
   Soot                          Disabled

Boundary Conditions
-------------------

   Zones

      name               id   type
      ---------------------------------------
      tank               2    fluid
      wall               3    wall
      top_surf           4    wall
      outlet             5    outflow
      inlet              6    mass-flow-inlet
      default-interior   8    interior

   Boundary Conditions

      tank

         Condition                                          Value
         ------------------------------------------------------------
         Material Name                                      xanthan-gum
         Specify source terms?                              no

         Source Terms                                       ((mass (inactive
. #f) (constant . 0) (profile  )) (x-momentum (inactive . #f) (constant
. 0) (profile  )) (y-momentum (inactive . #f) (constant . 0) (profile
)) (z-momentum (inactive . #f) (constant . 0) (profile  )) (energy
(inactive . #f) (constant . 0) (profile  )))

         Specify fixed values?                              no
         Local Coordinate System for Fixed Velocities       no
```

Fixed Values	((x-velocity (inactive . #f) (constant . 0) (profile)) (y-velocity (inactive . #f) (constant . 0) (profile)) (z-velocity (inactive . #f) (constant . 0) (profile)) (temperature (inactive . #f) (constant . 0) (profile)))
Motion Type	0
X-Velocity Of Zone	0
Y-Velocity Of Zone	0
Z-Velocity Of Zone	0
Rotation speed	0
X-Origin of Rotation-Axis	0
Y-Origin of Rotation-Axis	0
Z-Origin of Rotation-Axis	0
X-Component of Rotation-Axis	0
Y-Component of Rotation-Axis	0
Z-Component of Rotation-Axis	1
Deactivated Thread	no
Porous zone?	no
Conical porous zone?	no
X-Component of Direction-1 Vector	1
Y-Component of Direction-1 Vector	0
Z-Component of Direction-1 Vector	0
X-Component of Direction-2 Vector	0
Y-Component of Direction-2 Vector	1
Z-Component of Direction-2 Vector	0
X-Coordinate of Point on Cone Axis	1
Y-Coordinate of Point on Cone Axis	0
Z-Coordinate of Point on Cone Axis	0
Half Angle of Cone Relative to its Axis	0
Direction-1 Viscous Resistance	0
Direction-2 Viscous Resistance	0
Direction-3 Viscous Resistance	0
Direction-1 Inertial Resistance	0
Direction-2 Inertial Resistance	0
Direction-3 Inertial Resistance	0
C0 Coefficient for Power-Law	0
C1 Coefficient for Power-Law	0
Porosity	1
Solid Material Name	aluminum

wall

Condition	Value
Wall Thickness	0
Heat Generation Rate	0
Material Name	aluminum
Thermal BC Type	1
Temperature	300
Heat Flux	0
Convective Heat Transfer Coefficient	0
Free Stream Temperature	300
Enable shell conduction?	no
Wall Motion	0
Shear Boundary Condition	0
Define wall motion relative to adjacent cell zone?	yes
Apply a rotational velocity to this wall?	no
Velocity Magnitude	0
X-Component of Wall Translation	1

```
        Y-Component of Wall Translation                    0
        Z-Component of Wall Translation                    0
        Define wall velocity components?                   no
        X-Component of Wall Translation                    0
        Y-Component of Wall Translation                    0
        Z-Component of Wall Translation                    0
        External Emissivity                                1
        External Radiation Temperature                     300
        Discrete Phase BC Type                             2
        Normal
((polynomial angle 1))
        Tangent
((polynomial angle 1))
        Discrete Phase BC Function                         none
        Impact Angle Function
((polynomial angle 1))
        Diameter Function
((polynomial 1.8e-09))
        Velocity Exponent Function
((polynomial 0))
        Rotation Speed                                     0
        X-Position of Rotation-Axis Origin                 0
        Y-Position of Rotation-Axis Origin                 0
        Z-Position of Rotation-Axis Origin                 0
        X-Component of Rotation-Axis Direction             0
        Y-Component of Rotation-Axis Direction             0
        Z-Component of Rotation-Axis Direction             1
        X-component of shear stress                        0
        Y-component of shear stress                        0
        Z-component of shear stress                        0
        Surface tension gradient                           0
        Specularity Coefficient                            0
```

```
      top_surf

         Condition                                                Value
         ---------------------------------------------------------------
         Wall Thickness                                           0
         Heat Generation Rate                                     0
         Material Name                                            aluminum
         Thermal BC Type                                          1
         Temperature                                              300
         Heat Flux                                                0
         Convective Heat Transfer Coefficient                     0
         Free Stream Temperature                                  300
         Enable shell conduction?                                 no
         Wall Motion                                              0
         Shear Boundary Condition                                 0
         Define wall motion relative to adjacent cell zone?       yes
         Apply a rotational velocity to this wall?                no
         Velocity Magnitude                                       0
         X-Component of Wall Translation                          1
         Y-Component of Wall Translation                          0
         Z-Component of Wall Translation                          0
         Define wall velocity components?                         no
         X-Component of Wall Translation                          0
         Y-Component of Wall Translation                          0
         Z-Component of Wall Translation                          0
         External Emissivity                                      1
         External Radiation Temperature                           300
         Discrete Phase BC Type                                   2
         Normal
((polynomial angle 1))
         Tangent
((polynomial angle 1))
         Discrete Phase BC Function                               none
         Impact Angle Function
((polynomial angle 1))
         Diameter Function
((polynomial 1.8e-09))
         Velocity Exponent Function
((polynomial 0))
         Rotation Speed                                           0
         X-Position of Rotation-Axis Origin                       0
         Y-Position of Rotation-Axis Origin                       0
         Z-Position of Rotation-Axis Origin                       0
         X-Component of Rotation-Axis Direction                   0
         Y-Component of Rotation-Axis Direction                   0
         Z-Component of Rotation-Axis Direction                   1
         X-component of shear stress                              0
         Y-component of shear stress                              0
         Z-component of shear stress                              0
         Surface tension gradient                                 0
         Specularity Coefficient                                  0
```

```
      outlet

         Condition                      Value
         --------------------------------
         Flow rate weighting            1
         Discrete Phase BC Type         4
         Discrete Phase BC Function     none

      inlet

         Condition                                  Value
         ----------------------------------------------
         Mass Flow Specification Method             0
         Mass Flow-Rate                             0.050000001
         Mass Flux                                  1
         Average Mass Flux                          1
         Upstream Torque Integral                   1
         Upstream Total Enthalpy Integral           1
         Total Temperature                          300
         Supersonic/Initial Gauge Pressure          0
         Direction Specification Method             1
         Reference Frame                            0
         Coordinate System                          0
         X-Component of Flow Direction              1
         Y-Component of Flow Direction              0
         Z-Component of Flow Direction              0
         X-Component of Axis Direction              1
         Y-Component of Axis Direction              0
         Z-Component of Axis Direction              0
         X-Coordinate of Axis Origin                0
         Y-Coordinate of Axis Origin                0
         Z-Coordinate of Axis Origin                0
         Discrete Phase BC Type                     4
         Discrete Phase BC Function                 none
         is zone used in mixing-plane model?        no

      default-interior

         Condition   Value
         -----------------

Solver Controls
---------------

   Equations

      Equation   Solved
      -----------------
      Flow       yes
      Energy     yes
```

```
 Numerics

      Numeric                            Enabled
      -----------------------------------------
      Absolute Velocity Formulation      yes

   Relaxation

      Variable      Relaxation Factor
      -------------------------------
      Pressure      0.25
      Density       1
      Body Forces   1
      Momentum      0.5
      Energy        1

   Linear Solver

                    Solver     Termination   Residual Reduction
      Variable      Type       Criterion     Tolerance
      ------------------------------------------------------------
      Pressure      V-Cycle    0.1
      X-Momentum    Flexible   0.1           0.7
      Y-Momentum    Flexible   0.1           0.7
      Z-Momentum    Flexible   0.1           0.7
      Energy        Flexible   0.1           0.7

   Discretization Scheme

      Variable   Scheme
      ----------------------------
      Pressure   Standard
      Momentum   First Order Upwind
      Energy     First Order Upwind

   Solution Limits

      Quantity                      Limit
      --------------------------------
      Minimum Absolute Pressure     1
      Maximum Absolute Pressure     5e+10
      Minimum Temperature           1
      Maximum Temperature           5000

Material Properties
-------------------

   Material: anthracite (inert-particle)

      Property                Units    Method     Value(s)
      ------------------------------------------------------
      Density                 kg/m3    constant   1550
      Cp (Specific Heat)      j/kg-k   constant   1680
      Thermal Conductivity    w/m-k    constant   0.0454

   Material: xanthan-gum (fluid)

      Property                          Units      Method                 Value(s)
      ------------------------------------------------------------------------------
      Density                           kg/m3      constant                  1000
      Cp (Specific Heat)                j/kg-k     constant                  4182
      Thermal Conductivity              w/m-k      constant                  0.6
      Viscosity                         kg/m-s     non-newtonian-power-law
(0.126 0.48699999 298 0.0119 4.3590002 )
      Molecular Weight                  kg/kgmol   constant               18.0152
```

```
L-J Characteristic Length       angstrom   constant                0
L-J Energy Parameter            k          constant                0
Thermal Expansion Coefficient   1/k        constant                0
Degrees of Freedom                         constant                0
Speed of Sound                  m/s        none                    #f
```

Report #4

Geometry G1
Fluid TS8-manure (8% TS hog manure)
Flow rate 0.05 L/s

```
FLUENT
Version: 3d, dp, segregated, lam (3d, double precision, segregated,
laminar)
Release: 6.2.5
Title:

Models
------

   Model                         Settings
   ------------------------------------
   Space                         3D
   Time                          Steady
   Viscous                       Laminar
   Heat Transfer                 Enabled
   Solidification and Melting    Disabled
   Radiation                     None
   Species Transport             Disabled
   Coupled Dispersed Phase       Disabled
   Pollutants                    Disabled
   Soot                          Disabled

Boundary Conditions
-------------------

   Zones

      name               id   type
      ---------------------------------------
      tank               2    fluid
      wall               3    wall
      top_surf           4    wall
      outlet             5    outflow
      inlet              6    mass-flow-inlet
      default-interior   8    interior

   Boundary Conditions

      tank

         Condition                                          Value
         ------------------------------------------------------------
         Material Name                                      manure-ts8
         Specify source terms?                              no
         Source Terms                                       ((mass (inactive
. #f) (constant . 0) (profile  )) (x-momentum (inactive . #f) (constant
. 0) (profile  )) (y-momentum (inactive . #f) (constant . 0) (profile
)) (z-momentum (inactive . #f) (constant . 0) (profile  )) (energy
(inactive . #f) (constant . 0) (profile  )))
         Specify fixed values?                              no
         Local Coordinate System for Fixed Velocities       no
```

```
         Fixed Values                                    ((x-velocity
(inactive . #f) (constant . 0) (profile  )) (y-velocity (inactive . #f)
(constant . 0) (profile  )) (z-velocity (inactive . #f) (constant . 0)
(profile  )) (temperature (inactive . #f) (constant . 0) (profile  )))
         Motion Type                                     0
         X-Velocity Of Zone                              0
         Y-Velocity Of Zone                              0
         Z-Velocity Of Zone                              0
         Rotation speed                                  0
         X-Origin of Rotation-Axis                       0
         Y-Origin of Rotation-Axis                       0
         Z-Origin of Rotation-Axis                       0
         X-Component of Rotation-Axis                    0
         Y-Component of Rotation-Axis                    0
         Z-Component of Rotation-Axis                    1
         Deactivated Thread                              no
         Porous zone?                                    no
         Conical porous zone?                            no
         X-Component of Direction-1 Vector               1
         Y-Component of Direction-1 Vector               0
         Z-Component of Direction-1 Vector               0
         X-Component of Direction-2 Vector               0
         Y-Component of Direction-2 Vector               1
         Z-Component of Direction-2 Vector               0
         X-Coordinate of Point on Cone Axis              1
         Y-Coordinate of Point on Cone Axis              0
         Z-Coordinate of Point on Cone Axis              0
         Half Angle of Cone Relative to its Axis         0
         Direction-1 Viscous Resistance                  0
         Direction-2 Viscous Resistance                  0
         Direction-3 Viscous Resistance                  0
         Direction-1 Inertial Resistance                 0
         Direction-2 Inertial Resistance                 0
         Direction-3 Inertial Resistance                 0
         C0 Coefficient for Power-Law                    0
         C1 Coefficient for Power-Law                    0
         Porosity                                        1
         Solid Material Name                             aluminum

      wall

         Condition                                                Value
         ---------------------------------------------------------------
         Wall Thickness                                           0
         Heat Generation Rate                                     0
         Material Name                                            aluminum
         Thermal BC Type                                          1
         Temperature                                              300
         Heat Flux                                                0
         Convective Heat Transfer Coefficient                     0
         Free Stream Temperature                                  300
         Enable shell conduction?                                 no
         Wall Motion                                              0
         Shear Boundary Condition                                 0
         Define wall motion relative to adjacent cell zone?       yes
         Apply a rotational velocity to this wall?                no
         Velocity Magnitude                                       0
         X-Component of Wall Translation                          1
         Y-Component of Wall Translation                          0
         Z-Component of Wall Translation                          0
         Define wall velocity components?                         no
         X-Component of Wall Translation                          0
         Y-Component of Wall Translation                          0
         Z-Component of Wall Translation                          0
```

```
         External Emissivity                                  1
         External Radiation Temperature                       300
         Discrete Phase BC Type                               2
         Normal
((polynomial angle 1))
         Tangent
((polynomial angle 1))
         Discrete Phase BC Function                           none
         Impact Angle Function
((polynomial angle 1))
         Diameter Function
((polynomial 1.8e-09))
         Velocity Exponent Function
((polynomial 0))
         Rotation Speed                                       0
         X-Position of Rotation-Axis Origin                   0
         Y-Position of Rotation-Axis Origin                   0
         Z-Position of Rotation-Axis Origin                   0
         X-Component of Rotation-Axis Direction               0
         Y-Component of Rotation-Axis Direction               0
         Z-Component of Rotation-Axis Direction               1
         X-component of shear stress                          0
         Y-component of shear stress                          0
         Z-component of shear stress                          0
         Surface tension gradient                             0
         Specularity Coefficient                              0

      top_surf

         Condition                                            Value
         -------------------------------------------------------------
         Wall Thickness                                       0
         Heat Generation Rate                                 0
         Material Name                                        aluminum
         Thermal BC Type                                      1
         Temperature                                          300
         Heat Flux                                            0
         Convective Heat Transfer Coefficient                 0
         Free Stream Temperature                              300
         Enable shell conduction?                             no
         Wall Motion                                          0
         Shear Boundary Condition                             0
         Define wall motion relative to adjacent cell zone?   yes
         Apply a rotational velocity to this wall?            no
         Velocity Magnitude                                   0
         X-Component of Wall Translation                      1
         Y-Component of Wall Translation                      0
         Z-Component of Wall Translation                      0
         Define wall velocity components?                     no
         X-Component of Wall Translation                      0
         Y-Component of Wall Translation                      0
         Z-Component of Wall Translation                      0
         External Emissivity                                  1
         External Radiation Temperature                       300
         Discrete Phase BC Type                               2
         Normal
((polynomial angle 1))
         Tangent
((polynomial angle 1))
         Discrete Phase BC Function                           none
         Impact Angle Function
((polynomial angle 1))
         Diameter Function
((polynomial 1.8e-09))
```

```
         Velocity Exponent Function
((polynomial 0))
         Rotation Speed                                  0
         X-Position of Rotation-Axis Origin              0
         Y-Position of Rotation-Axis Origin              0
         Z-Position of Rotation-Axis Origin              0
         X-Component of Rotation-Axis Direction          0
         Y-Component of Rotation-Axis Direction          0
         Z-Component of Rotation-Axis Direction          1
         X-component of shear stress                     0
         Y-component of shear stress                     0
         Z-component of shear stress                     0
         Surface tension gradient                        0
         Specularity Coefficient                         0

      outlet

         Condition                    Value
         ---------------------------------
         Flow rate weighting          1
         Discrete Phase BC Type       4
         Discrete Phase BC Function   none
```

```
      inlet

         Condition                                  Value
         -----------------------------------------------
         Mass Flow Specification Method             0
         Mass Flow-Rate                             0.050000001
         Mass Flux                                  1
         Average Mass Flux                          1
         Upstream Torque Integral                   1
         Upstream Total Enthalpy Integral           1
         Total Temperature                          300
         Supersonic/Initial Gauge Pressure          0
         Direction Specification Method             1
         Reference Frame                            0
         Coordinate System                          0
         X-Component of Flow Direction              1
         Y-Component of Flow Direction              0
         Z-Component of Flow Direction              0
         X-Component of Axis Direction              1
         Y-Component of Axis Direction              0
         Z-Component of Axis Direction              0
         X-Coordinate of Axis Origin                0
         Y-Coordinate of Axis Origin                0
         Z-Coordinate of Axis Origin                0
         Discrete Phase BC Type                     4
         Discrete Phase BC Function                 none
         is zone used in mixing-plane model?        no

      default-interior

         Condition   Value
         -----------------

Solver Controls
---------------

   Equations

      Equation   Solved
      -----------------
      Flow       yes
      Energy     no

   Numerics

      Numeric                           Enabled
      ---------------------------------------
      Absolute Velocity Formulation     yes
```

```
 Relaxation

      Variable      Relaxation Factor
      ------------------------------
      Pressure      0.25
      Density       1
      Body Forces   1
      Momentum      0.5
      Energy        1

   Linear Solver

                    Solver     Termination   Residual Reduction
      Variable      Type       Criterion     Tolerance
      ------------------------------------------------------------
      Pressure      V-Cycle    0.1
      X-Momentum    Flexible   0.1           0.7
      Y-Momentum    Flexible   0.1           0.7
      Z-Momentum    Flexible   0.1           0.7
      Energy        Flexible   0.1           0.7

   Discretization Scheme

      Variable   Scheme
      ----------------------------
      Pressure   Standard
      Momentum   First Order Upwind
      Energy     First Order Upwind

   Solution Limits

      Quantity                     Limit
      -------------------------------
      Minimum Absolute Pressure    1
      Maximum Absolute Pressure    5e+10
      Minimum Temperature          1
      Maximum Temperature          5000

Material Properties
-------------------

   Material: anthracite (inert-particle)

      Property                Units    Method     Value(s)
      ------------------------------------------------------
      Density                 kg/m3    constant   1550
      Cp (Specific Heat)      j/kg-k   constant   1680
      Thermal Conductivity    w/m-k    constant   0.0454
```

```
   Material: manure-ts8 (fluid)

      Property                       Units      Method               Value(s)
      ------------------------------------------------------------------------
      Density                        kg/m3      constant                   1000
      Cp (Specific Heat)             j/kg-k     constant                   4182
      Thermal Conductivity           w/m-k      constant                   0.6
      Viscosity                      kg/m-s     non-newtonian-power-law
(0.439 0.51234 298 0.486 29.24 )
      Molecular Weight               kg/kgmol   constant                18.0152
      L-J Characteristic Length      angstrom   constant                   0
      L-J Energy Parameter           k          constant                   0
      Thermal Expansion Coefficient  1/k        constant                   0
      Degrees of Freedom                        constant                   0
      Speed of Sound                 m/s        none                       #f
```

Appendix D. Full residence time distribution experimental data

HRT = 639.34 s G1 H2O 0.05 L/s Run #1

Tube	Time	Theta	Fls1	Fls2	Fls3	Fls4	Average	StDev	% StDev	Trapezoid	C	SC*dt	St*C*dt	St*t*C*dt
0	0	0.0000					168.625	4.984	2.96		0.01958			
1	30	0.0469	54	60	95	59	67	18.850	28.13	5.528	0.00778	0.000642	0.000009	0.000000
2	60	0.0938	2283	2495	3457	2532	2691.75	521.828	19.39	64.725	0.31260	0.007517	0.000697	0.000065
3	90	0.1408	4092	4392	5928	4414	4706.5	827.474	17.58	173.575	0.54658	0.020158	0.002493	0.000319
4	120	0.1877	4578	4821	6017	4959	5093.75	635.332	12.47	229.930	0.59156	0.026703	0.004410	0.000743
5	150	0.2346	5094	5586	6526	5093	5574.75	675.329	12.11	250.301	0.64742	0.029068	0.006169	0.001325
6	180	0.2815	5592	5429	6407	4837	5566.25	647.602	11.63	261.387	0.64643	0.030356	0.007834	0.002038
7	210	0.3285	5358	5097	6056	5040	5387.75	466.515	8.66	256.999	0.62570	0.029846	0.009092	0.002786
8	240	0.3754	5432	5338	6531	4980	5570.25	669.450	12.02	257.093	0.64689	0.029857	0.010519	0.003723
9	270	0.4223	5111	4585	5917	4802	5103.75	583.547	11.43	250.430	0.59272	0.029083	0.011570	0.004619
10	300	0.4692	5005	4921	6147	5086	5289.75	575.457	10.88	243.849	0.61432	0.028319	0.012636	0.005654
11	330	0.5162	4768	5117	5662	4800	5086.75	414.590	8.15	243.450	0.59074	0.028273	0.013917	0.006866
12	360	0.5631	4202	4584	5574	4425	4696.25	605.779	12.90	229.526	0.54539	0.026656	0.014359	0.007750
13	390	0.6100	4027	4746	4573	4621	4491.75	318.299	7.09	215.566	0.52164	0.025034	0.014671	0.008611
14	420	0.6569	3890	4775	4942	4273	4470	479.937	10.74	210.258	0.51912	0.024418	0.015467	0.009810
15	450	0.7039	3634	4431	4962	4161	4297	553.247	12.88	205.689	0.49903	0.023887	0.016242	0.011056
16	480	0.7508	3598	4294	4641	3845	4094.5	464.480	11.34	196.879	0.47551	0.022864	0.016617	0.012089
17	510	0.7977	3922	4499	4279	3879	4144.75	296.511	7.15	193.307	0.48135	0.022449	0.017384	0.013474
18	540	0.8446	4141	4589	4736	4175	4410.25	297.715	6.75	200.715	0.51218	0.02331	0.019158	0.015759
19	570	0.8915	3790	3998	4349	3634	3942.75	309.166	7.84	195.976	0.45789	0.022759	0.019727	0.017111
20	600	0.9385	3585	3402	4174	3298	3614.75	391.254	10.82	177.312	0.41979	0.020592	0.018821	0.017213
21	630	0.9854	3347	3507	3789	3371	3503.5	202.954	5.79	167.006	0.40687	0.019395	0.018650	0.017943
22	660	1.0323	3210	3482	3468	3072	3308	200.978	6.08	159.809	0.38417	0.018559	0.018711	0.018874
23	690	1.0792	3235	3170	3498	3209	3278	149.079	4.55	154.519	0.38069	0.017945	0.018944	0.020008
24	720	1.1262	3116	3182	3250	3077	3156.25	76.054	2.41	150.958	0.36655	0.017531	0.019324	0.021310

25	750	1.1731	3231	3392	3309	2999	3232.75	169.132	5.23	149.897	0.37543	0.017408	0.020018	0.023028
26	780	1.2200	3089	3148	3007	2739	2995.75	180.668	6.03	146.131	0.34791	0.016971	0.020291	0.024271
27	810	1.2669	3174	3034	3282	2648	3034.5	276.947	9.13	141.480	0.35241	0.016431	0.020433	0.025420
28	840	1.3139	2473	2672	2397	2222	2441	186.442	7.64	128.465	0.28348	0.014919	0.019214	0.024752
29	870	1.3608	2574	2493	2708	2269	2511	184.089	7.33	116.182	0.29161	0.013493	0.018048	0.024150
30	900	1.4077	2239	2284	2605	1878	2251.5	297.589	13.22	111.736	0.26148	0.012976	0.017946	0.024825
31	960	1.5015	1983	2322	2383	2015	2175.75	206.022	9.47	207.742	0.25268	0.024126	0.035075	0.051045
32	1020	1.5954	1744	1831	1825	1957	1839.25	87.956	4.78	188.397	0.21360	0.021879	0.033793	0.052243
33	1080	1.6892	2102	2064	2186	2082	2108.5	53.948	2.56	185.242	0.24487	0.021513	0.035400	0.058298
34	1140	1.7831	2026	2067	1891	1674	1914.5	177.088	9.25	188.773	0.22234	0.021923	0.038012	0.065958
35	1200	1.8769	1641	1663	1441	1817	1640.5	154.336	9.41	166.813	0.19052	0.019373	0.035382	0.064664
36	1320	2.0646	1364	1488	1355	1165	1343	133.284	9.92	279.992	0.15597	0.032516	0.063779	0.125381
37	1440	2.2523	1300	1174	1231	1166	1217.75	62.002	5.09	240.318	0.14142	0.027909	0.060113	0.129721
38	1560	2.4400	1272	1146	1202	1006	1156.5	112.799	9.75	222.816	0.13431	0.025876	0.060648	0.142371
39	1680	2.6277	1014	952	978	751	923.75	117.939	12.77	195.225	0.10728	0.022672	0.057210	0.144559
40	1800	2.8154	816	711	802	621	737.5	90.548	12.28	155.903	0.08565	0.018106	0.049085	0.133228

SUMMARY OUTPUT

Linest		Y-int	3032.2	A =	6631.21	Mean RT =	1.418493
Slope m	Y-int b	Slope =	-801.839	b =	0.745411	var =	1.738106 non-dim
-801.839	*3032.2*	t(n-3)	2.440016			sigma =	1.318373 non-dim
		T(n)	2.815403	Integral1 =	7519.898		
		Fls(n-3) =	1075.7	Integral2 =	1090.867	A(adj) =	0.770107
		Fls(n)	774.7	TotInt =	8610.766	b(adj) =	0.745411
						Integral3 =	0.526628
						Int2(adj) =	0.126686
						Integral4 =	2.417167

HRT = **639.34** **s** **G1** **H2O** **0.05** **L/s** **Run #2**

Tube #	Time (s)	Theta	Fls#1	Fls#2	Fls#3	Fls#4	Average	StDev	%StDev	Trapezoid	C	SC*dt	St*C*dt	St*t*C*dt
0	0	0					39.25	5.4707	13.9381		0.00442			
1	30	0.046923	24	49	36	37	36.5	10.2144	27.9846	1.78	0.00411	0.00020	0.00000	0.00000
2	60	0.093847	3549	3544	3483	3259	3458.75	136.5049	3.9467	82.00	0.38969	0.00924	0.00086	0.00008
3	90	0.14077	6443	5927	5438	5654	5865.5	433.8882	7.3973	218.76	0.66085	0.02465	0.00304	0.00039
4	120	0.187694	6916	6051	5717	4785	5867.25	880.8104	15.0123	275.27	0.66105	0.03101	0.00509	0.00085
5	150	0.234617	7303	6383	6648	6198	6633	483.3391	7.2869	293.28	0.74732	0.03304	0.00702	0.00151
6	180	0.28154	7384	6090	6937	6038	6612.25	659.1835	9.9691	310.76	0.74499	0.03501	0.00903	0.00235
7	210	0.328464	7118	6281	6011	6383	6448.25	473.2803	7.3397	306.42	0.72651	0.03452	0.01052	0.00322
8	240	0.375387	6725	5811	6070	5661	6066.75	470.2286	7.7509	293.62	0.68353	0.03308	0.01162	0.00410
9	270	0.422311	6196	5677	5475	5581	5732.25	319.9848	5.5822	276.82	0.64584	0.03119	0.01242	0.00496
10	300	0.469234	6174	5839	5282	5429	5681	404.4412	7.1192	267.77	0.64006	0.03017	0.01345	0.00601
11	330	0.516157	5619	5466	5187	5321	5398.25	186.1135	3.4477	259.94	0.60821	0.02929	0.01441	0.00711
12	360	0.563081	5464	5197	4673	4941	5068.75	339.4156	6.6962	245.57	0.57108	0.02767	0.01491	0.00805
13	390	0.610004	5250	5176	4052	4857	4833.75	548.3529	11.3443	232.33	0.54461	0.02618	0.01534	0.00900
14	420	0.656927	5101	4660	4208	4524	4623.25	370.5306	8.0145	221.88	0.52089	0.02500	0.01582	0.01003
15	450	0.703851	4951	4487	4160	4369	4491.75	334.6933	7.4513	213.85	0.50607	0.02409	0.01639	0.01116
16	480	0.750774	4446	4221	4090	3971	4182	203.4715	4.8654	203.50	0.47118	0.02293	0.01666	0.01211
17	510	0.797698	4379	4202	3856	4230	4166.75	221.2531	5.3100	195.88	0.46946	0.02207	0.01709	0.01324
18	540	0.844621	4380	4003	3995	3952	4082.5	199.5938	4.8890	193.54	0.45997	0.02181	0.01790	0.01471
19	570	0.891544	4105	3829	3967	3723	3906	166.0723	4.2517	187.42	0.44008	0.02112	0.01832	0.01591
20	600	0.938468	3933	4014	3671	3669	3821.75	178.3206	4.6659	181.31	0.43059	0.02043	0.01869	0.01710
21	630	0.985391	3866	3524	3415	3479	3571	201.6879	5.6479	173.45	0.40234	0.01954	0.01878	0.01806
22	660	1.032315	3559	3478	2958	3401	3349	268.5306	8.0182	162.35	0.37732	0.01829	0.01844	0.01860
23	690	1.079238	3620	2830	3188	3315	3238.25	327.0152	10.0985	154.55	0.36485	0.01741	0.01838	0.01940
24	720	1.126161	3483	3180	2770	3062	3123.75	295.0575	9.4456	149.26	0.35195	0.01682	0.01854	0.02044
25	750	1.173085	2928	2871	2696	2847	2835.5	99.0101	3.4918	139.81	0.31947	0.01575	0.01809	0.02079
26	780	1.220008	3011	2541	2527	2798	2719.25	230.9782	8.4942	130.32	0.30637	0.01468	0.01756	0.02101

27	810	1.266932	2867	2439	2439	2417	2540.5	217.9136	8.5776	123.40	0.28623	0.01390	0.01728	0.02148
28	840	1.313855	2784	2685	2513	2525	2626.75	130.9106	4.9837	121.23	0.29595	0.01366	0.01763	0.02277
29	870	1.360778	2580	2484	2447	2255	2441.5	136.3830	5.5860	118.91	0.27508	0.01340	0.01790	0.02394
30	900	1.407702	2614	2284	2347	2376	2405.25	144.3685	6.0022	113.71	0.27099	0.01281	0.01773	0.02455
31	960	1.501548	1688	2100	2244	2254	2071.5	265.1710	12.8009	210.06	0.23339	0.02367	0.03434	0.04989
32	1020	1.595395	2138	2106	1964	2155	2090.75	86.9075	4.1568	195.31	0.23556	0.02200	0.03408	0.05283
33	1080	1.689242	2143	1884	1915	1993	1983.75	115.6471	5.8297	191.19	0.22350	0.02154	0.03535	0.05806
34	1140	1.783089	1835	1601	1636	1764	1709	109.3831	6.4004	173.28	0.19255	0.01952	0.03383	0.05865
35	1200	1.876936	1770	1764	1610	1716	1715	74.0540	4.3180	160.67	0.19322	0.01810	0.03313	0.06067
36	1320	2.064629	1625	1611	1443	1585	1566	83.6580	5.3421	307.91	0.17644	0.03469	0.06822	0.13446
37	1440	2.252323	1307	1309	1363	1329	1327	25.9743	1.9574	271.50	0.14951	0.03059	0.06579	0.14176
38	1560	2.440016	1000	1160	1064	1066	1072.5	65.8964	6.1442	225.19	0.12084	0.02537	0.05927	0.13869
39	1680	2.62771	1016	937	1004	1090	1011.75	62.6864	6.1958	195.60	0.11399	0.02204	0.05578	0.14138
40	1800	2.815403	751	787	784	753	768.75	19.3972	2.5232	167.09	0.08661	0.01883	0.05100	0.13830

SUMMARY OUTPUT

Linest		Y-int	3631.875	A =	9968.366	Mean RT =	1.303204	
Slope m	Y-int b	Slope =	-1017.48	b =	0.885384	var =	1.394699	non-dim
-1017.48	*3631.875*	t(n-3)	2.440016			sigma =	1.180974	non-dim
		T(n)	2.815403	Integral1 =	7944.734			
		Fls(n-3) =	1149.2	Integral2 =	930.9391	A(adj) =	1.123111	
		Fls(n)	767.25	TotInt =	8875.673	b(adj) =	0.885384	
						Integral3 =	0.413763	
						Int2(adj) =	0.104887	
						Integral4 =	1.766035	

HRT = **639.34** **s** **G1** **H2O** **0.05** **L/s** **Run #3**

Tube #	Time (s)	Theta	Fls#1	Fls#2	Fls#3	Fls#4	Average	StDev	%StDev	Trapezoid	C	SC*dt	St*C*dt	St*t*C*dt
0	0	0.0000					20.125	1.7269	8.5808		0.00431			
1	30	0.0469	21	16	16	10	15.75	4.5000	28.5714	0.842	0.00337	0.00018	0.00000	0.00000
2	60	0.0938	533	541	492	513	519.75	21.9298	4.2193	12.564	0.11130	0.00269	0.00025	0.00002
3	90	0.1408	3110	3257	3188	3300	3213.75	83.1399	2.5870	87.594	0.68818	0.01876	0.00252	0.00034
4	120	0.1877	4033	3923	3944	3995	3973.75	49.7418	1.2518	168.631	0.85092	0.03611	0.00602	0.00102
5	150	0.2346	3864	3941	3651	4156	3903	208.5490	5.3433	184.802	0.83577	0.03957	0.00835	0.00178
6	180	0.2815	4181	4024	4204	4118	4131.75	80.5083	1.9485	188.509	0.88475	0.04037	0.01044	0.00272
7	210	0.3285	4015	3969	3912	4223	4029.75	135.5467	3.3637	191.483	0.86291	0.04100	0.01249	0.00383
8	240	0.3754	3558	3608	3588	3785	3634.75	102.2525	2.8132	179.822	0.77833	0.03851	0.01350	0.00476
9	270	0.4223	3436	3374	3454	3530	3448.5	64.2365	1.8627	166.185	0.73844	0.03559	0.01417	0.00566
10	300	0.4692	3536	3371	3054	3406	3341.75	204.5456	6.1209	159.311	0.71558	0.03411	0.01519	0.00679
11	330	0.5162	3210	3193	2912	2776	3022.75	213.8526	7.0748	149.322	0.64728	0.03197	0.01572	0.00774
12	360	0.5631	2915	2788	2764	2502	2742.25	173.3289	6.3207	135.257	0.58721	0.02896	0.01560	0.00841
13	390	0.6100	2571	2688	2575	2334	2542	148.8959	5.8574	123.977	0.54433	0.02655	0.01555	0.00912
14	420	0.6569	2508	2274	2415	2195	2348	140.2070	5.9713	114.728	0.50279	0.02457	0.01554	0.00984
15	450	0.7039	2316	2590	2369	2041	2329	225.7093	9.6913	109.730	0.49872	0.02350	0.01598	0.01089
16	480	0.7508	2207	2275	2269	2129	2220	68.0098	3.0635	106.727	0.47538	0.02285	0.01661	0.01208
17	510	0.7977	2252	2350	2247	2394	2310.75	72.9994	3.1591	106.299	0.49481	0.02276	0.01763	0.01367
18	540	0.8446	2000	2159	1903	2107	2042.25	114.0157	5.5828	102.129	0.43732	0.02187	0.01793	0.01471
19	570	0.8915	2043	2008	2019	2068	2034.5	26.6896	1.3118	95.647	0.43566	0.02048	0.01778	0.01544
20	600	0.9385	1830	1824	1588	1683	1731.25	117.1932	6.7693	88.351	0.37072	0.01892	0.01728	0.01578
21	630	0.9854	1517	1583	1652	1350	1525.5	129.3329	8.4781	76.409	0.32666	0.01636	0.01571	0.01510
22	660	1.0323	1523	1652	1592	1427	1548.5	96.6385	6.2408	72.121	0.33159	0.01544	0.01558	0.01573
23	690	1.0792	1441	1582	1464	1271	1439.5	128.1939	8.9054	70.104	0.30825	0.01501	0.01584	0.01671
24	720	1.1262	1770	1530	1544	1176	1505	245.3650	16.3033	69.083	0.32227	0.01479	0.01632	0.01801
25	750	1.1731	1556	1345	1542	1167	1402.5	184.2001	13.1337	68.215	0.30032	0.01461	0.01678	0.01929
26	780	1.2200	1392	1369	1439	1031	1307.75	186.7858	14.2830	63.587	0.28003	0.01362	0.01628	0.01948
27	810	1.2669	1222	1439	1304	1318	1320.75	89.4851	6.7753	61.669	0.28282	0.01321	0.01642	0.02043

28	840	1.3139	1299	1369	1197	1128	1248.25	106.8375	8.5590	60.273	0.26729	0.01291	0.01665	0.02148
29	870	1.3608	1225	1242	1252	1106	1206.25	67.7563	5.6171	57.587	0.25830	0.01233	0.01649	0.02205
30	900	1.4077	1301	1337	1074	1208	1230	117.3456	9.5403	57.159	0.26339	0.01224	0.01695	0.02347
31	960	1.5015	1011	1090	896	897	973.5	94.5815	9.7156	103.396	0.20846	0.02214	0.03209	0.04654
32	1020	1.5954	1226	1294	1130	675	1081.25	279.0644	25.8094	96.416	0.23153	0.02065	0.03202	0.04971
33	1080	1.6892	1047	956	978	678	914.75	162.5246	17.7671	93.659	0.19588	0.02006	0.03286	0.05388
34	1140	1.7831	969	780	960	560	817.25	192.3285	23.5336	81.271	0.17500	0.01740	0.03017	0.05234
35	1200	1.8769	920	891	918	602	832.75	154.4007	18.5411	77.424	0.17832	0.01658	0.03035	0.05559
36	1320	2.0646	802	582	681	557	655.5	111.3807	16.9917	139.667	0.14037	0.02991	0.05861	0.11511
37	1440	2.2523	713	714	651	521	649.75	90.7501	13.9669	122.494	0.13913	0.02623	0.05661	0.12239
38	1560	2.4400	478	494	604	581	539.25	62.5427	11.5981	111.584	0.11547	0.02389	0.05585	0.13076
39	1680	2.6277	497	428	470	409	451	39.8748	8.8414	92.932	0.09657	0.01990	0.05026	0.12710
40	1800	2.8154	383	367	382	395	381.75	11.4710	3.0048	78.151	0.08175	0.01673	0.04541	0.12339

SUMMARY OUTPUT

Linest		Y-int	1505.575	A =	3277.713	Mean RT =	1.321903
Slope m	Y-int b	Slope =	-397.59	b =	0.742533	var =	1.701333 non-dim
-397.59	*1505.575*	t(n-3)	2.440016			sigma =	1.304352 non-dim
		T(n)	2.815403	Integral1 =	4124.267		
		Fls(n-3) =	535.45	Integral2 =	545.6934	A(adj) =	0.701872
		Fls(n)	386.2	TotInt =	4669.96	b(adj) =	0.742533
						Integral3 =	0.486354
						Int2(adj) =	0.116852
						Integral4 =	2.236211

HRT(nom) =	2400	s	HRT(act) =	2557.36	G1	H2O	0.0125	L/s

Tube #	Time (s)	Theta	Fls#1	Fls#2	Fls#3	Fls#4	Average	StDev	%StDev	Trapezoid	C	SC*dt	St*C*dt	St*t*C*dt
0	0	0.0000					42.25	6.9437	16.4347		0.00635			
1	120	0.0000	20	24	25	28	24.25	3.3040	13.6249	0.00	0.00364	0.00000	0.00000	0.00000
2	240	0.0469	440	494	435	468	459.25	27.3420	5.9536	11.34	0.06902	0.00170	0.00008	0.00000
3	360	0.0938	3427	2284	3678	2889	3069.5	618.5114	20.1502	82.79	0.46132	0.01244	0.00109	0.00010
4	480	0.1408	5405	5509	5921	5476	5577.75	232.9111	4.1757	202.88	0.83828	0.03049	0.00378	0.00049
5	600	0.1877	5442	4939	5678	5212	5317.75	316.1501	5.9452	255.63	0.79920	0.03842	0.00629	0.00105
6	720	0.2346	5004	4583	5059	4676	4830.5	236.2492	4.8908	238.10	0.72598	0.03578	0.00752	0.00160
7	840	0.2815	4504	4495	4643	4616	4564.5	75.9495	1.6639	220.42	0.68600	0.03313	0.00853	0.00221
8	960	0.3285	4348	4211	4462	4137	4289.5	144.4495	3.3675	207.73	0.64467	0.03122	0.00950	0.00291
9	1080	0.3754	4056	3962	4313	4174	4126.25	151.7330	3.6773	197.45	0.62013	0.02967	0.01043	0.00368
10	1200	0.4223	4026	3601	4105	3924	3914	221.4302	5.6574	188.64	0.58823	0.02835	0.01129	0.00451
11	1320	0.4692	3577	3917	3714	3739	3736.75	139.6815	3.7380	179.50	0.56160	0.02698	0.01201	0.00536
12	1440	0.5162	3616	3762	3942	3708	3757	137.2734	3.6538	175.82	0.56464	0.02642	0.01302	0.00643
13	1560	0.5631	3708	3811	3537	3676	3683	113.0988	3.0708	174.56	0.55352	0.02623	0.01415	0.00765
14	1680	0.6100	3613	3573	3674	3587	3611.75	44.6869	1.2373	171.15	0.54281	0.02572	0.01508	0.00886
15	1800	0.6569	3526	3306	3614	3495	3485.25	129.6955	3.7213	166.51	0.52380	0.02502	0.01584	0.01004
16	1920	0.7039	3273	3148	3297	3131	3212.25	84.8582	2.6417	157.13	0.48277	0.02362	0.01605	0.01091
17	2040	0.7508	3031	3033	3020	3078	3040.5	25.6450	0.8434	146.70	0.45696	0.02205	0.01602	0.01165
18	2160	0.7977	3066	2979	3210	3037	3073	98.2344	3.1967	143.43	0.46184	0.02156	0.01669	0.01294
19	2280	0.8446	2906	2889	2957	2954	2926.5	34.2199	1.1693	140.76	0.43982	0.02115	0.01736	0.01426
20	2400	0.8915	2805	2673	2872	2875	2806.25	94.5282	3.3685	134.50	0.42175	0.02021	0.01754	0.01523
21	2520	0.9385	2705	2639	2631	2713	2672	42.9729	1.6083	128.53	0.40157	0.01932	0.01766	0.01616
22	2640	0.9854	2677	2656	2661	2571	2641.25	47.6821	1.8053	124.66	0.39695	0.01873	0.01802	0.01734
23	2760	1.0323	2556	2487	2665	2408	2529	108.9801	4.3092	121.30	0.38008	0.01823	0.01838	0.01855
24	2880	1.0792	2430	2517	2498	2526	2492.75	43.4310	1.7423	117.82	0.37464	0.01771	0.01869	0.01974
25	3000	1.1262	2448	2382	2381	2320	2382.75	52.2773	2.1940	114.39	0.35810	0.01719	0.01895	0.02089
26	3120	1.1731	2314	2331	2357	2279	2320.25	32.6943	1.4091	110.34	0.34871	0.01658	0.01906	0.02191
27	3240	1.2200	2152	2254	2287	2178	2217.75	63.2791	2.8533	106.47	0.33331	0.01600	0.01914	0.02290

28	3360	1.2669	2127	2107	2088	2243	2141.25	69.6772	3.2540	102.27	0.32181	0.01537	0.01911	0.02376
29	3480	1.3139	1883	2165	2086	2085	2054.75	120.4779	5.8634	98.45	0.30881	0.01480	0.01908	0.02463
30	3600	1.3608	1955	1855	2078	1960	1962	91.2104	4.6488	94.24	0.29487	0.01416	0.01893	0.02532
31	3840	1.4077	1210	1865	1748	1908	1682.75	322.3367	19.1553	85.51	0.25290	0.01285	0.01777	0.02457
32	4080	1.5015	1781	1871	1768	1713	1783.25	65.5051	3.6734	162.64	0.26800	0.02444	0.03559	0.05187
33	4320	1.5954	1686	1779	1680	1543	1672	97.2111	5.8141	162.13	0.25128	0.02437	0.03769	0.05837
34	4560	1.6892	1603	1562	1593	1546	1576	26.5456	1.6844	152.41	0.23686	0.02291	0.03759	0.06173
35	4800	1.7831	1413	1400	1476	1474	1440.75	39.9114	2.7702	141.56	0.21653	0.02127	0.03689	0.06402
36	5280	1.8769	1310	1300	1250	1309	1292.25	28.5234	2.2073	128.24	0.19421	0.01927	0.03522	0.06441
37	5760	2.0646	1078	1101	1189	1149	1129.25	49.6143	4.3936	227.25	0.16971	0.03415	0.06709	0.13210
38	6240	2.2523	945	1025	933	960	965.75	41.0152	4.2470	196.61	0.14514	0.02955	0.06356	0.13699
39	6720	2.4400	714	790	784	742	757.5	36.0139	4.7543	161.72	0.11384	0.02431	0.05675	0.13271
40	7200	2.6277	685	627	732	678	680.5	42.9767	6.3155	134.95	0.10227	0.02028	0.05129	0.12988

SUMMARY OUTPUT

Linest		Y-int	2879.35	A =	7015.012	Mean RT =	1.284	
Slope m	Y-int b	Slope =	-849.923	b =	0.880703	var =	1.367237	non-dim
-849.923	*2879.35*	t(n-3)	2.252323			sigma =	1.169289	non-dim
		T(n)	2.62771	Integral1 =	5866.503			
		Fls(n-3) =	965.05	Integral2 =	787.3004	A(adj) =	1.054286	
		Fls(n)	646	TotInt =	6653.803	b(adj) =	0.880703	
						Integral3 =	0.44527	
						Int2(adj) =	0.118323	
						Integral4 =	1.828177	

targetHRT =	600	s	actualHRT =	639.34		**G2**	**H20**	**0.05 L/s**		Run # 1				
Tube #	Time (s)	Theta	Fls#1	Fls#2	Fls#3	Fls#4	Average	StDev	%StDev	Trapezoid	C	SC*dt	St*C*dt	St*t*C*dt
0	0	0					7.875	2.232071	28.34376		0.001122			
1	30	0.046923	27	21	22	17	21.75	4.112988	18.91029	0.695053	0.003099	9.9E-05	3.41E-06	1.6E-07
2	60	0.093847	4485	4726	4353	4813	4594.25	212.4043	4.623264	108.2992	0.654554	0.01543	0.001445	0.000135
3	90	0.14077	6761	6664	6536	6690	6662.75	93.91974	1.409624	264.1083	0.949258	0.037628	0.004576	0.000577
4	120	0.187694	5140	5074	4614	5087	4978.75	244.8365	4.91763	273.1293	0.709334	0.038913	0.006259	0.001028
5	150	0.234617	4380	4299	4318	1922	3729.75	1205.663	32.32557	204.3162	0.531386	0.029109	0.006049	0.001273
6	180	0.28154	4056	3752	3856	3749	3853.25	144.031	3.737908	177.91	0.548982	0.025347	0.006551	0.001707
7	210	0.328464	3866	4010	3808	3775	3864.75	103.8825	2.68795	181.0774	0.55062	0.025799	0.00787	0.002415
8	240	0.375387	3713	4021	3719	3735	3797	149.6217	3.940525	179.7576	0.540968	0.025611	0.009008	0.003182
9	270	0.422311	3844	3976	3742	3725	3821.75	115.4827	3.021723	178.7488	0.544494	0.025467	0.010159	0.004067
10	300	0.469234	3956	3359	3537	3503	3588.75	256.7026	7.152982	173.8629	0.511298	0.024771	0.011024	0.00492
11	330	0.516157	3651	3723	3581	3607	3640.5	62.12622	1.70653	169.6105	0.518671	0.024165	0.01191	0.005883
12	360	0.563081	3503	3568	3530	3435	3509	56.07733	1.5981	167.7394	0.499936	0.023898	0.012886	0.006961
13	390	0.610004	3399	3398	3442	3494	3433.25	45.39732	1.322284	162.877	0.489143	0.023205	0.013605	0.007989
14	420	0.656927	3228	3295	3222	3321	3266.5	49.14265	1.504444	157.1875	0.465386	0.022395	0.014173	0.008982
15	450	0.703851	3146	3019	2950	3039	3038.5	81.17676	2.671606	147.926	0.432902	0.021075	0.014322	0.009744
16	480	0.750774	2937	3048	2921	2977	2970.75	56.62964	1.906241	140.9872	0.42325	0.020087	0.014604	0.010629
17	510	0.797698	2840	2903	2695	2761	2799.75	90.83823	3.244512	135.3857	0.398887	0.019289	0.014921	0.011552
18	540	0.844621	2793	2749	2730	2636	2727	66.15638	2.425977	129.6669	0.388522	0.018474	0.015164	0.012458
19	570	0.891544	2588	2728	2537	2632	2621.25	81.0653	3.09262	125.479	0.373456	0.017877	0.015511	0.013467
20	600	0.938468	2667	2635	2394	2596	2573	122.8142	4.773192	121.8659	0.366581	0.017363	0.015883	0.014539
21	630	0.985391	2449	2416	2337	2106	2327	154.6458	6.645717	114.9623	0.331533	0.016379	0.015736	0.015127
22	660	1.032315	2209	2270	2259	2335	2268.25	51.81618	2.284412	107.8124	0.323163	0.01536	0.015492	0.015633
23	690	1.079238	2226	2148	2221	2244	2209.75	42.33497	1.915826	105.0615	0.314828	0.014968	0.015799	0.016683
24	720	1.126161	2197	2243	1999	2211	2162.5	110.6872	5.118485	102.5804	0.308097	0.014615	0.016112	0.017771
25	750	1.173085	2209	2163	2218	2261	2212.75	40.18603	1.816112	102.6508	0.315256	0.014625	0.016817	0.019346
26	780	1.220008	1919	2060	1935	1935	1962.25	65.6017	3.343188	97.95258	0.279566	0.013956	0.016679	0.019941

27	810	1.266932	1957	1982	1850	1938	1931.75	57.40136	2.97147	91.35984	0.275221	0.013016	0.016183	0.020127
28	840	1.313855	1792	1994	1811	1970	1891.75	104.9583	5.548213	89.70579	0.269522	0.012781	0.016489	0.02128
29	870	1.360778	1833	1862	1735	1890	1830	67.47345	3.687074	87.31856	0.260724	0.01244	0.016632	0.022243
30	900	1.407702	1799	1799	1695	1775	1767	49.31531	2.790906	84.39172	0.251749	0.012023	0.016638	0.023031
31	960	1.501548	1650	1683	1651	1504	1622	80.1457	4.941165	159.0234	0.23109	0.022656	0.032911	0.047857
32	1020	1.595395	1544	1556	1557	1575	1558	12.78019	0.820295	149.2164	0.221972	0.021259	0.032899	0.050959
33	1080	1.689242	1470	1469	1509	1480	1482	18.67262	1.259961	142.6471	0.211144	0.020323	0.033353	0.054783
34	1140	1.783089	1319	1394	1369	1351	1358.25	31.55287	2.323053	133.2742	0.193513	0.018988	0.032927	0.057142
35	1200	1.876936	1238	1234	1197	1232	1225.25	18.99781	1.550525	121.2266	0.174564	0.017271	0.031565	0.057726
36	1320	2.064629	1146	1167	1109	1199	1155.25	37.7569	3.268288	223.4023	0.164591	0.031829	0.06264	0.123556
37	1440	2.252323	966	986	1017	974	985.75	22.39606	2.271981	200.926	0.140442	0.028626	0.061577	0.132705
38	1560	2.440016	894	904	839	958	898.75	48.75363	5.424604	176.8543	0.128047	0.025197	0.059007	0.138406
39	1680	2.62771	3	0	0	3	1.5	1.732051	115.4701					
40	1800	2.815403	4	0	0	0	1	2	200					

SUMMARY OUTPUT

Linest		Y-int	2534.756	A =	3885.874	Mean RT =	1.612581	
Slope m	Y-int b	Slope =	-676.83	b =	0.595092	var =	2.687379	non-dim
-676.83	*2534.756*	t(n-3)	2.064629			sigma =	1.639323	non-dim
		T(n)	2.440016	Integral1 =	5490.301			
		Fls(n-3) =	1137.354	Integral2 =	1528.603	A(adj) =	0.55363	
		Fls(n)	883.2805	TotInt =	7018.903	b(adj) =	0.595092	
						Integral3 =	0.897362	
						Int2(adj) =	0.217784	
						Integral4 =	4.312494	

targetHRT =	600	s	actualHRT =	639.34		**G2**	**H20**	**0.05 L/s**		Run # 2				
Tube #	Time (s)	Theta	Fls#1	Fls#2	Fls#3	Fls#4	Average	StDev	%StDev	Trapezoid	C	SC*dt	St*C*dt	St*t*C*dt
0	0	0					63.625	4.688512	7.368977		0.009322			
1	30	0.046923	261	309	280	291	285.25	20.10597	7.048543	8.185199	0.041795	0.001199	4.6E-05	2.16E-06
2	60	0.093847	627	644	592	651	628.5	26.33755	4.190541	21.43812	0.092089	0.003141	0.000249	2.12E-05
3	90	0.14077	4099	3551	4047	3491	3797	320.3415	8.4367	103.8297	0.556342	0.015213	0.00204	0.000278
4	120	0.187694	4657	4506	4001	4569	4433.25	294.7455	6.64852	193.0956	0.649567	0.028293	0.004698	0.000796
5	150	0.234617	4480	4198	4427	4259	4341	134.0274	3.087477	205.8588	0.63605	0.030163	0.006362	0.001358
6	180	0.28154	4279	3959	2351	3296	3471.25	851.6714	24.53501	183.2886	0.508613	0.026856	0.006861	0.001767
7	210	0.328464	3724	4145	3730	4016	3903.75	210.7927	5.39975	173.03	0.571983	0.025353	0.007767	0.002394
8	240	0.375387	3769	3794	3781	3921	3816.25	70.57561	1.849345	181.1243	0.559163	0.026539	0.009333	0.003296
9	270	0.422311	3747	3733	3877	3587	3736	118.6198	3.175049	177.1886	0.547404	0.025962	0.010348	0.004139
10	300	0.469234	3707	3779	3855	3800	3785.25	61.22295	1.617408	176.4613	0.554621	0.025855	0.01153	0.005156
11	330	0.516157	3631	3761	3610	3637	3659.75	68.4854	1.871314	174.6723	0.536232	0.025593	0.0126	0.006217
12	360	0.563081	3403	3804	3726	3757	3672.5	182.5057	4.969522	172.027	0.5381	0.025206	0.013602	0.007355
13	390	0.610004	3799	3880	3660	3714	3763.25	96.60012	2.566933	174.4553	0.551397	0.025561	0.015	0.008817
14	420	0.656927	3768	3717	3425	3622	3633	151.29	4.164327	173.5286	0.532313	0.025426	0.016096	0.010203
15	450	0.703851	3598	3501	3427	3261	3446.75	142.2589	4.127333	166.1029	0.505023	0.024338	0.016544	0.01126
16	480	0.750774	3408	3242	3345	3186	3295.25	99.93123	3.032584	158.1787	0.482825	0.023177	0.016844	0.012255
17	510	0.797698	3279	3063	2935	3182	3114.75	148.8721	4.779586	150.3895	0.456378	0.022035	0.017046	0.013198
18	540	0.844621	3233	3180	3032	3223	3167	92.89062	2.933079	147.3805	0.464034	0.021594	0.017737	0.01458
19	570	0.891544	2989	3081	3141	3054	3066.25	63.04165	2.055985	146.2426	0.449272	0.021428	0.018593	0.016145
20	600	0.938468	2755	2926	2860	2813	2838.5	72.43618	2.551918	138.5354	0.415901	0.020298	0.018555	0.016972
21	630	0.985391	3079	3021	2935	2845	2970	102.1959	3.440939	136.2773	0.435169	0.019968	0.019218	0.018508
22	660	1.032315	2911	2965	2754	2822	2863	93.57706	3.268497	136.8521	0.419491	0.020052	0.020221	0.020402
23	690	1.079238	2904	2951	2756	2889	2875	83.61419	2.90832	134.6232	0.421249	0.019725	0.020826	0.022
24	720	1.126161	2680	2843	2597	2697	2704.25	102.2982	3.782867	130.8987	0.396231	0.019179	0.021135	0.023301
25	750	1.173085	2676	2773	2465	2539	2613.25	137.7785	5.272305	124.7576	0.382897	0.01828	0.021007	0.024152
26	780	1.220008	2411	2565	2377	2193	2386.5	152.7471	6.400464	117.3026	0.349674	0.017187	0.020547	0.024573

27	810	1.266932	2333	2375	2211	2191	2277.5	90.35301	3.967201	109.4253	0.333703	0.016033	0.019928	0.024778
28	840	1.313855	2130	2407	2157	2208	2225.5	125.2478	5.627848	105.648	0.326084	0.01548	0.019971	0.025773
29	870	1.360778	2202	2157	2147	1748	2063.5	211.6892	10.25875	100.6272	0.302347	0.014744	0.019704	0.026342
30	900	1.407702	1898	2171	2106	1989	2041	121.488	5.952376	96.29853	0.29905	0.01411	0.01953	0.027039
31	960	1.501548	2063	1981	1872	1058	1743.5	463.6482	26.59296	177.5816	0.25546	0.02602	0.037753	0.054834
32	1020	1.595395	1874	1886	1538	1592	1722.5	183.2621	10.63931	162.6365	0.252383	0.02383	0.036893	0.05717
33	1080	1.689242	1141	1662	1368	1510	1420.25	221.5166	15.59701	147.4685	0.208097	0.021607	0.035389	0.058007
34	1140	1.783089	1618	850	1497	1183	1287	344.2121	26.74531	127.0333	0.188573	0.018613	0.032272	0.055997
35	1200	1.876936	1470	1430	1529	1439	1467	44.74371	3.050015	129.227	0.214947	0.018935	0.034709	0.063665
36	1320	2.064629	1439	1489	1203	531	1165.5	441.003	37.8381	247.0516	0.170771	0.036198	0.07095	0.139379
37	1440	2.252323	1227	1181	1151	1249	1202	44.25683	3.681932	222.1823	0.176119	0.032554	0.070315	0.152162
38	1560	2.440016	900	970	974	1022	966.5	50.23611	5.197735	203.5067	0.141613	0.029818	0.069654	0.162971
39	1680	2.62771	846	694	760	801	775.25	64.55682	8.327226	163.4576	0.113591	0.02395	0.060439	0.152731
40	1800	2.815403	692	661	685	643	670.25	22.5	3.356956	135.6555	0.098206	0.019876	0.053959	0.14666

SUMMARY OUTPUT

Linest		Y-int	2798.325	A =	6568.743	Mean RT =	1.462481	
Slope m	Y-int b	Slope =	-755.087	b =	0.789923	var =	1.68008	non-dim
-755.087	*2798.325*	t(n-3)	2.440016			sigma =	1.296179	non-dim
		T(n)	2.815403	Integral1 =	5925.339			
		Fls(n-3) =	955.9	Integral2 =	899.5967	A(adj) =	0.962462	
		Fls(n)	672.45	TotInt =	6824.936	b(adj) =	0.789923	
						Integral3 =	0.537964	
						Int2(adj) =	0.13181	
						Integral4 =	2.406861	

target HRT = 600 s actual HRT = 639.34 **G2** **H20** **0.05 L/s** Run # 3

Tube #	Time (s)	Theta	Fls#1	Fls#2	Fls#3	Fls#4	Average	StDev	%StDev	Trapezoid	C	SC*dt	St*C*dt	St*t*C*dt
0	0	0					68.875	11.24325	16.32414		0.013921			
1	30	0.046923	72	96	56	63	71.75	17.44276	24.31047	3.299301	0.014502	0.000667	1.6E-05	7.49E-07
2	60	0.093847	4333	4484	4022	4395	4308.5	200.8026	4.660614	102.7681	0.870805	0.020771	0.001933	0.000181
3	90	0.14077	5123	5041	4885	5047	5024	99.89995	1.988454	218.9563	1.015417	0.044254	0.005271	0.000652
4	120	0.187694	4238	4082	4166	3636	4030.5	270.616	6.714203	212.4339	0.814617	0.042936	0.006941	0.001145
5	150	0.234617	3864	3992	3590	3628	3768.5	192.072	5.096777	182.9778	0.761663	0.036982	0.00778	0.001657
6	180	0.28154	3539	3674	3443	3260	3479	174.0517	5.002924	170.0386	0.703152	0.034367	0.008837	0.002291
7	210	0.328464	3166	3227	3052	3019	3116	97.16995	3.11842	154.7299	0.629785	0.031273	0.009498	0.002902
8	240	0.375387	2914	3248	2893	3111	3041.5	169.0966	5.559646	144.4654	0.614727	0.029198	0.010267	0.003626
9	270	0.422311	2976	3262	2954	2964	3039	148.9385	4.900904	142.6588	0.614222	0.028833	0.0115	0.004602
10	300	0.469234	2770	2738	2772	2912	2798	77.58007	2.772697	136.9459	0.565513	0.027679	0.012312	0.005491
11	330	0.516157	2676	2600	2489	2692	2614.25	92.64403	3.543809	126.9806	0.528374	0.025664	0.012624	0.006224
12	360	0.563081	2951	3018	2628	2768	2841.25	177.1315	6.234282	127.9953	0.574254	0.02587	0.013985	0.007574
13	390	0.610004	2683	2829	2517	2594	2655.75	133.9437	5.043536	128.9689	0.536762	0.026066	0.015268	0.008958
14	420	0.656927	2457	2553	2556	2597	2540.75	59.33169	2.335204	121.9187	0.513519	0.024641	0.015597	0.009885
15	450	0.703851	2759	2405	2444	2343	2487.75	185.5539	7.458704	117.9771	0.502807	0.023845	0.016218	0.011044
16	480	0.750774	2520	2520	2430	2312	2445.5	98.59513	4.031696	115.7424	0.494268	0.023393	0.017009	0.012381
17	510	0.797698	1970	2551	2312	2344	2294.25	240.7272	10.49263	111.2026	0.463698	0.022476	0.017385	0.013459
18	540	0.844621	2225	2339	2074	2229	2216.75	108.8435	4.91005	105.8357	0.448034	0.021391	0.017557	0.014421
19	570	0.891544	1772	2378	1984	2124	2064.5	254.204	12.3131	100.4454	0.417263	0.020301	0.017606	0.01528
20	600	0.938468	2022	1722	2072	1983	1949.75	156.1418	8.008297	94.18111	0.39407	0.019035	0.017405	0.015924
21	630	0.985391	1781	1888	1909	1808	1846.5	61.64684	3.338578	89.06646	0.373202	0.018002	0.017305	0.016645
22	660	1.032315	1644	1922	1555	1757	1719.5	158.2961	9.20594	83.6644	0.347534	0.01691	0.017045	0.017191
23	690	1.079238	1414	1903	1626	1707	1662.5	202.4064	12.17482	79.34745	0.336013	0.016037	0.016925	0.017871
24	720	1.126161	1750	1861	1773	1642	1756.5	90.08329	5.128568	80.21553	0.355012	0.016213	0.017888	0.019746
25	750	1.173085	1439	1554	1593	1527	1528.25	65.37775	4.277949	77.0658	0.308879	0.015576	0.017881	0.020536
26	780	1.220008	1386	1678	1522	1564	1537.5	120.6027	7.844075	71.92769	0.310749	0.014538	0.017396	0.020824

27	810	1.266932	1562	1601	1586	1546	1573.75	24.5	1.556791	72.9952	0.318076	0.014753	0.018349	0.02283
28	840	1.313855	1326	1415	1407	1510	1414.5	75.29719	5.323237	70.10941	0.285889	0.01417	0.018267	0.023557
29	870	1.360778	1403	1452	1407	1391	1413.25	26.71298	1.890181	66.34381	0.285636	0.013409	0.017932	0.023988
30	900	1.407702	994	1179	1307	1297	1194.25	145.6053	12.1922	61.17637	0.241374	0.012365	0.017091	0.023631
31	960	1.501548	1021	1216	1100	1219	1139	96.2185	8.44763	109.484	0.230207	0.022128	0.032164	0.046799
32	1020	1.595395	1187	1132	1083	1098	1125	46.13748	4.101109	106.2346	0.227377	0.021471	0.033242	0.051511
33	1080	1.689242	1120	1177	1089	966	1088	89.12538	8.191671	103.8415	0.219899	0.020988	0.034452	0.0566
34	1140	1.783089	968	1025	1079	836	977	104.3552	10.68118	96.8968	0.197465	0.019584	0.033952	0.058903
35	1200	1.876936	888	832	873	925	879.5	38.4751	4.374656	87.11327	0.177759	0.017607	0.032177	0.058844
36	1320	2.064629	952	925	904	893	918.5	25.98076	2.828608	168.7365	0.185641	0.034104	0.067281	0.133033
37	1440	2.252323	840	822	742	783	796.75	43.56891	5.468329	160.9707	0.161034	0.032534	0.070008	0.150929
38	1560	2.440016	623	578	611	627	609.75	22.23173	3.646041	131.9955	0.123239	0.026678	0.062258	0.145523
39	1680	2.62771	362	573	504	565	501	97.65586	19.49219	104.2403	0.101259	0.021068	0.053191	0.134473
40	1800	2.815403	310	447	509	450	429	84.31291	19.65336	87.2775	0.086707	0.01764	0.04788	0.130114

SUMMARY OUTPUT

Linest		Y-int	2308.175	A =	8300.685	Mean RT =	1.198624	
Slope m	Y-int b	Slope =	-679.166	b =	1.043265	var =	1.165333	non-dim
-679.166	*2308.175*	t(n-3)	2.440016			sigma =	1.079506	non-dim
		T(n)	2.815403	Integral1 =	4525.925			
		Fls(n-3) =	651	Integral2 =	421.7978	A(adj) =	1.677678	
		Fls(n)	396.05	TotInt =	4947.723	b(adj) =	1.043265	
						Integral3 =	0.321731	
						Int2(adj) =	0.085251	
						Integral4 =	1.292518	

targetHRT =	2400	s	actualHRT =	2557.36	G2	H20	0.0125	L/s

Tube #	Time (s)	Theta	Fls#1	Fls#2	Fls#3	Fls#4	Average	StDev	%StDev	Trapezoid	C	SC*dt	St*C*dt	St*t*C*dt
0	0	0					124.375	12.55772	10.09666		0.016839			
1	120	0.046923	165	202	206	236	202.25	29.10183	14.38904	7.663176	0.027382	0.001038	3.01E-05	1.41E-06
2	240	0.093847	152	195	163	193	175.75	21.56193	12.26852	8.868521	0.023794	0.001201	8.25E-05	6.33E-06
3	360	0.14077	3053	3270	3221	3054	3149.5	112.6425	3.57652	78.016	0.426405	0.010562	0.001461	0.000203
4	480	0.187694	3988	4665	4865	4547	4516.25	375.831	8.321749	179.8515	0.611447	0.02435	0.004101	0.000704
5	600	0.234617	5190	5081	5097	5086	5113.5	51.43604	1.005887	225.9303	0.692308	0.030588	0.006503	0.001399
6	720	0.28154	5213	4984	5458	4882	5134.25	256.3986	4.993886	240.4296	0.695117	0.032551	0.008402	0.002187
7	840	0.328464	4823	4755	4856	4483	4729.25	169.4666	3.583371	231.4144	0.640285	0.031331	0.009526	0.002913
8	960	0.375387	4481	4398	4785	4307	4492.75	207.3875	4.616049	216.3638	0.608265	0.029293	0.010291	0.003632
9	1080	0.422311	4327	4566	4751	4344	4497	201.3173	4.476703	210.9148	0.608841	0.028555	0.01139	0.004559
10	1200	0.469234	4589	4555	4693	4394	4557.75	123.9499	2.719542	212.4398	0.617066	0.028762	0.012826	0.005735
11	1320	0.516157	4158	3921	4000	4218	4074.25	137.4491	3.373605	202.5214	0.551606	0.027419	0.013473	0.006636
12	1440	0.563081	4146	4243	4193	4233	4203.75	44.14654	1.05017	194.2159	0.569138	0.026295	0.014199	0.007682
13	1560	0.610004	3949	3857	3997	4087	3972.5	95.92184	2.414647	191.8287	0.53783	0.025971	0.015216	0.008929
14	1680	0.656927	3684	3897	3969	3555	3776.25	190.7833	5.052188	181.7988	0.51126	0.024613	0.015577	0.009872
15	1800	0.703851	3163	3873	3652	3719	3601.75	306.7848	8.51766	173.1004	0.487635	0.023436	0.015932	0.010844
16	1920	0.750774	3552	3682	3702	3250	3546.5	208.553	5.880529	167.7101	0.480154	0.022706	0.01651	0.012018
17	2040	0.797698	3561	3442	3336	3198	3384.25	154.4806	4.564692	162.6071	0.458188	0.022015	0.017033	0.01319
18	2160	0.844621	3568	3471	3390	3310	3434.75	110.506	3.217295	159.9853	0.465025	0.02166	0.01779	0.014624
19	2280	0.891544	3188	3260	2982	2889	3079.75	173.3482	5.628644	152.8412	0.416962	0.020693	0.017937	0.015559
20	2400	0.938468	3027	3005	2950	3078	3015	53.03458	1.759024	142.9932	0.408196	0.01936	0.017709	0.01621
21	2520	0.985391	3103	3001	3060	2959	3030.75	63.53149	2.09623	141.8435	0.410328	0.019204	0.018474	0.017782
22	2640	1.032315	2867	2828	2875	2885	2863.75	24.94494	0.871059	138.295	0.387718	0.018724	0.018877	0.019042
23	2760	1.079238	2751	2710	2869	2924	2813.5	99.84822	3.548897	133.1979	0.380915	0.018033	0.019036	0.020103
24	2880	1.126161	2825	2760	2718	2752	2763.75	44.70925	1.617702	130.8517	0.374179	0.017716	0.019531	0.021543
25	3000	1.173085	2691	2602	2724	2596	2653.25	64.12163	2.41672	127.092	0.359219	0.017207	0.019773	0.022732
26	3120	1.220008	2563	2414	2511	2453	2485.25	65.38285	2.630836	120.5579	0.336474	0.016322	0.019518	0.023348

27	3240	1.266932	2332	2436	2357	2364	2372.25	44.66449	1.88279	113.9652	0.321175	0.01543	0.019178	0.023845
28	3360	1.313855	2111	2268	2154	2255	2197	76.70289	3.491256	107.2023	0.297448	0.014514	0.018716	0.024142
29	3480	1.360778	2236	2253	2256	2177	2230.5	36.73781	1.647066	103.8767	0.301983	0.014064	0.01881	0.025166
30	3600	1.407702	2149	2099	2074	1982	2076	69.99524	3.37164	101.0378	0.281066	0.013679	0.018924	0.026187
31	3840	1.501548	2051	1953	2043	2071	2029.5	52.34183	2.57905	192.644	0.27477	0.026082	0.037925	0.055204
32	4080	1.595395	1918	1916	1943	1956	1933.25	19.51709	1.009548	185.9457	0.261739	0.025175	0.038954	0.06033
33	4320	1.689242	1819	1817	1758	1538	1733	133.0439	7.677083	172.0329	0.234628	0.023291	0.038192	0.062677
34	4560	1.783089	1667	1376	1552	1664	1564.75	136.7415	8.738875	154.7416	0.211849	0.02095	0.036323	0.063022
35	4800	1.876936	1606	1583	1582	1686	1614.25	49.10109	3.041728	149.1695	0.21855	0.020196	0.036973	0.067733
36	5280	2.064629	1535	1528	1523	1626	1553	48.91489	3.149703	297.2362	0.210258	0.040242	0.079236	0.156367
37	5760	2.252323	1376	1496	1382	1450	1426	57.48043	4.030886	279.5696	0.193064	0.03785	0.081548	0.176025
38	6240	2.440016	1322	1378	1296	1390	1346.5	44.85161	3.330977	260.1902	0.1823	0.035227	0.082553	0.193771
39	6720	2.62771	986	962	829	1040	954.25	89.64513	9.394303	215.918	0.129194	0.029233	0.073604	0.185575
40	7200	2.815403	685	652	612	613	640.5	35.02856	5.46894	149.6622	0.086716	0.020262	0.054771	0.148224

SUMMARY OUTPUT

Linest		Y-int	4169.825	A =	14740.57	Mean RT =	1.373598	
Slope m	Y-int b	Slope =	-1223.67	b =	1.033462	var =	1.244326	non-dim
-1223.67	*4169.825*	t(n-3)	2.440016			sigma =	1.115494	non-dim
		T(n)	2.815403	Integral1 =	6608.86			
		Fls(n-3) =	1184.05	Integral2 =	777.3059	A(adj) =	1.9957	
		Fls(n)	724.7	TotInt =	7386.166	b(adj) =	1.033462	
						Integral3 =	0.398118	
						Int2(adj) =	0.105238	
						Integral4 =	1.604625	

targetHRT = 600 s actualHRT = 555.84 **G3** **H2O** **0.05** **L/s**

Tube #	Time (s)	Theta	Fls#1	Fls#2	Fls#3	Fls#4	Average	StDev	%StDev	Trapezoid	C	SC*dt	St*C*dt	St*t*C*dt
0	0	0					10.375	2.825269	27.2315		0.001641			
1	30	0.053972	380	392	370	349	372.75	18.20943	4.885159	10.33908	0.058963	0.001635	8.59E-05	4.64E-06
2	60	0.107945	55	49	31	28	40.75	13.27592	32.57894	11.15879	0.006446	0.001765	0.000105	6.66E-06
3	90	0.161917	428	435	368	374	401.25	35.13189	8.755612	11.92789	0.063471	0.001887	0.000296	4.69E-05
4	120	0.215889	430	523	355	433	435.25	68.73318	15.79166	22.57394	0.06885	0.003571	0.000678	0.000132
5	150	0.269862	519	595	549	510	543.25	38.31775	7.053429	26.40598	0.085934	0.004177	0.001027	0.000255
6	180	0.323834	745	893	827	833	824.5	60.80296	7.374525	36.91035	0.130423	0.005839	0.001766	0.000538
7	210	0.377807	1188	1158	1241	1250	1209.25	43.76738	3.619382	54.88315	0.191284	0.008682	0.00309	0.001106
8	240	0.431779	2151	2210	2083	2227	2167.75	65.21439	3.008391	91.13234	0.342904	0.014416	0.005946	0.002462
9	270	0.485751	3511	3505	3330	3464	3452.5	84.29512	2.441567	151.6691	0.546132	0.023992	0.011155	0.005203
10	300	0.539724	5041	4971	4839	5045	4974	96.20118	1.934081	227.3991	0.786809	0.035971	0.018619	0.009663
11	330	0.593696	6599	6883	6181	6120	6445.75	360.9611	5.599986	308.1755	1.019617	0.048749	0.027796	0.015884
12	360	0.647668	7357	7414	6961	6752	7121	317.9654	4.465179	366.1148	1.126431	0.057914	0.036024	0.02245
13	390	0.701641	7243	7136	6826	6522	6931.75	325.4088	4.694469	379.2301	1.096494	0.059988	0.04045	0.027318
14	420	0.755613	7104	7062	6610	6535	6827.75	296.8191	4.347246	371.3164	1.080043	0.058736	0.042785	0.031208
15	450	0.809585	6265	6555	6057	6030	6226.75	242.7185	3.897996	352.2911	0.984974	0.055727	0.043543	0.034063
16	480	0.863558	6099	5633	5846	5305	5720.75	336.3078	5.878736	322.4174	0.904933	0.051001	0.042608	0.035633
17	510	0.91753	5819	5733	5527	5359	5609.5	207.1223	3.69235	305.7602	0.887335	0.048366	0.04306	0.03837
18	540	0.971503	4939	5068	4842	5062	4977.75	108.2786	2.175251	285.7095	0.787402	0.045195	0.042614	0.040214
19	570	1.025475	4277	4523	4352	4407	4389.75	103.5869	2.359745	252.7931	0.69439	0.039988	0.03986	0.039761
20	600	1.079447	3781	3946	3845	4007	3894.75	101.0623	2.594833	223.567	0.616089	0.035365	0.037163	0.039078
21	630	1.13342	3725	3746	3421	3472	3591	168.3667	4.688573	202.0118	0.56804	0.031955	0.035321	0.039065
22	660	1.187392	3446	3579	3229	3173	3356.75	189.2483	5.637843	187.4933	0.530985	0.029659	0.034389	0.039895
23	690	1.241364	2923	3265	2804	3027	3004.75	195.9666	6.521894	171.6726	0.475304	0.027156	0.032937	0.039969
24	720	1.295337	2895	2720	2735	2750	2775	80.93207	2.916471	155.9734	0.438962	0.024673	0.031267	0.039642
25	750	1.349309	2503	2588	2417	2415	2480.75	82.43128	3.322837	141.8326	0.392416	0.022436	0.029633	0.039156
26	780	1.403282	2258	2412	2217	2389	2319	96.04513	4.141661	129.5269	0.36683	0.020489	0.02818	0.038774
27	810	1.457254	1713	2087	2126	2031	1989.25	188.2487	9.463302	116.2632	0.314668	0.018391	0.026266	0.037527
28	840	1.511226	1695	1869	1892	1958	1853.5	112.1977	6.053291	103.7012	0.293195	0.016404	0.024332	0.036103

29	870	1.565199	1754	1776	1673	1327	1632.5	208.4266	12.76733	94.07383	0.258236	0.014881	0.022865	0.035142
30	900	1.619171	1499	1330	1548	1483	1465	94.15236	6.426782	83.5897	0.23174	0.013223	0.021034	0.033468
31	960	1.727116	1333	1164	1408	1349	1313.5	104.7553	7.975278	149.9622	0.207775	0.023722	0.03962	0.066242
32	1020	1.83506	1312	1209	1262	1241	1256	43.22808	3.441726	138.682	0.19868	0.021937	0.039046	0.069561
33	1080	1.943005	1139	827	1023	1032	1005.25	129.9907	12.93118	122.045	0.159015	0.019306	0.036353	0.068511
34	1140	2.05095	943	702	932	844	855.25	111.3594	13.02068	100.4156	0.135287	0.015884	0.031651	0.063115
35	1200	2.158895	717	706	685	715	705.75	14.63728	2.074004	84.25086	0.111639	0.013327	0.027984	0.058797
36	1320	2.374784	625	491	684	626	606.5	81.79038	13.48564	141.6505	0.095939	0.022407	0.05061	0.114571
37	1440	2.590674	480	374	479	448	445.25	49.76863	11.17768	113.5309	0.070432	0.017959	0.04429	0.109431
38	1560	2.806563	337	271	316	290	303.5	28.9655	9.543821	80.82362	0.048009	0.012785	0.034241	0.091846
39	1680	3.022453	240	194	209	192	208.75	22.17168	10.62116	55.29469	0.033021	0.008747	0.025318	0.073382
40	1800	3.238342	133	106	156	178	143.25	30.89094	21.56435	37.99655	0.02266	0.00601	0.018694	0.058213

SUMMARY OUTPUT

Linest		Y-int	1853.35	A =	28597.72	Mean RT =	1.137916	
Slope m	Y-int b	Slope =	-538.702	b =	1.577688	var =	0.464773	non-dim
-538.702	*1853.35*	t(n-3)	2.806563			sigma =	0.681743	non-dim
		T(n)	3.238342	Integral1 =	6212.226			
		Fls(n-3) =	341.45	Integral2 =	109.5114	A(adj) =	4.523712	
		Fls(n)	108.85	TotInt =	6321.737	b(adj) =	1.577688	
						Integral3 =	0.067078	
						Int2(adj) =	0.017323	
						Integral4 =	0.266697	

targetHRT = 2400 s actualHRT = 2223.36 **G3 H2O 0.0125 L/s**

Tube #	Time (s)	Theta	Fls#1	Fls#2	Fls#3	Fls#4	Average	StDev	%StDev	Trapezoid	C	SC*dt	St*C*dt	St*t*C*dt
0	0	0					28.5	3.422614	12.00917		0.003974			
1	120	0.053972	258	282	213	173	231.5	48.36321	20.89124	7.016408	0.032277	0.000978	4.7E-05	2.54E-06
2	240	0.107945	27	29	29	21	26.5	3.785939	14.28656	6.962435	0.003695	0.000971	5.78E-05	3.7E-06
3	360	0.161917	225	265	274	237	250.25	23.05609	9.213223	7.468426	0.034891	0.001041	0.000163	2.58E-05
4	480	0.215889	229	271	290	244	258.5	27.25803	10.54469	13.72922	0.036041	0.001914	0.000362	7E-05
5	600	0.269862	331	299	239	306	293.75	38.99893	13.27623	14.90312	0.040956	0.002078	0.000508	0.000126
6	720	0.323834	381	357	278	364	345	45.78937	13.27228	17.23742	0.048101	0.002403	0.000719	0.000217
7	840	0.377807	1069	1036	947	1048	1025	53.75872	5.244753	36.97107	0.14291	0.005155	0.001877	0.000687
8	960	0.431779	1951	1921	1822	1925	1904.75	56.74725	2.979249	79.06277	0.265569	0.011023	0.004551	0.001887
9	1080	0.485751	3475	3432	3509	3459	3468.75	32.17012	0.927427	145.0103	0.483629	0.020218	0.009434	0.004416
10	1200	0.539724	4639	4654	4797	4654	4686	74.33707	1.586365	220.0656	0.653343	0.030683	0.015856	0.008216
11	1320	0.593696	5501	5282	5648	5439	5467.5	151.5751	2.772292	274.0042	0.762304	0.038203	0.021729	0.012387
12	1440	0.647668	6812	7100	6793	6445	6787.5	268.0752	3.949543	330.7157	0.946344	0.04611	0.028754	0.017964
13	1560	0.701641	7026	7360	6958	7333	7169.25	206.8387	2.885081	376.6394	0.999569	0.052513	0.035467	0.023992
14	1680	0.755613	7398	7359	6293	7402	7113	547.0107	7.690295	385.4234	0.991727	0.053737	0.039149	0.02856
15	1800	0.809585	7163	6761	7506	7003	7108.25	312.4435	4.395505	383.7773	0.991064	0.053508	0.041875	0.03281
16	1920	0.863558	6280	6505	6728	6288	6450.25	212.4875	3.294251	365.8922	0.899323	0.051014	0.04261	0.035628
17	2040	0.91753	6018	5847	5958	5802	5906.25	99.23835	1.680226	333.4548	0.823476	0.046492	0.041348	0.036807
18	2160	0.971503	5807	5713	5831	5700	5762.75	65.90081	1.143565	314.9018	0.803469	0.043905	0.041454	0.039173
19	2280	1.025475	5256	5321	5108	5212	5224.25	89.50372	1.713236	296.4972	0.728389	0.041339	0.041222	0.041135
20	2400	1.079447	4821	4726	4494	4673	4678.5	137.396	2.936754	267.2374	0.652298	0.037259	0.039159	0.041182
21	2520	1.13342	4447	4396	4367	3849	4264.75	279.1324	6.545107	241.3442	0.594611	0.033649	0.037189	0.041125
22	2640	1.187392	3905	4064	3791	3698	3864.5	157.6547	4.079562	219.3774	0.538806	0.030587	0.035452	0.041114
23	2760	1.241364	3797	3727	3598	3653	3693.75	86.7847	2.349501	203.9683	0.514999	0.028438	0.034517	0.041917
24	2880	1.295337	3411	3454	3370	2885	3280	265.5573	8.096258	188.1949	0.457312	0.026239	0.033238	0.042124
25	3000	1.349309	3044	3022	2940	2927	2983.25	58.38593	1.957125	169.0212	0.415938	0.023566	0.031131	0.041143
26	3120	1.403282	2359	2345	2597	2786	2521.75	210.7279	8.356415	148.5589	0.351594	0.020713	0.02846	0.03912
27	3240	1.457254	2463	2362	2459	2530	2453.5	69.1496	2.818406	134.263	0.342078	0.01872	0.026767	0.038288
28	3360	1.511226	2352	2375	2268	2314	2327.25	46.82859	2.012186	129.0142	0.324476	0.017988	0.026685	0.039601

29	3480	1.565199	2187	2166	2134	2156	2160.75	22.02082	1.019129	121.114	0.301262	0.016886	0.025958	0.039915
30	3600	1.619171	1908	1912	1846	1805	1867.75	51.60346	2.762867	108.7138	0.26041	0.015157	0.024104	0.038341
31	3840	1.727116	1665	1732	1326	1257	1495	238.2394	15.93574	181.4956	0.20844	0.025305	0.042187	0.070406
32	4080	1.83506	1565	1498	1237	1069	1342.25	230.6648	17.18494	153.1331	0.187143	0.021351	0.037965	0.067571
33	4320	1.943005	1189	1250	1302	1187	1232	55.06965	4.469939	138.9384	0.171771	0.019371	0.036548	0.069013
34	4560	2.05095	946	1001	939	718	901	125.1106	13.88575	115.1231	0.125622	0.016051	0.031919	0.06352
35	4800	2.158895	845	794	828	612	769.75	107.2827	13.93735	90.17433	0.107322	0.012573	0.026411	0.055517
36	5280	2.374784	712	735	704	627	694.5	46.87928	6.750076	158.0581	0.09683	0.022037	0.049832	0.112942
37	5760	2.590674	565	576	436	607	546	75.4586	13.82026	133.9054	0.076126	0.01867	0.046111	0.114099
38	6240	2.806563	375	425	490	450	435	48.13176	11.06477	105.8938	0.06065	0.014764	0.039663	0.10672
39	6720	3.022453	337	304	501	328	367.5	90.08329	24.51246	86.62565	0.051239	0.012078	0.035091	0.102094
40	7200	3.238342	351	327	370	355	350.75	17.82087	5.080789	77.5313	0.048903	0.01081	0.033812	0.105885

SUMMARY OUTPUT

Linest		Y-int	1604.55	A =	5027.706	Mean RT =	1.333966	
Slope m	Y-int b	Slope =	-401.131	b =	0.837872	var =	0.982339	non-dim
-401.131	*1604.55*	t(n-3)	2.806563			sigma =	0.99113	non-dim
		T(n)	3.238342	Integral1 =	6774.402			
		Fls(n-3) =	478.75	Integral2 =	397.9367	A(adj) =	0.700985	
		Fls(n)	305.55	TotInt =	7172.339	b(adj) =	0.837872	
						Integral3 =	0.245888	
						Int2(adj) =	0.055482	
						Integral4 =	1.168768	

targetHRT = 600 s actualHRT = 496.58 **G4 H2O 0.05 L/s**

Tube #	Time (s)	Theta	Fls#1	Fls#2	Fls#3	Fls#4	Average	StDev	%StDev	Trapezoid	C	SC*dt	St*C*dt	St*t*C*dt
0	0	0					22.5	3.070598	13.6471		0.002966			
1	30	0	174	160	188	142	166	19.66384	11.84569	0	0.021885	0	0	0
2	60	0.060413	32	51	32	35	37.5	9.110434	24.29449	6.147045793	0.004944	0.00081	9.02E-06	5.45E-07
3	90	0.120826	229	289	199	222	234.75	38.36991	16.34501	8.223750453	0.030949	0.001084	0.000122	1.42E-05
4	120	0.18124	263	345	223	194	256.25	65.58137	25.59273	14.8314471	0.033784	0.001955	0.000298	4.72E-05
5	150	0.241653	299	385	290	236	302.5	61.63603	20.37555	16.87794514	0.039881	0.002225	0.000476	0.000104
6	180	0.302066	286	351	196	324	289.25	67.64306	23.38567	17.87476338	0.038135	0.002357	0.000639	0.000175
7	210	0.362479	465	524	433	509	482.75	41.55619	8.608221	23.31950542	0.063646	0.003074	0.001045	0.000358
8	240	0.422893	344	440	391	410	396.25	40.25233	10.15832	26.55161303	0.052241	0.003501	0.001364	0.000535
9	270	0.483306	901	1060	933	865	939.75	84.8425	9.028199	40.35603528	0.123896	0.005321	0.002476	0.001156
10	300	0.543719	1843	1804	1764	1848	1814.75	39.13545	2.15652	83.20411615	0.239256	0.01097	0.005738	0.003011
11	330	0.604132	3419	3402	3286	3344	3362.75	60.40626	1.796335	156.39474	0.443344	0.020619	0.01202	0.007024
12	360	0.664545	6275	6187	5995	6070	6131.75	123.9445	2.021357	286.7966894	0.808407	0.037811	0.024318	0.015672
13	390	0.724959	9210	8542	8228	8308	8572	445.7114	5.19962	444.1504893	1.130129	0.058557	0.040976	0.028725
14	420	0.785372	10644	10579	10596	10128	10486.7	240.7452	2.295708	575.70029	1.382569	0.0759	0.057547	0.043701
15	450	0.845785	12135	12095	12866	12086	12295.5	380.9291	3.098118	688.1746144	1.621033	0.090729	0.074214	0.060788
16	480	0.906198	12096	12346	12364	11790	12149	268.7775	2.212342	738.3855572	1.601719	0.097348	0.085259	0.074759
17	510	0.966612	10901	11123	11515	11090	11157.2	257.7756	2.310386	704.0028797	1.470967	0.092815	0.086794	0.081247
18	540	1.027025	10061	9919	10343	9870	10048.2	212.5392	2.115186	640.5463369	1.324757	0.084449	0.084047	0.083724
19	570	1.087438	8511	8602	8484	8463	8515	61.23724	0.719169	560.7329131	1.122614	0.073927	0.077973	0.082308
20	600	1.147851	7330	7158	6878	7140	7126.5	186.4931	2.616896	472.4767409	0.939555	0.062291	0.069452	0.077493
21	630	1.208265	5590	5311	5453	5234	5397	157.4272	2.91694	378.2925208	0.711538	0.049874	0.058546	0.068771
22	660	1.268678	4767	4762	4555	4564	4662	118.4314	2.540356	303.8483225	0.614636	0.040059	0.049524	0.061261
23	690	1.329091	3936	3960	3527	3850	3818.25	199.8272	5.233477	256.1596319	0.503396	0.033772	0.043764	0.056744
24	720	1.389504	3289	3179	2660	2782	2977.5	303.678	10.19909	205.2765919	0.392552	0.027064	0.036686	0.049755
25	750	1.449917	2633	2550	2536	2542	2565.25	45.52929	1.774848	167.4277055	0.338201	0.022074	0.031289	0.04437
26	780	1.510331	2237	2163	1958	1614	1993	278.8679	13.99237	137.6892948	0.262756	0.018153	0.0268	0.039582
27	810	1.570744	1802	1687	1588	1398	1618.75	171.1868	10.57525	109.0987353	0.213415	0.014384	0.022113	0.03401
28	840	1.631157	1472	1504	1393	1329	1424.5	78.92824	5.540768	91.92627573	0.187805	0.01212	0.019379	0.030999
29	870	1.69157	1197	1204	1137	871	1102.25	157.0719	14.25012	76.32455999	0.14532	0.010063	0.016679	0.027654

30	900	1.751984	1084	1044	996	1066	1047.5	38.03069	3.630615	64.9366668	0.138102	0.008561	0.014734	0.025365
31	930	1.812397	1	1	0	0	0.5	0.57735	115.4701	31.65653067	6.59E-05	0.004174	0.007312	0.012811
32	960	1.87281	858	771	679	798	776.5	74.47818	9.591524	23.47053848	0.102373	0.003094	0.005795	0.010853
33	990	1.933223	567	590	395	566	529.5	90.34932	17.06314	39.44983688	0.069809	0.005201	0.009868	0.018727
34	1020	1.993636	534	479	378	512	475.75	68.97524	14.49821	30.36519795	0.062723	0.004003	0.007854	0.015411
35	1050	2.05405	443	392	367	421	405.75	33.22022	8.187363	26.62712957	0.053494	0.003511	0.007096	0.014348
36	1080	2.114463	354	354	393	374	368.75	18.71497	5.075245	23.39502195	0.048616	0.003084	0.006424	0.013383
37	1110	2.174876	278	290	287	285	285	5.09902	1.78913	19.7475734	0.037574	0.002604	0.005574	0.011934
38	1140	2.235289	254	276	302	262	273.5	21.0634	7.701425	16.87039349	0.036058	0.002224	0.004903	0.010811
39	1170	2.295703	210	197	116	185	177	41.92851	23.68842	13.60807926	0.023336	0.001794	0.004053	0.009157
40	1200	2.356116	173	171	181	168	173.25	5.560276	3.209394	10.57986629	0.022841	0.001395	0.003244	0.007545

SUMMARY OUTPUT

Linest		Y-int	2101.8	A =	351317.4	Mean RT =	1.025198364	
Slope m	Y-int b	Slope =	-825.978	b =	3.232791	var =	0.124068902	non-dim
-825.978	*2101.8*	t(n-3)	2.235289			sigma =	0.352234157	non-dim
		T(n)	2.356116	Integral1 =	7531.498			
		Fls(n-3) =	255.5	Integral2 =	53.47798	A(adj) =	46.31754282	
		Fls(n)	155.7	TotInt =	7584.976	b(adj) =	3.232790868	
						Integral3 =	0.018792765	
						Int2(adj) =	0.007050514	
						Integral4 =	0.050765731	

targetHRT = 2400 s actualHRT = 1986.32 **G4** **H2O** **0.0125** **L/s**

Tube #	Time (s)	Theta	Fls#1	Fls#2	Fls#3	Fls#4	Average	StDev	%StDev	Trapezoid	C	SC*dt	St*C*dt	St*t*C*dt
0	0	0					54.75	5.230406	9.553252		0.006633			
1	120	0	22	20	29	28	24.75	4.425306	17.88002	0	0.002999	0	0	0
2	240	0.060413	100	24	27	29	45	36.7242	81.60933	2.106911	0.005452	0.000255	9.95E-06	6.01E-07
3	360	0.120826	148	191	145	218	175.5	35.27511	20.09978	6.660558	0.021263	0.000807	8.76E-05	9.98E-06
4	480	0.18124	171	186	147	176	170	16.55295	9.737027	10.43638	0.020596	0.001264	0.00019	2.98E-05
5	600	0.241653	158	181	169	187	173.75	12.8938	7.42089	10.38352	0.021051	0.001258	0.000266	5.76E-05
6	720	0.302066	200	210	195	216	205.25	9.5	4.628502	11.44831	0.024867	0.001387	0.000381	0.000106
7	840	0.362479	219	263	219	270	242.75	27.57263	11.35845	13.53256	0.02941	0.00164	0.000549	0.000185
8	960	0.422893	218	231	250	250	237.25	15.64981	6.596339	14.49917	0.028744	0.001757	0.000689	0.000272
9	1080	0.483306	364	350	366	346	356.5	9.983319	2.80037	17.93518	0.043192	0.002173	0.000998	0.00046
10	1200	0.543719	438	489	468	492	471.75	24.90482	5.279241	25.01863	0.057155	0.003031	0.001569	0.000815
11	1320	0.604132	761	701	802	878	785.5	74.31689	9.461093	37.97726	0.095167	0.004601	0.002675	0.00156
12	1440	0.664545	1385	1700	2095	2187	1841.75	370.6061	20.1225	79.36032	0.223137	0.009615	0.006216	0.004026
13	1560	0.724959	5153	5251	5410	5779	5398.25	275.0386	5.094959	218.6959	0.654024	0.026496	0.018801	0.01336
14	1680	0.785372	10498	10050	11163	10496	10551.75	458.758	4.347696	481.7955	1.278395	0.058372	0.04465	0.034202
15	1800	0.845785	16130	15586	17332	16150	16299.5	736.2561	4.517047	811.0853	1.974762	0.098267	0.08078	0.06649
16	1920	0.906198	18899	18245	19416	17249	18452.25	934.3737	5.063739	1049.733	2.235578	0.12718	0.111647	0.098126
17	2040	0.966612	17669	17923	18201	18122	17978.75	237.3245	1.320028	1100.457	2.178212	0.133326	0.124794	0.116931
18	2160	1.027025	15047	14626	15013	14682	14842	218.7251	1.47369	991.4037	1.798179	0.120113	0.119384	0.118768
19	2280	1.087438	11096	10820	10753	10851	10880	149.6952	1.375875	776.9745	1.318164	0.094134	0.099084	0.104377
20	2400	1.147851	8057	7912	8085	8123	8044.25	92.22211	1.146435	571.6375	0.974599	0.069257	0.077091	0.085873
21	2520	1.208265	5769	5262	5804	5900	5683.75	286.5686	5.041894	414.6764	0.688613	0.05024	0.058925	0.069155
22	2640	1.268678	3854	3608	4030	4101	3898.25	219.5972	5.633224	289.4398	0.472292	0.035067	0.043232	0.053329
23	2760	1.329091	3111	2973	3179	3058	3080.25	86.97653	2.823684	210.7969	0.373187	0.025539	0.033082	0.042875
24	2880	1.389504	2461	2176	2445	2679	2440.25	205.9796	8.440921	166.7556	0.295648	0.020203	0.027391	0.037155
25	3000	1.449917	2021	1423	1821	2129	1848.5	311.0429	16.82677	129.5486	0.223955	0.015695	0.022218	0.031464
26	3120	1.510331	1700	1785	1830	1862	1794.25	70.32484	3.919456	110.0351	0.217382	0.013331	0.019726	0.0292
27	3240	1.570744	1362	1286	1399	1342	1347.25	47.16902	3.501134	94.89408	0.163226	0.011497	0.017662	0.027143
28	3360	1.631157	1094	1006	1135	1162	1099.25	68.16341	6.200901	73.90048	0.133179	0.008953	0.014307	0.022868

29	3480	1.69157	1096	978	1022	1018	1028.5	49.19011	4.782704	64.27212	0.124608	0.007787	0.012929	0.021474
30	3600	1.751984	811	787	818	749	791.25	31.13813	3.935309	54.96848	0.095864	0.00666	0.01144	0.019659
31	3720	1.812397	672	483	662	637	613.5	88.23642	14.38247	42.43274	0.074328	0.005141	0.009142	0.016263
32	3840	1.87281	677	475	755	667	643.5	119.0224	18.4961	37.96971	0.077963	0.0046	0.00848	0.015635
33	3960	1.933223	535	475	594	601	551.25	58.82389	10.671	36.08935	0.066787	0.004372	0.008311	0.0158
34	4080	1.993636	509	379	535	458	470.25	68.72833	14.61527	30.85606	0.056973	0.003738	0.007331	0.01438
35	4200	2.05405	422	361	467	468	429.5	50.4546	11.74729	27.1784	0.052036	0.003293	0.00666	0.013472
36	4320	2.114463	402	393	430	438	415.75	21.63909	5.204831	25.53214	0.05037	0.003093	0.006446	0.013434
37	4440	2.174876	393	371	321	348	358.25	30.89094	8.622732	23.37992	0.043404	0.002833	0.006069	0.013004
38	4560	2.235289	364	357	358	366	361.25	4.425306	1.224998	21.73366	0.043767	0.002633	0.005807	0.012807
39	4680	2.295703	235	267	266	295	265.75	24.5136	9.224309	18.93955	0.032197	0.002295	0.005188	0.011731
40	4800	2.356116	265	252	285	254	264	15.12173	5.727927	16.00195	0.031985	0.001939	0.004509	0.010489

SUMMARY OUTPUT

Linest		Y-int	1798.2	A =	27123.14	Mean RT =	1.064992	
Slope m	Y-int b	Slope =	-655.486	b =	1.968425	var =	0.139493	non-dim
-655.486	*1798.2*	t(n-3)	2.235289			sigma =	0.373488	non-dim
		T(n)	2.356116	Integral1 =	8120.542			
		Fls(n-3) =	333	Integral2 =	133.3625	A(adj) =	3.286098	
		Fls(n)	253.8	TotInt =	8253.904	b(adj) =	1.968425	
						Integral3 =	0.046277	
						Int2(adj) =	0.016158	
						Integral4 =	0.136714	

targetHRT =	600	s	actualHRT =	639.34		G1	XG	0.05	L/s

Tube #	Time (s)	Theta	Fls#1	Fls#2	Fls#3	Fls#4	Average	StDev	%StDev	Trapezoid	C	SC*dt	St*C*dt	St*t*C*dt
0	0	0					1.25	1.581139	126.4911		0.000238			
1	30	0.046923	18	4	6	12	10	6.324555	63.24555	0.263944	0.001907	5.03E-05	2.1E-06	9.85E-08
2	60	0.093847	22	16	12	25	18.75	5.85235	31.21253	0.674524	0.003575	0.000129	9.97E-06	8.37E-07
3	90	0.14077	26	17	12	23	19.5	6.244998	32.02563	0.89741	0.003718	0.000171	2.02E-05	2.47E-06
4	120	0.187694	22	31	6	16	18.75	10.5	56	0.89741	0.003575	0.000171	2.8E-05	4.68E-06
5	150	0.234617	17	124	14	17	43	54.01852	125.6245	1.44876	0.008199	0.000276	6.09E-05	1.35E-05
6	180	0.28154	9920	9013	6962	8269	8541	1250.553	14.64177	201.3952	1.628479	0.038399	0.010802	0.003039
7	210	0.328464	8423	8316	6939	7369.5	7761.875	724.6199	9.33563	382.4931	1.479926	0.072928	0.022162	0.006775
8	240	0.375387	6926	7619	6916	6470	6982.75	474.4831	6.795076	345.9339	1.331373	0.065958	0.02313	0.008148
9	270	0.422311	6336	6933	6372	5787	6357	468.0961	7.363476	312.9731	1.212064	0.059673	0.023735	0.009473
10	300	0.469234	5462	5700	5376	4996	5383.5	292.4306	5.43198	275.452	1.026451	0.052519	0.023309	0.010374
11	330	0.516157	4514	5267	3776	4401	4489.5	611.5611	13.62203	231.6373	0.855995	0.044165	0.021666	0.010653
12	360	0.563081	4075	4866	4198	4335	4368.5	348.2533	7.971919	207.8237	0.832925	0.039625	0.02137	0.011546
13	390	0.610004	3720	4683	4110	4282	4198.75	399.3773	9.511815	201.0022	0.800559	0.038324	0.022461	0.013185
14	420	0.656927	3801	4588	3770	3829	3997	394.7362	9.875812	192.2862	0.762092	0.036662	0.023203	0.014705
15	450	0.703851	3618	3988	3987	3392	3746.25	293.4534	7.833258	181.6698	0.714283	0.034638	0.023541	0.016018
16	480	0.750774	3551	3666	3507	3512	3559	73.9955	2.079109	171.3935	0.67858	0.032679	0.023748	0.017276
17	510	0.797698	3504	3177	3084	3292	3264.25	181.0642	5.546886	160.085	0.622382	0.030523	0.023601	0.018266
18	540	0.844621	3468	3132	2797	3216	3153.25	277.1105	8.788093	150.5654	0.601218	0.028708	0.023562	0.019354
19	570	0.891544	3461	3286	2613	3041	3100.25	367.6805	11.8597	146.7177	0.591112	0.027974	0.024278	0.021086
20	600	0.938468	2864	3134	2345	2602	2736.25	339.4234	12.40469	136.9342	0.52171	0.026109	0.023851	0.021804
21	630	0.985391	2481	2755	2190	2088	2378.5	301.2092	12.66383	120.0007	0.453499	0.02288	0.021971	0.021111
22	660	1.032315	2383	2377	2089	2025	2218.5	188.3215	8.488688	107.8534	0.422993	0.020564	0.020729	0.020907
23	690	1.079238	2281	2285	2157	2000	2180.75	134.3537	6.160894	103.2139	0.415795	0.019679	0.020773	0.021938
24	720	1.126161	2083	1932	2218	2396	2157.25	197.4359	9.152201	101.7768	0.411314	0.019405	0.021396	0.023601
25	750	1.173085	1911	2086	1782	1735	1878.5	157.0743	8.361687	94.68554	0.358166	0.018053	0.020725	0.023803
26	780	1.220008	1933	1936	1734	1650	1813.25	144.1513	7.949883	86.61471	0.345725	0.016514	0.019754	0.023637
27	810	1.266932	1677	1623	1554	1628	1620.5	50.58656	3.121664	80.56159	0.308974	0.01536	0.01908	0.023709

28	840	1.313855	1435	1568	1471	1350	1456	90.26997	6.19986	72.1799	0.27761	0.013762	0.017741	0.022879
29	870	1.360778	1516	1689	1460	1390	1513.75	127.6985	8.435907	69.67537	0.288621	0.013285	0.017772	0.023782
30	900	1.407702	1428	1405	1329	1153	1328.75	124.5696	9.374946	66.68987	0.253348	0.012715	0.017582	0.024318
31	930	1.454625	1116	1282	991	836	1056.25	189.1214	17.90499	55.95614	0.201391	0.010669	0.01524	0.021776
32	960	1.501548	1054	1091	922	921	997	88.47975	8.874599	48.17272	0.190094	0.009185	0.01357	0.020053
33	990	1.548472	928	1097	998	884	976.75	92.89914	9.511046	46.30752	0.186233	0.008829	0.013463	0.020532
34	1020	1.595395	937	1076	926	865	951	89.14782	9.374113	45.22828	0.181323	0.008623	0.013553	0.021305
35	1050	1.642319	913	758	841	832	836	63.3877	7.58226	41.92605	0.159397	0.007994	0.012929	0.020915
36	1080	1.689242	804	801	750	735	772.5	35.19943	4.556561	37.73814	0.14729	0.007195	0.011979	0.019948
37	1110	1.736165	811	760	716	684	742.75	55.14451	7.42437	35.55033	0.141617	0.006778	0.011606	0.019876
38	1140	1.783089	807	786	741	679	753.25	56.64142	7.519604	35.0987	0.143619	0.006692	0.011777	0.020728
39	1170	1.830012	700	691	680	621	673	35.61835	5.292474	33.46224	0.128318	0.00638	0.011518	0.020795
40	1200	1.876936	737	647	588	565	634.25	76.71321	12.09511	30.6703	0.12093	0.005848	0.010835	0.020077

SUMMARY OUTPUT

Linest		Y-int	2030.9	A =	4502.176	Mean RT =	0.999883	
Slope m	Y-int b	Slope =	-737.905	b =	1.031818	var =	0.721888	non-dim
-737.905	*2030.9*	t(n-3)	1.783089			sigma =	0.84964	non-dim
		T(n)	1.876936	Integral1 =	4615.643			
		Fls(n-3) =	715.15	Integral2 =	629.1293	A(adj) =	0.858412	
		Fls(n)	645.9	TotInt =	5244.772	b(adj) =	1.031818	
						Integral3 =	0.3414	
						Int2(adj) =	0.119954	
						Integral4 =	1.084327	

HRT = 600 s actualHRT = 555.84 **G2** **XG** **0.05** **L/s**

Tube #	Time (s)	Theta	Fls#1	Fls#2	Fls#3	Fls#4	Average	StDev	%StDev	Trapezoid	C	SC*dt	St*C*dt	St*t*C*dt
0	0	0					0.625	1.06066	169.7056		0.000202			
1	60	0	19	7	3	6	8.75	7.041543	80.47478	0	0.002822	0	0	0
2	120	0.107945	8	7	5	64	21	28.69379	136.6371	1.605678	0.006773	0.000518	3.95E-05	4.26E-06
3	135	0.215889	6	5	6	9	6.5	1.732051	26.64694	1.48424	0.002096	0.000479	6.39E-05	9.53E-06
4	150	0.242876	5483	5789	5611	5416	5574.75	164.1511	2.944546	75.30832	1.797867	0.024287	0.005898	0.001432
5	165	0.269862	9013	9640	9258	9914	9456.25	399.6135	4.225919	202.8147	3.049658	0.065408	0.016996	0.004428
6	180	0.296848	7630	7224	7411	7157	7355.5	212.2302	2.885327	226.8425	2.372162	0.073157	0.020606	0.005817
7	195	0.323834	2	0	1	0	6020.25	0.957427	0.015903	180.4802	1.941541	0.058205	0.017985	0.005568
8	210	0.35082	5080	4663	4275	4722	4685	329.6352	7.035969	144.4469	1.510921	0.046584	0.015636	0.005256
9	225	0.377807	5203	4771	4702	4686	4840.5	244.4647	5.050402	128.5284	1.56107	0.041451	0.01511	0.005516
10	240	0.404793	4286	4692	4859	4595	4608	240.7696	5.225035	127.4895	1.486088	0.041116	0.016075	0.006292
11	255	0.431779	3629	4650	3570	3810	3914.75	500.6898	12.78983	114.9982	1.262514	0.037087	0.015472	0.006462
12	270	0.458765	3336	3432	3189	3576	3383.25	162.7828	4.811434	98.47258	1.091104	0.031758	0.01411	0.006274
13	285	0.485751	3069	3395	3229	3174	3216.75	136.1136	4.231402	89.0544	1.037408	0.02872	0.013554	0.006401
14	300	0.512737	2829	3094	2610	3055	2897	224.177	7.738247	82.49339	0.934288	0.026604	0.013263	0.006617
15	330	0.539724	2664	2926	2410	2722	2680.5	212.4735	7.926638	75.25772	0.864466	0.024271	0.012759	0.006712
16	360	0.593696	2236	2794	1939	2292	2315.25	354.7707	15.32321	134.8162	0.746672	0.043478	0.024554	0.013898
17	390	0.647668	1809	2247	2068	1715	1959.75	242.8022	12.38945	115.3659	0.632023	0.037206	0.023009	0.014257
18	420	0.701641	1802	1808	1712	1787	1777.25	44.3875	2.497538	100.8474	0.573166	0.032523	0.021899	0.014769
19	450	0.755613	1398	1690	1308	1494	1472.5	163.6857	11.11617	87.69835	0.474884	0.028283	0.020536	0.014932
20	480	0.809585	1203	1309	1123	1217	1213	76.22773	6.284232	72.47139	0.391195	0.023372	0.01823	0.014236
21	510	0.863558	1059	1159	1023	1167	1102	72.02777	6.536096	62.47301	0.355397	0.020148	0.016829	0.014071
22	540	0.91753	1048	1094	1047	957	1036.5	57.35562	5.533586	57.70995	0.334273	0.018612	0.016559	0.014746
23	570	0.971503	1022	1048	1000	1110	1045	47.5675	4.551913	56.17174	0.337014	0.018115	0.017112	0.016178
24	600	1.025475	932	913	955	1061	965.25	66.10282	6.848259	54.24897	0.311295	0.017495	0.01745	0.017418
25	660	1.079447	884	817	779	905	846.25	58.4658	6.90881	48.88547	0.272917	0.015766	0.016565	0.017416
26	720	1.187392	833	749	720	723	756.25	52.79757	6.981497	86.49072	0.243892	0.027893	0.03153	0.035723
27	780	1.295337	762	675	543	650	657.5	90.17206	13.71438	76.30343	0.212045	0.024608	0.030455	0.037762

28	840	1.403282	655	657	496	610	604.5	75.51821	12.49267	68.11313	0.194952	0.021967	0.02959	0.039923
29	900	1.511226	511	607	507	517	535.5	47.84349	8.934359	61.5285	0.1727	0.019843	0.028852	0.042007
30	960	1.619171	475	566	393	427	465.25	75.11935	16.14602	54.01285	0.150044	0.017419	0.027199	0.042519
31	1020	1.727116	412	389	308	427	384	53.02201	13.80781	45.83603	0.123841	0.014782	0.024656	0.041169
32	1080	1.83506	350	381	345	340	354	18.45716	5.213886	39.83161	0.114166	0.012846	0.022851	0.040687
33	1140	1.943005	283	328	294	316	305.25	20.45116	6.699807	35.58128	0.098444	0.011475	0.021631	0.040808
34	1200	2.05095	295	292	273	310	292.5	15.19868	5.196131	32.26198	0.094332	0.010405	0.020766	0.041475

SUMMARY OUTPUT

Linest		Y-int	1081.425	A =	2667.641	Mean RT =	0.857459	
Slope m	Y-int b	Slope =	-393.025	b =	1.09113	var =	0.656927	non-dim
-393.025	*1081.425*	t(n-3)	1.83506			sigma =	0.81051	non-dim
		T(n)	2.05095	Integral1 =	2839.925			
		Fls(n-3) =	360.2	Integral2 =	260.8333	A(adj) =	0.860319	
		Fls(n)	275.35	TotInt =	3100.758	b(adj) =	1.09113	
						Integral3 =	0.249618	
						Int2(adj) =	0.084119	
						Integral4 =	0.811379	

HRT = 600 s actualHRT = 555.84 **G3** **XG** **0.05 L/s**

Tube #	Time (s)	Theta	Fls#1	Fls#2	Fls#3	Fls#4	Average	StDev	%StDev	Trapezoid	C	SC*dt	St*C*dt	St*t*C*dt
0	0	0					0.75	1.164965	155.3286		0.000244			
1	60	0.107945	16	23	13	14	16.5	4.50925	27.32879	0.931023	0.005374	0.000303	3.13E-05	3.38E-06
2	120	0.215889	13	17	12	34	19	10.23067	53.84565	1.916019	0.006189	0.000624	0.000103	1.89E-05
3	135	0.242876	12	14	11	83	30	35.35534	117.8511	0.661161	0.009772	0.000215	5.01E-05	1.17E-05
4	150	0.269862	8	11	11	20	12.5	5.196152	41.56922	0.573456	0.004072	0.000187	4.68E-05	1.18E-05
5	165	0.296848	10	15	9	57	22.75	22.98369	101.0272	0.475631	0.00741	0.000155	4.45E-05	1.28E-05
6	180	0.323834	12	12	9	7	10	2.44949	24.4949	0.441899	0.003257	0.000144	4.39E-05	1.34E-05
7	195	0.35082	10	29	9	17	16.25	9.215024	56.70784	0.354194	0.005293	0.000115	3.93E-05	1.34E-05
8	210	0.377807	13	26	12	18	17.25	6.396614	37.08182	0.452019	0.005619	0.000147	5.37E-05	1.96E-05
9	225	0.404793	15	16	11	18	15	2.94392	19.62614	0.435152	0.004886	0.000142	5.53E-05	2.16E-05
10	240	0.431779	1371	1315	1352	1442	1370	53.33542	3.893096	18.68793	0.446238	0.006087	0.002626	0.001133
11	255	0.458765	4853	5945	4753	4750	5075.25	581.8055	11.46358	86.96635	1.653116	0.028327	0.012833	0.005817
12	270	0.485751	6473	6346	5452	5697	5992	495.0764	8.26229	149.3314	1.951721	0.04864	0.023025	0.010908
13	285	0.512737	6191	6004	5481	5334	5752.5	410.0362	7.127965	158.4696	1.873711	0.051617	0.025755	0.01286
14	300	0.539724	6073	5699	5113	4293	5294.5	775.8065	14.65306	149.0582	1.72453	0.048551	0.025522	0.013425
15	315	0.56671	5436	4448	4184	4243	4577.75	583.2452	12.74087	133.2072	1.49107	0.043388	0.023961	0.01324
16	330	0.593696	5312	4268	4192	3668	4360	688.4417	15.78995	120.5979	1.420144	0.039281	0.022778	0.013216
17	345	0.620682	4156	3440	3304	3714	3653.5	375.8985	10.28872	108.1269	1.190022	0.035219	0.021343	0.01294
18	360	0.647668	3631	3200	3161	2910	3225.5	299.322	9.279864	92.81898	1.050613	0.030233	0.019148	0.012132
19	375	0.674655	3573	3080	2897	3037	3146.75	294.7116	9.365586	85.98135	1.024963	0.028006	0.018512	0.012241
20	390	0.701641	3465	3146	2728	2839	3044.5	331.4237	10.88598	83.5391	0.991658	0.02721	0.018719	0.012882
21	405	0.728627	3013	3063	2367	2563	2751.5	340.9726	12.39225	78.20596	0.896222	0.025473	0.018199	0.013007
22	420	0.755613	3306	3134	2719	2558	2929.25	349.2348	11.92233	76.65088	0.954119	0.024967	0.018539	0.01377
23	435	0.782599	3023	2684	2755	2869	2832.75	147.9648	5.223363	77.74719	0.922686	0.025324	0.019471	0.014976
24	450	0.809585	2944	2783	2530	3072	2832.25	233.6299	8.248914	76.43836	0.922524	0.024898	0.019821	0.015784
25	465	0.836572	3145	2497	2345	2436	2605.75	364.8848	14.00306	73.37543	0.848748	0.0239	0.019658	0.016173
26	480	0.863558	2756	2194	1997	2077	2256	343.0092	15.20431	65.60004	0.734827	0.021367	0.018143	0.015409
27	510	0.91753	2607	2218	2073	1812	2177.5	331.9744	15.24567	119.6432	0.709258	0.03897	0.034686	0.030901

28	540	0.971503	2328	2031	1767	2098	2056	230.8636	11.22877	114.246	0.669683	0.037212	0.035119	0.03317
29	570	1.025475	2020	1926	1508	1789	1810.75	223.0088	12.31582	104.3488	0.589799	0.033989	0.033879	0.033795
30	600	1.079447	1682	1605	1477	1505	1567.25	94.18554	6.009606	91.15933	0.510486	0.029693	0.031192	0.03279
31	660	1.187392	1353	1408	1178	1158	1274.25	124.9917	9.809038	153.3625	0.41505	0.049953	0.05634	0.063687
32	720	1.295337	1244	1213	937	957	1087.75	163.2205	15.00533	127.4827	0.354303	0.041524	0.051369	0.063669
33	780	1.403282	1079	843	854	842	904.5	116.4603	12.87565	107.5264	0.294615	0.035024	0.047084	0.063398
34	840	1.511226	862	848	768	772	812.5	49.43346	6.084118	92.67055	0.264648	0.030185	0.0439	0.063934
35	900	1.619171	744	604	630	628	651.5	62.788	9.637453	79.01554	0.212207	0.025737	0.040131	0.062649
36	960	1.727116	519	609	597	480	551.25	62.03426	11.25338	64.91526	0.179554	0.021144	0.035282	0.058935
37	1020	1.83506	516	486	387	400	447.25	63.48425	14.19435	53.89141	0.145679	0.017554	0.031166	0.055384
38	1080	1.943005	418	389	337	423	391.75	39.45778	10.07218	45.28282	0.127601	0.01475	0.02781	0.052477
39	1140	2.05095	354	554	248	299	363.75	134.0159	36.84285	40.77612	0.118481	0.013282	0.026497	0.052899
40	1200	2.158895	277	291	267	254	272.25	15.64981	5.748325	34.32642	0.088678	0.011181	0.023448	0.049206

SUMMARY OUTPUT

Linest		Y-int	1559.95	A =	7001.337	Mean RT =	1.032424	
Slope m	Y-int b	Slope =	-594.286	b =	1.466467	var =	0.420362	non-dim
-594.286	*1559.95*	t(n-3)	1.943005			sigma =	0.648353	non-dim
		T(n)	2.158895	Integral1 =	2868.759			
		Fls(n-3) =	405.25	Integral2 =	201.3518	A(adj) =	2.280483	
		Fls(n)	276.95	TotInt =	3070.111	b(adj) =	1.466467	
						Integral3 =	0.186313	
						Int2(adj) =	0.065585	
						Integral4 =	0.559776	

Target HRT =	600	s	Actual HRT =	496.58		G4	XG	0.05	L/s					

Tube #	Time (s)	Theta	Fls#1	Fls#2	Fls#3	Fls#4	Fls#5	Average	StDev	%StDev	Trapezoid	C	SC*dt	St*C*dt	St*t*C*dt
0	0	0	0	0	0	0	0	0.0	0.0000	#DIV/0!		0			
1	60	0.120826	0	0	0	0	0	0.0	0.0000	#DIV/0!	0.0000	0	0	0	0
2	120	0.241653	0	0	0	0	0	0.0	0.0000	#DIV/0!	0.0000	0	0	0	0
3	135	0.27186	0	0	0	0	0	0.0	0.0000	#DIV/0!	0.0000	0	0	0	0
4	150	0.302066	0	0	0	0	0	0.0	0.0000	#DIV/0!	0.0000	0	0	0	0
5	165	0.332273	0	0	0	0	0	0.0	0.0000	#DIV/0!	0.0000	0	0	0	0
6	180	0.362479	0	0	0	0	0	0.0	0.0000	#DIV/0!	0.0000	0	0	0	0
7	195	0.392686	0	0	0	0	0	0.0	0.0000	#DIV/0!	0.0000	0	0	0	0
8	210	0.422893	0	0	0	0	0	0.0	0.0000	#DIV/0!	0.0000	0	0	0	0
9	225	0.453099	0	0	0	0	0	0.0	0.0000	#DIV/0!	0.0000	0	0	0	0
10	240	0.483306	0	0	0	0	0	0.0	0.0000	#DIV/0!	0.0000	0	0	0	0
11	255	0.513512	74	126	74	124	91	97.8	25.7915	26.3716	1.4771	0.02672	0.00040	0.00021	0.00011
12	270	0.543719	6495	6638	6441	6466	7739	6755.8	554.9006	8.2137	103.5120	1.84604	0.02828	0.01537	0.00835
13	285	0.573926	9555	10079	9700	10075	11572	10196.2	802.9014	7.8745	256.0313	2.78614	0.06996	0.03931	0.02210
14	300	0.604132	8950	8700	9422	9934	8724	9146.0	527.3841	5.7663	292.1312	2.49917	0.07983	0.04695	0.02764
15	315	0.634339	8408	8403	8840	8201	7644	8299.2	434.1678	5.2314	263.4802	2.26778	0.07200	0.04453	0.02756
16	330	0.664545	7773	8361	7830	7913	8316	8038.6	278.7137	3.4672	246.7548	2.19657	0.06743	0.04377	0.02843
17	345	0.694752	6675	7162	6423	6548	6976	6756.8	305.7559	4.5252	223.4595	1.84632	0.06106	0.04142	0.02811
18	360	0.724959	5086	5227	4783	5764	6042	5380.4	512.8238	9.5313	183.3119	1.47021	0.05009	0.03547	0.02513
19	375	0.755165	4480	4684	4527	4790	5068	4709.8	235.3873	4.9978	152.3954	1.28697	0.04164	0.03078	0.02275
20	390	0.785372	3825	3928	4273	3746	4337	4021.8	267.4167	6.6492	131.8760	1.09897	0.03604	0.02771	0.02132
21	405	0.815579	3012	3416	3303	3418	3127	3255.2	180.4348	5.5430	109.9068	0.88949	0.03003	0.02399	0.01917
22	420	0.845785	2798	3461	3349	3161	3103	3174.4	254.7446	8.0250	97.1082	0.86741	0.02654	0.02204	0.01831
23	435	0.875992	2657	3224	2845	2900	2789	2883.0	210.9064	7.3155	91.4868	0.78779	0.02500	0.02150	0.01850
24	450	0.906198	2420	2332	2643	2487	2473	2471.0	113.7607	4.6038	80.8631	0.67521	0.02210	0.01966	0.01750
25	465	0.936405	2130	2343	2415	2141	2377	2281.2	135.4777	5.9389	71.7739	0.62335	0.01961	0.01806	0.01663
26	480	0.966612	1889	1938	1948	1841	2119	1947.0	105.1974	5.4031	63.8598	0.53202	0.01745	0.01658	0.01576

27	510	1.027025	1664	1820	1830	1489	2016	1763.8	197.8767	11.2188	112.0907	0.48196	0.03063	0.03049	0.03037
28	540	1.087438	1607	1603	1670	1470	1584	1586.8	72.8745	4.5925	101.2103	0.43360	0.02766	0.02919	0.03084
29	570	1.147851	1336	1231	1260	1412	1083	1264.4	123.4435	9.7630	86.1251	0.34550	0.02353	0.02622	0.02924
30	600	1.208265	1083	1139	1092	1035	1018	1073.4	48.1799	4.4885	70.6170	0.29331	0.01930	0.02268	0.02669
31	660	1.329091	785	860	806	724		793.8	56.2161	7.0823	112.8006	0.21689	0.03082	0.03883	0.04902
32	720	1.449917	722	771	660	774		731.8	53.4439	7.3036	92.1604	0.19995	0.02518	0.03493	0.04854
33	780	1.570744	515	548	506	638		551.8	60.2682	10.9231	77.5404	0.15077	0.02119	0.03182	0.04787
34	840	1.69157	443	418	457	441		439.8	16.1529	3.6732	59.8997	0.12016	0.01637	0.02659	0.04324
35	900	1.812397	457	362	348	369		384.0	49.4436	12.8759	49.7654	0.10493	0.01360	0.02377	0.04159
36	960	1.933223	298	313	305	337		313.3	16.9779	5.4199	42.1231	0.08560	0.01151	0.02149	0.04015
37	1020	2.05405	310	277	263	289		284.8	19.9060	6.9907	36.1271	0.07781	0.00987	0.01965	0.03916
38	1080	2.174876	237	276	207	282		250.5	35.1994	14.0517	32.3362	0.06845	0.00884	0.01865	0.03939
39	1140	2.295703	238	255	221	241		238.8	13.9613	5.8476	29.5572	0.06524	0.00808	0.01804	0.04033
40	1200	2.416529	222	250	230	239		235.3	12.0381	5.1172	28.6359	0.06428	0.00782	0.01843	0.04345

SUMMARY OUTPUT

Linest		Y-int	628.1	A =	1045.771781	Mean RT =	1.200612379	
Slope m	Y-int b	Slope =	-167.182	b =	0.632067801	var =	-1.33443198	non-dim
-167.1819	*628.1*	t(n-3)	2.174876			sigma =	#NUM!	non-dim
		T(n)	2.416529	Integral1 =	3300.416851			
		Fls(n-3) =	264.5	Integral2 =	359.1926382	A(adj) =	0.285760485	
		Fls(n)	224.1	TotInt =	3659.609489	b(adj) =	0.632067801	
						Integral3 =	0.39246845	
						Int2(adj) =	0.098150537	
						Integral4 =	1.815016664	

Appendix E. Residence time distribution experimental procedure

1 Prepare dilution of Rhodamine tracer
2 Fill syringe 1 with Rhodamine, syringe 2 with H2O
3 Ensure all valves are in correct position
  * Supply tank to FC
  * Discharge tank to drain
  * Inlet valve to appropriate inlet
  * Outlet valve to discharge tank
4 Check level of supply tank - fill if necessary
5 Ensure no bubbles in fluid column
6 Double check outlet valve
7 Turn on pump - set to correct flow rate
8 Place test tubes in position
9 Open needle valve 2 turns
10 Sample to beaker to get control sample
11 Reset stopwatch
  Connect syringe #1 to hose. Syringe #2 is ready
12 ----------
13 Inject syringe #1
14 Quickly replace syringes and inject syringe #2
15 Start timer
16 Take initial sample after time t
  Take samples every dt seconds
  ----
17 Shut off pump
18 Allow discharge tank to drain
19 Check level in tanks - fill supply tank if necessary
20 Turn pump back on and let run at 3 L/min
21 * Tanks are 200 L. A tank will drain in 1 h at 3 L/min
22 After running tanks, take a final sample to beaker to test residual tracer
23 Shut off pump
24 Set outlet valve to "off"
25 Analyze results

Appendix F. MATLAB code for PIV data

MATLAB code for PIV data

```
% PIV-mainG1.m
% Reads in PIV data for G1 and plots contours and vectors

% Read in data from several PIV vector maps and concatenates into one
readpiv
findframe
offset
concat

% Creates a “coarser” mesh so that the vector plot isn’t too busy
sparse

% Plots data
rangeU = [-0.015:0.00325:0.05];
rangeV = [0.0075:-0.001125:-0.015];
contourf(Xpos, Ypos, Umean, rangeU)
contourf(Xpos, Ypos, Vmean, rangeV)
quiver(XposSparse, YposSparse, UmeanSparse, VmeanSparse, 5)



%***************************************************************
%***************************************************************


%Concat.m
%Concatenates several vector plots into 1

%****************** Section A ***************************
temp = find(XposA > cutoffx(1));
colMin = temp(1);
temp = find(XposA < cutoffx(2));
len = length(temp);
colMax = temp(len);

Xpos = XposA(colMin:colMax);

temp = find(YposA < cutoffy(1));
len = length(temp);
rowMax = temp(len);
temp = find(YposA > cutoffy(2));
rowMin = temp(1);

Ypos = YposA(rowMin:rowMax);

Umean = UmeanA(colMin:colMax, rowMin:rowMax);
```

```
Vmean = VmeanA(colMin:colMax, rowMin:rowMax);

%****************** Section B ***************************
temp = find(XposB > cutoffx(2));
colMin = temp(1);
temp = find(XposB < cutoffx(3));
len = length(temp);
colMax = temp(len);

Xpos = [Xpos; XposB(colMin:colMax)];

temp = find(YposB < cutoffy(1));
len = length(temp);
rowMax = temp(len);
temp = find(YposB > cutoffy(2));
rowMin = temp(1);

Umean = [Umean UmeanB(colMin:colMax, rowMin:rowMax)];
Vmean = [Vmean VmeanB(colMin:colMax, rowMin:rowMax)];

%****************** Section C ***************************
temp = find(XposC > cutoffx(3));
colMin = temp(1);
temp = find(XposC < cutoffx(4));
len = length(temp);
colMax = temp(len);

Xpos = [Xpos; XposC(colMin:colMax)];

temp = find(YposC < cutoffy(1));
len = length(temp);
rowMax = temp(len);
temp = find(YposC > cutoffy(2));
rowMin = temp(1);

Umean = [Umean UmeanC(colMin:colMax, rowMin:rowMax)];
Vmean = [Vmean VmeanC(colMin:colMax, rowMin:rowMax)];

%****************** Section D ***************************
temp = find(XposD > cutoffx(1));
colMin = temp(1);
temp = find(XposD < cutoffx(2));
len = length(temp);
colMax = temp(len);

temp = find(YposD < cutoffy(2));
len = length(temp);
rowMax = temp(len);
temp = find(YposD > cutoffy(3));
rowMin = temp(1);

Ypos = [YposD(rowMin:rowMax); Ypos];

Umean2 = UmeanD(colMin:colMax, rowMin:rowMax);
```

```
Vmean2 = VmeanD(colMin:colMax, rowMin:rowMax);

%****************** Section E ***************************
temp = find(XposE > cutoffx(2));
colMin = temp(1);
temp = find(XposE < cutoffx(3));
len = length(temp);
colMax = temp(len);

temp = find(YposE < cutoffy(2));
len = length(temp);
rowMax = temp(len);
temp = find(YposE > cutoffy(3));
rowMin = temp(1);

Umean2 = [Umean2 UmeanE(colMin:colMax, rowMin:rowMax)];
Vmean2 = [Vmean2 VmeanE(colMin:colMax, rowMin:rowMax)];

%****************** Section F ***************************
temp = find(XposF > cutoffx(3));
colMin = temp(1);
temp = find(XposF < cutoffx(4));
len = length(temp);
colMax = temp(len);

temp = find(YposF < cutoffy(2));
len = length(temp);
rowMax = temp(len);
temp = find(YposF > cutoffy(3));
rowMin = temp(1);

Umean2 = [Umean2 UmeanF(colMin:colMax, rowMin:rowMax)];
Vmean2 = [Vmean2 VmeanF(colMin:colMax, rowMin:rowMax)];

%Final Concatenation of U and V fields

Umean = [Umean2; Umean];
Vmean = [Vmean2; Vmean];




%*************************************************************
%*************************************************************


% findframe.m
% Finds the illuminated frame in the initial image and determines the
coordinates of the centre of the image. This is used for locating the
PIV data within the flow field.

% findframe
```

```
scale = 12.799;

% Frames A, B, and C were determined manually.
centreA = [477.5 494];
centreB = [506 492];
centreC = [494.5 487];

% read in image
imgD = imread('Frame21.tif',2);
imshow(imgD);

% detect edges of frame in horizontal direction
img = imgD;

for i = 1:10
    slice = find(img((20*i+400),:) > 65);
    tempL = find(slice < 350);
    leftEdge(i) = slice(tempL(length(tempL)));
    tempR = find(slice > 650);
    rightEdge(i) = slice(tempR(1));
end

avgLeftEdge = mean(leftEdge);
avgRightEdge = mean(rightEdge);

centreD(1) = (avgLeftEdge + avgRightEdge)/2;

%detect edges of frame in vertical direction
for i = 1:10
    slice = find(img(:,(20*i+400)) > 65);
    tempB = find(slice < 350);
    bottomEdge(i) = slice(tempB(length(tempB)));
    tempT = find(slice > 650);
    topEdge(i) = slice(tempT(1));
end

avgBottomEdge = mean(bottomEdge);
avgTopEdge = mean(topEdge);

centreD(2) = (avgBottomEdge + avgTopEdge)/2;

%*********************************************************

% read in image
imgE = imread('Frame22.tif',2);
imshow(imgE);

% detect edges of frame in horizontal direction
img = imgE;

for i = 1:10
    slice = find(img((20*i+400),:) > 65);
```

```
    tempL = find(slice < 350);
    leftEdge(i) = slice(tempL(length(tempL)));
    tempR = find(slice > 650);
    rightEdge(i) = slice(tempR(1));
end

avgLeftEdge = mean(leftEdge);
avgRightEdge = mean(rightEdge);

centreE(1) = (avgLeftEdge + avgRightEdge)/2;

%detect edges of frame in vertical direction
for i = 1:10
    slice = find(img(:,(20*i+400)) > 65);
    tempB = find(slice < 350);
    bottomEdge(i) = slice(tempB(length(tempB)));
    tempT = find(slice > 650);
    topEdge(i) = slice(tempT(1));
end

avgBottomEdge = mean(bottomEdge);
avgTopEdge = mean(topEdge);

centreE(2) = (avgBottomEdge + avgTopEdge)/2;

%*****************************************************************

% read in image
imgF = imread('Frame23.tif',2);
imshow(imgF);

% detect edges of frame in horizontal direction
img = imgF;

for i = 1:10
    slice = find(img((20*i+400),:) > 65);
    tempL = find(slice < 350);
    leftEdge(i) = slice(tempL(length(tempL)));
    tempR = find(slice > 650);
    rightEdge(i) = slice(tempR(1));
end

avgLeftEdge = mean(leftEdge);
avgRightEdge = mean(rightEdge);

centreF(1) = (avgLeftEdge + avgRightEdge)/2;

%detect edges of frame in vertical direction
for i = 1:10
    slice = find(img(:,(20*i+400)) > 65);
    tempB = find(slice < 350);
    bottomEdge(i) = slice(tempB(length(tempB)));
    tempT = find(slice > 650);
    topEdge(i) = slice(tempT(1));
```

```
end

avgBottomEdge = mean(bottomEdge);
avgTopEdge = mean(topEdge);

centreF(2) = (avgBottomEdge + avgTopEdge)/2;




%*****************************************************************
%*****************************************************************

% offset.m
% Offsets the X and Y positions of the PIV data to match the location
within the flow field.

spacing = 88.9;
lengthIA = 1.8431;

cutoffx = spacing*[-1.5 -0.5 0.5 1.5];
cutoffy = spacing*[1.5 0.5 -0.5];

Xcentre = 0.115194*[centreA(1) centreB(1) centreC(1) centreD(1)
centreE(1) centreF(1)]
Ycentre = 0.115194*[centreA(2) centreB(2) centreC(2) centreD(2)
centreE(2) centreF(2)]

for i = 1:6
    IAx = round(Xcentre(i)/1.8431);
    IAy = round(Xcentre(i)/1.8431);
    Xcentre(i) = IAx*1.8431;
    Ycentre(i) = IAy*1.8431;
end

offsetx = [-spacing 0 spacing -spacing 0 spacing];
offsety = [spacing spacing spacing 0 0 0];

% Offsetting Section A
XposA = offsetx(1)+XposA-Xcentre(1)
YposA = offsety(1)+YposA-Ycentre(1)

% Offsetting Section B
XposB = offsetx(2)+XposB-Xcentre(2)
YposB = offsety(2)+YposB-Ycentre(2)

% Offsetting Section C
XposC = offsetx(3)+XposC-Xcentre(3)
YposC = offsety(3)+YposC-Ycentre(3)

% Offsetting Section D
XposD = offsetx(4)+XposD-Xcentre(4)
YposD = offsety(4)+YposD-Ycentre(4)
```

```
% Offsetting Section E
XposE = offsetx(5)+XposE-Xcentre(5)
YposE = offsety(5)+YposE-Ycentre(5)

% Offsetting Section F
XposF = offsetx(6)+XposF-Xcentre(6)
YposF = offsety(6)+YposF-Ycentre(6)


%****************************************************************
%****************************************************************

% sparse.m
% skips every n data point to create a coarse flow field.

%skip n values
n = 4;

lenX = length(Xpos);
lenY = length(Ypos);
countx = 1;
county = 1;

for i = 1:n:lenY
    YposSparse (county) = Ypos(i);
    for j = 1:n:lenX
        if (i == 1)
            XposSparse(countx) = Xpos(j);
        end
        UmeanSparse(county, countx) = Umean(i,j);
        VmeanSparse(county, countx) = Vmean(i,j);
        countx = countx + 1;
    end
    county = county + 1;
    countx = 1;
end
```

Appendix G. Fluid column drawings

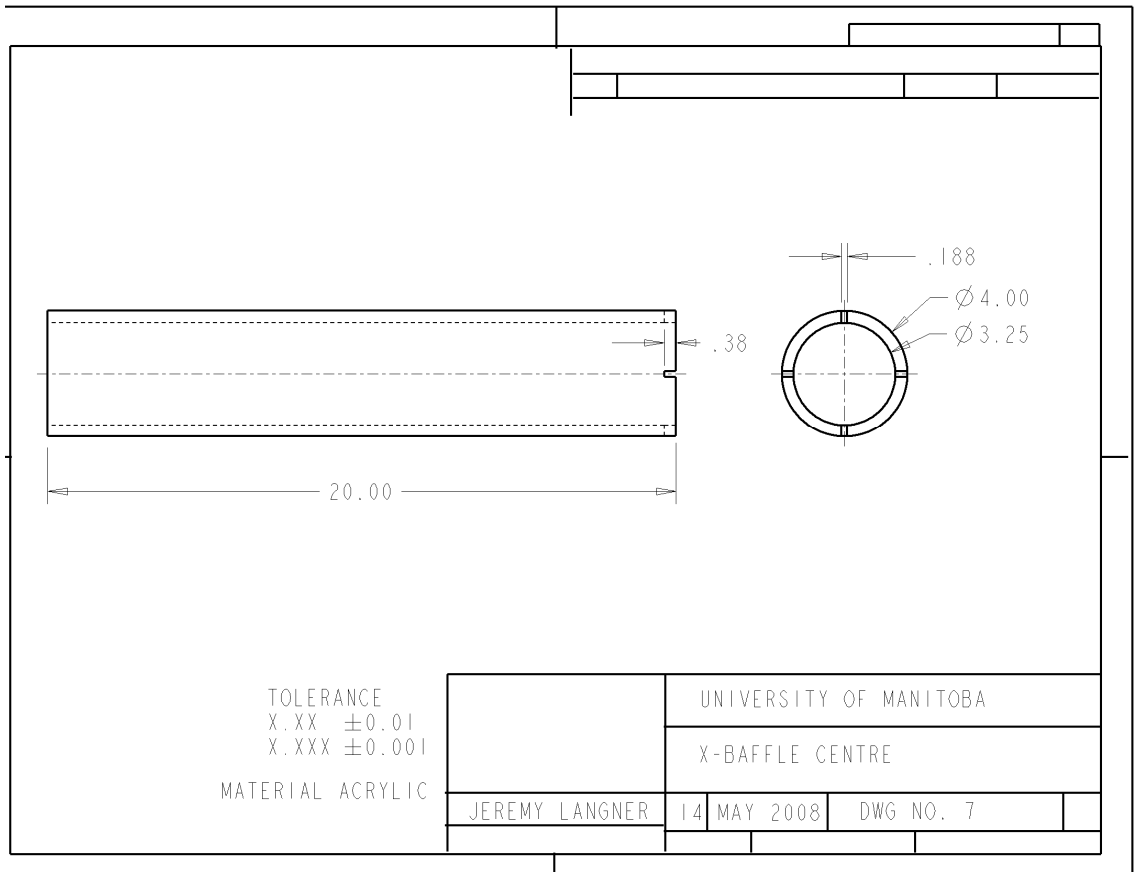

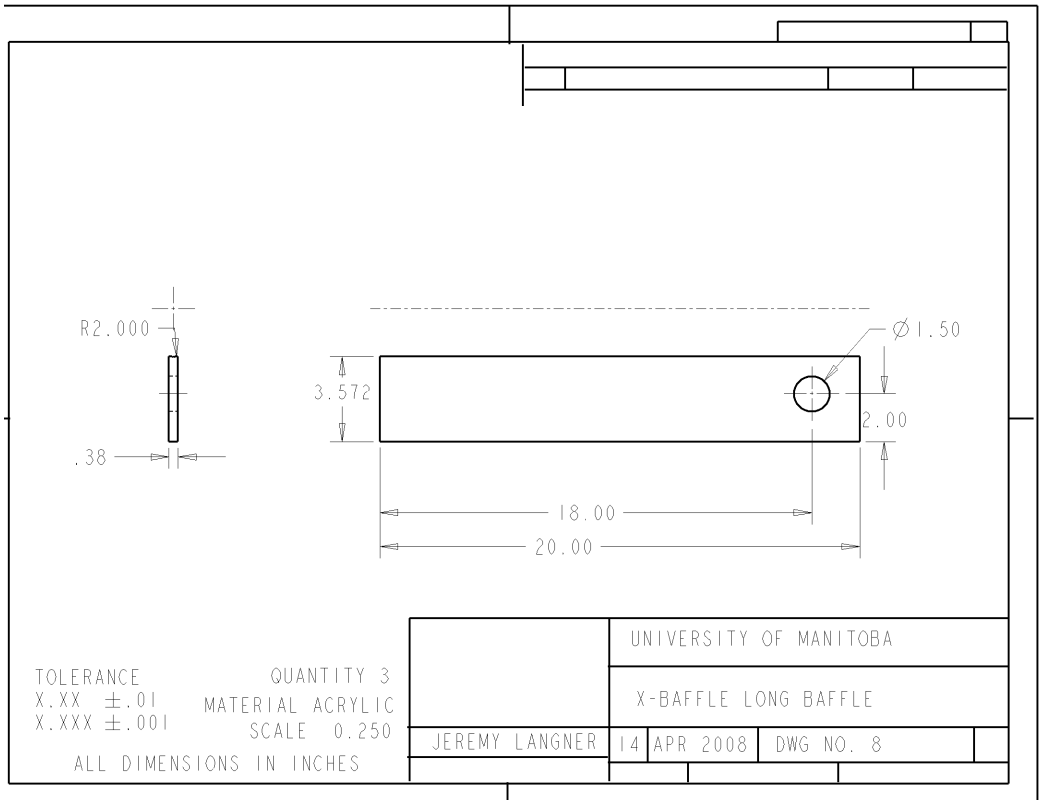
R2.000
.38
3.572
Ø1.50
2.00
18.00
20.00
TOLERANCE
X.XX ±.01
X.XXX ±.001
ALL DIMENSIONS IN INCHES
QUANTITY 3
MATERIAL ACRYLIC
SCALE 0.250
UNIVERSITY OF MANITOBA
X-BAFFLE LONG BAFFLE
JEREMY LANGNER
14 APR 2008
DWG NO. 8

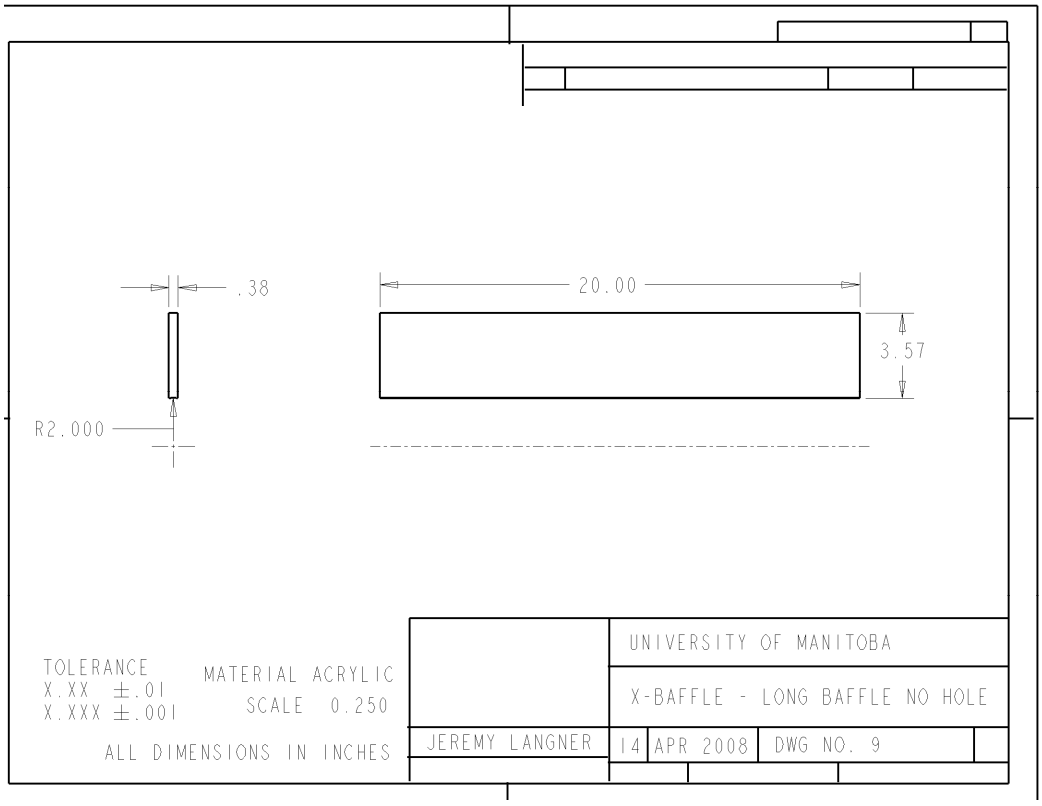
.38
20.00
3.57
R2.000
TOLERANCE
X.XX ±.01
X.XXX ±.001
ALL DIMENSIONS IN INCHES
MATERIAL ACRYLIC
SCALE 0.250
UNIVERSITY OF MANITOBA
X-BAFFLE - LONG BAFFLE NO HOLE
JEREMY LANGNER
14 APR 2008
DWG NO. 9

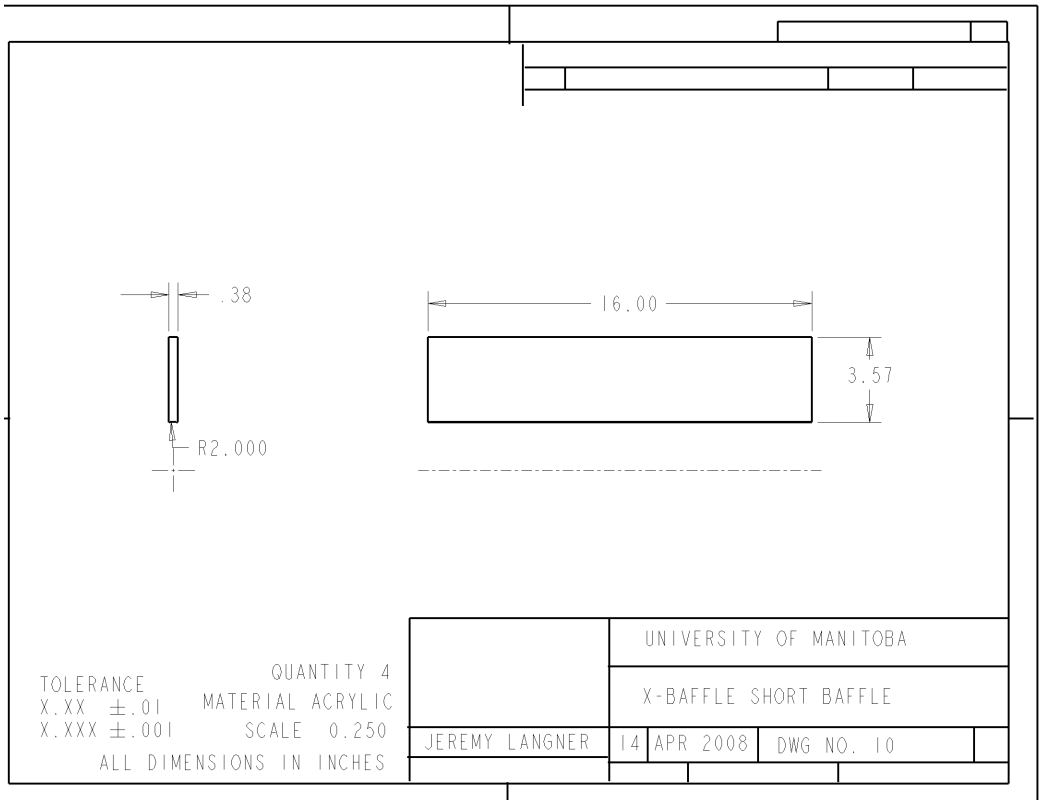
.38
16.00
3.57
R2.000
TOLERANCE
X.XX ±.01
X.XXX ±.001
ALL DIMENSIONS IN INCHES
QUANTITY 4
MATERIAL ACRYLIC
SCALE 0.250
UNIVERSITY OF MANITOBA
X-BAFFLE SHORT BAFFLE
JEREMY LANGNER
14 APR 2008
DWG NO. 10

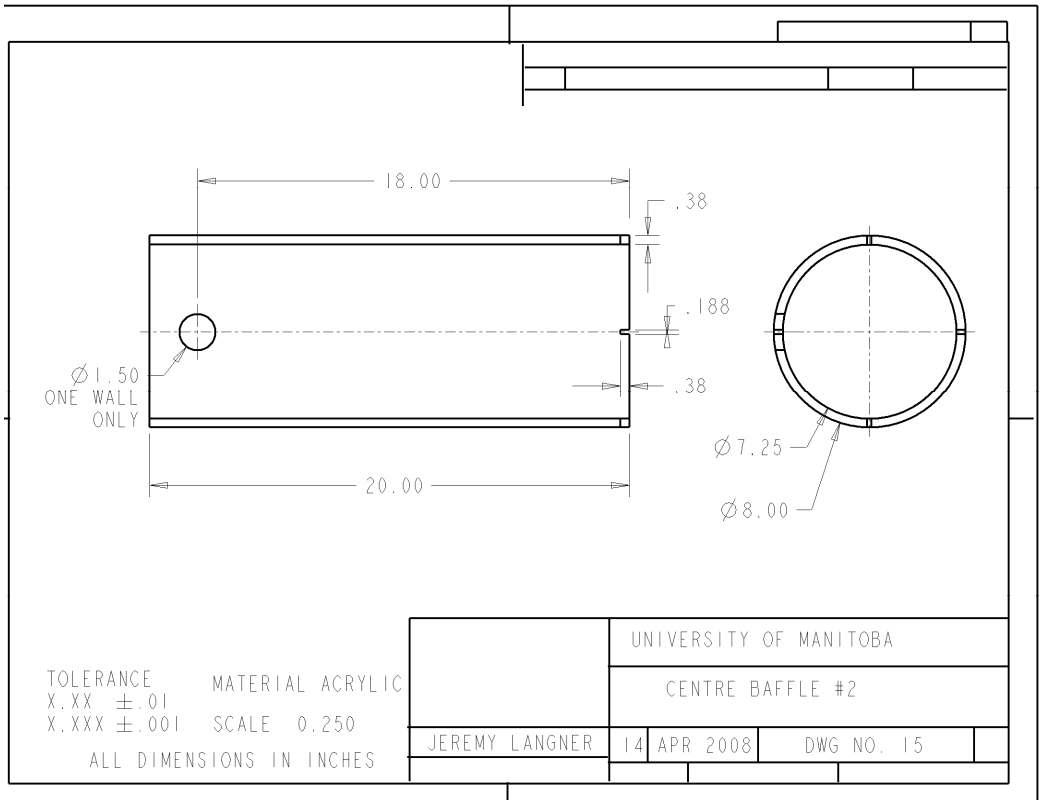
18.00
.38
.188
.38
Ø1.50
ONE WALL
ONLY
20.00
Ø7.25
Ø8.00
TOLERANCE
X.XX ±.01
X.XXX ±.001
ALL DIMENSIONS IN INCHES
MATERIAL ACRYLIC
SCALE 0.250
UNIVERSITY OF MANITOBA
CENTRE BAFFLE #2
JEREMY LANGNER
14 APR 2008
DWG NO. 15

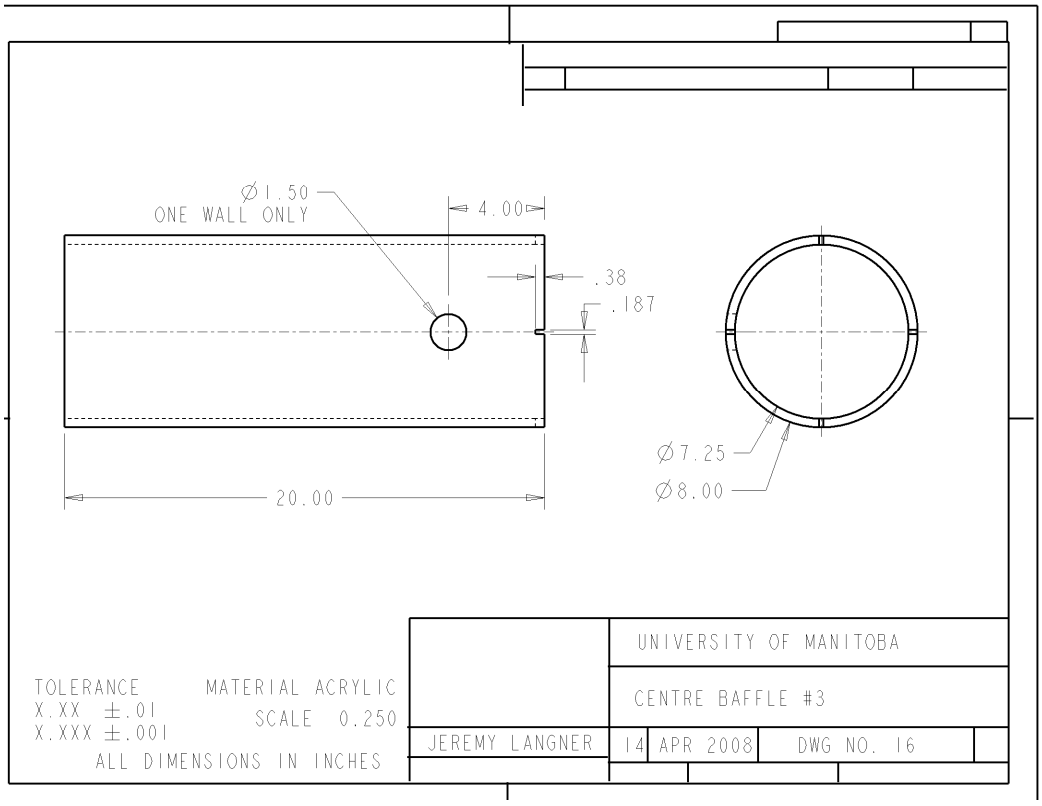
Ø1.50
ONE WALL ONLY
4.00
.38
.187
20.00
Ø7.25
Ø8.00
TOLERANCE
X.XX ±.01
X.XXX ±.001
ALL DIMENSIONS IN INCHES
MATERIAL ACRYLIC
SCALE 0.250
UNIVERSITY OF MANITOBA
CENTRE BAFFLE #3
JEREMY LANGNER
14 APR 2008
DWG NO. 16

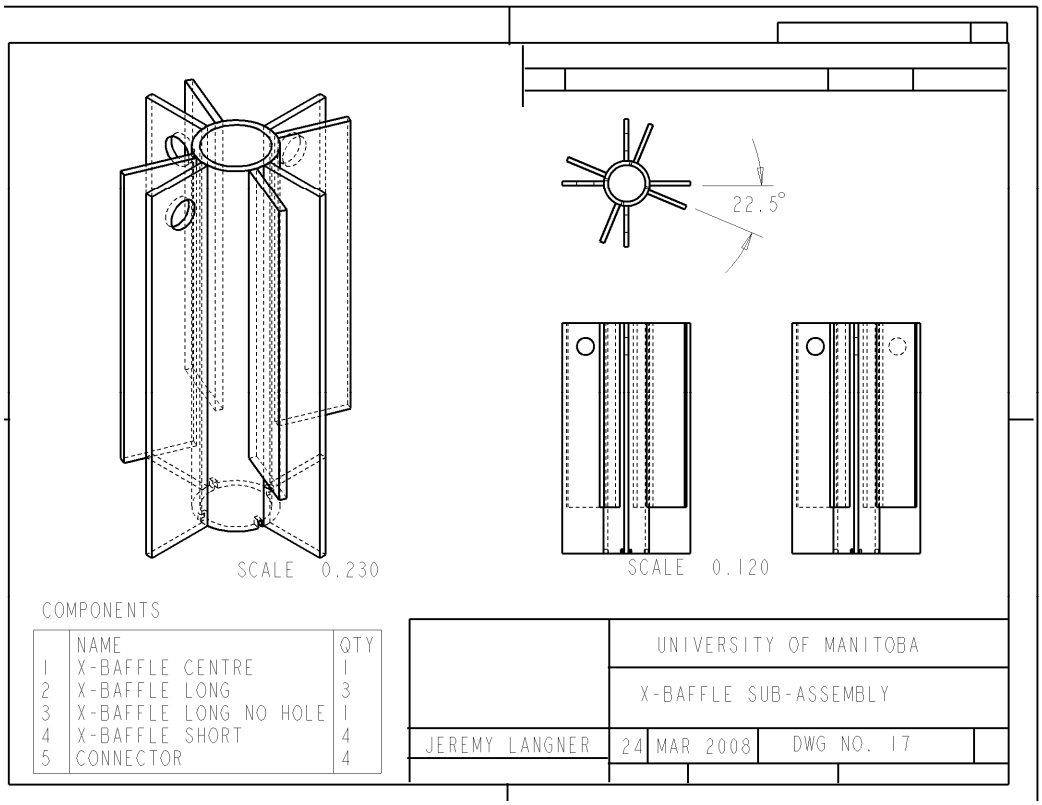
22.5°
SCALE 0.230
SCALE 0.120
COMPONENTS
NAME QTY
1 X-BAFFLE CENTRE 1
2 X-BAFFLE LONG 3
3 X-BAFFLE LONG NO HOLE 1
4 X-BAFFLE SHORT 4
5 CONNECTOR 4
UNIVERSITY OF MANITOBA
X-BAFFLE SUB-ASSEMBLY
JEREMY LANGNER
24 MAR 2008
DWG NO. 17

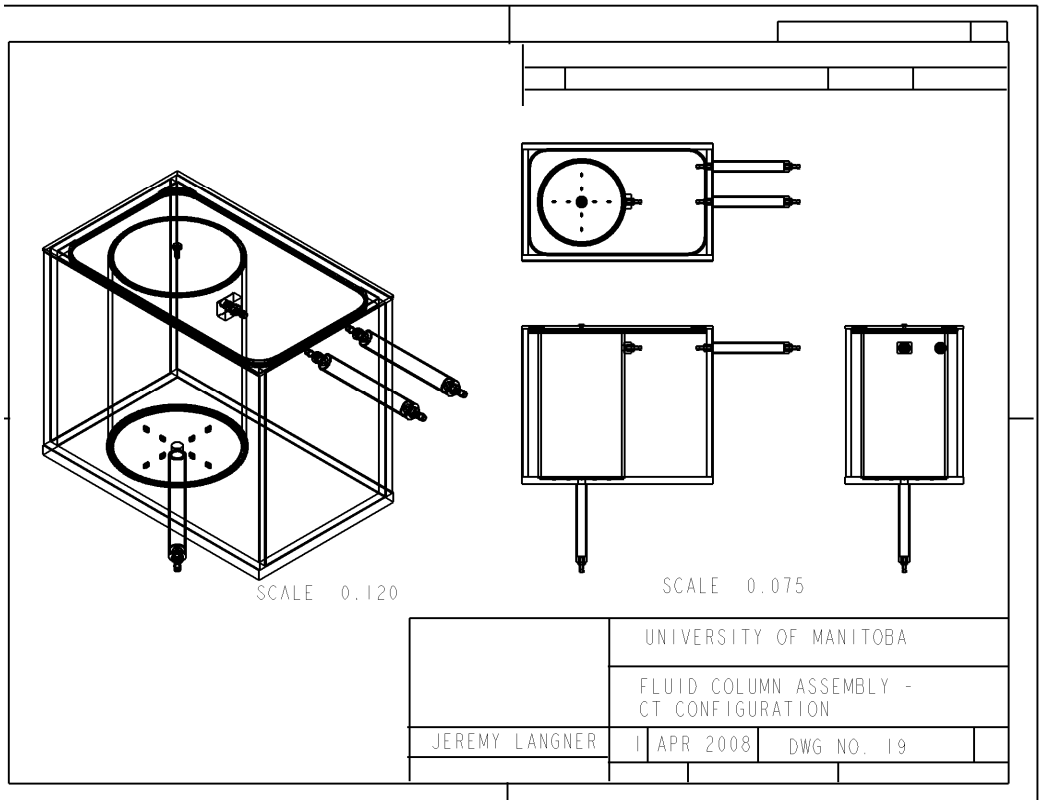
SCALE 0.120
SCALE 0.075
UNIVERSITY OF MANITOBA
FLUID COLUMN ASSEMBLY -
CT CONFIGURATION
JEREMY LANGNER
1 APR 2008
DWG NO. 19

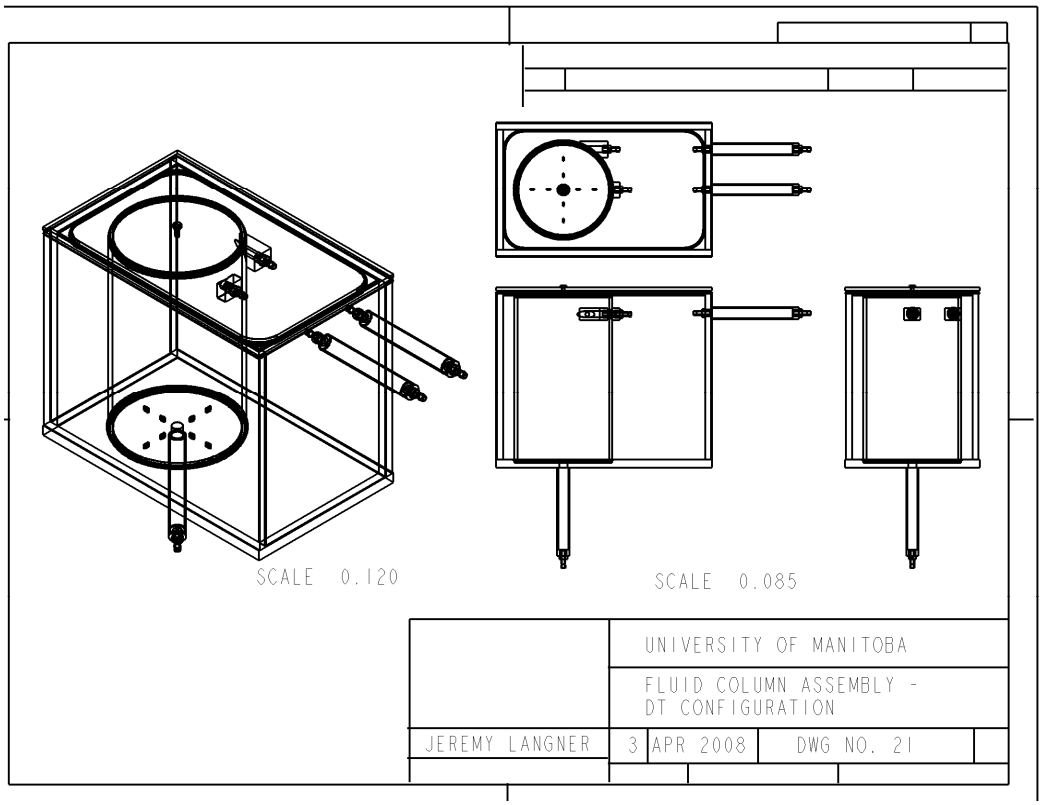
SCALE 0.120
SCALE 0.085
UNIVERSITY OF MANITOBA
FLUID COLUMN ASSEMBLY -
DT CONFIGURATION
JEREMY LANGNER
3 APR 2008
DWG NO. 21

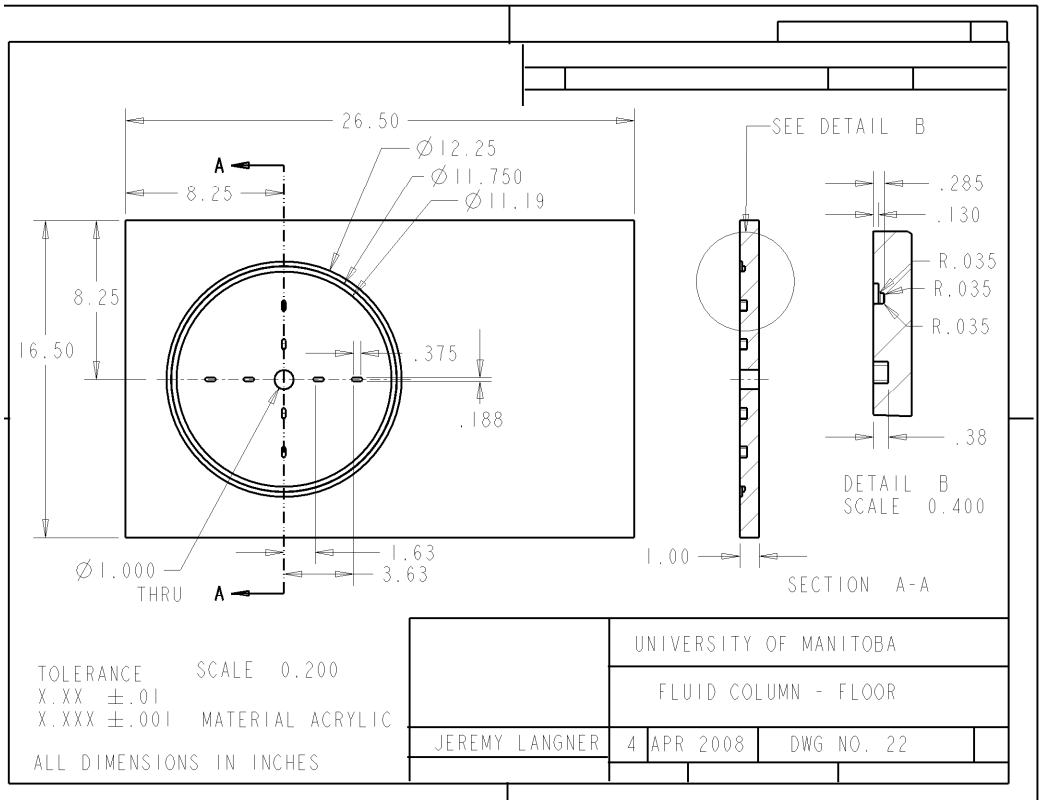
26.50
Ø12.25
Ø11.750
Ø11.19
A
8.25
8.25
16.50
.375
.188
Ø1.000
THRU
1.63
3.63
A
SEE DETAIL B
.285
.130
R.035
R.035
R.035
.38
DETAIL B
SCALE 0.400
1.00
SECTION A-A
TOLERANCE
X.XX ±.01
X.XXX ±.001
SCALE 0.200
MATERIAL ACRYLIC
ALL DIMENSIONS IN INCHES
UNIVERSITY OF MANITOBA
FLUID COLUMN - FLOOR
JEREMY LANGNER
4 APR 2008
DWG NO. 22

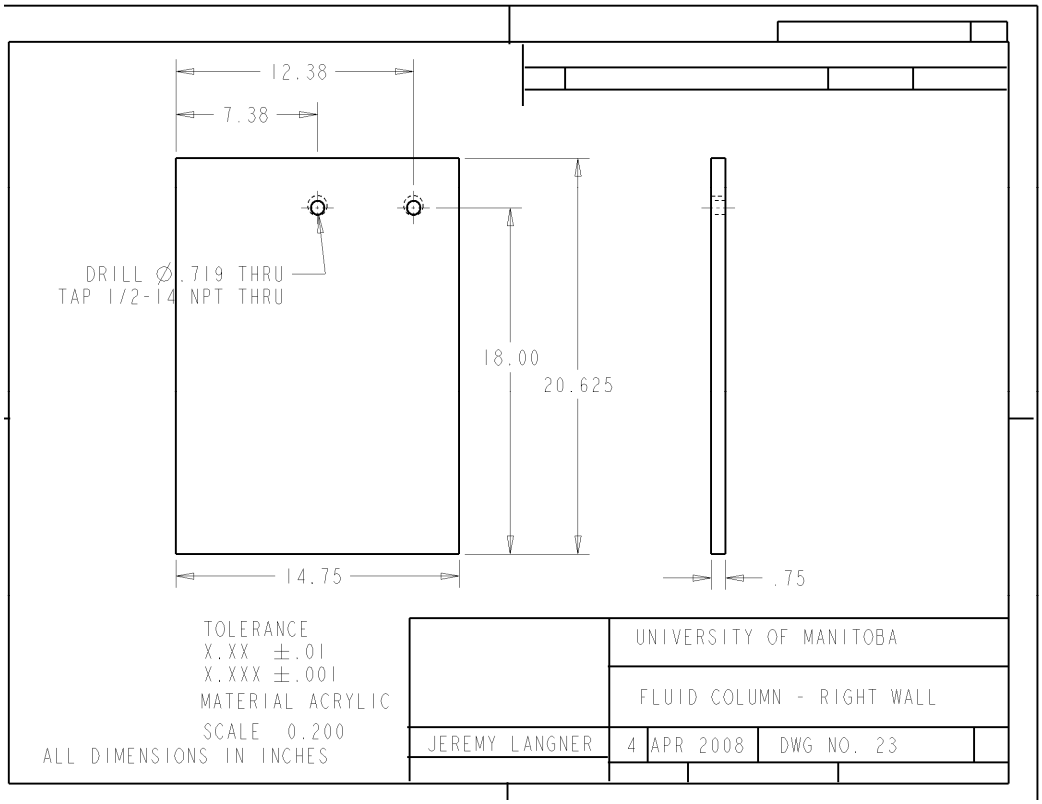
12.38
7.38
DRILL Ø.719 THRU
TAP 1/2-14 NPT THRU
18.00
20.625
14.75
.75
TOLERANCE
X.XX ±.01
X.XXX ±.001
MATERIAL ACRYLIC
SCALE 0.200
ALL DIMENSIONS IN INCHES
UNIVERSITY OF MANITOBA
FLUID COLUMN - RIGHT WALL
JEREMY LANGNER
4 APR 2008
DWG NO. 23

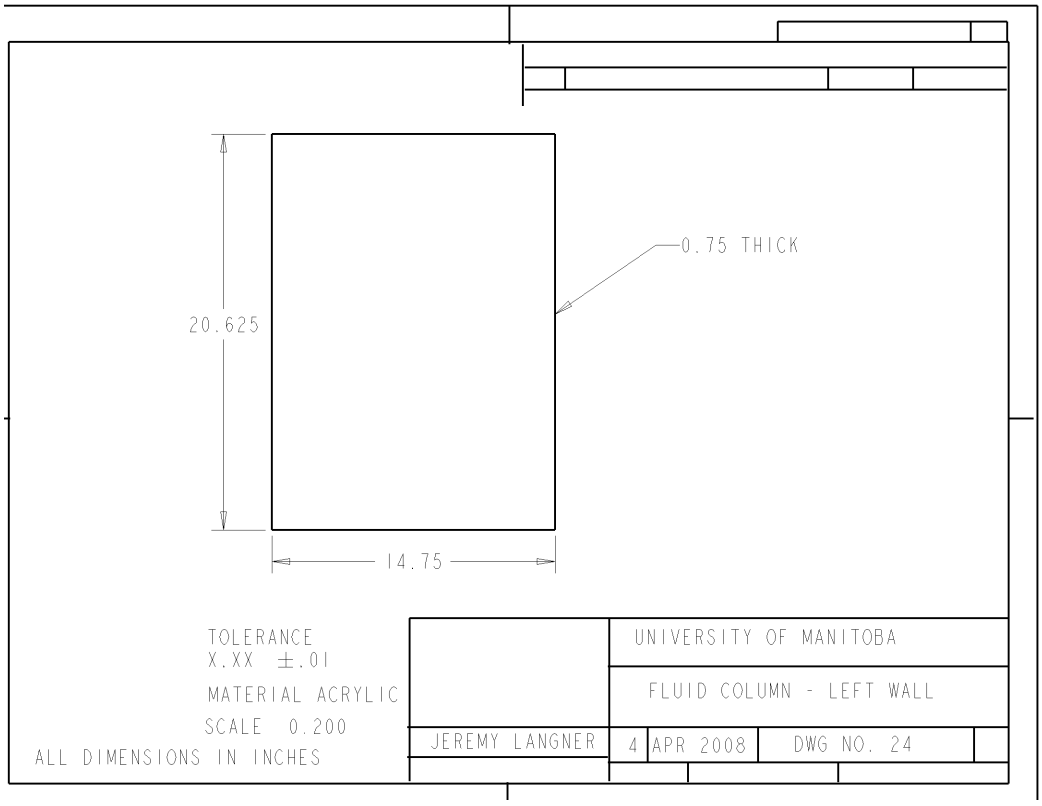
0.75 THICK
20.625
14.75
TOLERANCE
X.XX ±.01
MATERIAL ACRYLIC
SCALE 0.200
ALL DIMENSIONS IN INCHES
UNIVERSITY OF MANITOBA
FLUID COLUMN - LEFT WALL
JEREMY LANGNER
4 APR 2008
DWG NO. 24

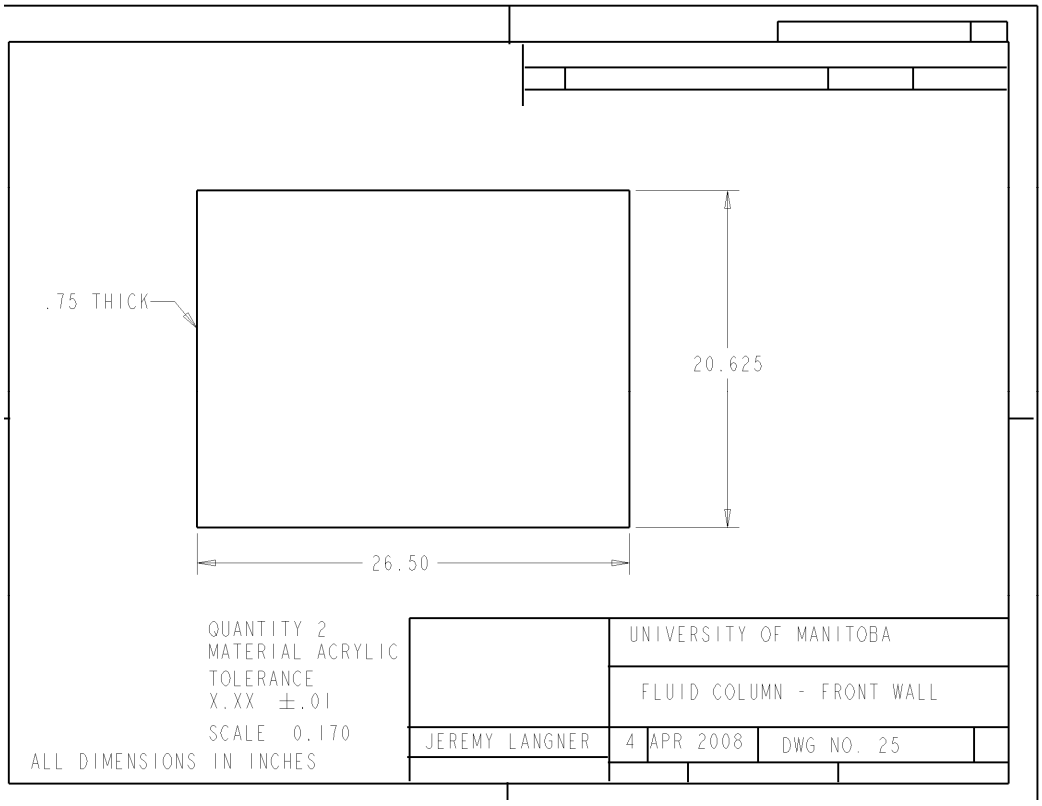
.75 THICK
20.625
26.50
QUANTITY 2
MATERIAL ACRYLIC
TOLERANCE
X.XX ±.01
SCALE 0.170
ALL DIMENSIONS IN INCHES
UNIVERSITY OF MANITOBA
FLUID COLUMN - FRONT WALL
JEREMY LANGNER
4 APR 2008
DWG NO. 25

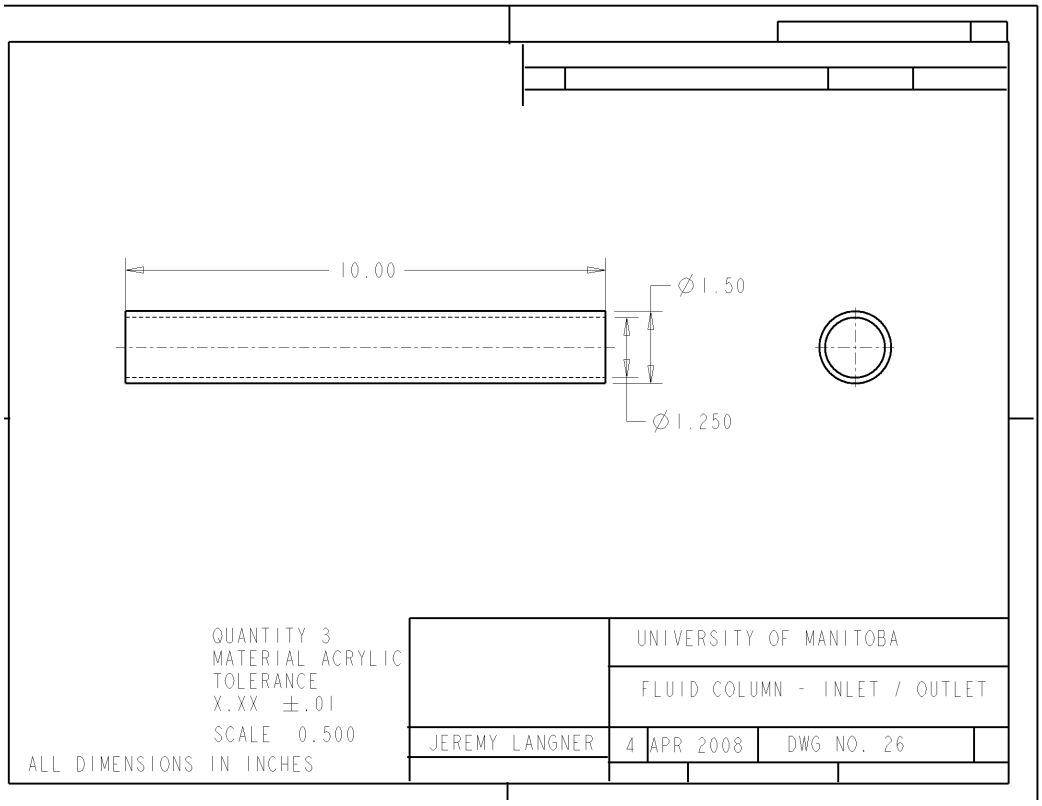
10.00
Ø1.50
Ø1.250
QUANTITY 3
MATERIAL ACRYLIC
TOLERANCE
X.XX ±.01
SCALE 0.500
ALL DIMENSIONS IN INCHES
UNIVERSITY OF MANITOBA
FLUID COLUMN - INLET / OUTLET
JEREMY LANGNER
4 APR 2008
DWG NO. 26

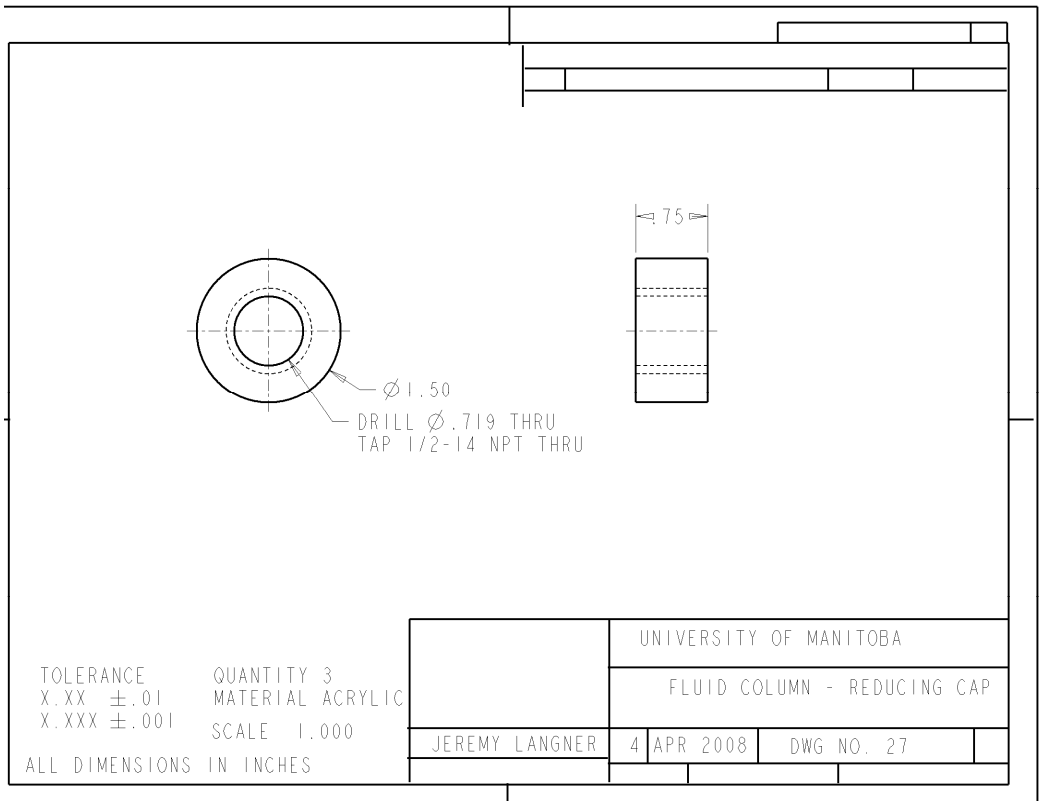
.75
Ø1.50
DRILL Ø.719 THRU
TAP 1/2-14 NPT THRU
TOLERANCE
X.XX ±.01
X.XXX ±.001
QUANTITY 3
MATERIAL ACRYLIC
SCALE 1.000
ALL DIMENSIONS IN INCHES
UNIVERSITY OF MANITOBA
FLUID COLUMN - REDUCING CAP
JEREMY LANGNER
4 APR 2008
DWG NO. 27

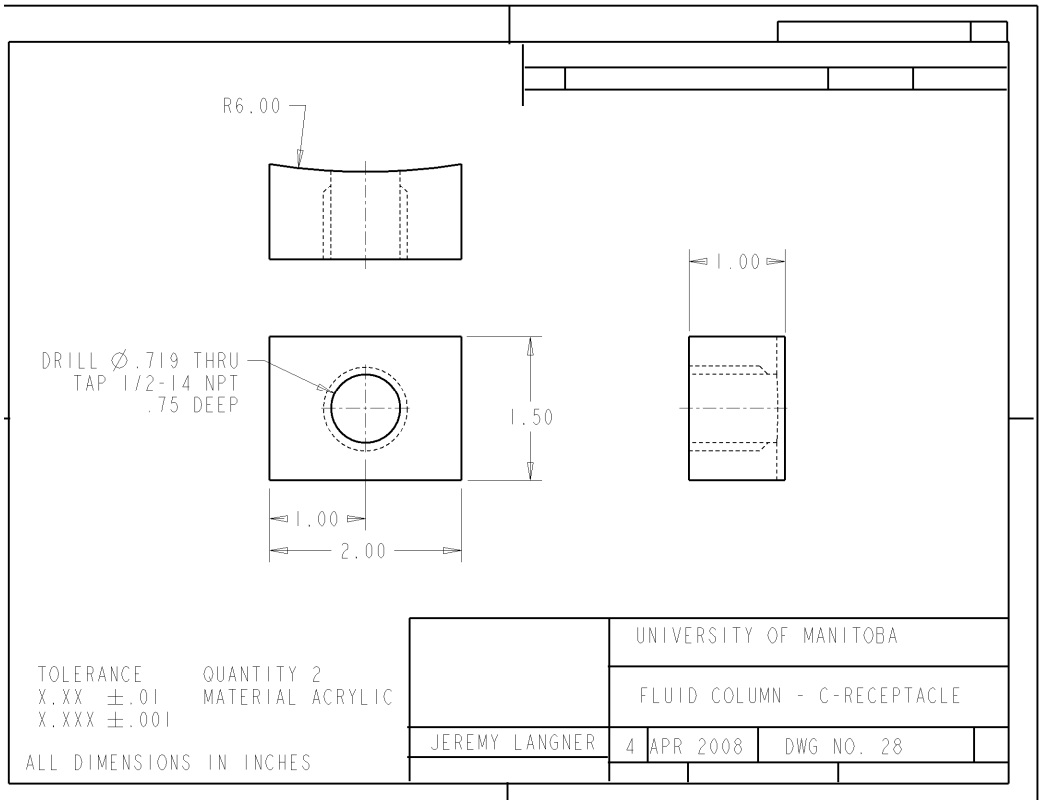
R6.00
1.00
DRILL Ø.719 THRU
TAP 1/2-14 NPT
.75 DEEP
1.50
1.00
2.00
TOLERANCE
X.XX ±.01
X.XXX ±.001
QUANTITY 2
MATERIAL ACRYLIC
ALL DIMENSIONS IN INCHES
UNIVERSITY OF MANITOBA
FLUID COLUMN - C-RECEPTACLE
JEREMY LANGNER
4 APR 2008
DWG NO. 28

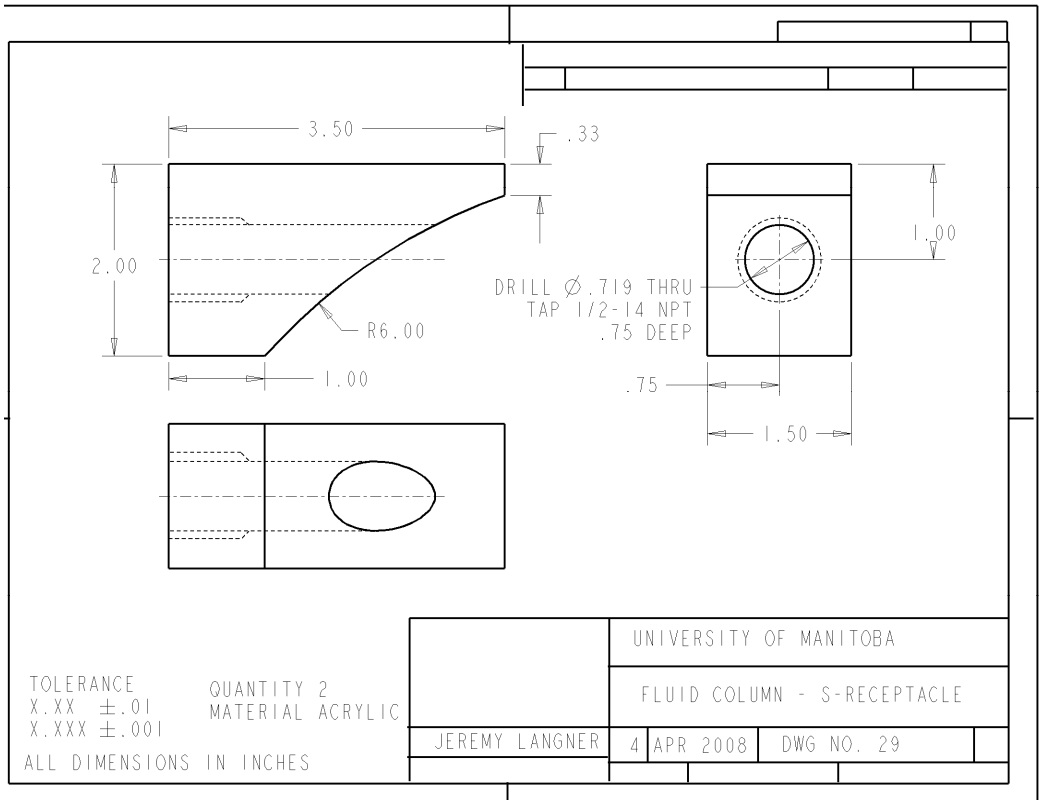
3.50
.33
2.00
R6.00
1.00
1.00
DRILL Ø.719 THRU
TAP 1/2-14 NPT
.75 DEEP
.75
1.50
TOLERANCE
X.XX ±.01
X.XXX ±.001
QUANTITY 2
MATERIAL ACRYLIC
ALL DIMENSIONS IN INCHES
UNIVERSITY OF MANITOBA
FLUID COLUMN - S-RECEPTACLE
JEREMY LANGNER
4 APR 2008
DWG NO. 29

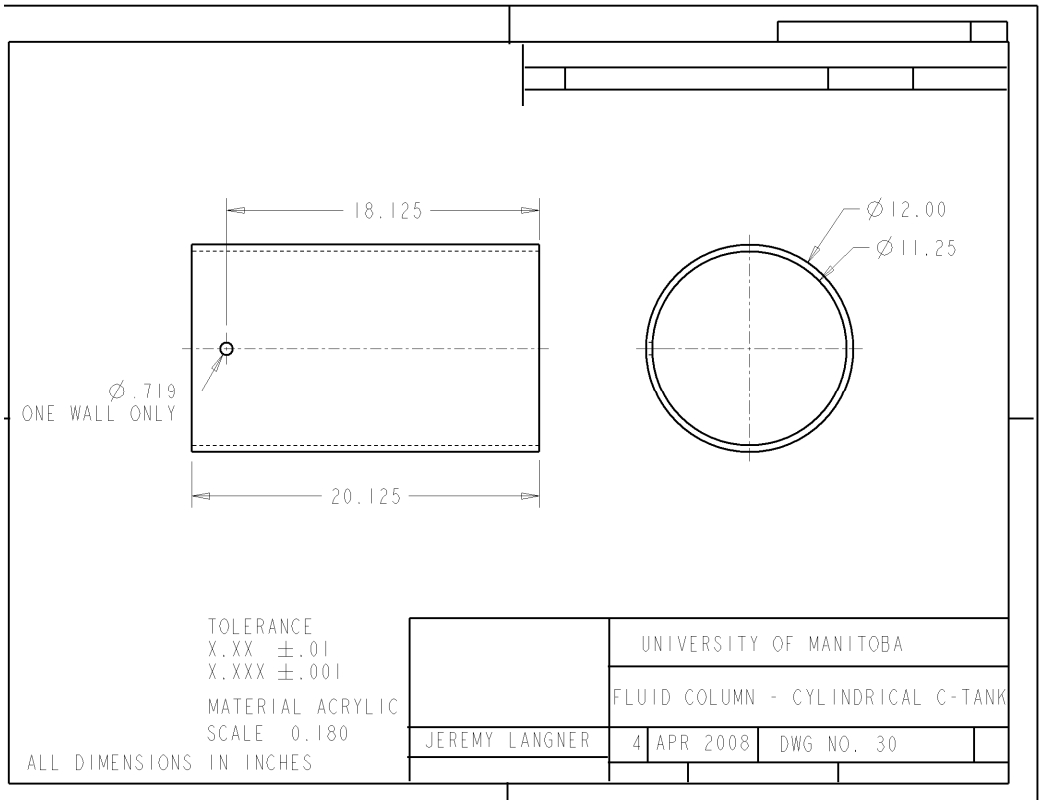
18.125
Ø12.00
Ø11.25
Ø.719
ONE WALL ONLY
20.125
TOLERANCE
X.XX ±.01
X.XXX ±.001
MATERIAL ACRYLIC
SCALE 0.180
ALL DIMENSIONS IN INCHES
UNIVERSITY OF MANITOBA
FLUID COLUMN - CYLINDRICAL C-TANK
JEREMY LANGNER
4 APR 2008
DWG NO. 30

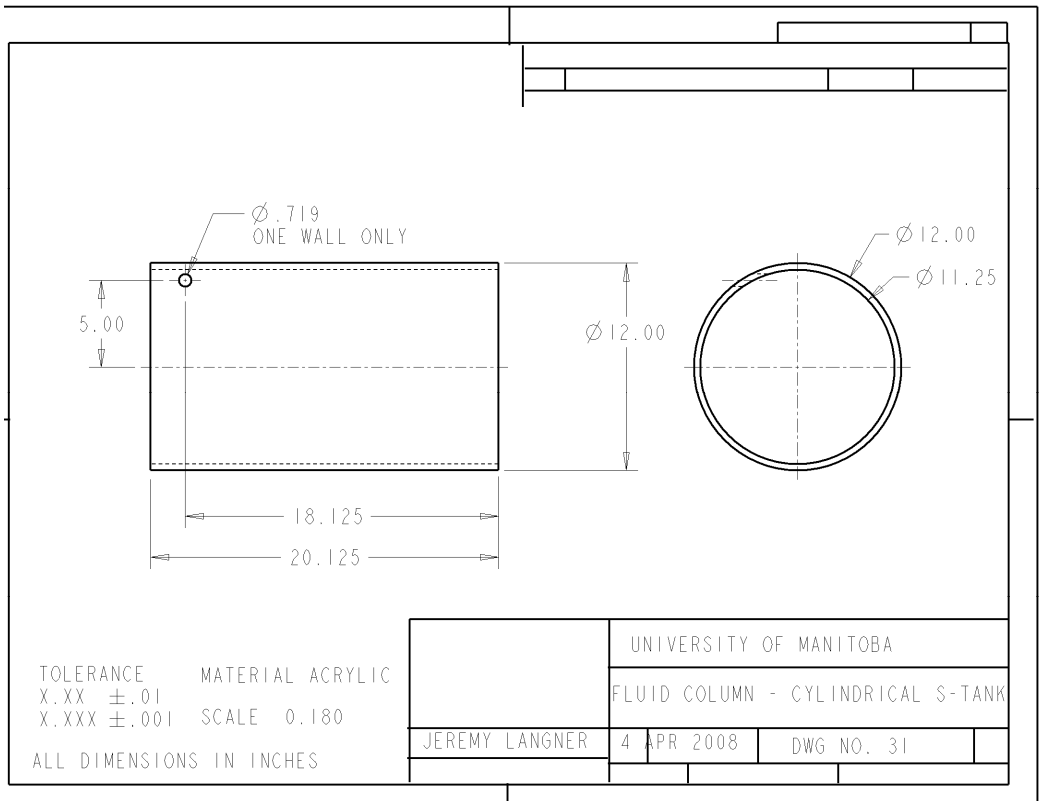
Ø.719
ONE WALL ONLY
5.00
Ø12.00
Ø12.00
Ø11.25
18.125
20.125
TOLERANCE
X.XX ±.01
X.XXX ±.001
MATERIAL ACRYLIC
SCALE 0.180
ALL DIMENSIONS IN INCHES
UNIVERSITY OF MANITOBA
FLUID COLUMN - CYLINDRICAL S-TANK
JEREMY LANGNER
4 APR 2008
DWG NO. 31

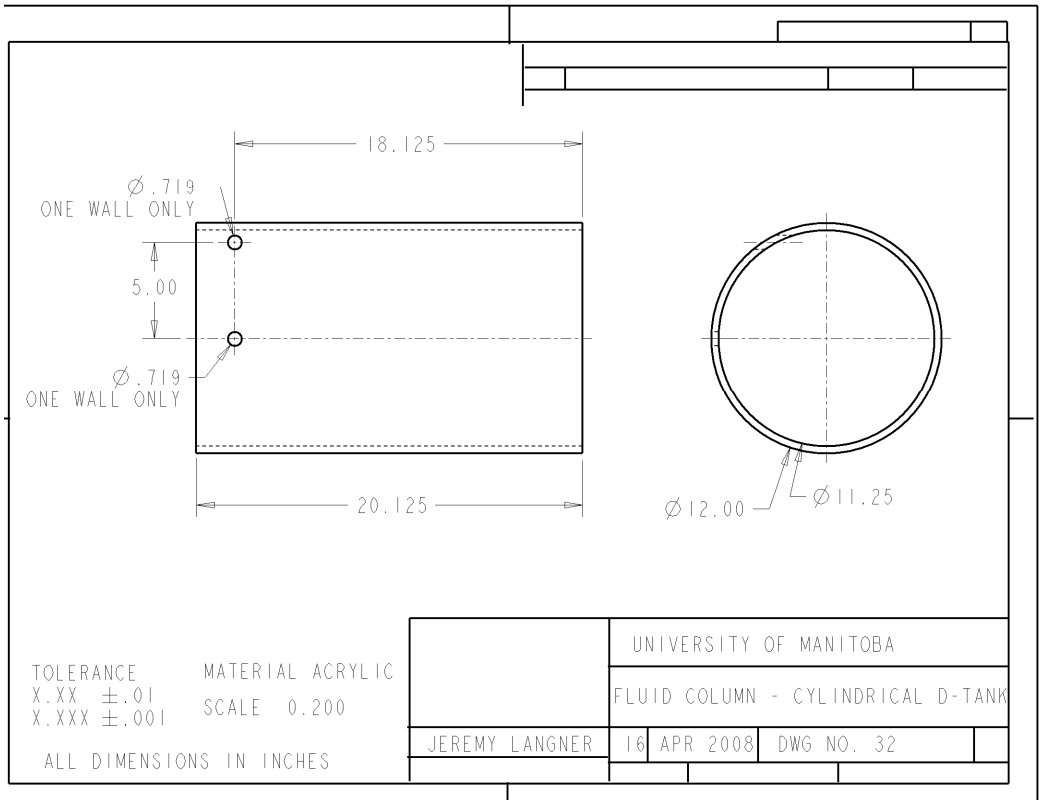
18.125
Ø.719
ONE WALL ONLY
5.00
Ø.719
ONE WALL ONLY
20.125
Ø12.00
Ø11.25
TOLERANCE
X.XX ±.01
X.XXX ±.001
MATERIAL ACRYLIC
SCALE 0.200
ALL DIMENSIONS IN INCHES
UNIVERSITY OF MANITOBA
FLUID COLUMN - CYLINDRICAL D-TANK
JEREMY LANGNER
16 APR 2008
DWG NO. 32

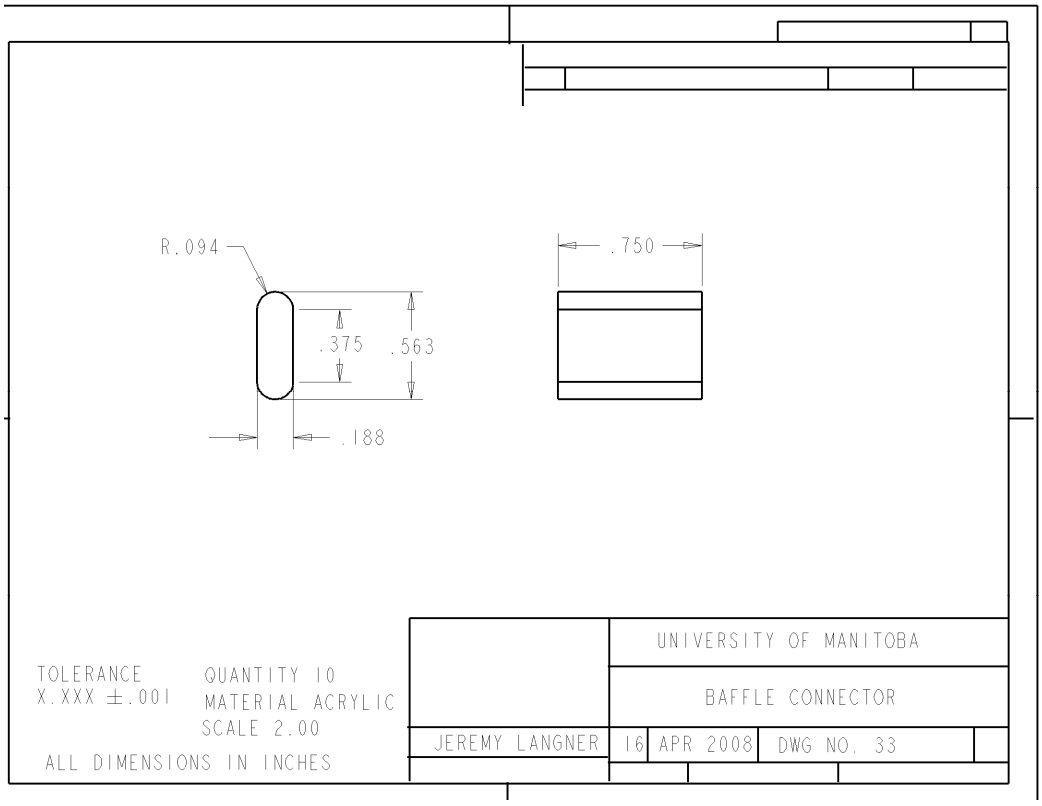
R.094
.375
.563
.188
.750
TOLERANCE
X.XXX ±.001
QUANTITY 10
MATERIAL ACRYLIC
SCALE 2.00
ALL DIMENSIONS IN INCHES
UNIVERSITY OF MANITOBA
BAFFLE CONNECTOR
JEREMY LANGNER
16 APR 2008
DWG NO. 33

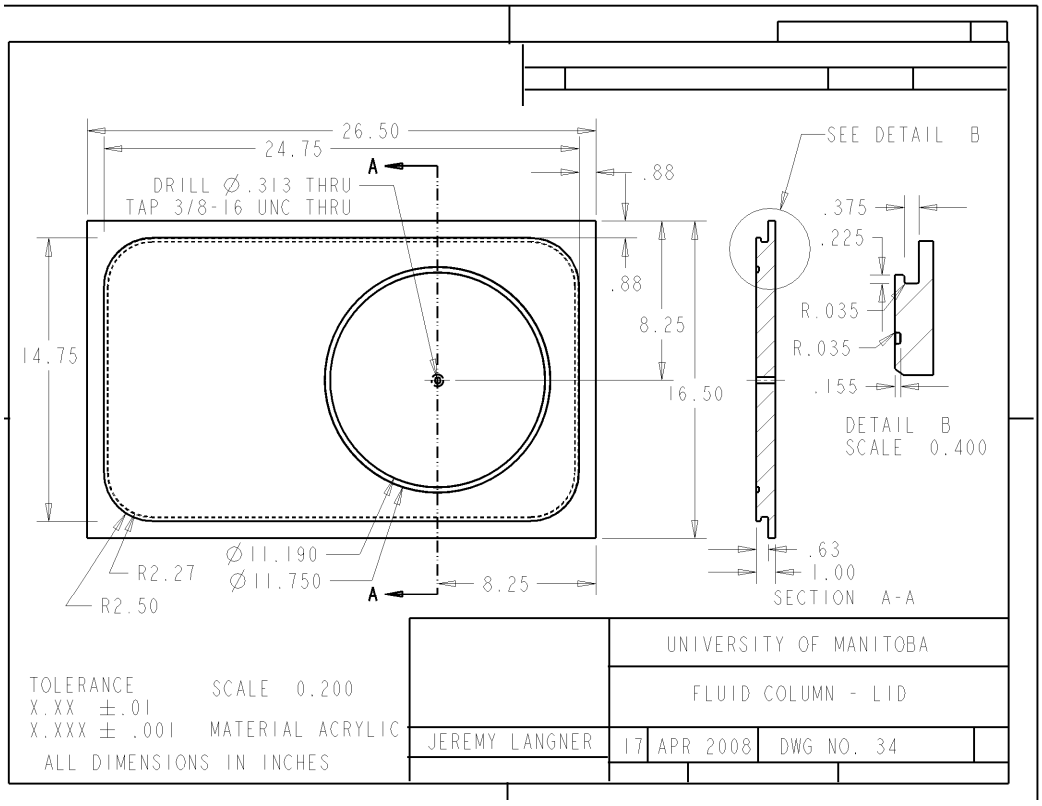
26.50
24.75
A
DRILL Ø.313 THRU
TAP 3/8-16 UNC THRU
.88
.88
8.25
16.50
14.75
Ø11.190
Ø11.750
R2.27
R2.50
8.25
A
SEE DETAIL B
.375
.225
R.035
R.035
.155
DETAIL B
SCALE 0.400
.63
1.00
SECTION A-A
TOLERANCE
X.XX ±.01
X.XXX ± .001
SCALE 0.200
MATERIAL ACRYLIC
ALL DIMENSIONS IN INCHES
UNIVERSITY OF MANITOBA
FLUID COLUMN - LID
JEREMY LANGNER
17 APR 2008
DWG NO. 34

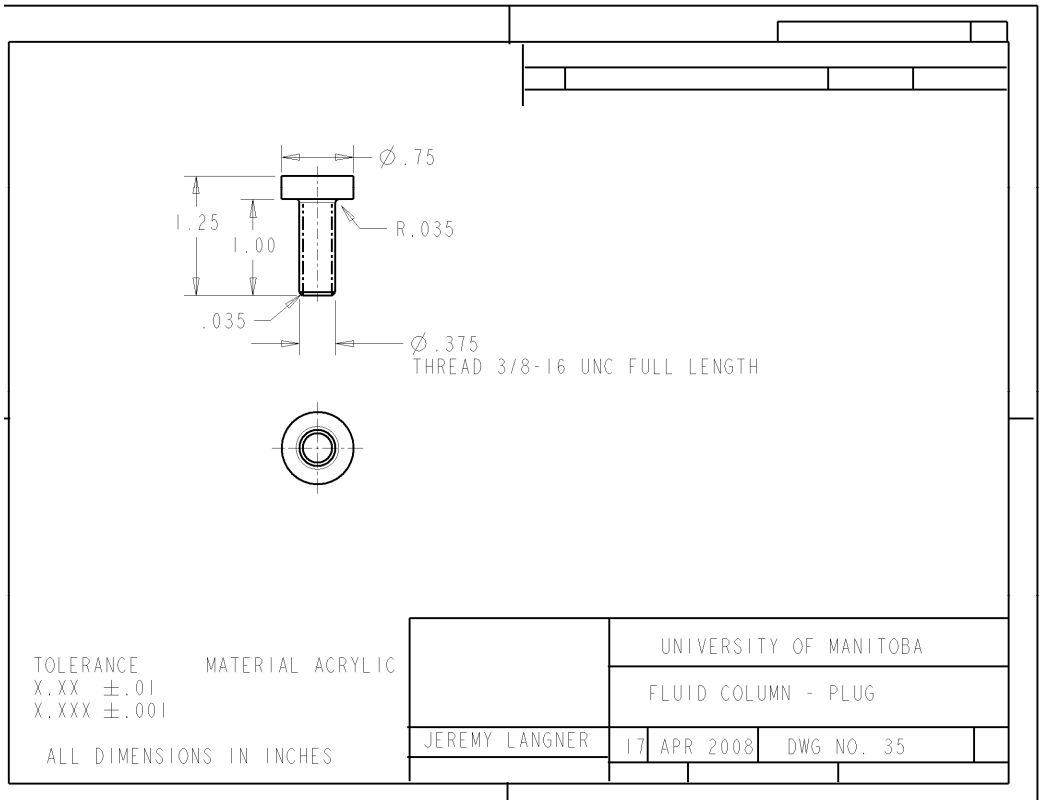
Ø.75
1.25
1.00
R.035
.035
Ø.375
THREAD 3/8-16 UNC FULL LENGTH
TOLERANCE
X.XX ±.01
X.XXX ±.001
MATERIAL ACRYLIC
ALL DIMENSIONS IN INCHES
UNIVERSITY OF MANITOBA
FLUID COLUMN - PLUG
JEREMY LANGNER
17 APR 2008
DWG NO. 35

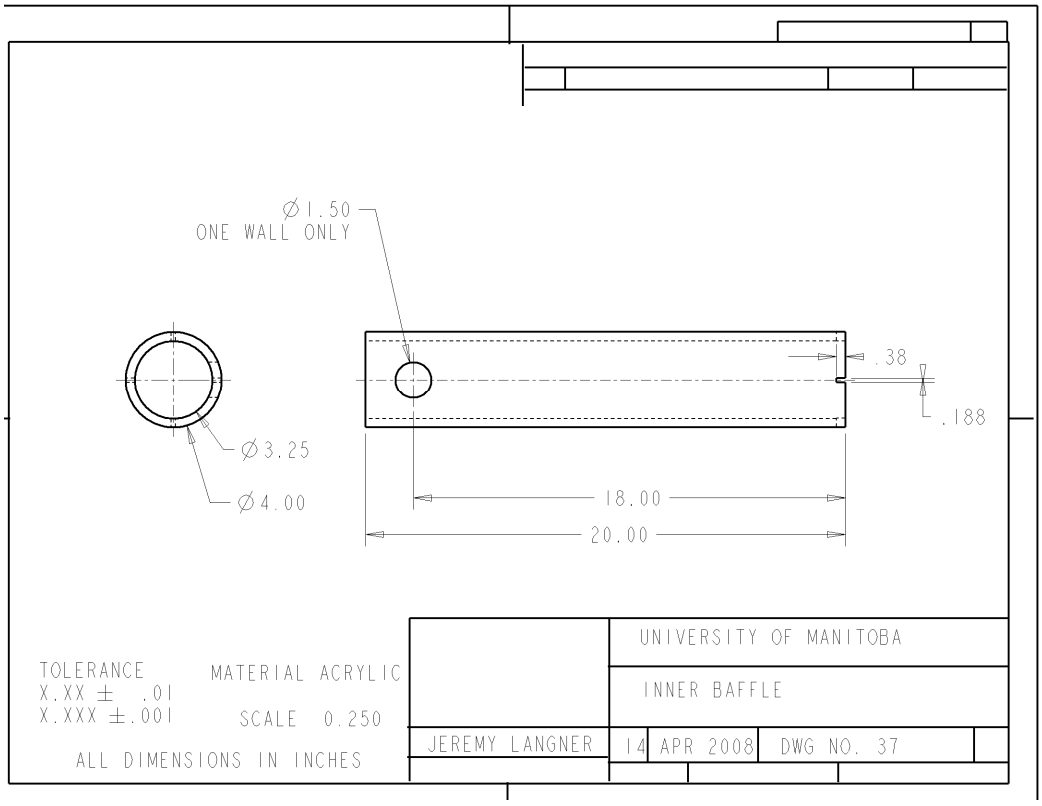
Ø1.50
ONE WALL ONLY
Ø3.25
Ø4.00
.38
.188
18.00
20.00
TOLERANCE
X.XX ± .01
X.XXX ±.001
MATERIAL ACRYLIC
SCALE 0.250
ALL DIMENSIONS IN INCHES
UNIVERSITY OF MANITOBA
INNER BAFFLE
JEREMY LANGNER
14 APR 2008
DWG NO. 37

Appendix H. Future expansion of the experimental fluid column facility

Currently, the fluid column facility is designed to simulate and study the flow characteristics of a continuous-flow anaerobic digester without forced mixing. However, many anaerobic digesters employ mixing in the form of mechanical agitation or bubble mixing. Thus, future expansion of the fluid column facility may be aimed at incorporating the ability to simulate these forms of mixing. Mixing often is used to increases the uniformity of the digestate within the tank; mixing may also mitigate settling. A key parameter in mixed digester tanks is the ratio of mixing momentum to inlet momentum. Since the hydraulic retention time of an anaerobic digester is very long—on the order of 10 to 30 days—the inlet momentum is very low. Thus, in a mixed digester, the effect of inlet velocity is very small compared to the velocities induced by mixing.

In a mechanically mixed digester, a mechanical impeller is used to agitate the fluid. This could easily be simulated using the fluid column facility. An impeller can be inserted through the threaded hole in the lid of the acrylic tank (see Figure H.1). The impeller would be rotated at a fixed RPM using an electric motor, based on the desired ratio of mixing momentum to inlet momentum. A seal would be required to prevent the leakage of fluid through the threaded hole. Both PIV and RTD experiments could be performed in this scenario; however, the position of the mechanical motor may obstruct the PIV camera at certain angles.

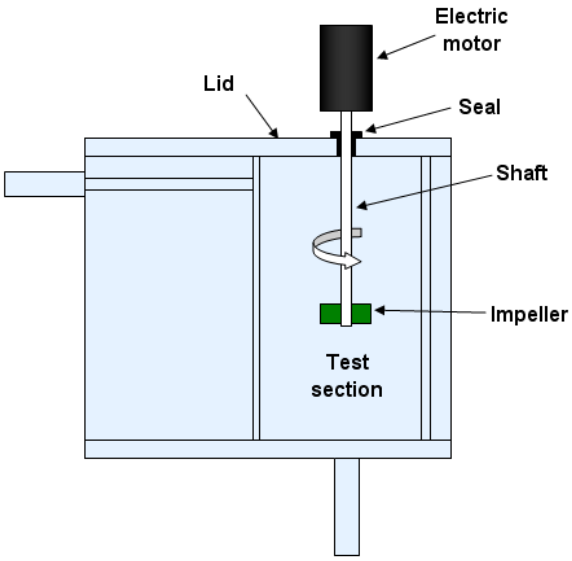

Figure H.1: Simulating mechanical mixing in the fluid column

Bubble mixing may be also simulated in the fluid column facility, though this requires more complex modifications. A straight tube may be inserted through the threaded hole in the tank lid, and air pushed through this tube using a small blower (see Figure H.2). The effect of a draft tube may be studied as well. However, air accumulation in the test section poses a problem. In this scenario, a constant volume of air must be maintained at the top of the test section. Probably the best way to do this is to recycle the air using the blower. The threaded hole in the top of the lid may have to be enlarged to allow both an air inlet tube and an exit tube. A seal would also be required; however, this seal must be air-tight as well as water-tight. RTD experiments may be performed in this scenario. However, PIV experiments could not, since the air bubbles would contaminate the PIV images.

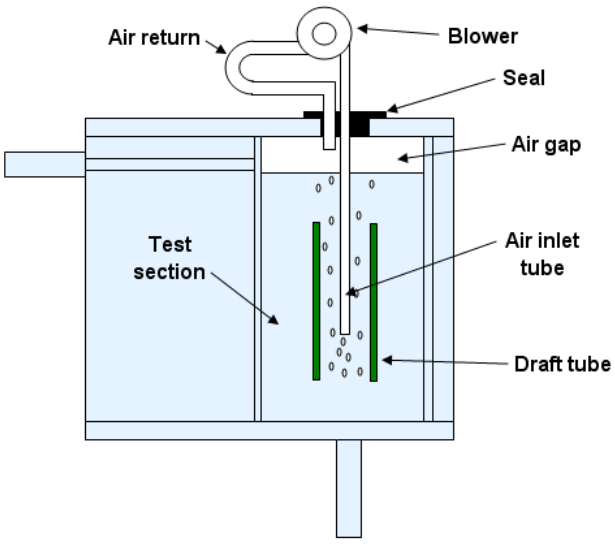

Figure H.2: Simulating bubble mixing with a draft tube in the fluid column

Only steady-flow conditions were investigated in the current study. However, the steady-flow assumption is rarely realistic when considering real-life anaerobic digesters; most anaerobic digesters operate in semi-batch or semi-continuous modes. For example, a digester may be fed once a day, with the pump running for only an hour or two. In the case of a mixed digester, mixing may not be continuous either; fluid may be agitated for half an hour every four hours, for example. These semi-continuous parameters vary from digester to digester. It would be valuable to use the fluid column facility to simulate these semi-continuous conditions; this could be done with only minor modifications.

Appendix I. Anaerobic Digester Economic Analysis

Case 1

Head (growers)	5000		Elec. Efficiency	30	%
Biogas	263,657	m3/yr	Heat recovery	65	%
HHV	25.2	MJ/m3	Heating months	6	
Energy	6,644	GJ/yr	Waste heat for drying	50	%
			Space heat efficiency	100	%
Energy Utilization			Dryer efficiency	70	%
Electricity generated	553,679	kWh/yr	HHV propane	24.8	GJ/m3
Space heat	1,512	GJ/yr			
Grain drying heat	756	GJ/yr			
Energy prices					
Electricity	$0.06	per kWh			
Propane	$191	per m3			

Annual Savings & Revenue

Item	Unit	Unit price	Quantity	Savings/Revenue
Electricity	kWh	$0.06	553,679	$33,221
Space heat (electric)	kWh	$0.06	419,873	$25,192
Propane (drying)	m3	$191	44	$8,315
Carbon credits	t CO2e	$10	2,504	$25,037
Gross savings & revenue				**$91,766**

Annual Expenses

Item	Unit	Unit price	Quantity	Expense
O&M based on BG prod.	m3 biogas	$0.04	263,657	$10,546
Total expenses				**$10,546**

Net revenue	**$81,219**
Max CapEx for 5 yr payback	**$406,097**

Case 2

Head (growers)	5000		Elec. Efficiency	30	%
Biogas	263,657	m3/yr	Heat recovery	65	%
HHV	25.2	MJ/m3	Heating months	6	
Energy	6,644	GJ/yr	Waste heat for drying	50	%
			Space heat efficiency	100	%
Energy Utilization			Dryer efficiency	70	%
Electricity generated	553,679	kWh/yr	HHV propane	24.8	GJ/m3
Space heat	1,512	GJ/yr			
Grain drying heat	756	GJ/yr			

Energy prices		
Electricity	$0.10	per kWh
Propane	$327	per m3

Annual Savings & Revenue

Item	Unit	Unit price	Quantity	Savings/Revenue
Electricity	kWh	$0.10	553,679	$55,368
Space heat (electric)	kWh	$0.10	419,873	$41,987
Propane (drying)	m3	$327	44	$14,236
Carbon credits	t CO2e	$30	2,504	$75,112
Gross savings & revenue				**$186,703**

Annual Expenses

Item	Unit	Unit price	Quantity	Expense
O&M based on BG prod.	m3 biogas	$0.04	263,657	$10,546
Total expenses				**$10,546**

Net revenue	**$176,157**
Max CapEx for 5 yr payback	**$880,785**